A STUDY OF SPACECRAFT TEMPERATURE PREDICTION BY THERMAL MODELING

By

DAGO MAPLES

Bachelor of Science
Mississippi State University
State College, Mississippi
1962

Master of Science
Mississippi State University
State College, Mississippi
1963

Submitted to the Faculty of the Graduate College
of the Oklahoma State University
in partial fulfillment of the requirements
for the Degree of
DOCTOR OF PHILOSOPHY
May, 1969

A STUDY OF SPACECRAFT TEMPERATURE PREDICTION

BY THERMAL MODELING

Thesis Approved:

J. A. Weitkult
Thesis Adviser

J. L. Fenton

James K. Partin

Robert D. Robinson, Jr.

D. D. Durham
Dean of the Graduate College

ACKNOWLEDGMENT

The author would like to express his sincere appreciation and extend his gratitude to the following individuals who provided help during his graduate program:

Particularly his graduate committee, composed of Dr. J. A. Wiebelt, Chairman, Dr. R. L. Panton, Dr. R. L. Robinson, and Dr. J. R. Partin, Jr.

Two brothers, Glennon and Dupree, for their encouragement, technical discussions, and most of all their daily association.

Mr. Harvey P. Metzler and Mr. Dick Bullock, for technical discussions and friendship during this investigation.

Mrs. Donna DeFrain and Mr. E. J. Hardy for assistance and advice in preparation of the manuscript.

Also Mr. Don Moore, Mr. David Phillip, and Mr. Bill Lewis for technical assistance.

Finally, Mother and Father, who have given the author love, respect, and continued encouragement from the beginning of his educational career.

In addition I would like to thank the National Aeronautics and Space Administration for financial support during this investigation.

TABLE OF CONTENTS

TABLE OF CONTENTS (Continued)

LIST OF TABLES

LIST OF TABLES (Continued)

LIST OF FIGURES

LIST OF FIGURES (Continued)

LIST OF FIGURES (Continued)

NOMENCLATURE

A	Surface area
$\bar{A}$	Dimensionless Area, A/L^2
ΔA	Surface Area of elemental volume
A_j	Effective area exposed to q_j and C_j
A_s	Irradiated area
A_2	Area of surface 2
A_5	Area of surface 5
${}^{s}A_j$	Projective area of surface j to sun
a	Exponent in the power function describing the dependence of thermal conductivity on temperature
a_1	Radius of inner cylinder
b	Exponent in the power function describing the dependence of heat capacity on temperature
C	Contact conductance
$\bar{C}$	Total heat capacity
C_p	Specific heat capacity at constant pressure
$\bar{C}_p$	Dimensionless specific heat capacity at constant pressure, $\frac{C_p}{C_{p_o}}$
C_{p_o}	A constant in the function that describes the dependence of heat capacity on temperature
C_{kj}	Conduction exchange coefficient between regions k and j
D	Diameter
d	Thickness

d_i . . . . . Diameter of inner cylinder

d_o . . . . . Diameter of outer cylinder

E_b . . . . . Black body emitted energy

E_j . . . . . Emitted energy from j th element

E_s . . . . . Solar radiation, $\int_o^\infty E_{s,\lambda} d\lambda$

$\bar{E}_s$ . . . . . Dimensionless solar radiation

F_{ij} or F_{i-j} . . . . Configuration factors = the fraction of energy directly incidental on the surface, i, from surface, j, which is assumed to be emitting energy diffusely

F_{2-w} . . . . . Configuration factor between the outer cylinder and the space chamber

$f_{j,k}$ . . . . . Distance between surface elements j and k

$\bar{f}_{j,k}$ . . . . . Dimensionless distance between surface elements j and k, $f_{j,k}/L$

F . . . . . Shape factor

F_s . . . . . Shape factor that accounts for all solar energy reaching area A_s by both direct and multiple reflection paths

Gr_δ . . . . . Grashof number based on the gap width

g . . . . . Acceleration due to gravity

h . . . . . Convective film coefficient

I . . . . . Intensity of radiation

$\bar{I}$ . . . . . Dimensionless intensity of radiation

I_λ . . . . . Monochromatic intensity of radiation, the rate at which radiant energy leaves a surface in the direction, per unit solid angle, per wavelength, per unit surface area perpendicular to the pencil of rays

$I_{b,\lambda}$ . . . . . Monochromatic intensity of radiation of a black surface

J . . . . . Radiosity function

k . . . . . Thermal conductivity

$\bar{k}$ . . . . . Dimensionless thermal conductivity, k/k_o

k_o . . . . . A constant in the function that describes the dependence of thermal conductivity on temperature

(k) . . . . . Quantities associated with A_k

k_c . . . . . $\bar{Q} \ln (\frac{d_o}{d_i})/2\pi(T_o-T_i)$ = "effective" thermal conductivity

L . . . . . Characteristic length

L_x . . . . . Characteristic dimension in X-direction

$\bar{L}_x$ . . . . . Dimensionless X-coordinate, X/L_x

L_y . . . . . Characteristic dimension in y-direction

$\bar{L}_y$ . . . . . Dimensionless Y-coordinate, Y/L_y

L_z . . . . . Characteristic dimension in Z-direction

$\bar{L}_z$ . . . . . Dimensionless Z-coordinate, Z/L_z

L_1 . . . . . Height of top cylinders

L_2 . . . . . Height of middle cylinders

L_3 . . . . . Height of bottom cylinders

Nu . . . . . Nusselt number

Nu_δ . . . . . Nusselt number based on the gap width

p . . . . . Static pressure

Pr . . . . . Prandtl number

PrGr . . . . . Rayleigh number

Q . . . . . Total heat input

$\bar{Q}$ . . . . . Heat transfer by convection per unit length

$\bar{q}$ . . . . . Dimensionless heat transfer rate $q/q_o = q/\sigma T^4$

q_α . . . . . Energy due to planetary albedo

q_c . . . . . Heat convected across annulus of test section

q_θ . . . . . Energy due to planatary emission

q_z . . . . . Heat transfer by convection and radiation across the gap

q_{in} . . . . . Net radiation energy received from other bodies

q_f . . . . . Heat conducted by fin

q_k . . . . . Heat conducted through the cylindrical wall

q_{net} . . . . . Net rate at which radiation leaves a surface

$\bar{q}_{net}$ . . . . . Dimensionless net rate at which radiation leaves a surface, $q_{net}/\sigma T_o^4$

q_o . . . . . Characteristic heat transfer rate, σT_o^4

q_r . . . . . Radiant energy exchange

q_{rr} . . . . . Heat flux in radial direction

q_s . . . . . Energy due to incident solar energy

q_3 . . . . . Heat flux in axial direction

$\overset{\circ}{q}$ . . . . . Heat transfer rate per unit area

$\overset{\circ}{q}_1$ . . . . . Heat transfer rate per unit area at surface 10

$\overset{\circ}{q}_2$ . . . . . Heat transfer rate per unit area at surface 2i

$\overset{\circ}{q}_3$ . . . . . Heat transfer rate per unit area at surface 20

$\overset{\circ\circ\circ}{\bar{q}}$ . . . . . Dimensionless heat transfer per unit volume

$\overset{\circ\circ\circ}{q}$ . . . . . Heat transfer rate per unit volume

R . . . . . Characteristic length

ΔR . . . . . Thickness of element

R_i . . . . . Radius of inner cylinder

R_{kj} . . . . . Radiative exchange coefficient between regions k and j

R_f . . . . . Radius of fin

R_o . . . . . Radius of outer cylinder

r . . . . . Radial direction in cylindrical coordinates

$\bar{r}$ . . . . . Dimensionless radius, r/R

S . . . . . Solar intensity

$\bar{S}$ . . . . . Dimensionless solar intensity, S/rt_o^4

S_o . . . . . Sutherland constant

T . . . . . Temperature

$\bar{T}$ . . . . . Dimensionless temperature, T/T_o

T_b . . . . . Temperature of fin's root

T_k . . . . . Temperature of area, A_k

T_j . . . . . Temperature of area, A_j

T_o . . . . . Characteristic temperature

T_R . . . . . Constant temperature of outer cylinder

T_* . . . . . Constant temperature of inner cylinder

T_w . . . . . Chamber wall temperature

$T(r,n)$ . . . . . Temperature deviation of the fluid field from some constant value

T_2 . . . . . Temperature of surface 2

T_5 . . . . . Temperature of surface 5

T_∞ . . . . . Temperature of the surroundings

$(\Delta T)_z$ . . . . . Measured minus predicted temperatures by the Zero Surroundings Technique

$(\Delta T)_I$ . . . . . Measured minus predicted temperatures by the Technique I

$(\frac{\Delta T}{T})_z$ . . . . . Temperature error in predicted values obtained through the Zero Surroundings Technique

$(\frac{\Delta T}{T})_I$ . . . . . Temperature error in predicted values obtained through Technique I

V . . . . . Volume

U . . . . . Current

v . . . . . Velocity

v_r . . . . . Radial velocity

v_n . . . . . Tangential velocity

x,y,z . . . . . Orthogonal coordinates

$\bar{x},\bar{y},\bar{z}$ . . . . . Dimensionless orthogonal coordinates, x/L, y/L, z/D

x_o . . . . . Characteristic length in x-direction

y_o . . . . . Characteristic length in y-direction

z_o . . . . . Characteristic length in z-direction

Greek

α . . . . . Absorptance, the fraction of energy absorbed from the total energy incoming to a surface element

α' or δ' . . . . . Angle defining the direction at which incoming radiation strikes a surface coming from another surface

α_{kj} . . . . . Absorptance for radiation interchange between k and j surfaces

α_s . . . . . Absorptance with respect to solar radiation

β . . . . . Volumetric coefficient of expansion

β' . . . . . Angle defining direction at which incoming radiation strikes a surface coming from another part of the same body

δ/d_i . . . . . Relative gap width

ϵ . . . . . Emittance

ϵ_w . . . . . Emittance of chamber wall

ϵ_λ . . . . . Directional monochromatic emittance

ϵ_{20} . . . . . Emittance of the exterior surface of outer cylinder

η . . . . . Angle direction in cylindrical coordinates

θ . . . . . Time

$\bar{\theta}$ . . . . . Dimensionless time, $k_o T_o^{\ a}/C_{p_o} T_o^{\ b} L^2 \rho_o$

θ' . . . . . Angle defining the direction at which radiation leaves a surface

θ_o . . . . . Characteristic time

λ . . . . . Wavelength

μ . . . . . Dynamic viscosity

ν . . . . . Kinematic viscosity

ρ . . . . . Density

$\bar{\rho}$ . . . . . Dimensionless density, ρ/ρ_o

$\bar{\bar{\rho}}$ . . . . . Reflectance

ρ_o . . . . . Characteristic density

σ . . . . . Stefan-Boltzmann Constant

τ . . . . . Dimensionless time, θ/θ_o

ϕ_{kj} . . . . . $\varepsilon_j A_j F_{jk} \sigma T_j^4/A_k$ in which F_{jk} is the configuration factor and the A's are surface area = energy flux leaving surface k and arriving at surface j

ϕ' . . . . . The angle at which radiation leaves a surface

ψ . . . . . Stream function

ω' . . . . . Solid angle

Ω . . . . . Resistivity

Subscripts

i,j,k . . . . . Regions of uniform temperature

n . . . . . Normal

m . . . . . Model

p . . . . . Prototype

s . . . . . Surface

20 . . . . . Exterior surface of outer cylinder

2i . . . . . Interior surface of outer cylinder

10 . . . . . Exterior surface of inner cylinder

1i . . . . . Interior surface of inner cylinder

Superscripts

* . . . . . Ratio of model property to prototype property

CHAPTER I

INTRODUCTION

For the past five years the principles of dimensional analysis and similitude have been applied to the thermal aspects of spacecraft and space related research problems. This activity has been particularly intense during the last two years. Published results have included both the analyses and experiments to confirm the analyses for radiation-conduction coupled heat transfer problems. In the process various thermal scale modeling techniques have been identified and used.

Interest in the thermal modeling of spacecraft has increased with the advent of larger and more complex spacecrafts which are necessary for more extensive observations and experiments in space. Space chambers capable of environmentally testing full scale spacecraft are extremely expensive to build and to operate. Since scale-model testing can be a valuable thermal design tool in the early stages of spacecraft design, a simple, valid thermal modeling technique is needed to predict the thermal behavior of a spacecraft from model test data.

The principles of similarity are well established in References [1]*, [2], and [3]. These concepts have been employed successfully in wind tunnel testing for years. For a spacecraft the temperature distribution within the vehicle is an important consideration; hence,

---

*Numbers in brackets designate References listed in Bibliography.

thermal similarity between the small-scale object (the model) in the test chamber and the spacecraft in flight (the prototype) is the desired goal.

The thermal characteristics of spacecraft impose a number of heat flow simulation modes (radiation, conduction, and convection) which must be duplicated in the laboratory to provide engineering data for a system design. A survey of the literature reveals that considerable attention has been focused on thermal similitude of the solid components of a spacecraft. The similarity parameters for models containing fluids have been discussed by Shih [13] and Katzoff [2], but there has been no attempt to verify experimentally a group of similarity parameters for a system of this type. The need for such an investigation is apparent, since fluid is a vital component of many satellites. Fluids are used to establish a habitable environment for crew members of manned spacecraft and to fill the pressurized cell detectors of a micrometeroid detection satellite, to mention two familiar applications.

The primary objectives of this investigation were to develop a practical method for thermal modeling of a system which contains a gas and to validate this method through tests performed on carefully designed models and prototypes. The system selected for this investigation consisted of concentric cylinders with a gas contained in the annulus between the cylinders. Dry air was selected as the fluid in the annulus in order to insure a medium which would not participate in the transfer of radiant energy between the concentric cylinders. The prototype and model were tested in a cold, high-vacuum environment.

This investigation included the following phases:

I. A group of similarity parameters which would thermally model a

system containing a fluid was developed. In order to model the convection mode of heat transfer, an empirical correlation for the convection film coefficient must be known. Since previously established empirical correlations for the convective film coefficient were incompatible, the desired correlation was established from data obtained by tests performed on the prototype.

II. A thermal analysis of the basic test configuration was performed. This analysis furnished valuable information for designing the system and provided a basis for the comparison of the steady-state experimental results.

III. An experimental investigation was performed in order to determine the validity of the similarity ratios. This required construction of three half-scale models and three full-scale prototypes. The test sections used in this investigation were designed to permit only one-dimensional, radial heat flow.

CHAPTER II

LITERATURE SURVEY

Approximately five years ago work on thermal modeling of spacecraft and their component parts was started. Generally, a thermal model is defined if the termperature, temperature distribution, internal energy, and flow of heat in the model are related in a known manner to the same quantities in the larger prototype. Since experimentation has been the only means of substantiating modeling criteria, the literature survey has been divided into two major categories: theory and experiments.

Theory

The theory of thermal modeling is based on both dimensional analysis and similitude. In dimensional analysis the pertinent variables are identified at the outset. Some insight into the problem and the knowledge of at least one combination of parameters are considered essential to the success of this method. The entire group of dimensionless combinations of these parameters formulates the modeling criteria.

The similitude approach consists of writing the governing differential equation for the model and prototype thermal behavior. The model equation is identical to the prototype equation if the dimensional elements multiplying corresponding terms are identical in value. The

modeling criteria are established by equating the ratios of corresponding dimensional multiplying elements in the model and the prototype differential equations. The previous theory of thermal scale modeling is surveyed below according to the classification of either similitude or dimensional analysis.

Similitude

Wainwright, Kelly, and Keesee [4] applied the theory of similitude to the differential equation which describes the thermal behavior of a thin shell vehicle. The differential equation is

$$\frac{\partial(\rho C_p T)}{\partial t}\,\Delta R\,\Delta A = \Delta R\,\Delta A\left\{\frac{\partial}{\partial X_1}\left(k\,\frac{\partial T}{\partial X_1}\right) + \frac{\partial}{\partial X_2}\left(k\,\frac{\partial T}{\partial X_2}\right)\right\}$$

$$- \sigma\epsilon T^4 \Delta A + \Sigma\,\dot{q}\,\Delta A, \qquad (2\text{-}1)$$

where x_1 and x_2 denote orthogonal axes in the plane of the wall, and $\Sigma\,\dot{q}$ is the sum of all external and internal sources. If a set of dimensionless quantities are introduced into Equation (2-1), the

$$\bar{X}_1,\ \bar{X}_2,\ \bar{\tau},\ \bar{T},\ \bar{k},\ \text{and}\ \bar{\rho}\,\bar{C}_p \qquad (2\text{-}2)$$

differential equation in dimensionless form becomes

$$\frac{\partial}{\partial \tau}\left(\bar{T}\bar{\rho}\bar{C}_p\right) = \frac{k_o\,\theta_o}{\rho_o C_{p_o} L^2}\left\{\frac{\partial}{\partial \bar{X}_1}\left(\bar{k}\,\frac{\partial \bar{T}}{\partial \bar{X}_1}\right) + \frac{\partial}{\partial \bar{X}_2}\left(\bar{k}\,\frac{\partial \bar{T}}{\partial \bar{X}_2}\right)\right.$$

$$\left. - \frac{\sigma\epsilon L^2 T_o^3}{k_o \Delta R}\left(\bar{T}^4 - \Sigma\,\frac{\dot{q}}{\sigma\epsilon T_o^4}\right)\right\}. \qquad (2\text{-}3)$$

The following ratios of quantities must be the same in the model and the prototype in order to obtain thermal similarity in the thermal

experiments:

$$\frac{k_o \theta_o}{\rho_o C_{p_o} L^2}, \frac{\sigma \epsilon L^2 T_o^3}{k_o \Delta R}, \frac{\ddot{q}}{\sigma \epsilon T_o^4} . \tag{2-4}$$

Hrycak and Unger [5] developed the same thin shell thermal modeling criteria that are presented in Equation (2-4) when the system was referred to in spherical coordinates.

Jones [6] and [7] applied the similitude method to a set of simultaneous, first-order differential equations. These equations were used to describe the thermal behavior of isothermal elements which were at different but uniform temperatures. These elements were considered to comprise the space vehicle under consideration. The describing equations are:

$$\overline{C}_j \left.\frac{\partial T_j}{\partial \theta}\right]_p = \left.\sum_{\substack{k=1 \\ k\neq j}}^{n} C_{kj} (T_k - T_j)\right]_p + \left.\sum_{\substack{k=1 \\ k\neq j}}^{n} R_{kj} (T_k^4 - T_j^4)\right]_p + \left. q_j \right]_p$$

$$+ \left. {}^{s}A_j \alpha_j S \right]_p - \left. A_j \epsilon_j \sigma T_j^4 \right]_p ; \quad j=1, \ldots, n, \tag{2-5}$$

where j, k are indices for regions that may be represented by a single temperature. Equation (2-5) was considered to represent the thermal behavior of the prototype. For a thermally similar model the differential equation is

$$\bar{C}_j \frac{\partial T_i}{\partial \theta}\Big]_m = \sum_{\substack{k=1 \\ k\neq j}}^{n} C_{kj} (T_k - T_j)\Big]_m + \sum_{\substack{k=1 \\ k\neq j}}^{n} R_{kj} (T_k^4 - T_j^4)\Big]_m$$

$$+ q_j\Big]_m + {}^{s}A_j \alpha_j S\Big]_m - A_j \epsilon_j \sigma T_j^4\Big]_m ; \quad j=1, \ldots, n. \tag{2-6}$$

The ratios of the prototype to the model quantities were represented by the following variables:

$$T_j^*, q_j^*, {}^{s}A_j^*, S^*, \alpha_j^*, C_{kj}^*, R_{kj}^*, A_j^*, \epsilon_j^*, \bar{C}_j^*, \theta^*$$

$$j = 1, \ldots, n,$$

$$j, k = 1, \ldots, n; k \neq j. \tag{2-7}$$

The dimensionless quantities in Equation (2-7) were introduced into Equation (2-5) and then the result was compared with Equation (2-6). From the comparison Equation (2-8) was obtained.

$$\bar{C}_j^* T_j^*/\theta^* = A_j^* \alpha_j^* S^* = A_j^* \epsilon_j^* T_j^{*4} = q_j^* = C_{1,j}^* T_1^* =$$

$$C_{2,j}^* T_2^* = \ldots = C_{j-1,j}^* T_{j-1}^* = C_{j+1,j}^* T_{j+1}^* = \ldots = C_{n,j}^* T_n^* =$$

$$C_{2,j}^* T_2^* = \ldots = C_{j-1,j}^* T_j^* = C_{j+1,j}^* T_j^* = \ldots = C_{n,j}^* T_j^* = R_{1,j}^* T_1^{*4} =$$

$$R_{2,j}^* T_2^{*4} = \ldots = R_{j-1,j}^* T_{j-1}^{*4} = R_{j+1,j}^* T_{j+1}^{*4} = R_{n,j}^* T_j^{*4} = R_{1,j}^* T_j^{*4} =$$

$$R_{2,j}^* T_j^{*4} = R_{2,j}^* T_j^{*4} = R_{j-1,j}^* T_{j-1}^{*4} = R_{j+1,j}^* T_{j+1}^{*4} = \ldots = R_{n,j}^* T_n^{*4};$$

$$j=1, \ldots, n. \tag{2-8}$$

All of the ratios contained in Equation (2-8) are the necessary and sufficient conditions for complete thermal similarity between the model

and prototype. These conditions, together with Equation (2-7) yield twenty eight ratios that must be constant from prototype to model if complete similarity is to be established. All the ratios contained in Equations (2-7) and (2-8) are not independent. Several independent groups of ratios can be deduced from these. One group is:

$$\frac{T_j}{T_k}, \frac{E_{kj}F_{kj}A_k}{\epsilon_j A_j}, \frac{\alpha_j {}^{s}A_j S\theta}{\overline{C}_j T_j}, \frac{\epsilon_j \sigma A_j T_j^3 \theta}{\overline{C}_j}, \frac{C_{kj}\theta}{\overline{C}_j}, \text{ and } \frac{q_j \theta}{\overline{C}_j T_j} . \qquad (2\text{-}9)$$

This particular group was selected with reference to the differential [Equation (2-5)]. For another independent group, see Reference [7]. Seven independent groups of ratios were established.

Chao and Wedeking [8] used the method of similitude to develop the thermal modeling criteria from the governing equations. The differential equations were written for n thin walls in two- and three-dimensions. The surfaces were assumed to be opaque and nondiffuse, and variations of bulk thermal properties with temperature were considered. The property variations of thermal conductivities and heat capacities were expressed as

$$k = k_o T^a; \; C_p = C_{p_o} T^b, \; (T = {}^{o}R)$$

where k, C_p, a, and b are constants. The governing nonlinear integro-differential equations in curvilinear coordinates for the surfaces are

$$C_{p_j} \frac{\partial T_j}{\partial t} = \dot{q}_j - \frac{q_{net,j}}{d_j} + \frac{\partial}{\partial y_j}\left(k_j \frac{\partial T}{\partial y_j}\right) + \frac{\partial}{\partial x_j}\left(k_j \frac{\partial T}{\partial x_j}\right), \qquad (2\text{-}10)$$

where

$$q_{net,j} = - \sum_{\substack{k=1 \\ k\neq j}}^{n} \int_{A_k} I_k \frac{\text{Cos } \alpha'_j \text{ Cos } \phi'_k}{r^2_{jk}} dA_k$$

$$- \int_{A_{(j)}} I_{(j)} \frac{\text{Cos } \delta'_j \text{ Cos } \phi'_{(j)}}{r^2_{j(j)}} dA_{(j)}$$

$$- E_s \text{ Cos } B'_j + \int_{hs} I_j \text{ Cos } \phi_j \, d\omega'_j; \quad (j=1,\ldots,n), \tag{2-11}$$

and the terms in the braces account for radiative interchange. The series of terms under the summination sign account for radiant energy exchange between different surfaces, excluding surfaces that can "see" themselves the next to the last term represents solar energy, and the last term accounts for radiation on the surface. Introducing the dimensionless variables

$$\overline{T}_j, \ \overline{X}_j, \ \overline{Y}_j, \ \overline{\theta}_j, \ \overline{I}_j, \ \overline{f}_{j,k}, \ \overline{A}_j, \text{ and } \overline{E}_s \tag{2-12}$$

$$(k, \ j=1, \ \ldots, \ n; \ k\neq j),$$

into Equation (2-10), together with the power law variation of conductivity and specific heat with temperature, the following equations are obtained:

$$(\overline{T}_j)^{b_j - a_j} \frac{\partial \overline{T}_j}{\partial \overline{\theta}_j} = \frac{\partial^2 \overline{T}_j}{\partial \overline{X}_j^2} + \frac{\partial^2 \overline{T}_j}{\partial \overline{Y}_j^2} + \frac{a_j}{\overline{T}_j} \left\{ \left(\frac{\partial \overline{T}_j}{\partial \overline{X}_j} \right)^2 + \left(\frac{\partial \overline{T}_j}{\partial \overline{Y}_j} \right)^2 \right\}$$

$$+ \frac{\sigma L^2 T_o^{3-a_j}}{k_{oj} d_j (\overline{T}_j)^{a_j}} \left\{ \sum_{\substack{k=1 \\ k\neq j}}^{n} \int_{\overline{A}_k} \overline{I}_k \frac{\text{Cos } \alpha'_j \text{ Cos } \phi'_k}{\overline{f}^2_{j,k}} d\overline{A}_k + \right.$$

$$\int_{\bar{A}_{(j)}} \bar{I}_{(j)} \frac{\cos \delta'_j \cos \phi'_{(j)}}{\bar{f}^2_{j(j)}} d\bar{A}_{(j)} \Bigg\} + \frac{L^2}{k_{oj} T_o^{1+a_j} \bar{T}_j^{a_j}} \bar{\dddot{q}}_j$$

$$- \frac{\sigma L^2 T_o^{3-a_j}}{k_{oj} d_j \bar{T}_j^{a_j}} \int_{hs} \bar{I}_j \cos \phi_j \, d\omega'_j$$

$$+ \frac{\sigma L^2 T_o^{3-a_j}}{k_{cj} d_j \bar{T}_j^{a_j}} \bar{E}_s \cos B'_j \qquad (j = 1, \ldots, n). \qquad (2\text{-}13)$$

The following groups of quantities must be the same in the model and the prototype in order for steady-state similarity to exist:

$$a_j, \frac{T_o^{3-a_j} L^2}{k_{oj} d_j}, \frac{E_s}{\sigma T_o^4}, \frac{\int_o^\infty I_{b,\lambda} \epsilon_{\lambda,(k)} d\lambda}{\sigma T_o^4}, \frac{\int_o^\infty I_{\lambda(k)} \bar{\bar{\rho}}_{\lambda(k)} d\lambda}{\sigma T_o^4},$$

$$\frac{\int_o^\infty E_{s(\lambda)} \bar{\bar{\rho}}_{\lambda(k)} d\lambda}{\sigma T_o^4}, \frac{\int_o^\infty I_{\lambda(j)} \bar{\bar{\rho}}_{\lambda(k)} d\lambda}{\sigma T_o^4}, \frac{\dddot{q}_j L^2}{k_{oj} T_o^{1+a_j}},$$

$$(j, k=1, \ldots, n; k \neq j). \qquad (2\text{-}14)$$

In addition to Equation (2-14), the group between model and prototype of b_j and $\frac{C_{p_o} T_o^b L^2}{k_o T_o^a \theta}$ are needed to establish transient thermal modeling.

Rolling [9] and [10] selected the similitude approach for developing the modeling criteria for space vehicles. The general differential equation expressing the energy balance for a single elemental volume

was given by

$$\rho V C_p \frac{dT}{d\theta} = A_s S \mathcal{F}_s + A_r R \mathcal{F}_r + A_e E \mathcal{F}_e + \dddot{q} +$$

$$+ \sum_{n=1}^{N} k_n A_n \frac{dT}{dX} + \sum_{j=1}^{J} \sigma A_j \mathcal{F}_j (T_j^4 - T^4), \qquad (2\text{-}15)$$

where $\rho V C_p (dT/d\theta)$ is the rate of change in sensible heat of the element, and $A_s S \mathcal{F}_s$ is the total energy rate absorbed by the element due to incident solar energy. $A_r R \mathcal{F}_r$ and $A_e E \mathcal{F}_e$ represent energy transfer to or from the element due to albedo absorption and earth emission absorption, respectively. The term $\sum_{n=1}^{N} k_n A_n \frac{dT}{dX}$ represents the conducted energy between the elemental volume and the surroundings, and $\sum_{j=1}^{J} \sigma A_j \mathcal{F}_j (T_j^4 - T^4)$ represents energy transfer along all radiative paths.

Rolling's procedure was identical to Chao and Wedekind. The ratio of model to prototype properties were expressed as

$$\rho^* = \rho_m/\rho_p, \; V^* = V_m/V_p, \; T^* = T_m/T_p, \; \theta^* = \theta_m/\theta_p, \qquad (2\text{-}16)$$

etc.

Where ρ_m is a model property and ρ_p is a property of the prototype. Substitution of the relations in Equation (2-16) for all terms in the model energy balance results in an equation for model behavior which is mathematically identical to that written for the prototype as long as the following conditions are satisfied:

$$\frac{\rho^* V^* C_p^* T^*}{\theta^*} = A_s^* S^* \mathcal{F}_s^* = A_r^* R^* \mathcal{F}_r^* = A_e^* E^* \mathcal{F}_e^* = \dddot{q}^*$$

$$= k_n^* A_n^* \left(\frac{T^*}{X^*}\right) = A_j^* \mathcal{F}_j^* T^{*4}. \qquad (2\text{-}17)$$

The ratios in Equation (2-17) are the governing similitude criteria for

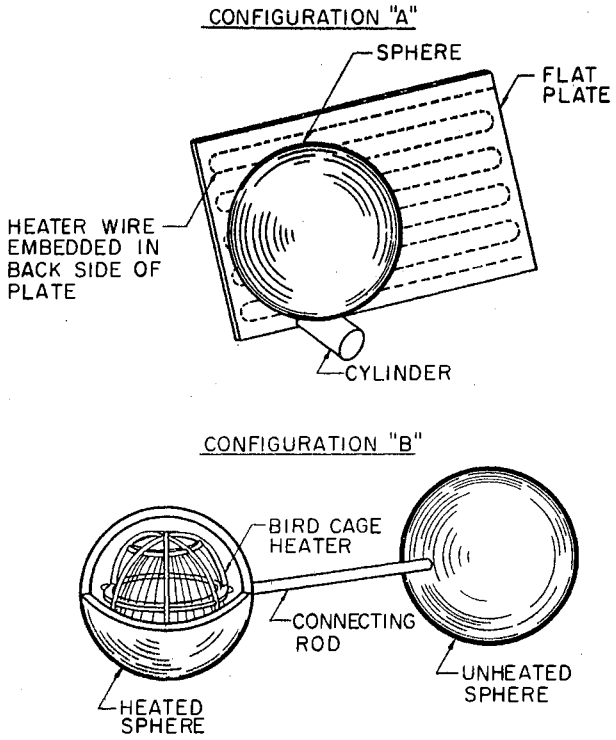

Figure 1. Test Configurations (Source: Ref. 11)

prediction of prototype behavior from model behavior for a radiation-conduction coupled problem.

Adkins [11] used the Fourier conduction equation with radiation boundary conditions, to establish the similarity criteria for two different configurations: A, the nonconduction array, and B, the conduction array that is shown in Figure 1. In configuration A, conduction heat transfer takes place only inside the bodies, whereas heat exchange between the bodies is accomplished by radiation. In configuration B, conduction heat exchange between the bodies takes place in addition to radiation exchange.

Assuming that the properties do not vary with temperature, then

the heat conduction equation can be written as

$$\frac{\partial T}{\partial \theta} = \frac{k}{\rho C_p}\left\{\frac{\partial^2 T}{\partial X^2} + \frac{\partial^2 T}{\partial Y^2} + \frac{\partial^2 T}{\partial Z^2}\right\}, \tag{2-18}$$

with boundary conditions

$$k\left(\frac{\partial T}{\partial Z}\right)_{z=d} = q_{1n}\ , \tag{2-19}$$

$$s = -\,k\left(\frac{\partial T}{\partial Z}\right)_{z=0}\ . \tag{2-20}$$

The following variables were used to write Equations (2-18), (2-19), and (2-20) in dimensionless form:

$$\overline{T},\ \overline{\tau},\ \overline{X},\ \overline{Y},\ \overline{Z},\ \overline{q},\ \overline{S}.$$

Equations (2-18), (2-19), and (2-20) written in dimensionless form are:

$$\frac{\partial \overline{T}}{\partial \tau} = \frac{k\theta_o}{\rho C_p L^2}\left\{\frac{\partial^2 \overline{T}}{\partial \overline{X}^2} + \frac{\partial^2 \overline{T}}{\partial \overline{Y}^2} + \left(\frac{L}{d}\right)^2 \frac{\partial^2 \overline{T}}{\partial \overline{Z}^2}\right\} \tag{2-21}$$

$$\left(\frac{\partial \overline{T}}{\partial \overline{Z}}\right)_{z=1} = \left\{(\sigma\, T_o^{\,3}\, d)/k\right\} \overline{q} \tag{2-22}$$

$$-\left(\frac{\partial \overline{T}}{\partial \overline{Z}}\right)_{z=0} = \left\{(\sigma\, T_o^{\,3}\, d)/k\right\} \overline{S}. \tag{2-23}$$

From inspection of Equations (2-21), (2-22), and (2-23), the similarity ratios are:

$$\frac{L^2\, \rho\, C_p}{k\ \theta_o},\ \frac{L}{d},\ (\sigma\, T_o^{\,3}\, d)/k. \tag{2-24}$$

The similitude method was applied by Young and Shanklin [12] to a

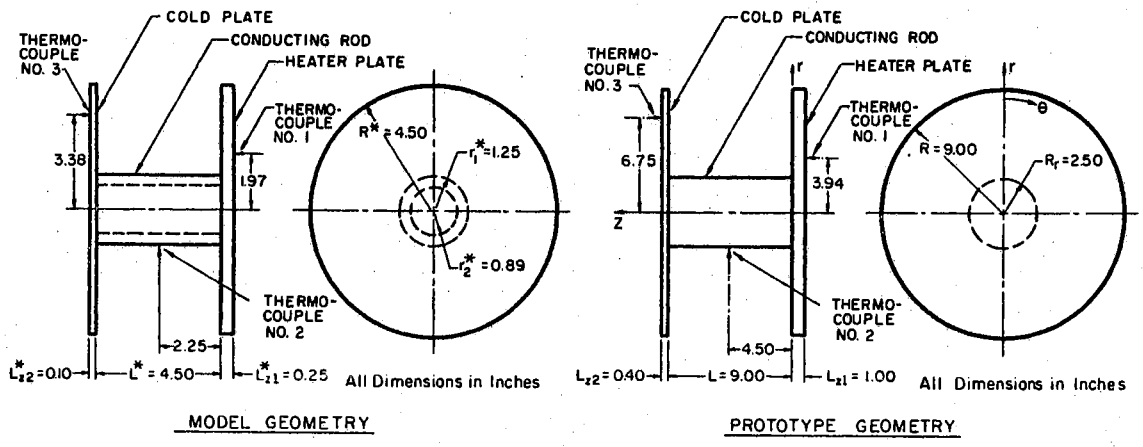

Figure 2. Spool Configuration (Source: Ref. 12)

set of differential equations used to describe the temperature behavior of the "spool-type" configuration shown in Figure 2. The system was made up of three sections; a heater-plate containing an electrical resistance heating element which represents an internal energy source of variable strength, a cold-plate having no internal energy source, and a cylindrical rod connecting the two plates. The differential equation for an elementary volume of the system was:

$$\frac{\partial T_i}{\partial \theta} = \frac{k}{\rho C_p} \nabla^2 T_i - \frac{2\epsilon_i \sigma T_i^4}{\rho C_p L_z} + \frac{1}{\rho C_p L_z} \sum_j^J \alpha_j \epsilon_j F_{i-j} \sigma T_j^4 + \frac{q}{\rho C_p}. \tag{2-25}$$

The initial condition was

$$T_i = T_{io} \text{ at } \theta = 0, \tag{2-26}$$

and the boundary conditions were:

$$k\,(2\pi R_r)\,L_z\left(\frac{\partial T_i}{\partial r}\right)_{r=Rr} = k\,(\pi R_r^2)\left(\frac{\partial T_i}{\partial z}\right)_{z=0,L} \qquad (2\text{-}27)$$

Applying the transformations

$$T_i = \bar{T}_i\,T_{io},\ \bar{r},\ \bar{z},\ \bar{\theta}$$

the following similarity parameters were obtained for the heater plate:

$$\frac{R^2\,\epsilon_i\,\sigma\,T_o^3}{k\,L_z},\ \frac{q\,R^2}{k\,T_{io}},\ \frac{R_r}{R},\ \frac{R_r\,R}{L_z\,L},\ \frac{\theta\,k}{R^2\,\rho\,C_p},\ \frac{R^2\,\alpha_i\,\epsilon_i\,F_{i-j}\,\sigma\,T_{jo}^4}{k\,L_z\,T_{io}}. \qquad (2\text{-}28)$$

The similarity parameters for the cold plate were the same as those for the hot plate with the exception of the ratio, $\frac{q\,R^2}{k\,T_{io}}$. Utilizing a similar approach for the connecting rod with an appropriate change in coordinates, the following similarity parameters were obtained in addition to the existing parameters:

$$\frac{L^2\,\epsilon_i\,\sigma\,T_{io}^3}{k\,R_r},\ \frac{L^2\,\alpha_i\,\epsilon_j\,F_{i-j}\,\sigma\,T_{jo}^4}{k\,R_r\,T_{io}}. \qquad (2\text{-}29)$$

Shih [13] considered the temperature field on a spacecraft with on-board equipment and personnel to be expressed as:

$$C_p\,\rho\,\frac{\partial T}{\partial \theta} = \nabla\cdot(k\nabla T) + \frac{h_s T}{dZ} + \frac{h_{ij} T}{dZ} + \frac{I}{dZ} + q. \qquad (2\text{-}30)$$

The transformations $L_x = \frac{x}{L_x}$, $T = \frac{T}{T_o}$, ..., were used to obtain the following similarity ratios.

$$\frac{L_x}{L_y}, \frac{q\ L_x\ L_y}{k\ T}, \frac{I\ L_x\ L_y}{k\ T\ L_z}, \frac{h_{ij}\ L_x\ L_y}{k\ L_z}, \frac{h_s\ L_x\ L_y}{k\ L_z}, \frac{C_p\ \rho\ L_x\ L_y}{k\ \theta}. \quad (2\text{-}31)$$

Miller [14] investigated the applicability of thermal modeling to steady-state and transient conduction in cylindrical solid rods, for both single and multiple material systems. By performing a similitude analysis, Miller obtained the following relations:

$$\overset{\circ\circ}{q}{}^* = L^{*-2},\ \ddot{q}^* = L^{*-1},\ q^* = L^{*3},\ T^* = 1,\ \theta^* = L^{*2},\ R^* = L^{*2}, \quad (2\text{-}32)$$

where the starred quantities represent the model to prototype ratio of the parameter (i.e., $T^* = \frac{T_m}{T_p}$, $q^* = \frac{q_m}{q_p}$, etc.).

Geometrically scaled models may be used to measure the classical diffuse radiation geometry factor (see References [4] and [5]). Matheny [15] has made such measurements for a number of configurations, including a plate, cylinder, and sphere arranged axisymmetrically in such a way that there was mutual shadowing. Kokorev [16] and [17] has proposed another method, also using scaling, where the factors are determined from the measurement of temperatures.

Clark and Leband [18] and Katz [19] were the first investigators to use dimensional analysis for establishing the thermal modeling criteria in space applications. (The dimensional ratios that they derived were used to study the temperature of composite wall constructions exposed to an external radiation environment.) Leband and Clark presented the ratios in Equation (2-33)

$$\frac{\sigma T^4}{\ddot{q}}, \frac{\ddot{q}L}{kT}, \frac{C_p L^2}{k\ \theta}, \quad (2\text{-}33)$$

and Katz presented the ratios listed in Equation (2-34)

$$\frac{\sigma T^3 L}{k}, \frac{\ddot{q} L^2}{k T}, \frac{C_p L^2}{k \theta}. \tag{2-34}$$

The last ratio in Equation (2-33) and Equation (2-34) is common. If $\ddot{q}$ does not enter into the problem, then the ratios in Equation (2-33) are not independent. The ratios in Equation (2-34) are independent if $\ddot{q}$ is not required. The two groups of ratios in Equation (2-33) and Equation (2-34) may be combined to form Equation (2-35)

$$\frac{\dddot{q} L^2}{k T}, \frac{\ddot{q} L}{k T}, \frac{\sigma T^3 L}{k}, \frac{C_p L^2}{k \theta}, \text{ and } \frac{\sigma T^4}{\ddot{q}} \tag{2-35}$$

where it is assumed that both $\ddot{q}$ and $\dddot{q}$ enter the problem. The three approaches listed in Equations (2-33), (2-34), and (2-35) are correct, depending on the specific application.

The basic dimensionless groups for thermal scale modeling in a high vacuum, for the case of conduction and radiation heat transfer, have been presented by Vickers [20] (see also References [23] and [24]). The dimensionless groups are:

$$\frac{\rho C_p L^2}{k \theta}, \frac{\epsilon \sigma T^3 L}{k}, \frac{CL}{k}, \frac{\alpha_{kj} \phi_{jk} L}{k T}, \frac{\alpha_s S L}{k T}, \frac{q}{LkT}, \frac{\ddot{q}L}{kT}, \frac{\dddot{q}L^2}{kT}. \tag{2-36}$$

By considering q, $\ddot{q}$, and $\dddot{q}$ as distinct physical quantities, Equation (2-36) forms one group of independent ratios. The last three ratios listed in Equation (2-36) may be reduced to one by introducing the following relations $\ddot{q} = q/L^2$ and $\dddot{q} = q/L^3$. The resulting group contains six independent ratios which includes one for joint interface conduct-

ance. In this case, q, is a characteristic power; however, in certain modeling it may be desirable to consider q, $\ddot{q}$, and $\dddot{q}$ as distinct quantities.

Katzoff [21] derived five dimensionless similitude parameters for the design and testing of thermal models of spacecraft. These ratios were concerned with the radiation, internal heat generation, thermal conductivities of materials, heat capacities of materials, and joint conductance. The five parameters are

$$\frac{\sigma T^4}{\ddot{q}}, \frac{\dddot{q} L}{\ddot{q}}, \frac{\ddot{q}L}{kT}, \frac{C_p L T}{\ddot{q}\,\theta}, \text{ and } \frac{CL}{k}, \tag{2-37}$$

where the last ratio in Equation (2-37) applies to joint conductance. This group of ratios does not explicitly include radiation exchange between surfaces; however, they form an independent group. The ratios in Equation (2-35) that form an independent group are

$$\frac{\sigma T^3 L}{k}, \frac{C_p L^2}{k\,\theta}, \frac{\ddot{q}L}{kT}, \text{ and } \frac{\dddot{q} L^2}{kT}. \tag{2-38}$$

If joint conductance is neglected, Equation (2-37) becomes

$$\frac{C T^4}{\ddot{q}}, \frac{C_p L T}{\ddot{q}\,\theta}, \frac{\ddot{q}L}{kT}, \text{ and } \frac{\dddot{q} L}{\ddot{q}}. \tag{2-39}$$

Evidently, Equations (2-38) and (2-39) are not identical groups of independent ratios, although they apply to the same physical problem. Either of the groups may be derived from the other. The ratio, $\ddot{q}$ L/kT, is common in Equation (2-38) and Equation (2-39). Equation (2-38) can be obtained from the product of the common ratio and the remaining

ratios of Equation (2-39).

All the thermal modeling criteria that have been listed above under dimensional analysis were developed from a knowledge of the physical phenomena involved. However, this gives no indication of their usefulness in the design of thermal models.

Watkins [22] developed forty-nine groups each of which contained seven independent similarity ratios for the general case of thermal modeling. The groups of similarity ratios were the result of a dimensional analysis study of the physical quantities defining the energy transfer to and from single, elemental, isothermal volumes of the prototype and model in a simulated space environment that was performed on the computer. For the general case that Watkins considered, the physical quantities defining the energy exchange between elemental isothermal volumes of the prototype and model in a simulated space environment are:

$$\overline{C}_j,\ C_{kj},\ q,\ R_{kj},\ \theta,\ T_j,\ T_k,\ q_e,\ q_a,\ \text{and}\ q_s.$$

A numerical approach to dimensional analysis was also applied to the physical quantities that describe the thermal behavior of two radiating disks connected by a conducting rod. One disk was exposed to external heating (radiation). The entire system was exposed to a low temperature environment. Joint interface conduction and internal energy release were not considered. The numerical solution yielded fifty-seven groups each of which contained five independent ratios. These ratios are presented in Reference [25]. Any one of these groups may be used for model design, the selection depending upon what is to be the purpose of the model experiments. One such group is

$$\frac{\bar{C}_j\, T_k}{\ddot{q}\, A_j\, \theta},\ \frac{T_k\, C_{kj}}{A_j\, \ddot{q}},\ \frac{T_k^4\, R_{kj}}{A_j\, \ddot{q}},\ \frac{\ddot{\ddot{A}}_j}{A_j},\ \frac{T_j}{T_k}, \tag{2-40}$$

where $\ddot{\ddot{A}}_j$ is the effective area exposed to $\ddot{q}_j$ and $\bar{C}_j$ is the total heat capacity.

Experiments

There have been several investigations performed to determine the validity of the derived similarity parameters. A brief review of these investigations is given in this section.

Gabron, Johnson, and Fowle, in collaboration with Vickers and Lucas [24, 26, 27, 28] carried out a series of experiments on models to predict the temperature of the Mariner IV spacecraft. The Mariner IV mission was, such that, the spacecraft spent long periods of time away from any planet. The spacecraft was exposed only to external radiation from the sun, and was at a fixed altitude with respect to the sun. Thus, steady-state modeling was applied.

The scale model of the Mariner IV was designed in accordance with the principles of the temperature preservation technique. "Temperature preservation" is where temperature at homologous locations in model and prototype are predicted by theory to be identical. Since the temperature measurements in the model and the prototype were made at thermal equilibrium, no consideration was given to the thermal scaling of temperature transients. The surface optical properties of the model and the prototype were made identical by use of the same thermal control coatings. The group of ratios in Equation (2-36) for this application are

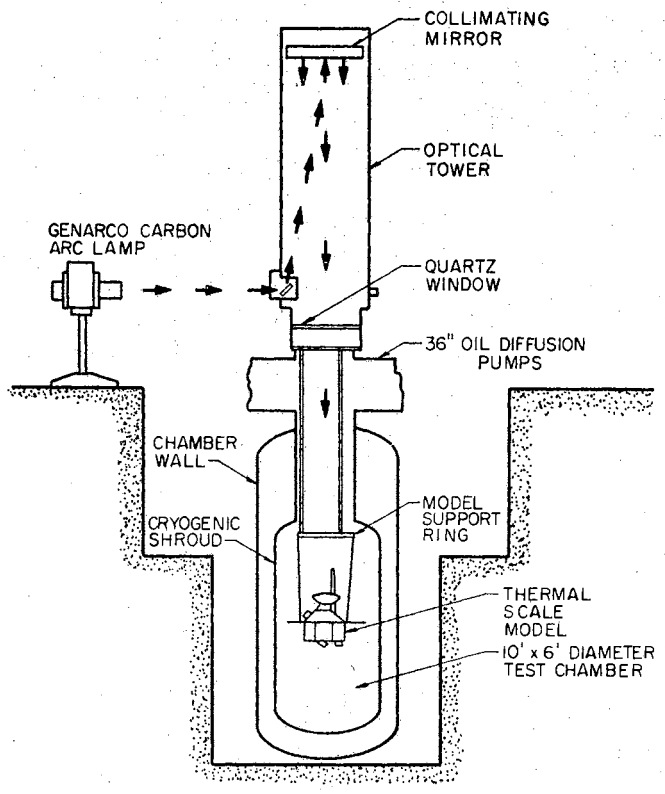

Figure 3. Schematic of Space Simulator with Model of Mariner IV Located Inside (Source: Ref. 26)

$$T,\ L/k,\ C,\ q/L^2,\ \ddot{q},\ \dddot{q}L \qquad (2\text{-}41)$$

These must have the same values at similar points on the prototype and the model. The ratio L^2/kd was kept constant (geometric distortion of minor dimensions) in the thin plates.

The one-half scale model in a space simulator is shown in Figure 3. Comparison of measured temperatures of the scale model and actual flight temperatures are shown in Table I for one mode of spacecraft operation (see Reference [29]). The basis for the comparison was temperature data telemetered to Earth from the Mariner IV spacecraft. The

TABLE I

MARINER IV TEMPERATURES

Source: Ref. 29
Earth Cruise - 2
98 Days from lunch
Solar intensity $\doteq$ 0.091 w/Cm^2 ($\frac{S}{S_o}$ = 0.655)

Location	Temperature ($^\circ$K) Flight Minus Scale Model
Sunlit Appendages	
Magnetometer	-6.12*
Ion Chamber	-7.78
Trapped Radiation Detection	+3.89
Internal Bus Locations	
Bay 1	-3.33
Bay 2	-3.33
Bay 3	0.0
Bay 4	-3.89
Bay 5	-2.78
Bay 6	-7.22
Bay 7	-2.22
Power Regulator (Bay 8)	-2.78
Battery (Bay 8)	0.0
Lower Ring (Bay 8)	12.8
Upper Ring (Bay 2)	-1.11
M/C Fuel Tank	-1.67
N_2 Tank (Bottom)	7.22
N_2 Tank (Top)	-1.11
Shaded Appendages	
Canopus Tracker	24.4
Television Camera	-0.55
Spits	-2.78

*Reference [29] gives values to nearest 0.0°F.

results show that successful modeling was accomplished.

Matheny [15] conducted some experiments that involved transient thermal modeling. The system selected for investigation was two disks connected by a conducting member. The conducting member was made large enough to enter into the radiant interchange. The models were designed according to the criteria given in Equation (2-38). The exterior of one of the disks was suddenly exposed to radiant energy from an electrical resistance heater. The results of the transient tests which were conducted on the prototype and one-half scale model are shown in Figure 4. The temperature of the model was within $3^{\circ}K$ of that of the prototype.

Folkman, Baldwin, and Wainwright [30] applied the modeling criteria given in Equation (2-4) to the conceptual space station illustrated in Figure 5. Geometric scaling was used and external radiation sources were preserved. The experimental results obtained from tests performed on the model were compared with three-dimensional transient analysis; a typical comparison is shown in Figure 6.

Jones and Harrison [31] used the group of ratios given in Equation (2-9) to model a system composed of a plate, cylinder, and sphere which were exchanging thermal energy by radiation only. The three components of the system were located relative to one another as shown in Figure 7.

If electrical resistance heaters are used to obtain the simulated heating effects of the sun, and if the space chamber is regarded as incorporated in the ratio involving radiative interchange between surfaces, then Equation (2-9) reduces to

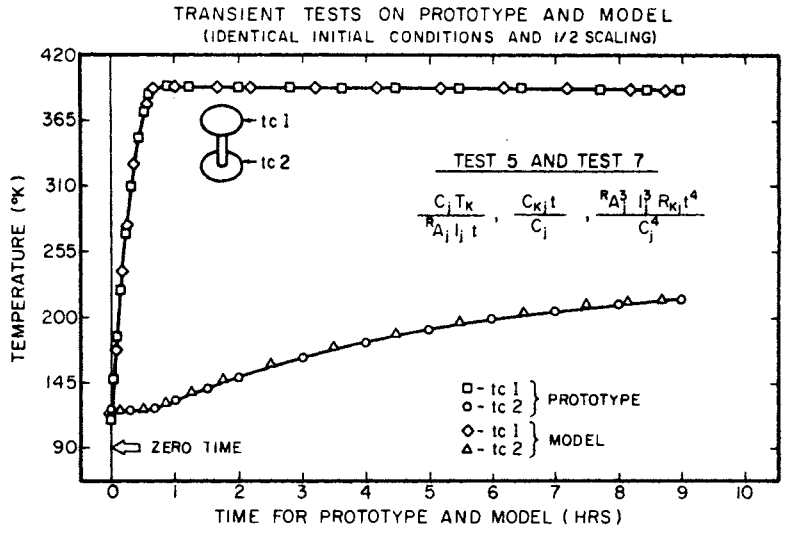

Figure 4. Two Opposed Discs Connected by a Conducting Member (Source: Ref. 15)

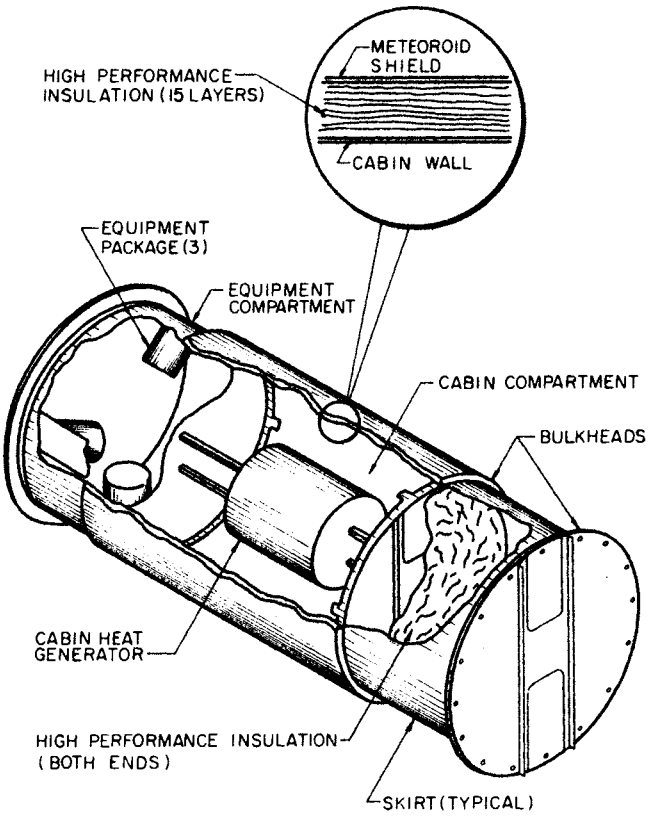

Figure 5. Conceptual Space Station (Source: Ref. 30)

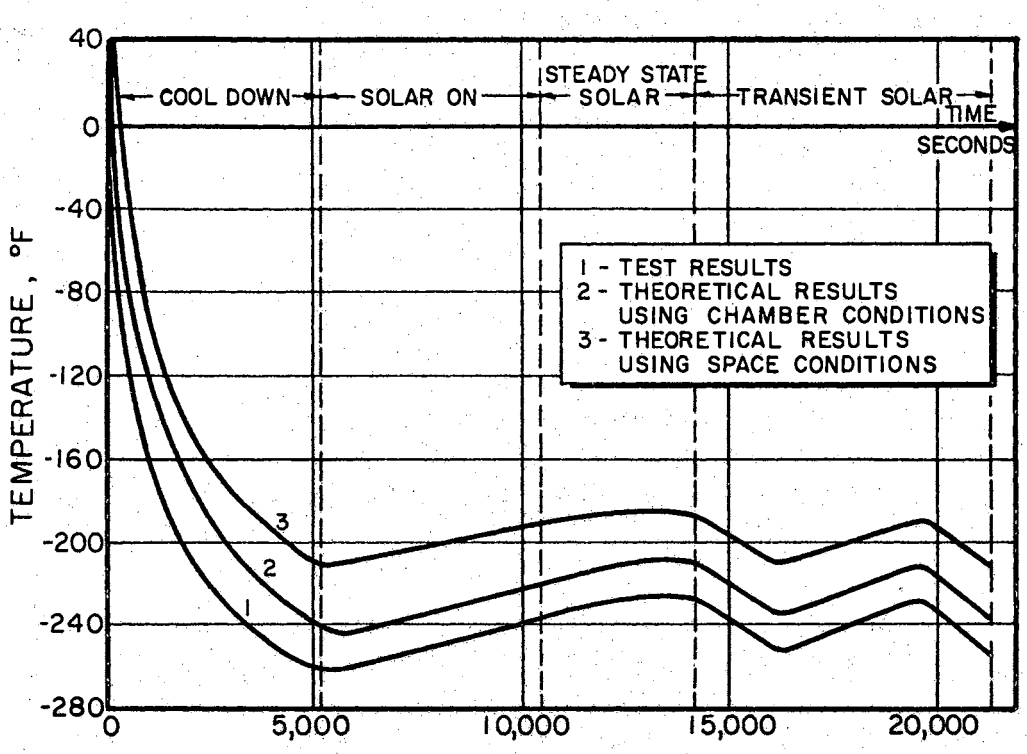

Figure 6. Temperature History of Conceptual Space Station (Source: Ref. 30)

$$\frac{T_j}{T_k}, \frac{R_{kj} T_j^3 \theta}{\overline{C}_j}, \frac{q_j \theta}{\overline{C}_j T_j} \quad (j, k=1, \ldots, n; k \neq j). \tag{2-41}$$

All major external dimensions were scaled by one-half. It was assumed that the materials were not changed from prototype to model, that the radiation geometry factors remain unchanged, that the temperatures of the model at a particular time were equal to the corresponding prototype temperatures at the same time, and that the thickness of the cylinder end caps was not changed from prototype to model. Some results of this experimental investigation are shown in Table II. Thermocouples 1-15 were for the sphere, 16-19 for the cylinder, and 20-25 for the plate. The experimental results generally confirm the

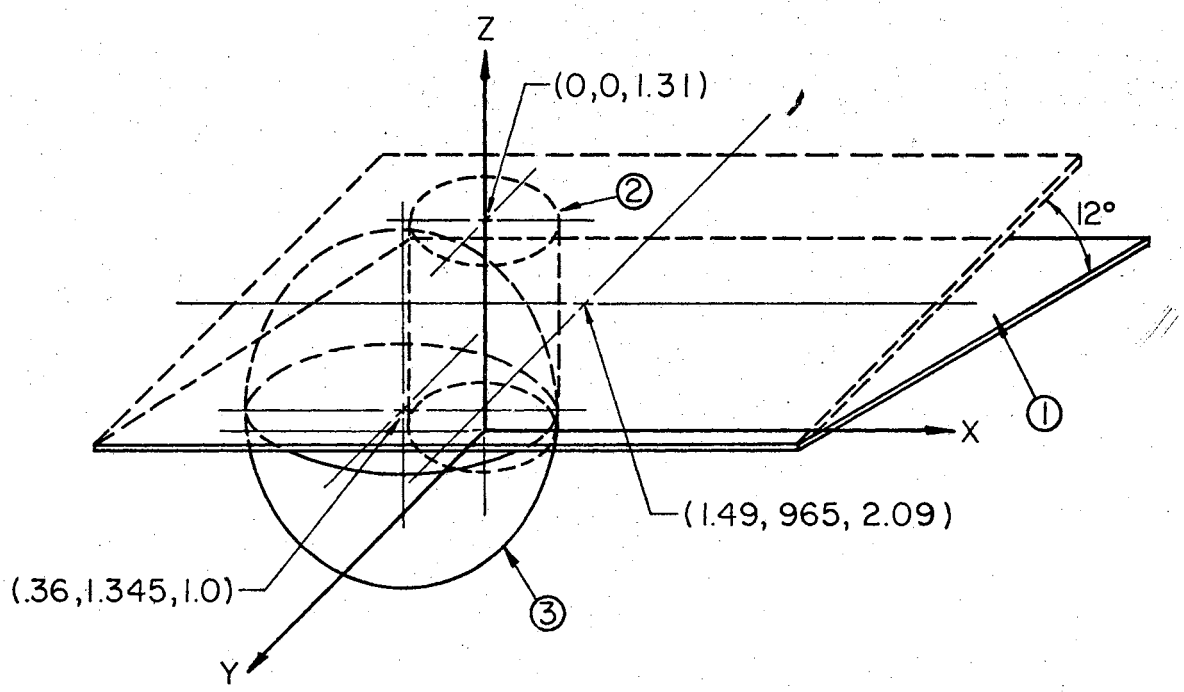

Figure 7. Geometric Arrangement of Plate, Cylinder, and Sphere. Numbers Shown are Based on Outside Dimensions of Sphere's Radius. Co-ordinate System Shown is Centered at Base of Cylinder. (Source: Ref. 31)

modeling rules, with some exceptions in the details, due largely to the assumption made regarding the volume partitioning of the objects being modeled. Adkins [11] has also presented experimental results for the same prototype configuration. These results are shown in Figure 8.

Adkins also applied the modeling criteria given in Reference [11] to a configuration consisting of two hollow spheres connected by a conducting member.

TABLE II

RADIATIVE MODEL EXPERIMENTAL RESULTS

Fraction of Time in Percent Where the Difference Between the Prototype and Model Temperatures of the Individual Thermocouple Measurements are Equal to or Less than 5, 10, 15, 20, and 25 degrees Kelvin. +

Thermocouple Number	5	10	15	20	25
1	59.2	75.5	89.8	95.9	98.0
2	26.5	46.9	63.3	79.6	95.9
3	51.0	79.6	89.8	89.8	93.9
4	55.1	73.5	89.8	93.9	93.9
5	44.9	57.1	69.4	79.6	89.8
6	51.0	65.3	85.7	89.8	91.8
7	51.0	75.5	83.7	85.7	87.8
8	55.1	71.4	85.7	89.8	89.8
10	53.1	67.3	87.8	89.8	91.8
11	42.9	61.2	81.6	89.8	91.8
12	2.0	6.1	10.2	14.3	14.3
13	0.0	2.0	18.4	40.8	44.9
14	38.8	51.0	55.1	57.1	59.2
15	10.2	28.6	59.2	79.6	95.9
16	6.1	36.7	75.5	93.9	100.0
17	4.1	30.6	67.3	81.6	93.9
18	4.1	8.2	32.7	63.3	79.6
19	4.1	10.2	49.0	71.4	81.6
20	32.7	46.9	46.9	46.9	59.2
21	42.9	49.0	53.1	59.2	83.7

+ Detrimental from discrete points in time corresponding to data read-out times. Source: Ref. 31

The different arrangements of this system are shown in Figure 1. Again, geometric distortion in the minor dimensions was permitted. The experimental results obtained from the system are shown in Figure 9.

Rolling [9] and [10] used the ratios in Equation (2-17) to model the two opposed disks with four connecting tubular members as shown in

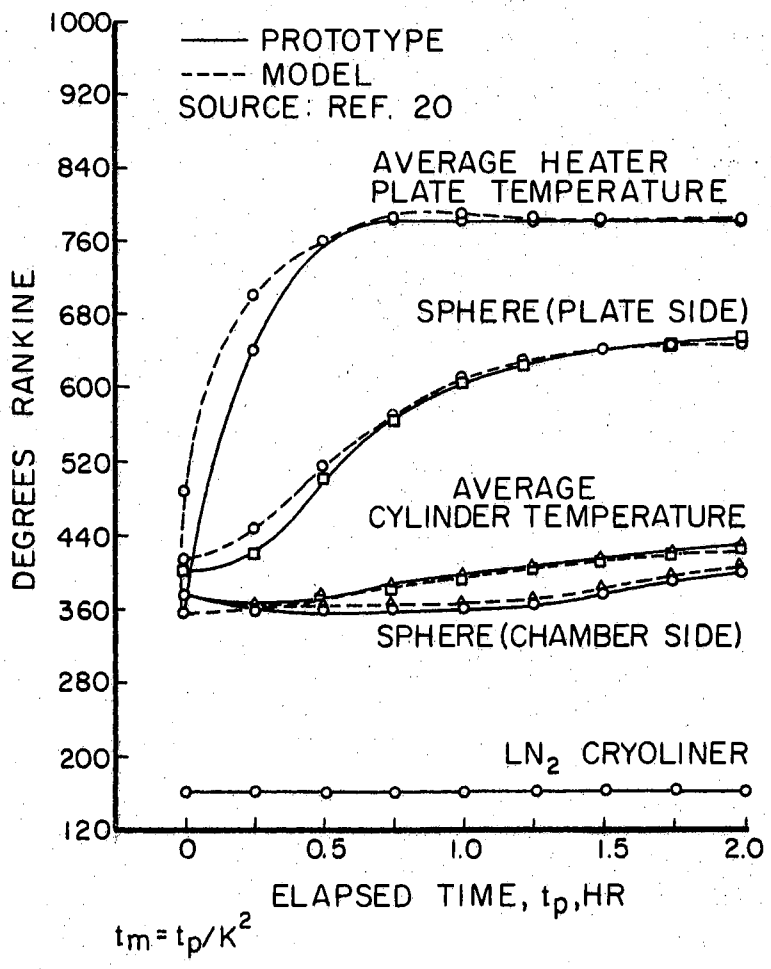

Figure 8. Temperature - Time Characteristics of Configuration A

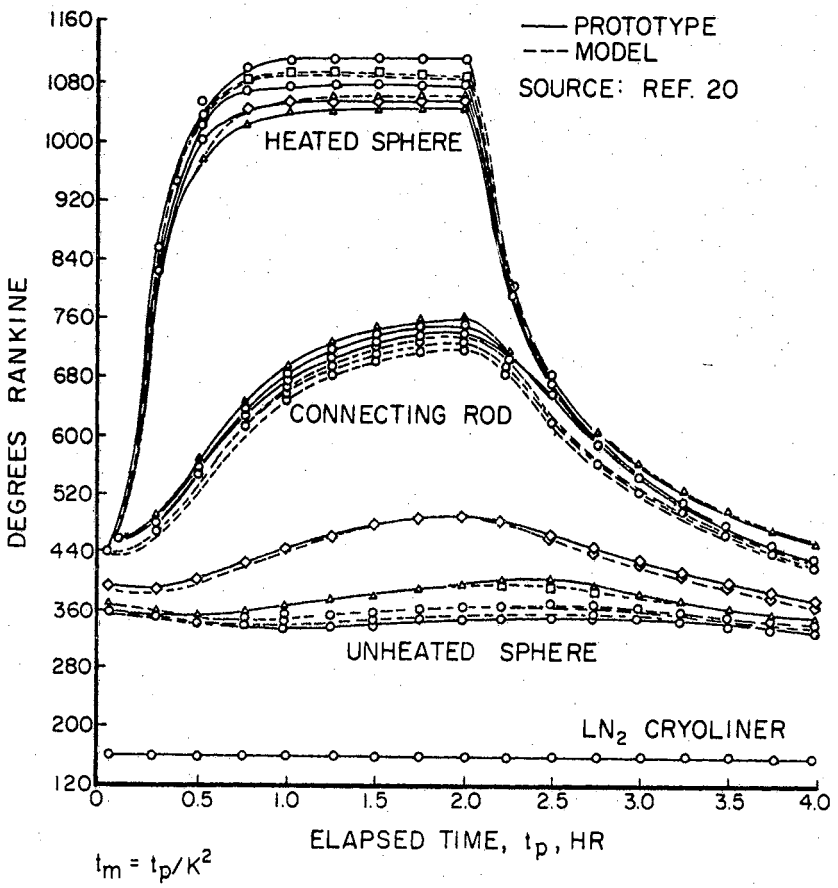

Figure 9. Temperature - Time Characteristics of Configuration B.

Figure 10 and the truncated cones shown in Figure 11. Models of one-half and one-quarter scale based on the exterior dimensions were used for the two systems. Material thermophysical properties were fixed while temperature and time were scaled. Geometric distortion in the minor dimensions was permitted. Arrays of tungsten filament lamps were used for external radiation sources. Some of the results for the opposed connected disks and for the cones are shown in Figure 12 and Figure 13, respectively. The temperatures of the model for the disks were within $9^{\circ}K$ of the prototype, and for the cones all model tempera-

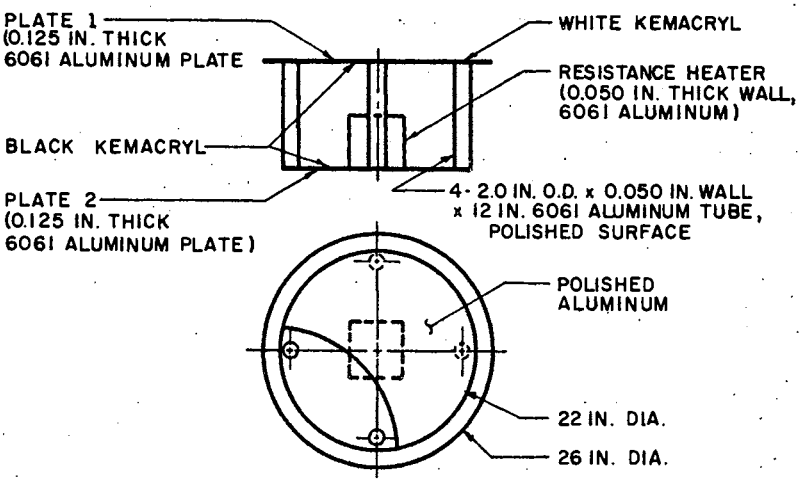

Figure 10. Opposed Disks Geometry (Source: Ref. 9)

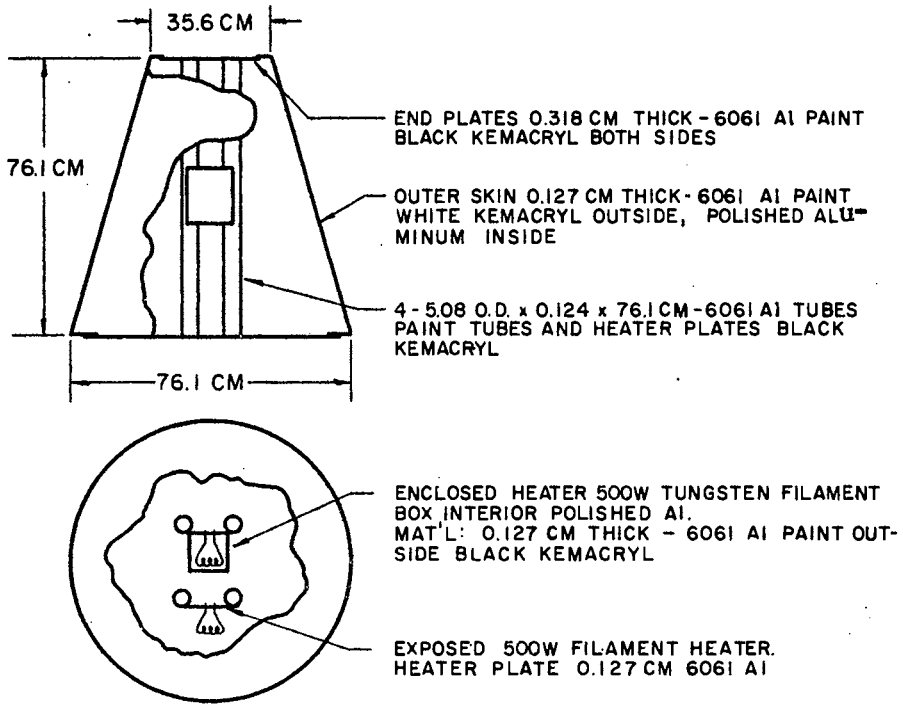

Figure 11. Truncated Cone Geometry (Source: Ref. 10)

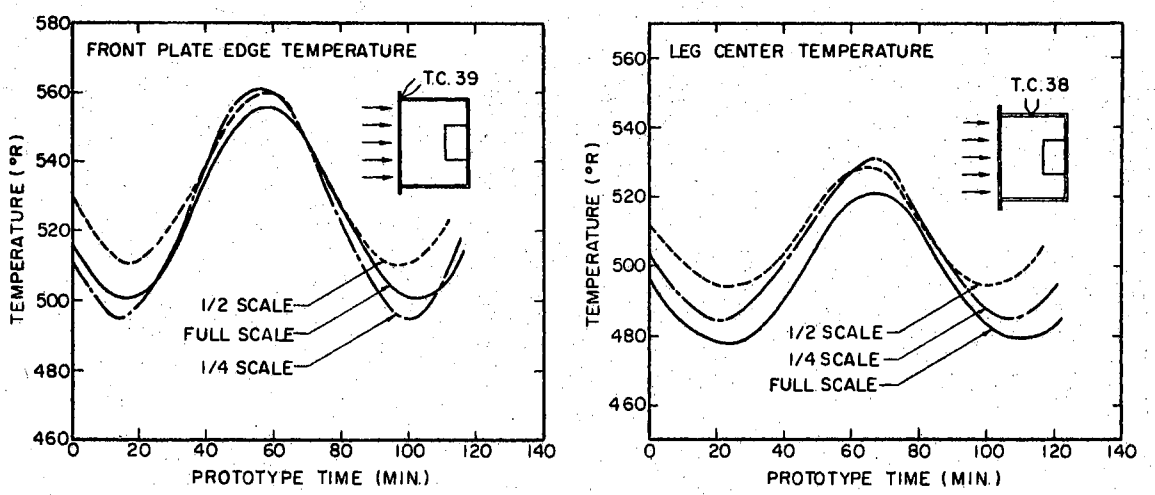

Figure 12. Temperature - Time Characteristics of the Opposed Disks (Source: Ref. 9)

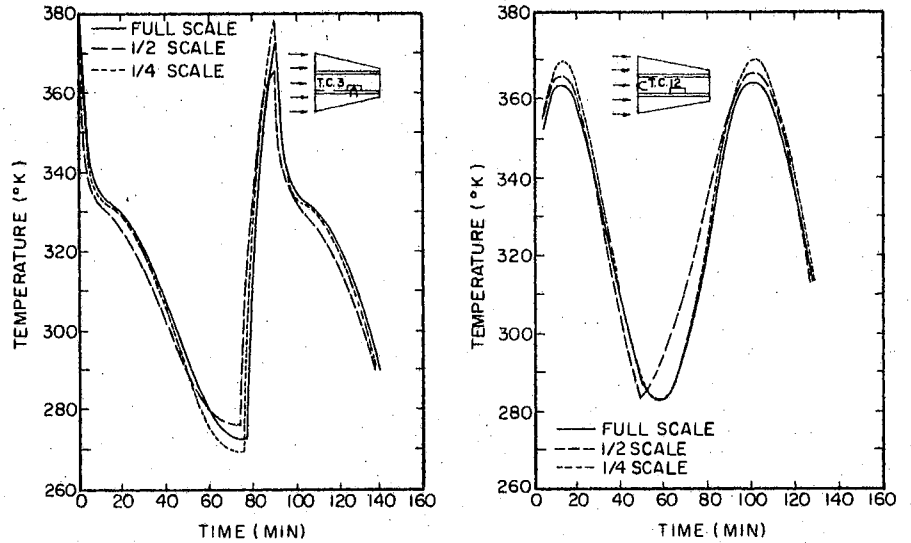

Figure 13. Temperature - Time Characteristics of the Truncated Cones (Source: Ref. 10)

tures were within 8°K of the prototype.

Young and Shanklin [12] applied the ratios below

$$\frac{R^2}{L_z}, \frac{R^2 F_{i-j}}{L_z}, qR^2, \frac{R_r}{R}, \frac{R_r R}{L_z L}, \frac{\theta}{R^2}, \frac{L^2}{R_r}, \text{ and } \frac{L^2 F_{i-j}}{R_r} \qquad (2\text{-}42)$$

to the system shown in Figure 12. This system was composed of three sections: a heater plate containing an electrical resistance heating element which represented an internal energy source of variable strength, a cold-plate having no internal energy source, and a cylindrical rod connecting the two plates. The prototype and the one-half scale model were fabricated of the same material with identical values of ϵ, a, b, and α. The prototype and the model were exposed to identical simulated space conditions and were started at the same initial temperature, T_{io}. Furthermore, the prototype and model surfaces were blackened such that ϵ and α approached unity. The ratios in Equation (2-42) were used in designing the model. Thermal similarity exists when identical temperatures are observed at corresponding locations on the prototype and the model at properly scaled times ($Q = 4Q^*$) for appropriately scaled power inputs ($q = 4q^*$). A large portion of the results of this investigation is presented in Figure 14. Prototype and model temperatures at three thermocouple locations were compared at reduced times for both high and low power test runs. Model temperatures deviated from those of the prototype by an average of approximately 1.5 percent.

Miller [14] applied the ratios in Equation (2-32) for the model design of cylindrical rods. The results from the application of

Equation (2-32) are shown in Table III and Table IV. The prototype and the models were fabricated of the same material with identical values of ϵ, a, b, and α. The prototype and model were started at the same initial temperature and were exposed to the same simulated space conditions. Furthermore, the prototype and model surfaces were blackened such that ϵ and α approached unity. The experimentally obtained temperatures of the prototype and model were consistently less than five degrees Fahrenheit apart. Miller concluded that temperature preservation between model and prototype was a necessity for proper thermal modeling.

Thompson, Klockzien and Dufoe [32] performed experimental investigations on a prototype and scaled models of a simulated spacecraft in a simulated space environment. Three models were designed and constructed according to the temperature-preservation technique. The

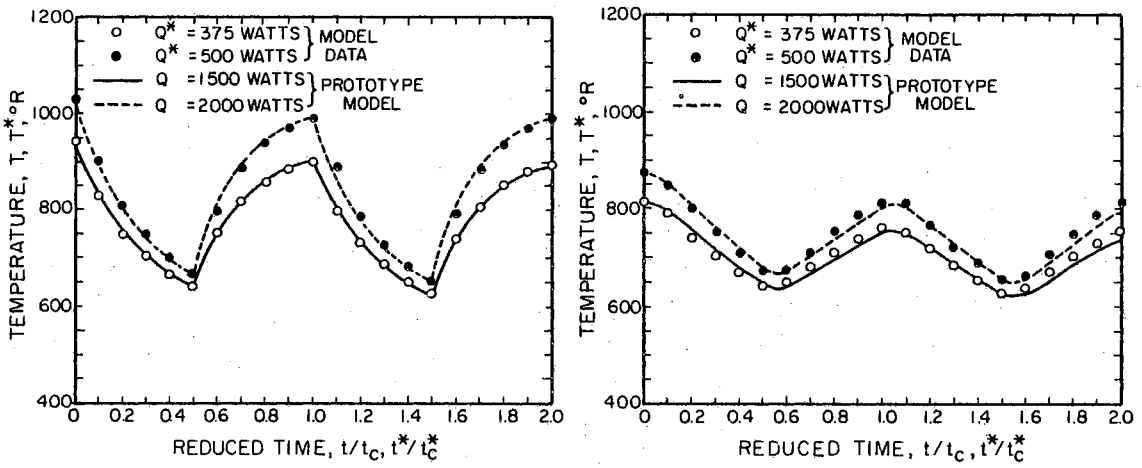

Figure 14. Temperature - Time Characteristics of the System Shown in Figure 2 (Source: Ref. 12)

TABLE III

PROTOTYPE AND MODEL DIMENSIONS, SINGLE MATERIAL

Source: Ref. 14

Model No.	Length L (in.)	Heater Length L_H (in.)	Diameter D (in.)	L*	R*
Proto. 1	17.242	2.25	2.001	-	-
1-1	8.637	1.13	1.001	0.501	0.500
1-2	5.714	0.75	0.661	0.331	0.331
1-3	8.641	1.13	0.498	0.501	0.249
1-4	6.120	0.80	0.249	0.355	0.125

TABLE IV

PROTOTYPE AND MODEL DIMENSIONS, TWO MATERIALS

Source: Ref. 14

Model No.	Al. Length L_{AL} (In.)	Htr. Length L_H (in.)	S.S. Length L_{SS} (in.)	Al.Dia. D (In.)	S.S.Dia D (In.)	L*	R*
Proto. 2	9.750	2.25	7.440	2.002	1.995	-	-
2-1	4.871	1.13	3.735	0.497	0.499	0.501	0.249
2-2	3.456	0.80	2.657	0.252	0.248	0.356	0.125

models consisted of a full-scale prototype, half-scale model, and a 0.285 scale model. The model configuration was designed to investigate the thermal scale-modeling criteria presented in the equation below.

$$\frac{k_m}{k_p} = \frac{L_m}{L_p}, \frac{\theta_m}{\theta_p} = \frac{L_m (\rho C_p)_m}{L_p (\rho C_p)_p}, \frac{\dot{q}_m}{\dot{q}_p} = \frac{L_p}{L_m}, \frac{q_m}{q_p} = \frac{L_m^2}{L_p^2}, \frac{\ddot{q}_m}{\ddot{q}_p} = 1, \frac{C_m}{C_p} = 1. \quad (2\text{-}43)$$

The basic test configuration used by Thompson, Klockzien and Dufoe was a double walled cylinder enclosed at both ends (Figure 15). A thermal analysis of the basic test configuration shown in Figure 15 was performed concurrency with the test program. The purpose of the thermal analysis was twofold: First, to provide a basis for comparison for the experimental results; and second, to provide a means for adjusting the test results from the existing test environment to the expected space environment.

Presented in Figure 16 are transient analytical and test results for two heater power levels of the system shown in Figure 15. Both solar-off and solar-on transient conditions are shown. The data shown are for two thermocouple locations on the outer and inner cylinder that are normal to the simulated solar radiation. The differences in the inner cylinder test results presented in Figure 16 were due primarily to the differences in the initial temperature. This is apparent in that the shapes of the transient curves agree closely. The differences in the test results for the outer cylinder were due primarily to the lower solar intensity of the solar simulation.

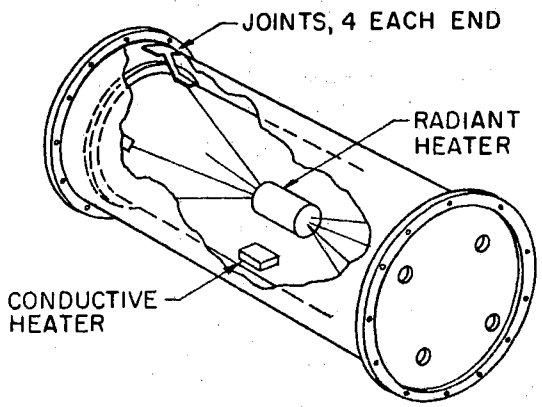

Figure 15. Basic Test Configuration (Source: Ref. 32)

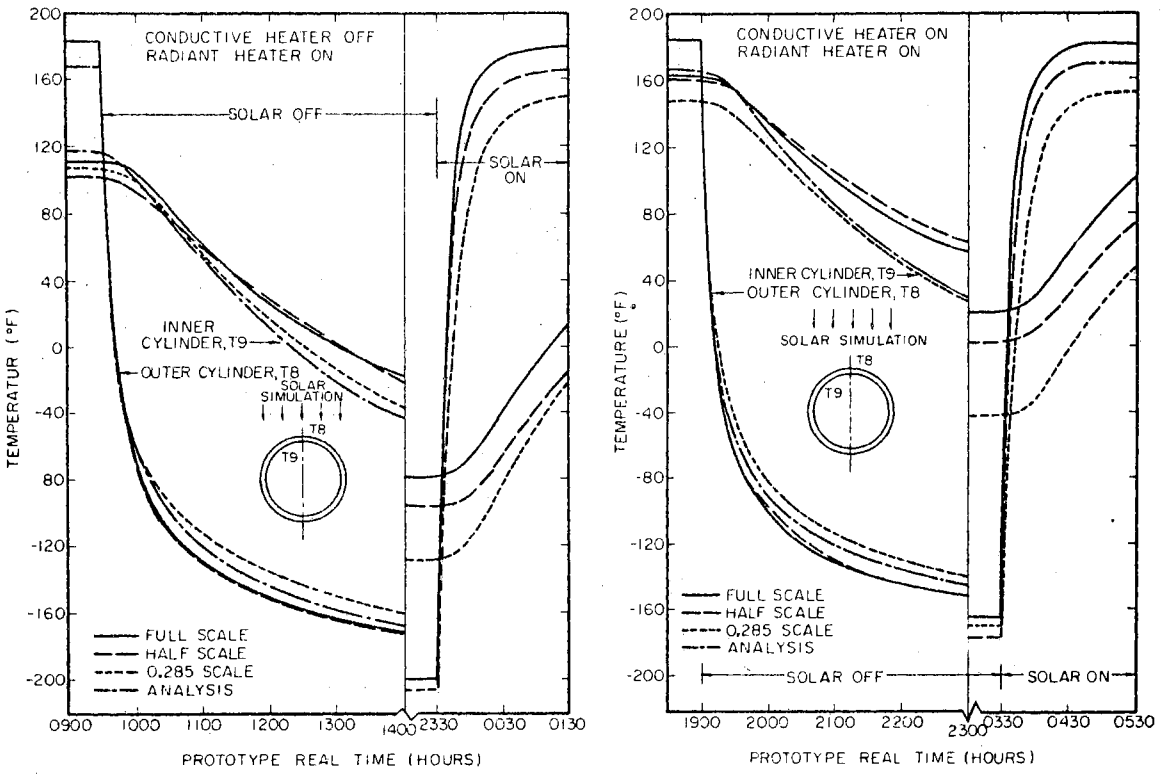

Figure 16. Transient Temperature Histories (Source: Ref. 32)

Summary

Analytical and experimental research in thermal similitude in space-related thermophysics problems is very active. Much progress has been made in confirming the analyses by experiments in both steady-state and transient cases. In the former case, a complicated spacecraft, Mariner IV, has been successfully modeled. However, there has been no attempt to experimentally verify a group of similarity parameters for a system that contains a fluid. The remaining part of this investigation was concerned with the applicability of thermal modeling to steady-state conditions for a system containing a gas.

CHAPTER III

MODELING CRITERIA

Thermal similarity parameters can be identified from either dimensional analysis or from energy balance considerations of the thermal system being investigated. The latter is a method using differential equations and boundary conditions and is perhaps the more attractive technique since the actual physical laws governing the system are used. The results of either approach, however, are clearly only as comprehensive as the number of system parameters considered in the derivation.

General Criteria

The basic modeling criteria for thermal scale modeling of a system were developed using the differential method. This method utilizes the energy equation for the model and the prototype. In order to account for the total heat transfer, the thermal scale modeling criteria for a radiation-conduction-convection coupled heat-transfer system were developed.

In order to develop the modeling criteria utilizing the differential method, the energy equation was written for a differential element. For the ith element, the energy equation is:

$$\rho_i V_i C_{p_i} \frac{\partial T_i}{\partial \theta} = q_i + \sum_{s=1}^{S} \sum_{j=1}^{J} \alpha_{sj} \phi_{js} A_s + \sum_{n=1}^{N} k_n A_n \frac{\partial T_{i-n}}{\partial L_{i-n}}$$

$$- \sum_{s=1}^{S} \epsilon_s \sigma A_s T_i^4 + \sum_{j=1}^{J} A_n C_s (T_i - T_j) + \sum_{j=1}^{J} h_s A_n (T_i - T_j). \quad (3\text{-}1)$$

Equation (3-1) was made dimensionless and applied to the model and prototype separately. In order for point-to-point similarity to exist between the model and the prototype, the following identities were obtained (see Appendix A for development):

$$\frac{\rho^* V^* C_p^* T^*}{\theta^*} = q^* = \alpha_{sj}^* \phi_{js}^* A_s^* = \epsilon_s^* A_s^* T^{*4} = k_n^* A_n^* \left(\frac{T^*}{L^*}\right)_n$$

$$= A_n^* C_s^* T^* = A_n^* h_s^* T^*, \quad (3\text{-}2)$$

where $j=1, 2, \ldots, J$

$n=1, 2, \ldots, N$

and $s=1, 2, \ldots, S$.

The superscript star indicates the quantity is a ratio of model value to prototype value of that quantity at corresponding points. The subscript s refers to a surface of the isothermal region under study. Subscript, j, is an isothermal region radiating or conducting energy to the isothermal element under study, and n denotes the normal to the region and gives the direction of conduction and convection to the isothermal region. The various subscripts for a typical system are illustrated in Figure 17. An algebraic solution of the radiation-conduction-convection coupled heat transfer problem is extremely difficult to obtain even for simple geometric shapes. However, the thermal behavior of a prescribed system may be predicted from an experimental

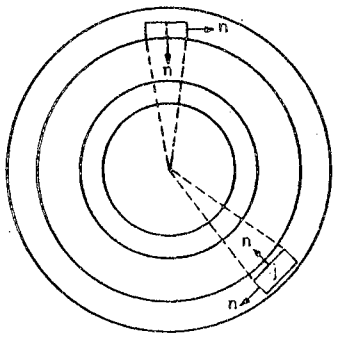

Figure 17. Typical System Showing Elements i and j.

investigation of a small-scale model. The identities in Equations (3-2) serve as the governing similitude criteria for predicting prototype behavior from observed model behavior.

Application of the General Criteria

The thermal behavior of a system may be determined by obtaining the performance of a model, through experimental methods, and then applying the modeling identities in Equations (3-2). In thermal modeling of a system some of the identities may be unimportant and can be neglected. This places certain constraints upon the modeling identities. These constraints will depend upon the particular system to be investigated and the final results will be only as good as the assumed constraints.

The configuration selected to illustrate the modeling criteria was two concentric cylinders. The geometry and notation nomenclature is shown in Figure 18. This was the geometry employed in the experimental

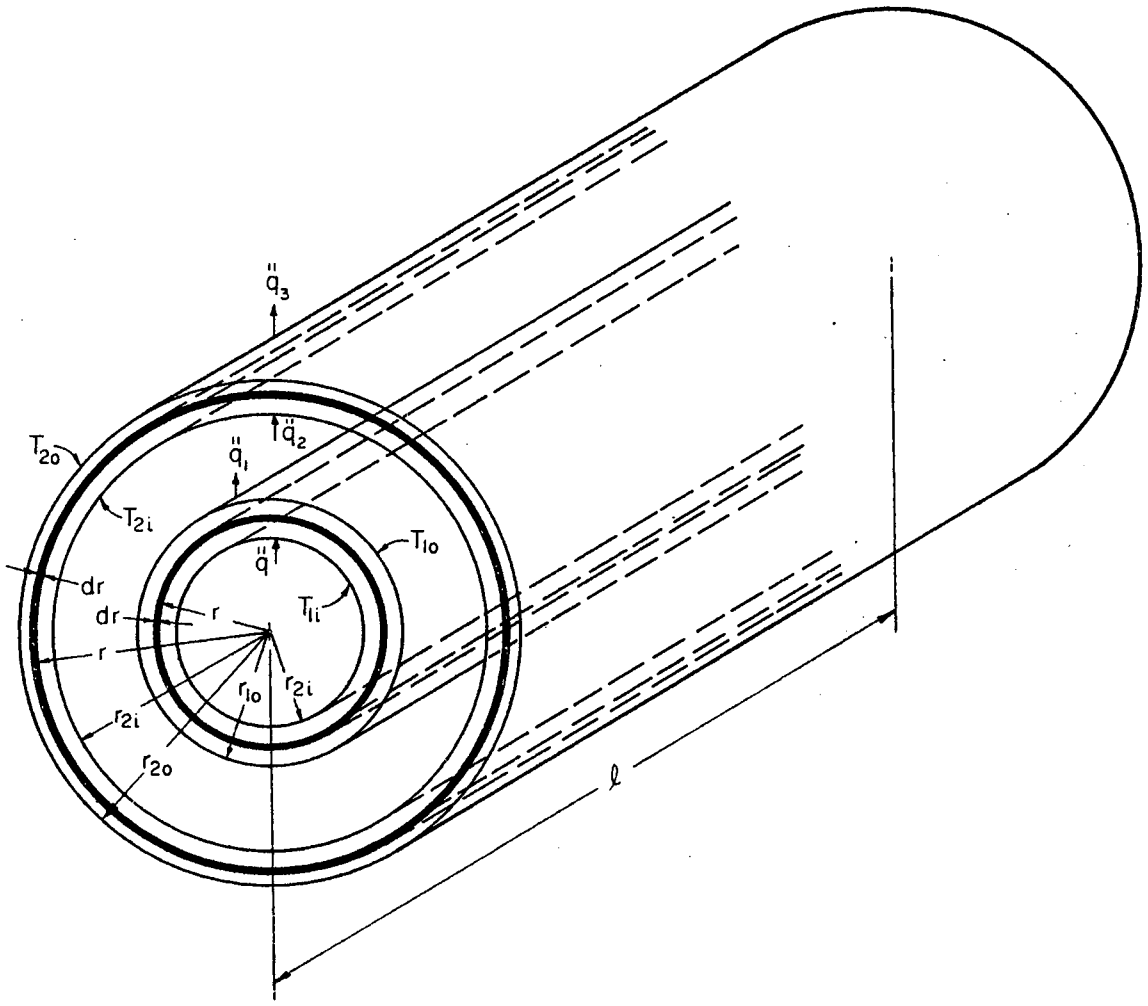

ℓ = LENGTH OF TEST SECTION

$r_{1i} = \frac{D_{1i}}{2}$ = INNER RADIUS OF INNER CYLINDER

$r_{1o} = \frac{D_{1o}}{2}$ = OUTER RADIUS OF INNER CYLINDER

$r_{2i} = \frac{D_{2i}}{2}$ = INNER RADIUS OF OUTER CYLINDER

$r_{2o} = \frac{D_{2o}}{2}$ = OUTER RADIUS OF OUTER CYLINDER

T_{1i} = UNIFORM TEMPERATURE OF THE INTERIOR OF THE INNER CYLINDER

T_{1o} = UNIFORM TEMPERATURE OF THE EXTERIOR OF THE INNER CYLINDER

T_{2i} = UNIFORM TEMPERATURE OF THE INTERIOR OF THE OUTER CYLINDER

T_{2o} = UNIFORM TEMPERATURE OF THE EXTERIOR OF THE OUTER CYLINDER

$\ddot{q}_1 = \ddot{q}_{R1} + \ddot{q}_{C1}$ = UNIFORM HEAT FLUX LEAVING THE EXTERIOR OF THE INNER CYLINDER

$\ddot{q}_2 = \ddot{q}_{R2} + \ddot{q}_{C2}$ = UNIFORM HEAT FLUX ENTERING THE INTERIOR OF THE OUTER CYLINDER

$\ddot{q}_3$ = UNIFORM HEAT FLUX LEAVING THE EXTERIOR OF THE OUTER CYLINDER

Figure 18. Sketch Illustrating the Nomenclature

investigation with the cylinders located in a simulated space environment.

The general modeling criteria were expressed in a more convenient form by equating each of the terms in Equations (3-2) to the conduction term. This yields the following equations:

$$\alpha^*_{sj}\ \phi^*_{js}\ A^*_s = k^*_n\ A^*_n\ \left(\frac{T^*}{L^*}\right)_n , \tag{3-3}$$

$$\epsilon^*_s\ A^*_s\ T^{*4} = k^*_n\ A^*_n\ \left(\frac{T^*}{L^*}\right)_n , \tag{3-4}$$

$$A^*_s\ h^*_s\ T^* = k^*_n\ A^*_n\ \left(\frac{T^*}{L^*}\right)_n , \tag{3-5}$$

$$q^* = k^*_n\ A^*_n\ \left(\frac{T^*}{L^*}\right)_n , \tag{3-6}$$

$$\overset{\circ\circ}{q}{}^* = k^*_n\ \left(\frac{T^*}{L^*}\right)_n , \tag{3-7}$$

$$\overset{\circ\circ\circ}{q}{}^* = \frac{k^*_n}{e^*}\ \left(\frac{T^*}{L^*}\right)_n , \tag{3-8}$$

and

$$\rho^*\ V^*\ C^*_p\ \frac{T^*}{\theta^*} = k^*_n\ A^*_n\ \left(\frac{T^*}{L^*}\right)_n , \tag{3-9}$$

where

$$\phi^*_{js} = \frac{F^*_{js}\ \epsilon^*_s\ T^{*4}_j\ A^*_j}{A^*_s},$$

$$A^*_s = D^*_{20}\ L^*,\ D^*_{2i}\ L^*,\ \text{or}\ D^*_{i0}\ L^*,$$

$$A^*_n = A^*_1,\ \text{or}\ A^*_2,$$

$$A_1^* = \frac{(D_{10} - D_{1i})^* L^*}{\left\{ \ln \frac{D_{10}}{D_{1i}} \right\}^*}, \text{ or } (D_{10}^2 - D_{1i}^2)^*,$$

and

$$A_2^* = \frac{(D_{20} - D_{2i})^* L^*}{\left\{ \ln \frac{D_{20}}{D_{2i}} \right\}^*}, \text{ or } (D_{20}^2 - D_{2i}^2)^*.$$

It should be noted that the ratios presented in Equations (3-2) must be the same for all isothermal regions of the system for point-to-point similarity to exist. Therefore, the ratios applied to an element which has an external surface is the same as the ratios for an internal element of the solid.

The effect of joint interface resistance will be neglected in this analysis since it was not of primary concern. Also, it is possible to design a test section which is free of joints.

The influence of spectral and angular distributions of the emitted and absorbed radiation may be eliminated by controlling the surface properties (emissivity and absorptivity) throughout the system. These properties may be controlled by proper selection of a material to coat the surfaces. Thus, this constraint requires that the emissivity and absorptivity of all surfaces throughout the model and prototype be constant and independent of temperature.

If the radiant flux ϕ_{js} from the surroundings to the system is the same for model and prototype, then ϕ_{js}^* is unity (referred to hereafter as "Technique I"). This may be accomplished by controlling the properties of the surroundings. In a simulated space environment, the

radiant flux from the surroundings is very low if solar energy is not simulated. This is due to the fact that the temperature is very low. Thus, for this case, the radiant flux ϕ_{js} will be considered zero (referred to hereafter as "Zero Surroundings Technique"). These two techniques will be discussed in the following sections.

Technique I

Technique I was limited to those situations where the radiant flux from the surroundings to the system was the same for both model and prototype. Thus,

$$\phi^*_{js} = 1.$$

Since the emissivity and absorptivity of all surfaces throughout the model and prototype were constant, the ratios of these properties must be constant. That is,

$$\alpha^*_{sj} = \epsilon^*_s = 1.$$

If Equations (3-3) through (3-9) are applied to the system shown in Figure 18 and the conditions listed above are considered, the following equations are obtained. These equations are:

for outside surface of outer cylinder, A_{20}

$$A^*_{20} = \left\{ k^*_n \, A^*_n \, \frac{T^*}{L^*} \right\}_2 , \qquad (3\text{-}10)$$

and

$$A^*_{20}\ T^{*4}_{20} = \left\{k^*_n\ A^*_n \frac{T^*}{L^*}\right\}_2 , \tag{3-11}$$

for inside surface of outer cylinder, A_{2i}

$$F^*_{10\rightarrow 2i}\ T^{*4}_{10}\ A^*_{10} = \left\{k^*_n\ A^*_n \frac{T^*}{L^*}\right\}_2 , \tag{3-12}$$

$$A^*_{2i}\ T^{*4}_{2i} = \left\{k^*_n\ A^*_n \frac{T^*}{L^*}\right\}_2 , \tag{3-13}$$

and

$$A^*_{2i}\ h^*_{2i}\ T^*_{2i} = \left\{k^*_n\ A^*_n \frac{T^*}{L^*}\right\}_2 , \tag{3-14}$$

for outside surface of inner cylinder, A_{10}

$$F^*_{2i\rightarrow 10}\ T^{*4}_{2i}\ A^*_{2i} = \left\{k^*_n\ A^*_n \frac{T^*}{L^*}\right\}_1 , \tag{3-15}$$

$$A^*_{10}\ T^{*4}_{10} = \left\{k^*_n\ A^*_n \frac{T^*}{L^*}\right\}_1 , \tag{3-16}$$

and

$$A^*_{10}\ h^*_{10}\ T^*_{10} = \left\{k^*_n\ A^*_n \frac{T^*}{L^*}\right\}_1 , \tag{3-17}$$

for the inner cylinder, 1

$$q^*_1 = \left\{k^*_n\ A^*_n \frac{T^*}{L^*}\right\}_1 , \tag{3-18}$$

$$\dot{q}_1^* = \left\{ k_n^* \frac{T^*}{L^*} \right\}_1 , \tag{3-19}$$

$$\ddot{q}_1^* = \left\{ k_n^* \frac{T^*}{L^* L^*} \right\}_1 , \tag{3-20}$$

and

$$\left\{ \rho^* V^* C_p^* \frac{T^*}{\theta^*} \right\}_1 = \left\{ k_n^* A_n^* \frac{T^*}{L^*} \right\}_1 , \tag{3-21}$$

for the outer cylinder, 2

$$q_2^* = \left\{ k_n^* A_n^* \frac{T^*}{L^*} \right\}_2 , \tag{3-22}$$

$$\dot{q}_2^* = \left\{ k_n^* \frac{T^*}{L^*} \right\}_2 , \tag{3-23}$$

$$\ddot{q}_2^* = \left\{ k_n^* \frac{T^*}{L^* L^*} \right\}_2 , \tag{3-24}$$

and

$$\left\{ \rho^* V^* C_p^* \frac{T^*}{\theta^*} \right\}_2 = \left\{ k_n^* A_n^* \frac{T^*}{L^*} \right\}_2 . \tag{3-25}$$

If Equation (3-10) is substituted into Equation (3-11), the resulting equation is

$$T_{20}^* = 1. \tag{3-26}$$

For exact geometric similitude (equal scaling in all directions) between the model and prototype, Equation (3-10) can be expressed as

$$\left\{\frac{T^*}{L^*}\right\}_2 = \left\{\frac{1}{k_n^*}\right\}_2 . \tag{3-27}$$

Substituting Equation (3-27) into Equations (3-12), (3-13), (3-14), (3-22), (3-23), (3-24), and (3-25) yields the following equations:

$$T_{10}^* = 1, \tag{3-28}$$

$$T_{2i}^* = 1, \tag{3-29}$$

$$h_{2i}^* = \frac{1}{T_{2i}^*} = 1, \tag{3-30}$$

$$q_2^* = (A_n^*)_2 = A_{20}^* = L^{*2}, \tag{3-31}$$

$$\dot{q}_2^* = 1, \tag{3-32}$$

$$\dddot{q}_2^* = \frac{1}{L^*}, \tag{3-33}$$

and

$$\theta_2^* = L^* C_{p_2}^* \rho_2^* , \tag{3-34}$$

where the initial time is defined as zero.

If Equation (3-28) is substituted into Equation (3-16), the resulting equation is

$$\left\{\frac{T^*}{L^*}\right\}_1 = \left\{\frac{1}{k_n^*}\right\}_1 . \tag{3-35}$$

Substituting Equation (3-35) into Equations (3-17), (3-18), (3-19),

(3-20), and (3-21) yields the following equations:

$$h_{10}^{*} = 1, \tag{3-36}$$

$$q_1^{*} = (A_n^{*})_1 = A_{10}^{*} = L^{*2}, \tag{3-37}$$

$$\mathring{q}_1^{*} = 1, \tag{3-38}$$

$$\dddot{q}_1^{*} = \frac{1}{L^{*}}, \tag{3-39}$$

and

$$\theta_1^{*} = L^{*}\, C_{p_1}^{*}\, \rho_1^{*}. \tag{3-40}$$

Equations (3-26), (3-28) through (3-34), and (3-36) through (3-40) may be reduced to the following equations:

$$T_{20}^{*} = T_{10}^{*} = T_{2i}^{*} = h_{2i}^{*} = h_{10}^{*} = \mathring{q}_2^{*} = \mathring{q}_1^{*} = 1, \tag{3-41}$$

$$q_2^{*} = q_1^{*} = L^{*2}, \tag{3-42}$$

$$\dddot{q}_2^{*} = \dddot{q}_1^{*} = \frac{1}{L^{*}}, \tag{3-43}$$

$$\theta_1^{*} = L^{*}\, C_{p_1}^{*}\, \rho_1^{*}, \tag{3-44}$$

and

$$\theta_2^{*} = L^{*}\, C_{p_2}^{*}\, \rho_2^{*}. \tag{3-45}$$

Equations (3-41) through (3-45) must be satisfied at corresponding locations on the model and prototype if thermal modeling of a system,

under the conditions of Technique I, is to be accomplished.

Zero Surroundings Technique

The radiant flux from a simulated space environment is approximately zero. Under this condition together with the conditions imposed in the development of the modeling equations for Technique I ($\alpha^*_{sj} = \epsilon^*_s = 1$, and geometric similarity between model and prototype), Equations (3-11) through (3-25) yield the following equations:

$$T^*_{20} = T^*_{21} = \left\{\frac{k^*_2}{L^*}\right\}^{\frac{1}{3}}, \tag{3-46}$$

$$T^*_{10} = \left\{\frac{k^*_1}{L^*}\right\}^{\frac{1}{3}}, \tag{3-47}$$

$$h^*_{2i} = \frac{k^*_2}{L^*}, \tag{3-48}$$

$$h^*_{10} = \frac{k^*_1}{L^*}, \tag{3-49}$$

$$q^*_2 = (k^*_2)^{\frac{4}{3}} (L^*)^{\frac{2}{3}}, \tag{3-50}$$

$$q^*_1 = (k^*_1)^{\frac{4}{3}} (L^*)^{\frac{2}{3}}, \tag{3-51}$$

$$\ddot{q}^*_2 = \left(\frac{k^*_2}{L^*}\right)^{\frac{4}{3}} \tag{3-52}$$

$$q_1^* = \left(\frac{k_1^*}{L^*}\right)^{\frac{4}{3}}, \tag{3-53}$$

$$\overset{\circ\circ}{q}{}_2^* = (k_2^*)^{\frac{4}{3}} \left(\frac{1}{L^*}\right)^{\frac{7}{3}}, \tag{3-54}$$

$$\overset{\circ\circ\circ}{q}{}_1^* = (k_1^*)^{\frac{4}{3}} \left(\frac{1}{L^*}\right)^{\frac{7}{3}}, \tag{3-55}$$

$$\theta_1^* = \frac{\rho_1^* L^{*2} C_{p_1}^*}{k_1^*} \tag{3-56}$$

and

$$\theta_2^* = \frac{\rho_2^* L^{*2} C_{p_2}^*}{k_2^*}. \tag{3-57}$$

In the above equations the directional variation of thermal conductivity was neglected.

Variable Specific Heat and Thermal Conductivity

The specific heat and thermal conductivity of the solid parts of a system was a function of temperature. Chao [8] suggested the use of a power law to describe the property variation over a specified range of temperatures. These relations are

$$k = k_o T^a,$$

and

$$C_p = C_{p_o} T^b,$$

where the temperature is in degrees Rankine. If the above expression for the specific heat is substituted into Equation (3-44) or (3-45), the following equation is obtained for the dimensionless time variable in Technique I:

$$\theta^* = \frac{\theta_m}{\theta_p} = L^* C_{p_o}^* \rho^* \frac{(T^b)_m}{(T^b)_p} . \tag{3-58}$$

For the Zero Surroundings Technique, the expressions for the specific heat and thermal conductivity were substituted into Equations (3-46), (3-48), (3-50), (3-52), (3-54), and (3-56) and the following equations were obtained:

$$T^* = \left\{ \frac{k_o^*}{L^*} \frac{(T^a)_m}{(T^a)_p} \right\}^{\frac{1}{3}} , \tag{3-59}$$

$$h^* = \frac{K_o^*}{L^*} \frac{(T^a)_m}{(T^a)_p} , \tag{3-60}$$

$$q^* = (L^*)^{\frac{3}{2}} \left\{ k_o^* \frac{(T^a)_m}{(T^a)_p} \right\}^{\frac{4}{3}} , \tag{3-61}$$

$$\dot{q}^* = \left\{ \frac{k_o^*}{L^*} \frac{(T^a)_m}{(T^a)_p} \right\}^{\frac{4}{3}} , \tag{3-62}$$

$$\dot{q}^* = \left\{ k_o^* \frac{(T^a)_m}{(T^a)_p} \right\}^{\frac{4}{3}} \left(\frac{1}{L^*}\right)^{\frac{7}{3}} , \tag{3-63}$$

and

$$\theta^* = \rho^* (L^*)^2 \frac{c_{p_o}^*}{k_o^*} \frac{(T^b)_m}{(T^b)_p} \frac{(T^a)_p}{(T^a)_m} . \tag{3-64}$$

A basic requirement for similarity between the model and prototype was that the dimensionless ratios of properties remain constant throughout the two systems for all thermal levels. Equations (3-58) through (3-64) indicate that dimensionless ratios of properties remain constant only for the case where $b_m = b_p$ and $a_m = a_p$. If these conditions are not met, strict similarity will not be obtained. Equal exponents were obtained by selecting the same material for both model and prototype. The material preservation requirement reduces Equations (3-58) through (3-64) to the following:

For Technique I

$$\theta^* = L^* \tag{3-65}$$

and for the Zero Surroundings Technique,

$$T^* = \left\{ \frac{1}{L^*} \right\}^{\frac{1}{3-a}} , \tag{3-66}$$

$$q^* = \left\{ L^{*2(1-a)} \right\}^{\frac{1}{3-a}} , \tag{3-67}$$

$$\overset{\circ}{q}{}^* = \left\{ \frac{1}{L^{*4}} \right\}^{\frac{1}{3-a}} , \tag{3-68}$$

$$\overset{\circ\circ}{q}{}^* = \left\{ \frac{1}{L^{*7-a}} \right\}^{\frac{1}{3-a}} , \tag{3-69}$$

$$\theta^* = \left\{ \frac{L^{*6-a}}{L^{*b}} \right\}^{\frac{1}{3-a}} , \tag{3-70}$$

and

$$h^* = \left\{ \frac{1}{L^{*3}} \right\}^{\frac{1}{3-a}} . \tag{3-71}$$

A summary of the modeling criteria for Technique I and the Zero Surroundings Technique is shown in Table V. For Technique I and the Zero Surroundings Technique with constant thermal properties, the modeling criteria is only a function of the geometric scaling factor. For the Zero Surroundings Technique with variable thermal properties, the modeling criteria is a function of the geometric scaling factor and the constants a and b.

Discussion of Assumptions

Several assumptions were made in order to reduce the modeling criteria given in Equation (3-2) to a usable form. For Technique I, the assumptions were:

1. The emissivity and absorptivity of all surfaces throughout the model and prototype were constant.
2. The radiant flux ϕ_{js} from the surroundings to the system was the same for both model and prototype.
3. The thermal properties of the solid parts (specific heat and thermal conductivity) were constant or varied with temperature according to a power law.
4. Exact geometric similitude.

For the Zero Surroundings Technique, the assumptions were the same as

TABLE V

MODELING CRITERIA FOR TECHNIQUE I AND ZERO SURROUNDINGS TECHNIQUE

Variables	Technique I	Zero Surroundings Technique	
	Constant or Variable, k	Constant, k	Variable, k
D^*	L^{*2}	L^{*2}	L^{*2}
T^*	1	$(1/L^*)^{1/3}$	$(1/L^*)^{\frac{1}{3-a}}$
h^*	1	$1/L^*$	$(1/L^{*3})^{\frac{1}{3-a}}$
θ^*	L^*	L^{*2}	$(\frac{L^{*6-a}}{L^{*b}})^{\frac{1}{3-a}}$
$\dddot{q}^*$	$1/L^*$	$(1/L^*)^{7/3}$	$(\frac{1}{*7-a})^{\frac{1}{3-a}}$
$\ddot{q}^*$	1	$(1/L^*)^{4/3}$	$(1/L^{*4})^{\frac{1}{3-a}}$
q^*	L^{*2}	$(L^*)^{2/3}$	$(L^{*2-2a})^{\frac{1}{3-a}}$

those of Technique I with the exception of the second assumption listed above. In this assumption the energy absorbed by the model and prototype from the surroundings was neglected. This can be obtained if the temperature of the surroundings approaches absolute zero. Several previous investigators have made this assumption [6], [9], [14], [20], and [26].

The first assumption may be satisfied by coating all surfaces throughout the model and prototype with a material which has uniform radiant properties. These surfaces were coated with flat black paint. Flat black paint (velvet coating 101-C10) is a product of Minnesota Mining and Manufacturing Company, and has been shown to have high and uniform values of emittance and absorptance [26].

The radiant flux ϕ_{js} from the surroundings to the system may be controlled by fixing the properties of the surroundings and those of the system where it is visible to the surroundings. In order for the incident flux on the model and prototype to be the same, the following expression must be satisfied:

$$\left\{\frac{F_{js}\ \epsilon_j\ \sigma\ T_j^{\,4}\ A_j}{A_s}\right\}_p = \left\{\frac{F_{js}\ \epsilon_j\ \sigma\ T_j^{\,4}\ A_j}{A_s}\right\}_m . \qquad (3\text{-}72)$$

If the properties ϵ_j, T_j, and A_j of the surroundings are fixed, Equation (3-72) will be satisfied if

$$[F_{js}]_p = \frac{(A_s)_p}{(A_s)_m}\,[F_{js}]_m .$$

For exact geometric similarity and a scaling factor of one-half between prototype and model

$$[F_{js}]_p = 4\,[F_{js}]_m \,.$$

In order to investigate experimentally the incident flux on a model and its geometrically similar prototype, the surroundings were specified. The surroundings consisted of a cylindrical container and the systems were centrally located within the container, then for the concentric cylinder systems considered in the experimental investigation

$$[F_{js}]_p = 4.01\,[F_{js}]_m \,.$$

Thus, the magnitude of the incident flux from the surroundings, for the model and prototype, will differ by less than one-half of one percent.

The thermal conductivity and specific heat of the solid components of a system are functions of temperature. In modeling, the variation in thermal properties may be controlled, to a certain degree, by selecting the same material for model and prototype. For certain materials the thermal property variations with temperature are small. A discussion of the error introduced by thermal property variations in the solid components of the systems used in this investigation can be found in Appendix G. It was concluded that for engineering applications the variations in thermal properties may be neglected in this investigation.

As stated earlier, the only method available for checking the validity of the developed modeling criteria is through experimentation. The systems designed for checking the modeling criteria are shown in Figures 36 through 41. They were scaled such that $D^* = e^*$ which satisfies both techniques listed in Table V.

Similarity in Natural Convection Heat Transfer in the Annulus Between Horizontal Concentric Cylinders

The fluid contained in the annulus between concentric cylinders, with a horizontal axis, will be in motion if a temperature difference exists between the two cylinders. The heat transfer associated with this motion is natural convection. In order to establish similarity in natural convection, the equations of motion, continuity, and energy will be examined. This analysis will be restricted to laminar flow, which will exist for Grashof numbers, Gr_δ, less than 10^7 [36]. Assumptions considered in formulating the equations of motion, continuity, and energy for the system shown in Figure 19 were; steady-flow, nondissipa-

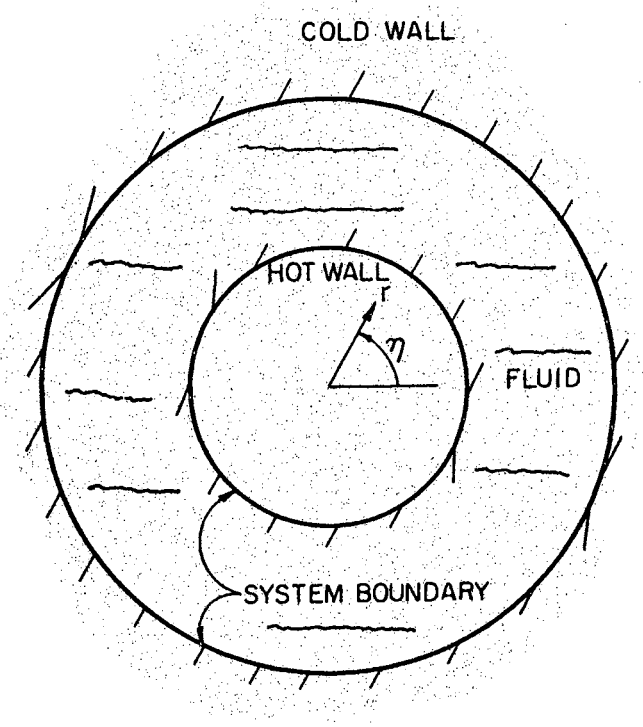

Figure 19. The End View of a Long Horizontal Cylindrical Annulus

tive processes, axisymmetric, and density was dependent only on temperature and that otherwise the fluid is incompressible.

With these assumptions the continuity equation in cylindrical coordinates, (r, η), is

$$\frac{\partial V_r}{\partial r} + \frac{V_r}{r} + \frac{1}{r}\frac{\partial V_\eta}{\partial \eta} = 0. \tag{3-73}$$

This equation may be satisfied by a stream function, $\psi(r, \eta)$, which is defined for subsequent use as

$$V_r = \frac{1}{r}\frac{\partial \psi}{\partial \eta}, \qquad V_\eta = -\frac{\partial \psi}{\partial r}. \tag{3-74}$$

The equations of motion in cylindrical coordinates are:

r-Component

$$\frac{DV_r}{Dt} - \frac{V_\eta^2}{r} = -\frac{1}{\rho}\frac{\partial p}{\partial r} + \nu\left(\nabla^2 V_r - \frac{2}{r^2}\frac{\partial V_\eta}{\partial \eta} - \frac{V_r}{r^2}\right) + g\,\beta\,T\sin\eta; \tag{3-75}$$

η-Component

$$\frac{DV_\eta}{Dt} + \frac{V_r V_\eta}{r} = -\frac{1}{\rho r}\frac{\partial p}{\partial \eta} + \nu\left(\nabla^2 V_\eta + \frac{2}{r^2}\frac{\partial V_r}{\partial \eta} - \frac{V_\eta}{r^2}\right) + g\,\beta\,T\cos\eta; \tag{3-76}$$

where the operators D/Dt and ∇^2 are given by

$$\frac{D}{Dt} = V_r\frac{\partial}{\partial r} + \frac{V_\eta}{r}\frac{\partial}{\partial \eta} = \frac{1}{r}\left(\frac{\partial \psi}{\partial \eta}\frac{\partial}{\partial r} - \frac{\partial \psi}{\partial r}\frac{\partial}{\partial \eta}\right) \tag{3-77}$$

and

$$\nabla^2 = \frac{\partial^2}{\partial r^2} + \frac{1}{r}\frac{\partial}{\partial r} + \frac{1}{r^2}\frac{\partial^2}{\partial \eta^2} \quad , \tag{3-78}$$

respectively.

For negligible frictional and compressional heating the energy equation in cylindrical coordinates is

$$\frac{1}{r}\frac{\partial(T,\psi)}{\partial(r,\eta)} = \frac{k}{\rho\, c_p}\nabla^2 T \quad , \tag{3-79}$$

where $\partial(T,\psi)/\partial(r,\eta)$ is the Jacobian. The boundary conditions are that the velocity is zero both at the surfaces and at a distance far removed from the surfaces.

By substituting Equation (3-74) into Equations (3-75) and (3-76) and eliminating the pressure by cross-differentiation, an equation for the stream function may be obtained. This equation is

$$\frac{1}{r}\frac{\partial(\nabla^2\psi,\psi)}{\partial(r,\eta)} = g\,\beta\left(\frac{\sin\eta}{r}\frac{\partial T}{\partial \eta} - \cos\eta\frac{\partial T}{\partial r}\right) + \nu\nabla^4\psi \,. \tag{3-80}$$

The problem now is to determine the conditions for which the velocity field in one free-convection system is similar to the velocity field in another. Similarity of velocity fields for different systems exists when Equation (3-80) written in dimensionless form is the same for model and prototype. The variables used to nondimensionalize Equation (3-80) are defined as follows:

$$\bar{r} = r/R_i \;;\; \bar{\psi} = \psi/RV;\; \bar{T}_w = (T-T_w)/(T_R-T_w). \tag{3-81}$$

Equation (3-80) in dimensionless form is

$$\frac{1}{\bar{r}} \frac{\partial(\nabla^2\bar{\psi},\bar{\psi})}{\partial(\bar{r},\eta)} = \frac{Gr}{2R_e^2}\left\{\frac{\sin\eta}{\bar{r}}\frac{\partial\bar{T}}{\partial\eta} - \cos\eta\frac{\partial\bar{T}}{\partial\bar{r}}\right\} + \frac{2}{Re}\nabla^4\bar{\psi}. \qquad (3\text{-}82)$$

Dynamic similarity between two geometric similar systems, A and B, exists if

$$\frac{(Gr/R_e^2)_A}{(Gr/R_e^2)_B} = \frac{(1/Re)_A}{(1/Re)_B} = 1, \qquad (3\text{-}83)$$

where $Gr = \frac{(2R_i)^3 g\beta}{\mu^2}(T_R - T_*)$, and $Re = \frac{2R_i V}{\nu}$. Equation (3-83) was obtained by comparing Equation (3-84) for the two systems. By combining the first and third terms of Equation (3-83) the result is

$$\left(\frac{Gr}{R_e^2}\right)_A = \left(\frac{Gr}{R_e^2}\right)_B . \qquad (3\text{-}84)$$

Combining the second and the third terms of Equation (3-83) the following expression is obtained

$$(Re)_A = (Re)_B . \qquad (3\text{-}85)$$

From the physical aspects of the problem the velocity of the fluid is not an independent quantity, but depends upon the buoyant driving force. Hence, v, can be eliminated from Equation (3-84) by substituting its value from Equation (3-85). The resulting expression is

$$(Gr)_A = (Gr)_B . \qquad (3\text{-}86)$$

The dimensionless modulus, $\frac{(2R_i)^3 g\beta}{\nu^2}(T_R - T_*)$, is called the Grashof number, Gr, and represents the ratio of buoyant to viscous forces.

When the buoyancy is the only driving force, the fluid velocity is determined entirely by the quantities contained in the Grashof modulus. Therefore, the Reynolds number, Re, is superfluous for free convection, and equality of the Grashof numbers establishes dynamic similarity.

The conditions for similarity of temperature fields in free-convection were obtained by writing Equation (3-79) in dimensionless form as

$$\frac{1}{\bar{r}} \frac{\partial(\bar{T}, \bar{\Psi})}{\partial(\bar{r}, \eta)} = \frac{2}{P_r R_e} \nabla^2 \bar{T} , \qquad (3\text{-}87)$$

where, $P_r = \frac{\mu c_p}{K}$, is the Prandtl number. Thus, similarity of temperature fields in free-convection exist for equal Prandtl numbers in systems that are dynamically similar. Therefore, when geometrically similar bodies are cooled or heated by free convection, both the velocity and temperature fields are similar provided the Grashof numbers and the Prandtl numbers are equal, respectively, at corresponding points. When the Grashof numbers are equal and the Prandtl numbers are equal, according to Schlichting [46], the Nusselt numbers for the bodies are the same. Hence, experimental results for free-convection heat transfer can be correlated by an equation of the form

$$Nu = C(GrP_r), \qquad (3\text{-}88)$$

Where c denotes a functional relationship. For a group of gases having the same number of atoms per molecule, the Prandtl number is nearly the

same [48]. Equation (3-88), for these gases, was reduced to

$$Nu = \phi(Gr). \tag{3-89}$$

A detail discussion of empirical data for the Nusselt number in horizontal cylindrical annuli is presented in Chapter IV.

CHAPTER IV

THERMAL ANALYSIS

Before the modeling criteria, which were developed in Chapter III, were experimentally examined, a thermal analysis of several selected systems was made. This analysis was necessary in order to design a system which was simple, yet flexible enough so that a radiation-conduction-convection coupled heat transfer problem could be experimentally investigated. The thermal analysis also illustrates the complexity which arises in the analytical approach to such a problem and the importance of being able to correctly model a system.

In order to check the modeling criteria a radiation-conduction-convection coupled heat transfer problem had to be selected so that all three modes of heat transfer were present. This meant that the system had to be capable of containing a fluid. Since the system was to be tested in a simulated space environment, proper sealing of all connections was important. The first system for analysis consisted of two concentric spheres with a fluid in the annular space. This system had the merit of simplicity; however, sufficient information on the convective film coefficient was not available from the literature. Thus, before a reliable experimental program could be conducted, sufficient tests would have been necessary to determine the necessary convective coefficient.

The second system for analysis consisted of two concentric

rectangular tubes. This geometry was also restricted by a lack of information on the convective film coefficient.

The third system for analysis consisted of two long concentric cylinders. Considerable information has been reported in the literature ([36], [37], [38], [39], and [40]) on the convective film coefficient for horizontal cylindrical annuli. The concentric cylinder system was selected for the experimental program and is discussed in the following sections.

Governing Equations for Concentric Cylinders

The concentric cylinders shown in Figure 20 were divided into two systems in order to perform the thermal analysis. One system consisted of the inner cylinder; the other cylinder comprised the other system. The solution to the thermal fields in these cylinders were connected through the boundary conditions. The inner cylinder was subjected to a uniform heat flux and the outer cylinder was exposed to a simulated space environment. In formulating this problem the following assumptions were made:

1. Steady-state conditions,
2. Symmetrical temperature distributions in the angular direction.

These assumptions reduced the problem to thermal variations in the radial and axial directions. Applying the first law of thermodynamics to a small element in the cylinder, as shown in Figure 21, the following equation was obtained:

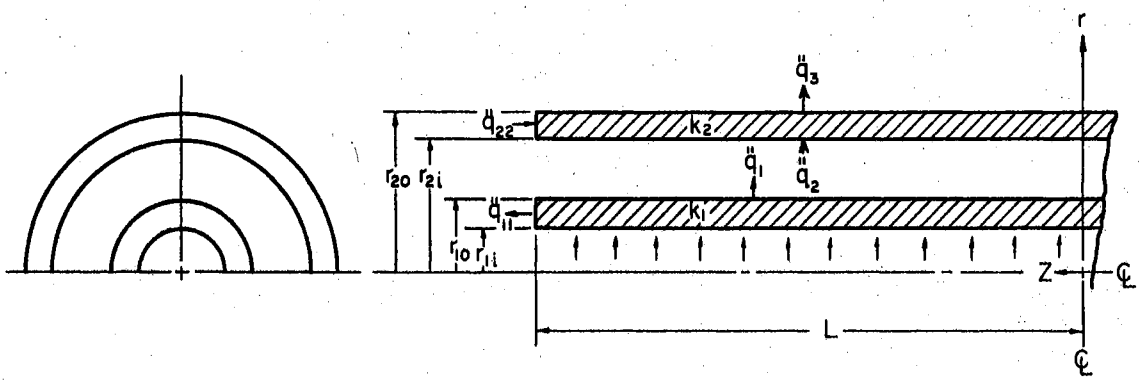

Figure 20. System with Two-Dimensional Heat Flow

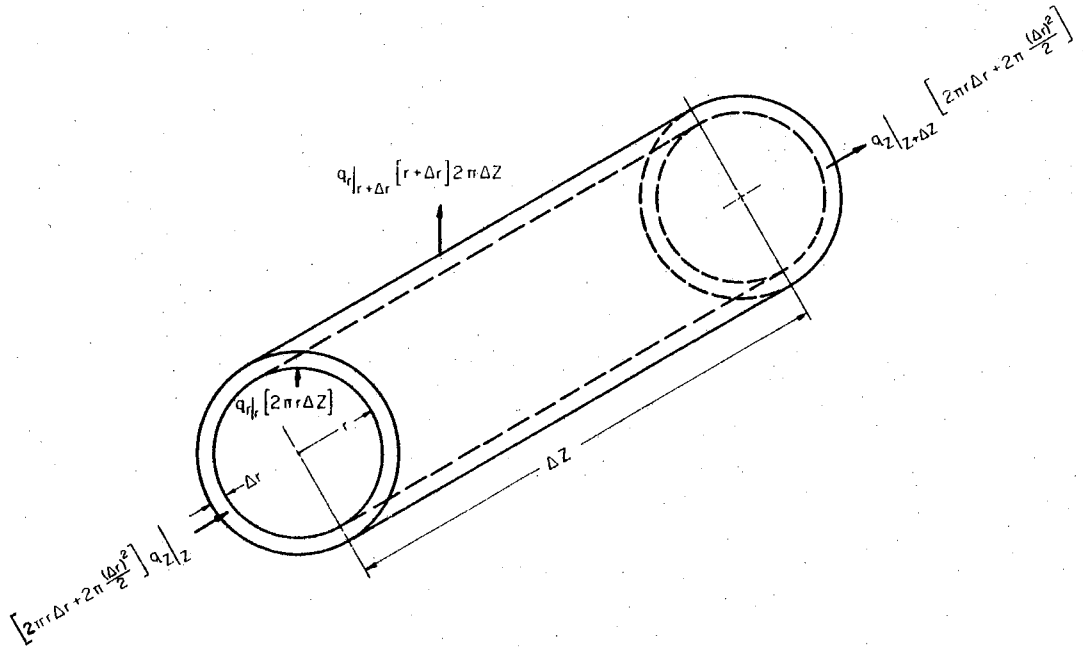

Figure 21. Volume Element of Two-Dimensional System

$$\frac{1}{r}\frac{\partial}{\partial r}(q_{rr}r) + \frac{\partial q_z}{\partial z} = 0, \qquad (4\text{-}1)$$

where q_{rr} and q_z are the r and z components of the heat flux, respectively. Fourier's law of heat conduction was used and obtain expression for q_{rr} and q_z. That is,

$$q_{rr} = - k \frac{\partial T}{\partial r} \quad \text{and} \quad q_z = - k \frac{\partial T}{\partial z} .$$

By substituting these expressions into Equation (4-1) the following equation was obtained:

$$\frac{1}{r}\frac{\partial}{\partial r}(kr\frac{\partial T}{\partial r}) + \frac{\partial}{\partial z}(k\frac{\partial T}{\partial z}) = 0. \qquad (4\text{-}2)$$

Equation (4-2) was used to analyze both cylinders. Using subscripts of 1 and 2 to denote the inner and outer cylinders, respectively, Equation (4-2) becomes:

$$\frac{1}{r}\frac{\partial}{\partial r}(k_1 r\frac{\partial T_1}{\partial r}) + \frac{\partial}{\partial z}(k_1\frac{\partial T_1}{\partial z}) = 0, \quad (r_{1i} \leq r \leq r_0) \qquad (4\text{-}3)$$

and

$$\frac{1}{r}\frac{\partial}{\partial r}(k_2 r\frac{\partial T_2}{\partial r}) + \frac{\partial}{\partial z}(k_2\frac{\partial T_2}{\partial z}) = 0. \quad (r_{2i} \leq r \leq r_{2o}) \qquad (4\text{-}4)$$

If the thermal conductivity, k, is such that it is approximately constant over a selected temperature range the temperature fields, $T_1(r,z)$ and $T_2(r,z)$, in the cylinders must satisfy Laplace's equation.

Thus, Equations (4-3) and (4-4) become

$$\frac{1}{r}\frac{\partial}{\partial r}\left(r\frac{\partial T_1}{\partial r}\right)+\frac{\partial^2 T_1}{\partial z^2}=0,\quad (r_{1i}\leq r\leq r_{10}) \tag{4-5}$$

$$\frac{1}{r}\frac{\partial}{\partial r}\left(r\frac{\partial T_2}{\partial r}\right)+\frac{\partial^2 T_2}{\partial z^2}=0,\quad (r_{2i}\leq r\leq r_{20}) \tag{4-6}$$

The boundary conditions for the systems shown in Figure 20 are:

$$\frac{\partial T_1(r,0)}{\partial z}=0 \qquad \frac{\partial T_2(r,0)}{\partial z}=0,$$

$$-k\frac{\partial T_1(r,L)}{\partial z}=\mathring{q}_{11}, \qquad -k\frac{\partial T_2(r,L)}{\partial z}=\mathring{q}_{22} \tag{4-7}$$

$$T_1(r_{1i},z)=T_{1i}, \qquad -k\frac{\partial T_2(r_{2i},z)}{\partial r}=\mathring{q}_{2},$$

$$-k\frac{\partial T_1(r_{10},z)}{\partial r}=\mathring{q}_{1}, \qquad -k\frac{\partial T_2(r_{20},z)}{\partial r}=\mathring{q}_{3}.$$

Equations (4-5) and (4-6) are second order linear partial differential equations. The separation of variables technique can be used to obtain product type solutions, but the complex boundary conditions make it difficult to obtain the constants in these solutions. Thus, it is possible to solve for the temperature fields numerically when sufficient boundary data are known. For the concentric cylinder system, a two-

dimensional thermal analysis could not be performed because of insufficient information on the convective boundary conditions. Thus, in order to simplify the problem, the horizontal test arrangement was designed to permit only one-dimensional heat flow in the solid cylinders.

Thermal Analysis of System with One-Dimensional Conduction

In order to simplify the thermal analysis, the system was designed to permit only radial heat transfer through the mid-section of the concentric cylinders. This was accomplished with guard heaters. For the concentric cylinder system, the heat conducted through the inner cylinder was approximately equal to the energy transferred through the annulus by convection and radiation. If the energy input to the system is known, the temperatures throughout the solid cylinders may be determined, provided a model can be developed to predict the energy transferred across the annulus. The fluid properties within the annulus were such that the gas did not participate in the radiant exchange. Thus, each mode of heat transfer was examined separately and the findings were combined to complete the thermal analysis. The nomenclature used in this analysis is shown in Figure 18.

Radial Conduction Through Solid Cylinders

In performing the thermal analysis of the solid cylinders, the following assumptions were made:

1. Steady-state heat transfer,
2. No axial or angular temperature gradients,
3. Uniform heat fluxes, $\overset{\circ\circ}{q}_1$, and $\overset{\circ\circ}{q}_2$,
4. Constant thermophysical properties,

5. Constant surface temperatures on each cylinder.

Under these assumptions the heat transfer is in the radial direction and can be expressed as

$$q_k = - k A \frac{dT}{dr} . \tag{4-8}$$

Integrating Equation (4-8) between the limits of T_o at V_o and T_i at V_i yields

$$q_k = \frac{2 \quad ke \ (T_i - T_o)}{\ln \frac{r_o}{r_i}} \tag{4-9}$$

The heat transfer through the inner cylinder (subscript 1) and that through the outer cylinder (subscript 2) may be expressed as

$$q_{k_1} = \overset{\circ\circ}{q}_{1(2 \pi r_{10} L)} = 2 \pi L k \frac{(T_{1i} - T_{10})}{\ln \frac{r_{10}}{r_{1i}}} , \tag{4-10}$$

and

$$q_{k_2} = q_{2(2 \pi r_{2i} L)} = 2 \pi L k \frac{(T_{2i} - T_{20})}{\ln \frac{r_{20}}{r_{2i}}} , \tag{4-11}$$

respectively.

Equations (4-10) and (4-11) may be solved for the unknown temperatures provided the heat transfer and one temperature on each cylinder is specified. A thermal analyses performed in this manner has restrictions. During any test the temperature of the surroundings was speci-

fied. Thus, this provides a starting point for determining the temperatures throughout the system, provided models can be formulated to accurately predict the heat transfer by radiation and convection.

Radiant Exchange Between System and Surroundings

The heat transfer by radiation will depend upon the properties of all systems participating in the exchange. In order to simplify this analysis, the emissivity and absorptivity of all surfaces throughout the system and surroundings were assumed to remain constant. These properties were controlled by the use of selected coating materials.

The concentric cylinder system was tested in a simulated space environment. In this environment the pressure was low enough so that radiation was the only mode of heat exchange between the system and the surroundings. Therefore, the net heat transfer, q_3, between the system and the surroundings may be evaluated by.

$$q_3 = A_{20}\, \ddot{q}_3 = A_{20}\, \sigma\, \epsilon_{20}\, F_{20\text{-}\omega}\, (T_{20}^4 - T_w^4). \qquad (4\text{-}12)$$

For a given heat transfer q_3 (which is approximately constant throughout the system) and a known constant temperature of the surroundings, the temperature, T_{20}, of the outside surface of the system can be determined from Equation (4-12). This temperature (T_{20}), together with the constant heat transfer, may be used to obtain the inside surface temperature, T_{2i}, of the outer cylinder (See Equation (4-11)).

Radiant Exchange Between Concentric Cylinders

The radiant energy leaving the outer surface of the inner cylinder was not equal to that entering the inner surface of the outer cylinder.

This difference was primarily caused by the ends which were needed in sealing the annulus. The relative magnitude of this difference was established through an example utilizing typical conditions during a test. This, together with a technique for evaluating the radiant exchange between the concentric cylinders, is presented below.

The integral equation for evaluating the net heat transfer by radiation at the j th surface is [34]

$$q_{net,j} = \left\{ \sum_{k=1}^{n} \int_{A_k} J_k \, F_{dA_k - A_j} \, dA_k \right\} - \int_{A_j} J_j \, dA_j, \qquad (4\text{-}13)$$

where J_k represents the function J over the area of the k th element. The radiosity functions, J_j, in Equation (4-13) are

$$J_j = E_j + \bar{\bar{\rho}}_j \left\{ \frac{1}{A_j} \sum_{k=1}^{n} \int_{A_k} J_k \, F_{dA_k \; A_j} \, dA_k \right\}; \; j=1,2,\ldots,n \qquad (4\text{-}14)$$

Where E_j represents the emitted energy from the j th element and $\bar{\bar{\rho}}$ represents the reflectance of the j th element. Equation (4-13) was solved by finite difference approximations for the annulus between the concentric cylinders. This method of solution is discussed in detail in Reference [34].

In order to write the integral equations as finite-difference approximations, the following assumptions were necessary:

1. The enclosure has n isothermal surfaces or elements.
2. The emissivity and reflectivity of all surfaces are constant.
3. The incident radiation is uniformly distributed over the surface of an element.

The above assumptions imply that emissions and reflections are "gray

and diffuse." Thus, J_k is constant over the area A_k and the radiosity function given by Equation (4-14) becomes

$$J_j = E_j + \bar{\rho}_j \sum_{k=1}^{n} J_k F_{A_j \rightarrow A_k}; \quad j=1,2,\ldots,n, \tag{4-15}$$

or

$$J_j = \epsilon_j E_{b_j} + \bar{\rho}_j \sum_{k=1}^{n} J_k F_{A_j \rightarrow A_k}; \quad j=1,2,\ldots,n. \tag{4-16}$$

If $F_{A_j \rightarrow A_k}$ is represented as F_{jk} Equation (4-13) becomes

$$q_{net,j} = \sum_{k=1}^{n} (J_k - J_j) F_{jk} A_j. \tag{4-17}$$

Equation (4-17) was used to obtain approximate values for the radiant exchange between the concentric cylinders. The accuracy depends upon the temperature difference between adjacent isothermal elements. As the temperature difference decreases the accuracy increases.

In selecting a model to describe the radiant exchange between the concentric cylinders, the system was analyzed for two different temperature distributions. First, each cylinder of the concentric cylinder system was divided into isothermal elements (referred to hereafter as nonisothermal case) and Equation (4-17) was used to obtain the net heat transfer from each element. Second, the surface of each cylinder was isothermal (referred to hereafter as isothermal case).

1. Nonisothermal Case

From initial tests performed on a concentric cylinder system, the temperature drop from the center to one end was less than $3^{\circ}F$. For the

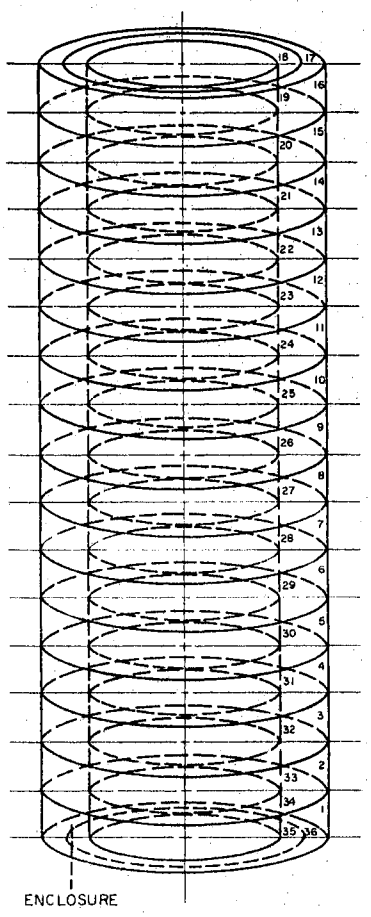

Figure 22. Isothermal Surfaces for Radiation Calculations

first attempt to evaluate the radiant heat transfer between the cylindrical surfaces, the enclosure was divided into isothermal elements as shown in Figure 22. This selection of isothermal elements allowed the temperature difference between adjacent elements to be less than three sixteenths of a degree. The system shown in Figure 22 consisted of 36 isothermal elements. For this enclosure, 1296 configuration factors and 1296 radiosity values must be determined in order to evaluate the radiant heat transfer between the cylindrical surfaces. This selection of isothermal elements was abandoned because of the labor

required in obtaining a solution. For larger temperature drops or greater accuracy, the temperature difference between adjacent elements must approximate the actual temperature distribution.

Since the inner and outer cylindrical surfaces were approximately uniform in temperature, three isothermal elements on each cylinder were selected for the radiant heat transfer calculations. The isothermal elements are shown in Figure 23. In order to determine a typical value for the net radiant exchange of an isothermal element, it was necessary to select typical values for the geometric dimensions, temperatures, and emissivities.

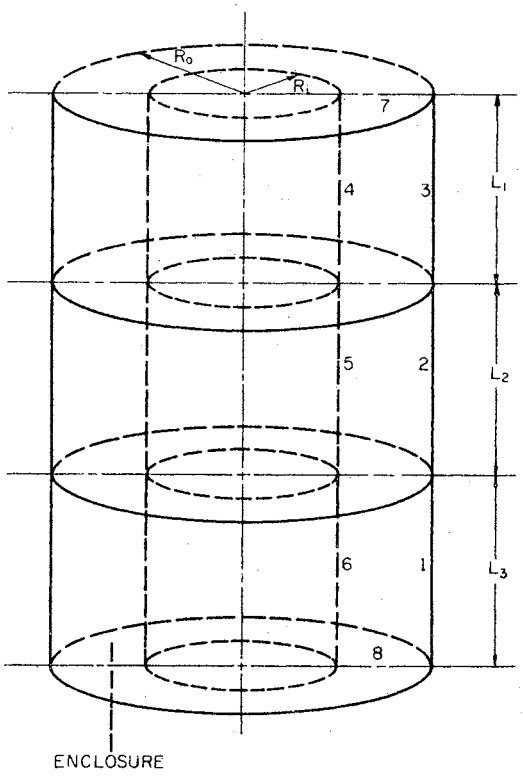

Figure 23. Isothermal Surfaces for Radiation Calculations

Before evaluating the net radiant exchange, the configuration factors and radiosities had to be determined. The configurations factors were determined from configuration factors for equal length concentric cylinders and flux algebra. The concentric cylinders consisted of lengths of L_1, L_2, L_3, $L_1 + L_2$, and $L_1 + L_2 + L_3$. A typical concentric cylinder system is shown in Figure 24. From Reference [35] together with the notation shown in Figure 24, the various factors are:

$$F_{21} = \frac{R_i}{R_o}\left\{1 - \frac{1}{\pi}\left\{\cos^{-1}\left(\frac{L^2 - R_o^2 + R_i^2}{L^2 + R_o^2 - R_i^2}\right) - \frac{1}{2(R_i)L}\right.\right.$$

$$\left.\sqrt{(L^2 + R_o^2 + R_i^2)^2 - (2R_iR_o)^2}\cdot \cos^{-1}\frac{R_i}{R_o}\frac{(L^2 - R_o^2 + R_i^2)}{(L^2 + R_o^2 - R_i^2)} + \right.$$

$$\left.\left.(L^2 - R_o^2 + R_i^2)\sin\frac{R_i}{R_o} - \frac{\pi}{2}(L^2 + R_o^2 - R_i^2)\right]\right\}\right\} , \quad (4\text{-}18)$$

$$F_{22} = 1 - \frac{R_i}{R_o} + \frac{1}{\pi}\left\{\frac{2R_i}{R_o}\tan^{-1}\frac{2\sqrt{R_o^2 - R_i^2}}{R_o} - \frac{L}{2R_o}\left[\frac{\sqrt{4R_o^2 + L^2}}{L}\cdot\right.\right.$$

$$\sin^{-1}\frac{4(R_o^2 - R_i^2) + \frac{L^2}{R_o^2}(R_o^2 - 2R_i^2)}{L^2 + 4(R_o^2 - R_i^2)} - \sin^{-1}\frac{R_o^2 - 2R_i^2}{R_o^2}$$

$$\left.\left.+ \frac{\pi}{2}\left\{\frac{\sqrt{4R_o^2 + L^2}}{L} - 1\right\}\right]\right\} , \quad (4\text{-}19)$$

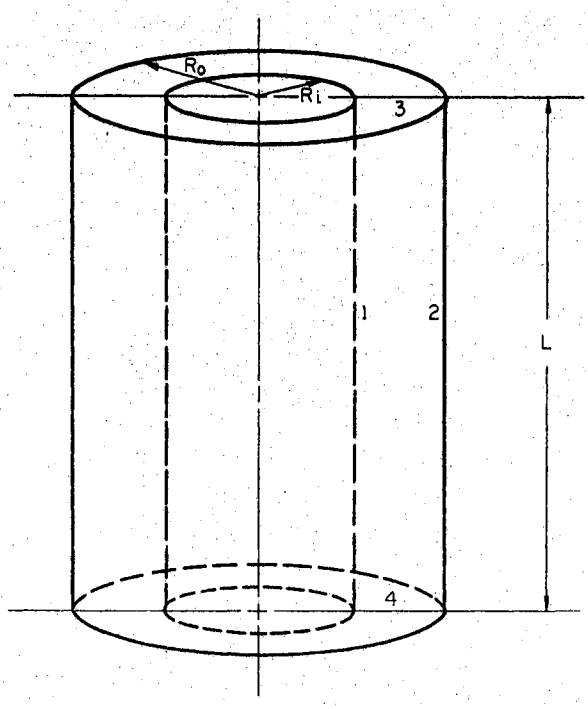

Figure 24. Two Equal Length Concentric Cylinders

$$F_{34} = 1 - \left\{\frac{L}{R_o^2 - R_i^2}\right\}\left\{R_i - R_o\,(F_{22} + 2F_{21} - 1)\right\}, \qquad (4\text{-}20)$$

and

$$F_{23} = \frac{1}{2}\,(1 - F_{21} - F_{22}). \qquad (4\text{-}21)$$

These equations were solved on a digital computer for the system shown in Figure 23. The computer program used in obtaining the configuration factors is listed in Appendix B and the resulting configuration factors are presented in Table VI.

The radiosity equations were obtained from the following expressions [34]

TABLE VI

COMPUTED CONFIGURATION FACTORS

F_{11} = 0.00000	F_{21} = 0.00000	F_{31} = 0.00000	F_{41} = 0.2774432
F_{12} = 0.0000000	F_{22} = 0.0000000	F_{32} = 0.0000000	F_{42} = 0.027783537
F_{13} = 0.0000000	F_{23} = 0.0000000	F_{33} = 0.0000000	F_{43} = 0.000011966
F_{14} = 0.8323296	F_{24} = 0.0512925	F_{34} = 0.0000358	F_{44} = 0.4679458
F_{15} = 0.0833509	F_{25} = 0.8952903	F_{35} = 0.0833509	F_{45} = 0.0968046
F_{16} = 0.0000358	F_{26} = 0.0512925	F_{36} = 0.8323296	F_{46} = 0.0017800
F_{17} = 0.0838352	F_{27} = 0.0010544	F_{37} = 0.0001448	F_{47} = 0.1273055
F_{18} = 0.0001448	F_{28} = 0.0010544	F_{38} = 0.0838352	F_{48} = 0.0008543
0.9996963	0.9999841	0.9996963	0.999928903

F_{51} = 0.0170924	F_{61} = 0.000011966	F_{71} = 0.1676704	F_{81} = 0.00028932
F_{52} = 0.2984301	F_{62} = 0.02778353	F_{72} = **0.003452**	F_{82} = 0.003452
F_{53} = 0.0170924	F_{63} = 0.2774432	F_{73} = 0.00028932	F_{83} = 0.1676704
F_{54} = 0.0595720	F_{64} = 0.0017849	F_{74} = 0.7638330	F_{84} = 0.0051199
F_{55} = 0.5372593	F_{65} = 0.0968046	F_{75} = 0.05248637	F_{85} = 0.0524863
F_{56} = 0.0595720	F_{66} = 0.4679458	F_{76} = 0.0051199	F_{86} = 0.7638330
F_{57} = 0.0054858	F_{67} = 0.0008543	F_{77} = 0.0000000	F_{87} = 0.0061476
F_{58} = 0.0054858	F_{68} = 0.1273055	F_{78} = 0.0061476	F_{88} = 0.0000000
0.9999898	0.9999289	0.99899859	0.998998

$$J_j = \left\{ \frac{\epsilon_j}{1 - \bar{\bar{\rho}}_j E_{jj}} \right\} E_{b_j} + \left\{ \frac{\bar{\bar{\rho}}_j}{1 - \bar{\bar{\rho}}_j E_{jj}} \right\} \sum_{\substack{k=1 \\ k \neq j}}^{n} J_k F_{jk}. \qquad (4\text{-}22)$$

For the system shown in Figure 23, two sets of equations were established from Equation (4-22) for the isothermal and nonisothermal cases. These equations were solved on the digital computer (See Appendix C for listing of program). The radiosity, net radiant flux, and total radiant exchange for the various isothermal surfaces shown in Figure 23, are listed in Table VII.

2. Isothermal Case

For this case, the surface of each cylinder was assumed to be isothermal. This particular temperature distribution was selected in order to demonstrate the importance of maintaining each cylinder at a constant temperature. The geometric dimensions, temperatures, and emissivities used in performing the calculations are listed in Table VII. The radiosity, net radiant flux, and total radiant exchange are listed in Table VIII.

As a matter of comparison, the infinite cylinder approximation was used to compute the radiant exchange between the concentric cylinders. In this approximation each cylinder must be isothermal. For two infinitely long isothermal cylinders, the radiant exchange at the midsection is

$$q_{2 \rightleftarrows 5} = \frac{A_2 \sigma \quad (T_2^4 - T_5^4)}{\left(\frac{1}{\epsilon_2} - 1 \right) \left(1 + \frac{A_2}{A_5} \right) + 1} . \qquad (4\text{-}23)$$

TABLE VII

TEMPERATURE, EMITTANCE, AND DIMENSIONS OF THE ELEMENTS

NONISOTHERMAL CASE			ISOTHERMAL CASE		
Surface	Emittance	Temperature	Emittance	Temperature	Size
1	0.97	598°R	0.97	600°R	
2	0.97	600°R	0.97	600°R	R_i = 0.50"
3	0.97	598°R	0.97	600°R	R_0 = 1.50"
4	0.97	495°R	0.97	500°R	L_1 = 4.00"
5	0.97	500°R	0.97	500°R	L_2 = 6.50"
6	0.97	495°R	0.97	500°R	L_3 = 4.00"
7	0.10	546.5°R	0.10	550°R	
8	0.10	546.5°R	0.10	550°R	

(The surfaces were assumed gray.)

TABLE VIII

HEAT TRANSFER AT SURFACE OF ELEMENTS

Surface	J-Values Btu/hr-ft^2	qnet, j-values Btu/hr-ft^2	q-values Btu/hr	J-values Btu/hr/ft^2	qnet, j-values Btu/hr-ft^2	q-values Btu/hr
1	210.02284	-103.8790678	- 9.05825472	218.64478	-108.574023	- 9.47487498
2	218.57807	-110.7939577	-15.670583	218.5921171	-110.339745	-15.64705857
3	210.02284	-103.879067	- 9.058254	-218.64478	-108.574023	- 9.4748749
4	103.9538	35.778434	9.3381714	108.19468	36.52188	9.561407308
5	108.1793	36.1602324	15.368098	108.20537	36.9469	15.71810038
6	103.9538	35.77843	9.3381714	108.19568	36.52188	9.561407308
7	125.453	- 2.9127529	- 0.126996	130.11423	- 3.8391085	- 0.1675127
8	125.453	- 2.9127529	- 0.126996	130.11423	- 3.8391085	- 0.1675127

The temperature and emissivities used in computing the radiant exchange were those listed in Table VII for the midsection of the concentric cylinder system. For these conditions, the radiant exchange at the midsection is 15.1841 Btu/hr.

In conclusion, the radiant exchange computed by the infinite cylinder approximation was in close agreement with the isothermal and nonisothermal cases presented in Table VIII for the midsection of the concentric cylinder system. According to this typical example, the maximum difference was less than 3 percent. Therefore, the radiant exchange between the concentric cylinders, at the midsection, can be obtained from the infinite cylinder approximation.

Convective Heat Transfer Across the Annulus Between Horizontal Concentric Cylinders

Whenever a fluid is present within the annulus between concentric cylinders, energy will be convected across the gap if a temperature difference exists. The quantity of energy convected across the gap may be determined if the convective flim coefficient is known. An estimate of the magnitude of this coefficient may be obtained from previous investigations of natural convection between concentric cylinders. The exact magnitude depends upon the exact conditions within the annulus, and as these conditions change the coefficient will change. Changes in film coefficient are associated with changes in flow patterns. If the gap temperature difference exceeds certain limits, the flow may become unstable.

The dependence of the film coefficient on the conditions within the annulus may be explained by examining the flow patterns for the

various flow regimes. Typical flow patterns for a few of the flow regimes are shown in Figure 26. Under certain conditions the flow between the concentric cylinders will oscillate [47]. The exact cause and occurrence of these oscillations has not been established.

The convection heat transfer associated with the various flow regimes is shown in Figure 25. These results point out the variation in convection heat transfer as observed by several investigators. Empirical correlations by Beckmann [38], Liu, Mueller, and Landis [40], Grigull and Hauf [36], and Lis [37] have been formulated for the overall convection heat transfer in long horizontal cylindrical annuli. These correlations and their ranges of application are listed in Table IX.

In order to obtain an estimate of the energy convected across the annulus, an empirical correlation of the film coefficient was selected. Figures 27, 28, and 29 show data generated from the relations presented in Table IX for the three different relative gap widths used in the experimental program. As can be seen from these figures, there was considerable variation in the Nusselt number for a given Grashof number. For this reason, it was necessary to use several different convection film coefficient correlations in performing the analytical investigations. In the experimental program a correlation was established from measurements taken on the prototype.

TABLE IX

EMPIRICAL CORRELATIONS OF HEAT TRANSFER IN LONG CYLINDRICAL ANNULI

Empirical Correlation	Source	Fluid	Indicated Deviations	Range of Dia. Ratios	Range of Grashof No.
$\frac{Kc}{k} = 1.0$	Kraussold	Air, Hydrogen, CO_2, Water, Transformer oil, Machine oil	+22.9% and -20%	$1.2 \leq \frac{do}{di} \leq 3.0$	$\log PrGr_\delta \leq 3.0$
$\frac{Kc}{k} = 0.11 (PrGr_\delta)^{0.29}$	Kraussold	Air, H_2, CO_2, Water, Transformer oil, Machine oil	+22.9% and -20%	$1.2 \leq \frac{do}{di} \leq 3.0$	$3.8 \log (PrGr_\delta) \leq 6.0$
$\frac{Kc}{k} = 0.4 (PrGr_\delta)^{0.20}$	Kraussold	Air, H_2, CO_2, Water, Transformer oil, Machine oil	+22.9% and -20%	$1.2 \leq \frac{do}{di} \leq 3.0$	$\log (PrGr_\delta) > 6.0$
$\frac{Kc}{k} = 0.135 \left[\frac{(Pr^2 Gr_\delta)}{(1.36+Pr)}\right]^{0.278}$ $\frac{Kc}{k} = 1.0$	Liu, Mueller, and Landis	Air, Water and Silicone	--	$1.15 \leq \frac{do}{di} \leq 7.5$	$3.5 \log \frac{(Pr^2 Gr_\delta)}{(1.36+Pr)} \leq 8.0$, $\log \frac{(Pr^2 Gr_\delta)}{(1.36+Pr)} \leq 3.0$
$Nu_s = [0.20+0.145(\delta/d_i)]Gr_e^{0.25} - .02(\delta/di)$	Grigull and Hauf	Air	--	$1.3 \leq \frac{do}{di} \leq 6.3$	$3{,}000 \leq Gr_\delta \leq 1{,}000{,}000$
$\frac{Kc}{k} = 0.389(GR_i Pr[1-(\frac{di}{do})]^{6.5})^{0.237}$	Lis	Air	$\pm$ 15%	$2 \leq \frac{do}{di} \leq 4$	$4x10^4 \leq (GrPr)i \leq 10^8$
$\frac{Kc}{k} = 0.087(GR_i Pr[1-(\frac{di}{do})]^{6.5})^{0.329}$	Lis	Air	$\pm$ 9%	$2 \leq \frac{do}{di} \leq 4$	$10^8 \leq Gr_i Pr \leq 5x10^{10}$

Before the film coefficient can be obtained from the correlations listed in Table IX, the dependency of the transport properties upon pressure and temperature must be established. Once this dependency has been established, the convective film coefficient can be obtained.

The convective heat flux, in terms of the film coefficient, may be computed by the relation

$$q_c = \mathring{q}_{c_1} = h\,(T_{10} - T_{2i}). \tag{4-24}$$

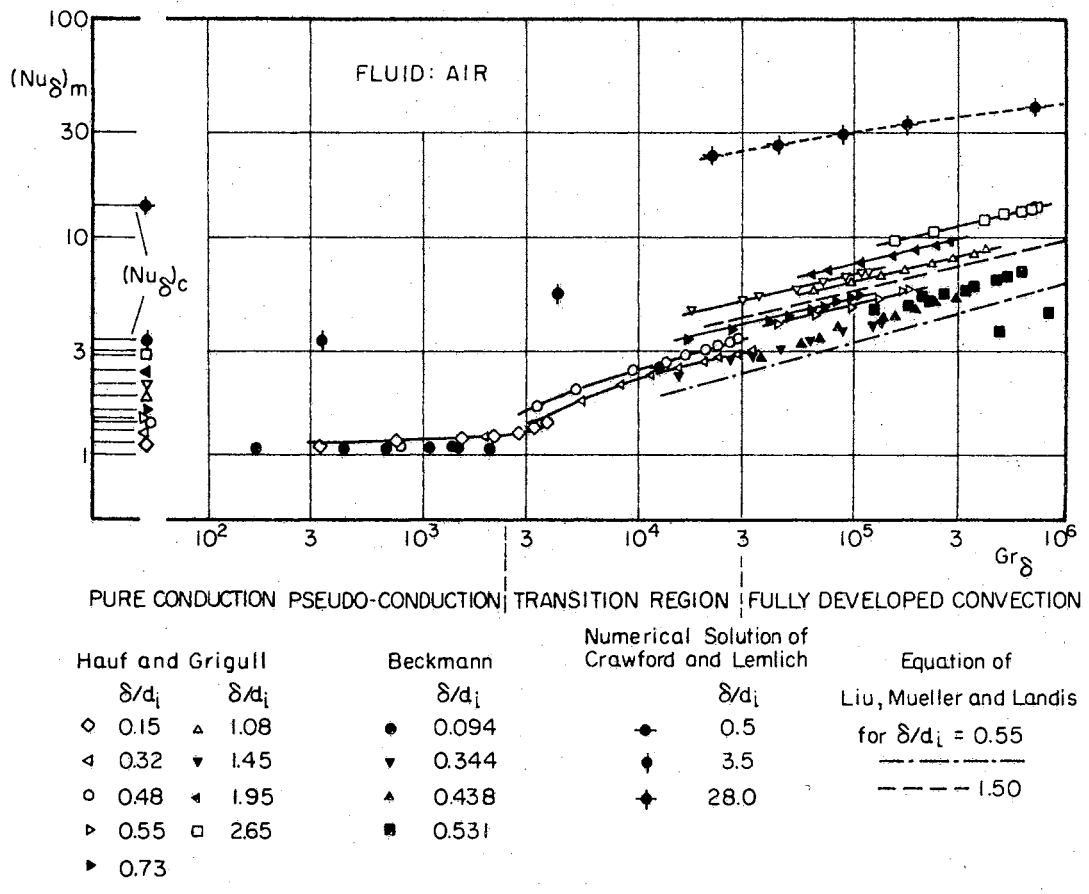

Figure 25. Heat Transfer by Natural Convection in Horizontal Cylindrical Annuli. Pr=0.71

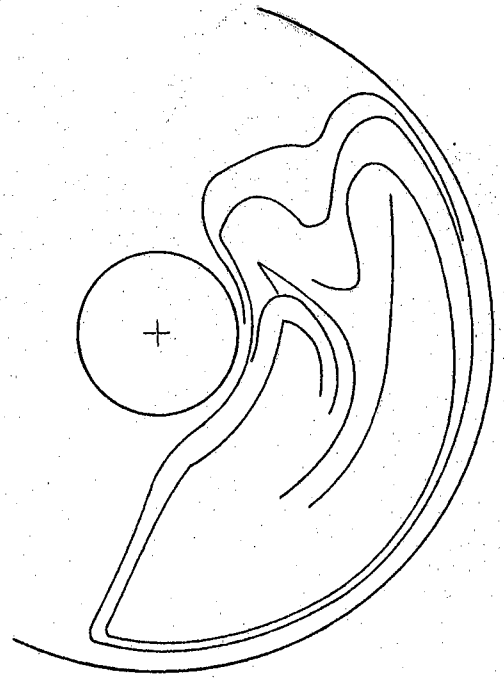

(a) Unstable Flow Pattern in Turbulent Region.

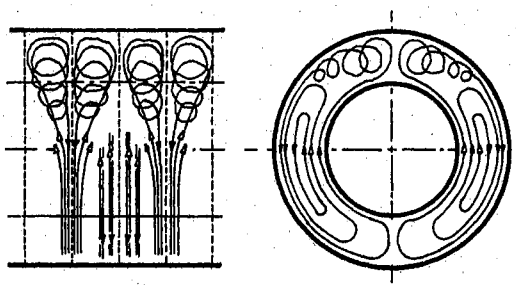

(b) Flow Pattern in Transition Regime.

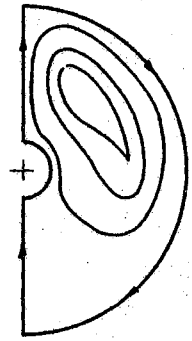

(c) Kidney Shaped Eddy Pattern in Fully Developed Region.

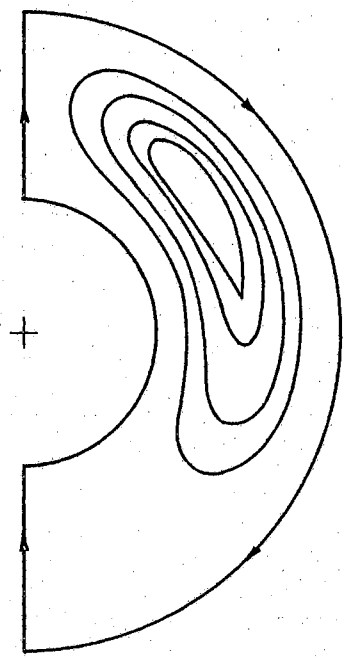

(d) Cresent Eddy Pattern in Fully Developed Regime.

Figure 26. Representation of Flow Patterns Which Exist in the Fully Developed Regime. Source: Ref. 36.

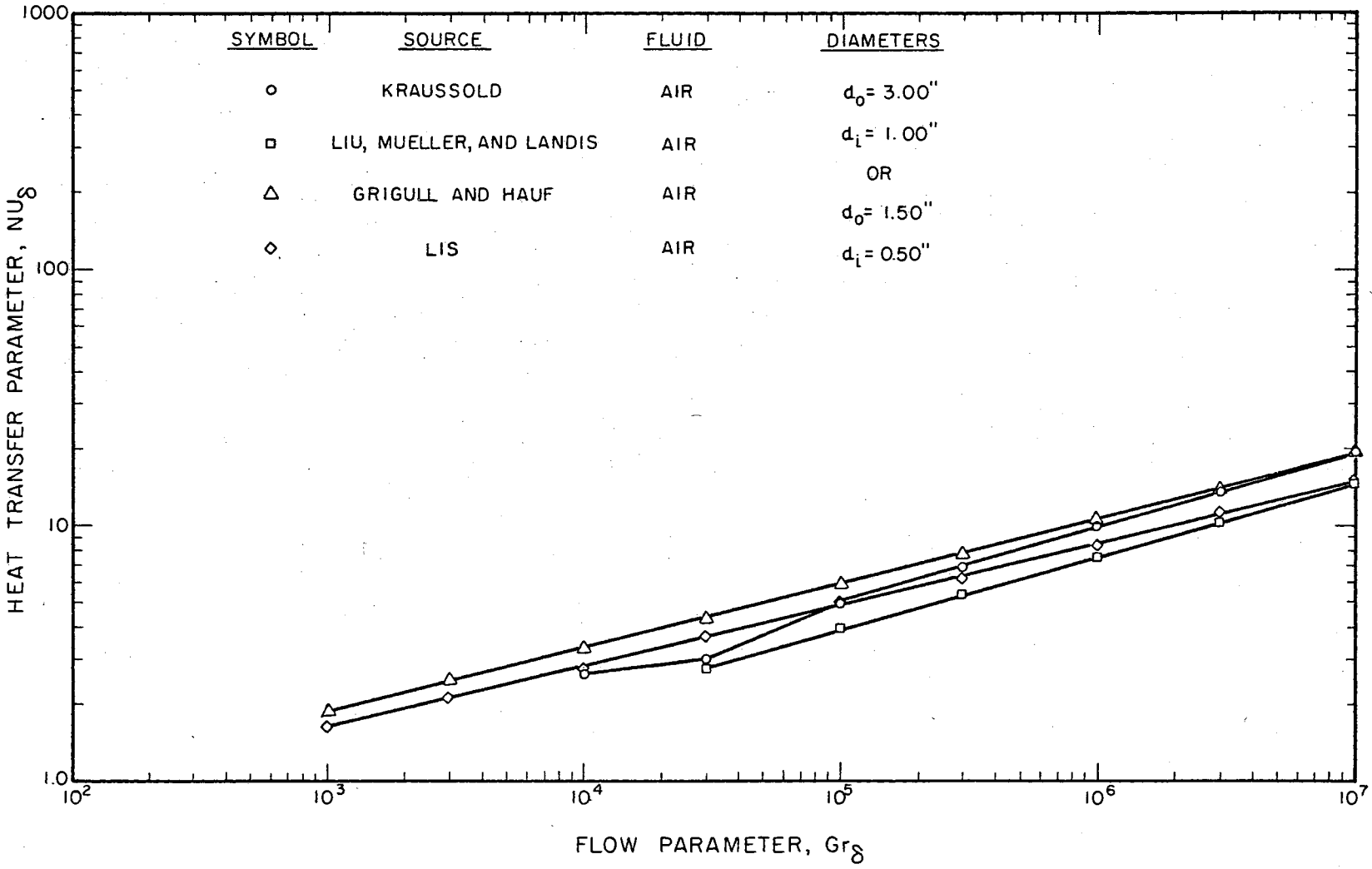

Figure 27. Empirical Curves for Natural Convection Heat Transfer in Annulus

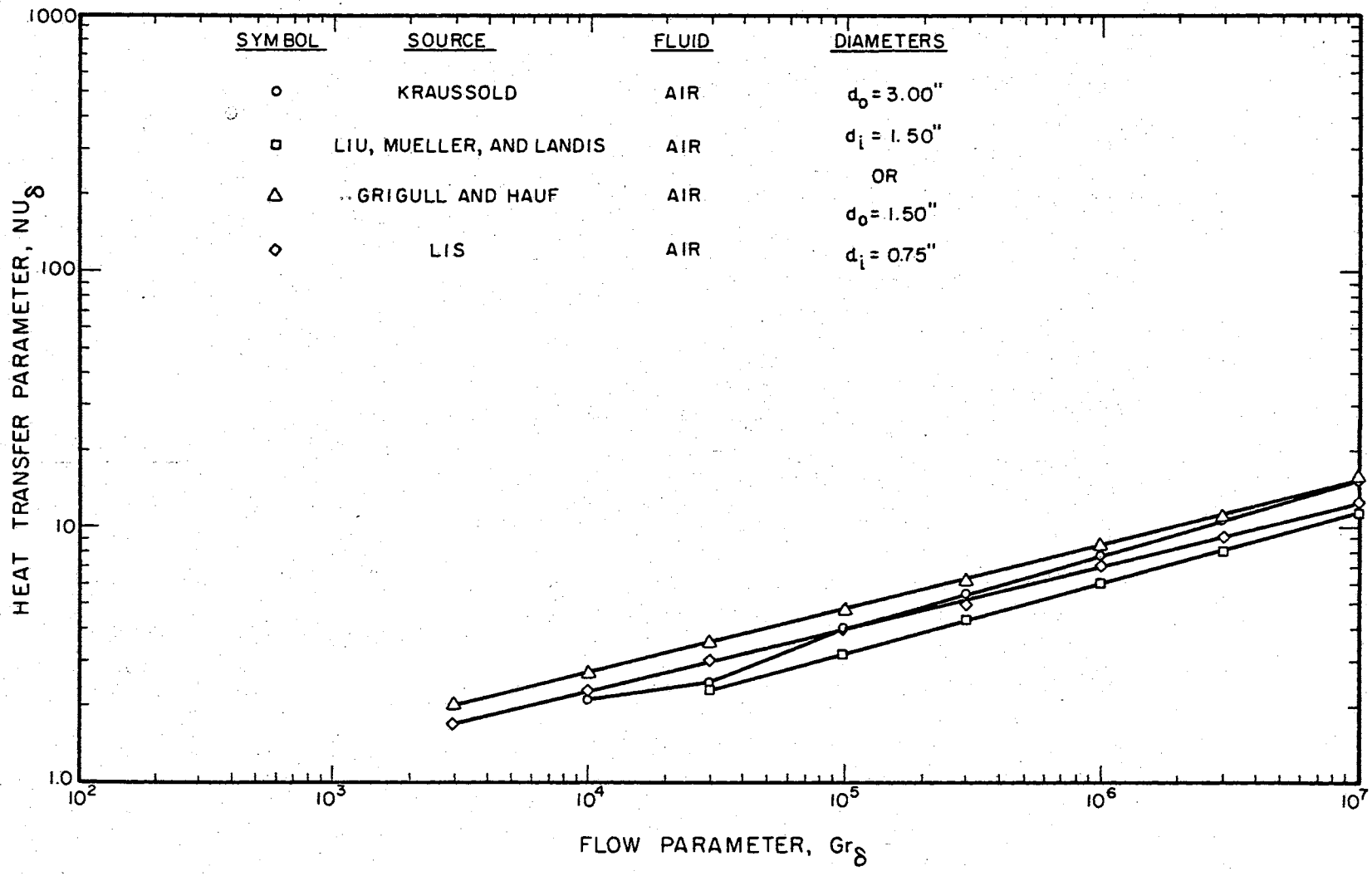

Figure 28. Empirical Curves for Natural Convection Heat Transfer in Annulus

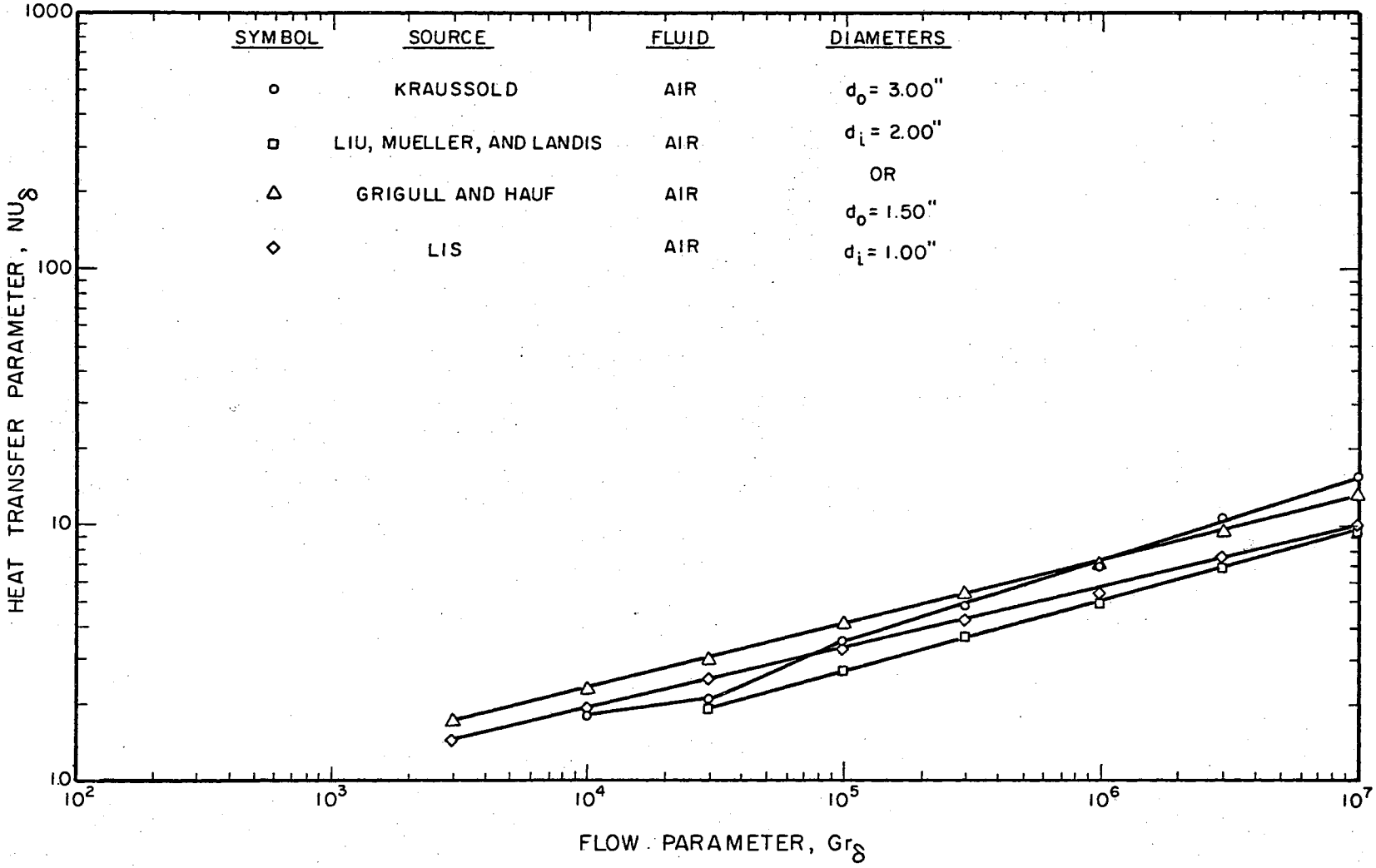

Figure 29. Empirical Curves for Natural Convection Heat Transfer in Annulus

The total heat transferred across the annulus is

$$q = q_c + q_r, \tag{4-25}$$

where q_r is the energy transferred by radiation. Since the total heat transfer and the inside surface temperature of the outer cylinder are known, Equations (4-11), (4-12), and (4-25) may be used to obtain the outer surface temperature of the inner cylinder.

Dependence of Transport Properties on Pressure and Temperature

The pressures (2 to 30 psia) within the annuli of the models and prototypes used in the experimental investigation had very little effect on the thermal conductivity and viscosity of the gas. The effect of pressure on these transport properties is shown in Table X. Table X is based on data taken from Reid and Sherwood [42]. In this table the explanation used in describing the behavior of thermal conductivity and viscosity, in each pressure range, should be interpreted for increases in pressure.

The effect of temperature on the low-pressure thermal conductivity of air can be established from experimental data. Experimental data for viscosity and thermal conductivity have been reported in Reference [43]. Various empirical methods may be used to relate thermal conductivity to temperature; in this case, the representation selected was a polynomial in temperature. The polynomial which describes the experimental data to within $\pm$ 0.25 percent is

$$k = 0.35145532 \times 10^{-3} + 0.32041684 \times 10^{-4}\, T - 0.10027234 \times 10^{-7}\, T^2; \quad (360^{\circ}R \leq T \leq 920^{\circ}R). \tag{4-26}$$

TABLE X

PRESSURE EFFECT ON VISCOSITY AND THERMAL CONDUCTIVITY OF AIR

Viscosity	Thermal Conductivity	Pressure Range
Nearly no effect	Increases rapidly	$0.0 \leq p \leq 1$ mm Hg.
Very slight effect	Increases about 1% per Atmos.	1 mm Hg. $\leq p \leq 10$ atmospheres (Known as low-pressure region)
Increases	Increases rapidly	10 atmospheres $\leq p$

Equation (4-26) was obtained by applying the least square curve fit computer program (listed in Appendix D) to the experimental data presented in Reference [43].

The two-constant Sutherland equation has been shown to be reliable in correlating viscosity-temperature data [44]. The Sutherland equation is

$$\mu = b_1 \, T^{3/2}/(S_o + T), \qquad (4\text{-}27)$$

where a plot of $T^{3/2}/\mu$ versus T should yield a straight line with a slope of $1/b$, and an intercept of S_o, the so-called "Sutherland Constant." The Sutherland equation was obtained from the plot of experimental data shown in Figure 33. This equation is

$$\mu = T^{3/2}/(375\ T + 77{,}700). \qquad (360^{\circ}R \leq T \leq 920^{\circ}R) \qquad (4\text{-}28)$$

Equations (4-26) and (4-28) were substituted into the selected convective film coefficient correlation in order to obtain an estimate of the film coefficient. This film coefficient was substituted into Equation (4-24) to obtain the convection heat transfer across the annulus.

Theoretical Calculations of Temperatures on Models and Prototype for Various Energy Inputs

The governing heat flux equations have been developed in the preceding sections. These equations were used in conjunction with the

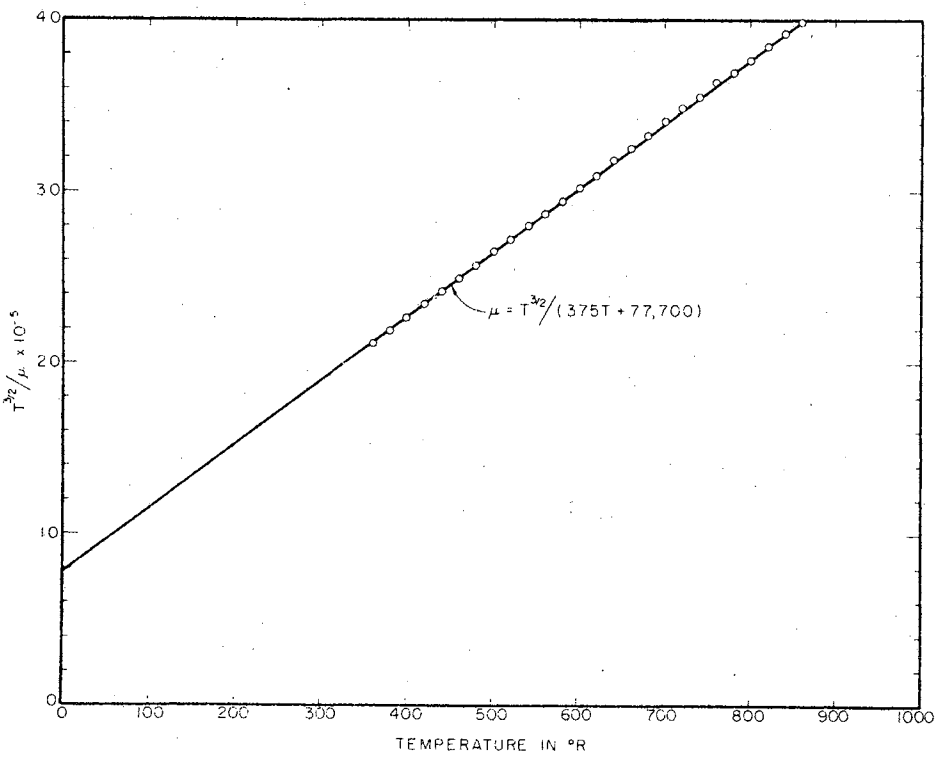

Figure 30. Viscosity versus Temperature at Atmospheric Pressure

convective film coefficient correlations to obtain a thermal analysis of the test section. The thermal analysis was performed for horizontal orientation of the system, and this analysis is valid only for the center section of the system.

Numerical solutions to Equations (4-10), (4-11), (4-12), and (4-25) were obtained (See Appendix E) for various energy inputs and convective film coefficient correlations. The results obtained from the solutions to these equations are presented in Table XXII (See Appendix E) for the models and prototypes used in the experimental program. The important conclusions drawn from the thermal analysis are:

1. A test section with one-dimensional heat flow is essential for accurate thermal analysis and to establish the modeling of convection heat transfer.
2. The radiant exchange between the concentric cylinders may be accurately evaluated by the infinite cylinder approximation. This approximation predicts the radiant exchange more accurately when there is a small temperature drop from the center to one end in the axial direction.
3. The temperature difference across the gap should be low (depends upon relative gap width) in order to eliminate flow oscillations within the fluid contained in the annulus. The occurrence of these oscillations was difficult to predict.
4. The correct convective film coefficient was obtained from tests performed on the prototype. This was necessary because of the disagreement between published correlations of the convective film coefficient.

5. The theoretical calculations furnished a basis for comparing the steady-state experimental results.

CHAPTER V

TEST SECTIONS

The test sections were designed so that the thermal modeling of a radiation-conduction-convection coupled heat transfer problem could be experimentally investigated. Several factors entered into the selection of a particular geometric shape for the test section. These factors ranged from fabrication difficulties to problems associated with determining the amount of energy transferred by natural convection. A concentric cylinder system was the simplest shape to construct with available equipment. Also, several investigations of natural convection between concentric cylinders have been reported in the literature. These previous investigations permitted a check on the amount of heat transferred by convection. For these reasons, the concentric cylinder system was selected to check the validity of the thermal modeling criteria developed in Chapter III.

The concentric cylinder system was designed to give one-dimensional (radial) heat flow through the solid components of the system. For a constant heat flux in the radial direction, the surface of each cylinder was nearly isothermal. Isothermal surfaces were necessary in order to separate the amount of energy transferred across the annulus by convection from that transferred by radiation (See Chapter IV). In order to achieve the desired isothermal surfaces, guard heaters were used during steady state testing. An assembly drawing of the system

is shown in Figure 31.

Description of Test Sections

Three prototype and three one-half scale models were designed and constructed in order to check the validity of the modeling criteria. These test sections were designed with relative gap widths, δ/di, of 1.0, 0.50, and 0.25. This range of relative gap widths allowed the investigation to cover the convective regimes from pseudo-conduction to fully developed laminar flow without exceeding the upper temperature limit of the test sections and without developing flow oscillations. Several systems could have been designed with the same δ/di. Since the energy transferred from the test section was absorbed by a liquid nitrogen cooled liner (enclosure), a system with a low total heat flow to the liner was less expensive to test. This together with the size of the liner, limited the size of the prototype.

Each test section consisted of concentric cylinders, heaters, end plates, and several miscellaneous parts. Detail drawings of each part of the test sections are shown in Figures 33 through 38 and photographs of a prototype and the corresponding model are shown in Figure 39. A description of the components is given in the following sections.

Cylinders

The prototypes or models consisted of an outer cylinder and three interchangeable inner cylinders. Each cylinder was constructed from 6061-T6 drawn aluminum tubing. Thick wall tubing was cut to size and an o-ring groove was cut in each end of each cylinder. Three small aluminum tubes were welded to the outer cylinder. A gas fill line was

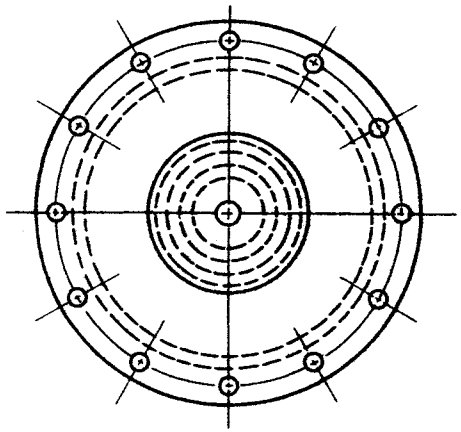

PART NO.	DESCRIPTION	MATERIAL
1	OUTER CYLINDER	6061-T6 Al
2	INNER CYLINDER	6061-T6 Al
3	HEATER CORE	PHENOLIC
4	SPACER RING	PHENOLIC
5	END FLANGE	LEXAN
6	ROD	6061-T6 Al
7	WASHER	304 S.S.
8	ULTRA-TORR ADAPTER	BRASS
9	ULTRA-TORR UNION	BRASS
10	GAS FILL LINE	TEFLON
11	EXTENSION LEADS	COPPER
12	RADIATION SHIELD	Al MYLAR
13	THERMO. WIRES	CU AND COPPER
14	WIRE FOR HEATERS	NICHROME V

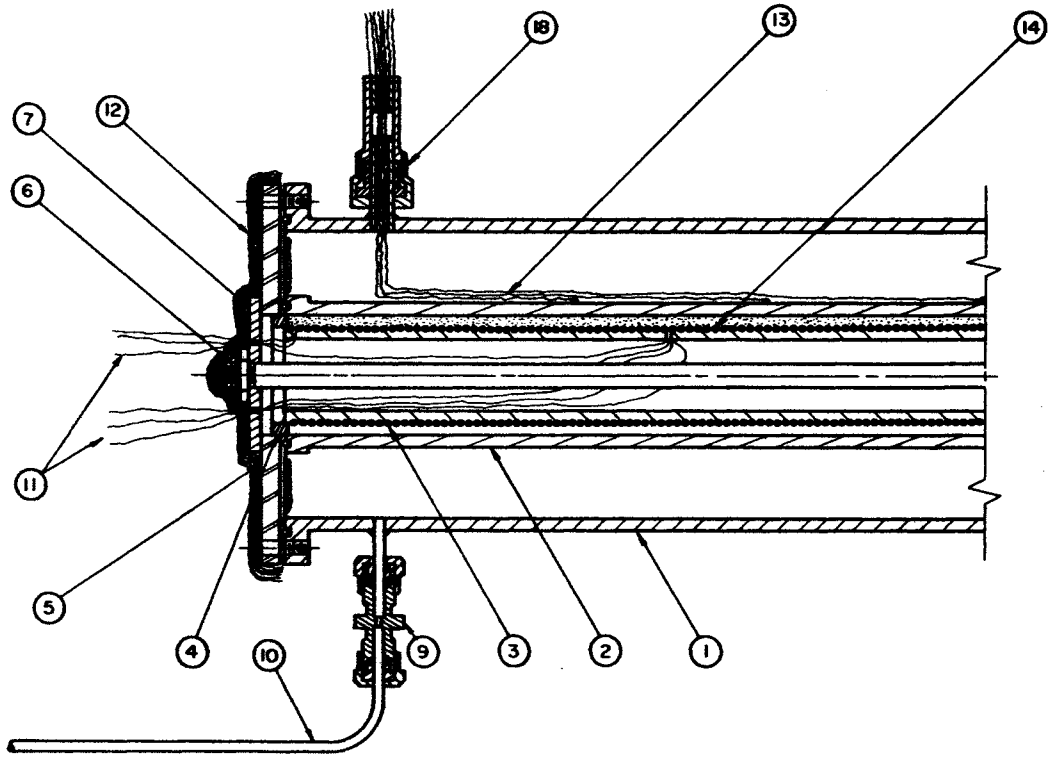

ASSEMBLY OF TYPICAL TEST SECTION

Figure 31. Schematic of Typical Test Section

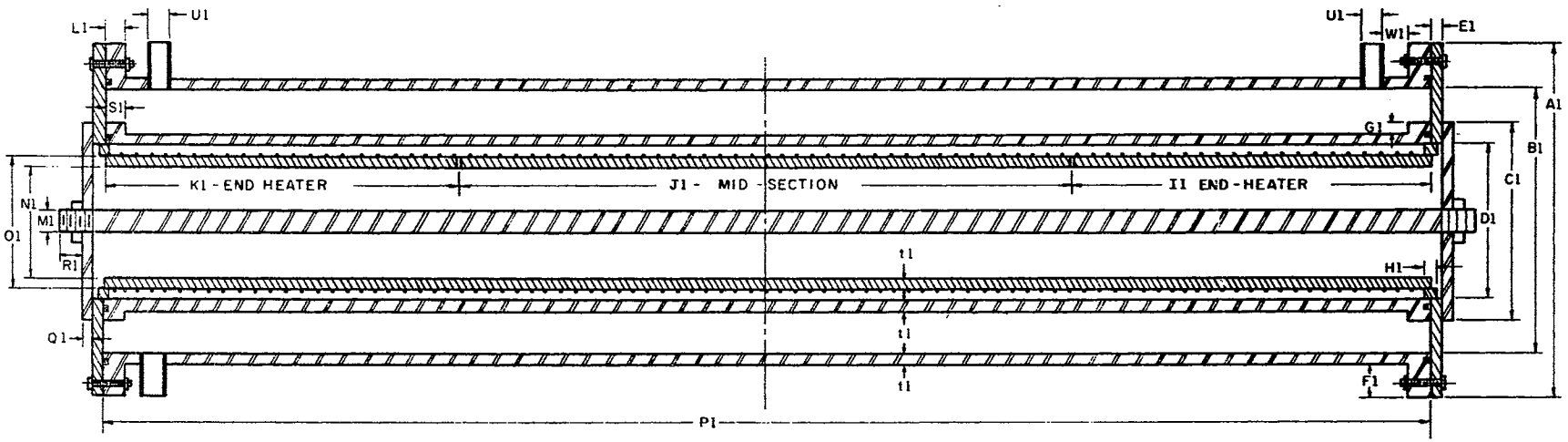

DIMENSION	MODEL - 1M	MODEL-2M	MODEL-3M	MODEL-1P	MODEL-2P	MODEL-3P	DIMENSION	MODEL-1M	MODEL-2M	MODEL-3M	MODEL-1P	MODEL-2P	MODEL-3P
A1	2.0"	2.00"	2.00"	4.00"	4.00"	4.00"	M1	0.125"	0.125"	0.125"	0.25"	0.25"	0.25"
B1	1.5"	1.50"	1.50"	3.00"	3.00"	3.00"	N1	0.375"	0.625"	0.125"	0.75"	0.75"	0.75"
C1	0.877"	1.127"	0.628"	1.625"	2.125"	1.25"	O1	0.500"	0.725"	0.25"	1.25"	1.45	0.500"
D1	0.625"	0.875"	0.375"	1.250"	1.750"	0.75"	P1	7.25"	7.25"	7.25"	14.50"	14.5"	14.500"
E1	3/32"	3/32"	3/32"	3/16"	3/16"	3/16"	Q1	1/16"	3/32"	3/32"	1/8"	1/8"	1/8"
F1	0.25"	0.25"	0.25"	0.50"	0.50"	0.50"	R1	3/8"	3/8"	3/8"	3/4"	3/4"	3/4"
G1	0.0625"	0.0625"	0.0625"	0.0625"	0.0625"	0.125"	S1	0.0625"	0.0625"	0.0625"	0.125"	0.125"	0.125"
H1	3/32"	3/32"	3/32"	3/16"	3/16"	3/16"	t1	0.0625"	0.0625"	0.0625"	0.125"	0.125"	0.125"
I1	1.995"	1.995"	1.997"	3.996"	3.996"	3.996"	U1	0.125"	0.0625"	0.125"	0.25"	0.25"	0.25"
J1	3.250"	3.250"	3.255"	6.508"	6.508"	6.508"	W1	0.60"	0.60"	0.60"	1.00"	1.00"	1.00"
K1	1.995"	1.995"	1.997"	3.996	3.996	3.996							
L1	0.125"	0.125"	0.125"	0.25"	0.25"	0.25"							

Figure 32. Prototype and Model Dimensions

attached to one tube and thermocouple feed-throughs were attached to the other two tubes. Prototype and model dimensions are listed in Figure 32.

Heaters

The heaters used in each test section, during the steady state investigation, consisted of a main heater and two guard heaters. These three heaters were made of fiberglass insulated nichrome wire spiral wrapped around a grooved phenolic tube. Each heater contained the same number of turns per inch and the same gage wire was used for all three heaters. Separate power and potential leads were connected to each of the three heaters. A list of the wire gages used in each test section is shown in Table XI.

For the transient investigation only one heater was used in each test section. This heater was made of 24 gage fiberglass insulated nichrome wire spiral wrapped around a grooved aluminum tube. Potential leads were connected to a 6.50 inch long section in the prototype and a 3.25 inch long section in the model. This was necessary in order to determine the power dissipated in the middle portion of the test section.

End Plates

The end plates were cut from a sheet of Lexan. This material had a thermal conductivity of approximately 0.11 Btu/hr ft$^{\circ}$F. This low value of thermal conductivity restricted the flow of heat, by conduction, between the inner and outer cylinders and made it easier to achieve isothermal cylinders. The Lexan had a maximum operating

temperature of approximately 250°F.

The inner surface of each end plate which was exposed to the annulus, was covered with aluminized mylar (two layers on prototypes and one on models). This reduced the amount of energy transferred to the ends by radiation. The mylar was not in contact with either cylinder.

Miscellaneous Parts

Several miscellaneous parts were used in assembling each test section. These miscellaneous parts included; phenolic spacer rings, viton o-rings, aluminized mylar, aluminum powder, aluminum rod, stainless steel washers, and aluminum screws. The locations of these parts are shown in Figure 31.

Assembly of Thermocouples, Power Leads, Potential Leads, and Gas Fill Line

The instrumentation attached to a test section consisted of thermocouples, power leads, electrical potential leads, and a gas fill line. The wire gages are listed in Table XI.

The thermocouple junction was formed by welding copper-constantan wires together. This junction was then shaped to fit the curvature of the test section. A spot of high vacuum grease was placed between the metal and the thermocouple junction to provide a good thermal contact. For the thermocouples on the inner cylinder, the lead wires were extended in an axial direction from each junction to the nearest end. At this point, they passed across the annulus and out through two small tubes. Ultra-Torr adapters were used to connect these small tubes to

TABLE XI

HEATER AND THERMOCOUPLE WIRE GAGES

Test Section	Heater Potential (Copper)	Wire Gage Current (Constantan)	Thermocouple Wire Gage (Copper-Constantan)
1 P	30	24	30
2 P	30	24	30
3 P	30	24	30
1 M	30	30	36
2 M	30	30	36
3 M	30	30	36

"Conax" thermocouple feed-throughs. The thermocouple junction and lead wires were kept in place by a light covering of epoxy cement. The thermocouples were located on the model and prototype as shown in Figure 40.

Two copper leads, enameled and fiberglass wrapped, were soldered to each end of the heater wires. These leads were passed through small holes in the wall of the heater core and out through the stainless steel washer. One of these leads was used for carrying current, and the other was used for electrical potential measurement. The soldered connections between the copper leads and the nichrome heater wire were coated with an enamel and a fiberglass resin.

All wires were polished for about twelve inches from the point where they left the test section. These wires were then extended and

soldered to a junction plate. This junction plate was used to facilitate the changing of test sections. The wires were extended from the junction plate to feed-throughs located in the chamber wall (See Figure 42).

Air was supplied to the test section through one-eighth inch diameter teflon tubing, as shown in Figure 42. An Ultra-Torr union was used to connect the teflon tubing to the test section (See Figure 31). This tubing was not modeled because of the low thermal conductivity and because the volume of the tubing was approximately two hundred times less than the volume of the smallest annulus.

Assembly of Test Sections

After installing the thermocouples, heater wires, power leads, and potential leads the cylinders were painted with "Velvet Coating 101-C10," a product of Minnesota Mining and Manufacturing Company. Both cylindrical surfaces of the outer cylinder and the outside surface of the inner cylinder were spray painted with this flat black paint to a mean thickness of approximately 0.003 inches.

At this point, the heater section was installed inside the inner cylinder and the space between these two parts was filled with atomized aluminum powder. Phenolic spacer rings were used to align the heater section within the inner cylinder. This assembly was placed inside the outer cylinder and the ends were installed. The ends were held in place by an aluminum rod passing axially through the test section and by aluminum screws located around the outer edge of each end. Each end was then covered with layers (six on prototype and 3 on model) of aluminized mylar.

Convection shields were used during the steady-state tests performed while the test sections were located in the vertical position. These shields were necessary to ensure that the power input to the main heater was transferred across the annulus to the outer cylinder. They were made of Lexan ($\frac{3}{32}$ -inch thick sheet for the prototype and $\frac{3}{64}$ -inch thick sheet for the model). A typical location of these shields is shown in Figure 41.

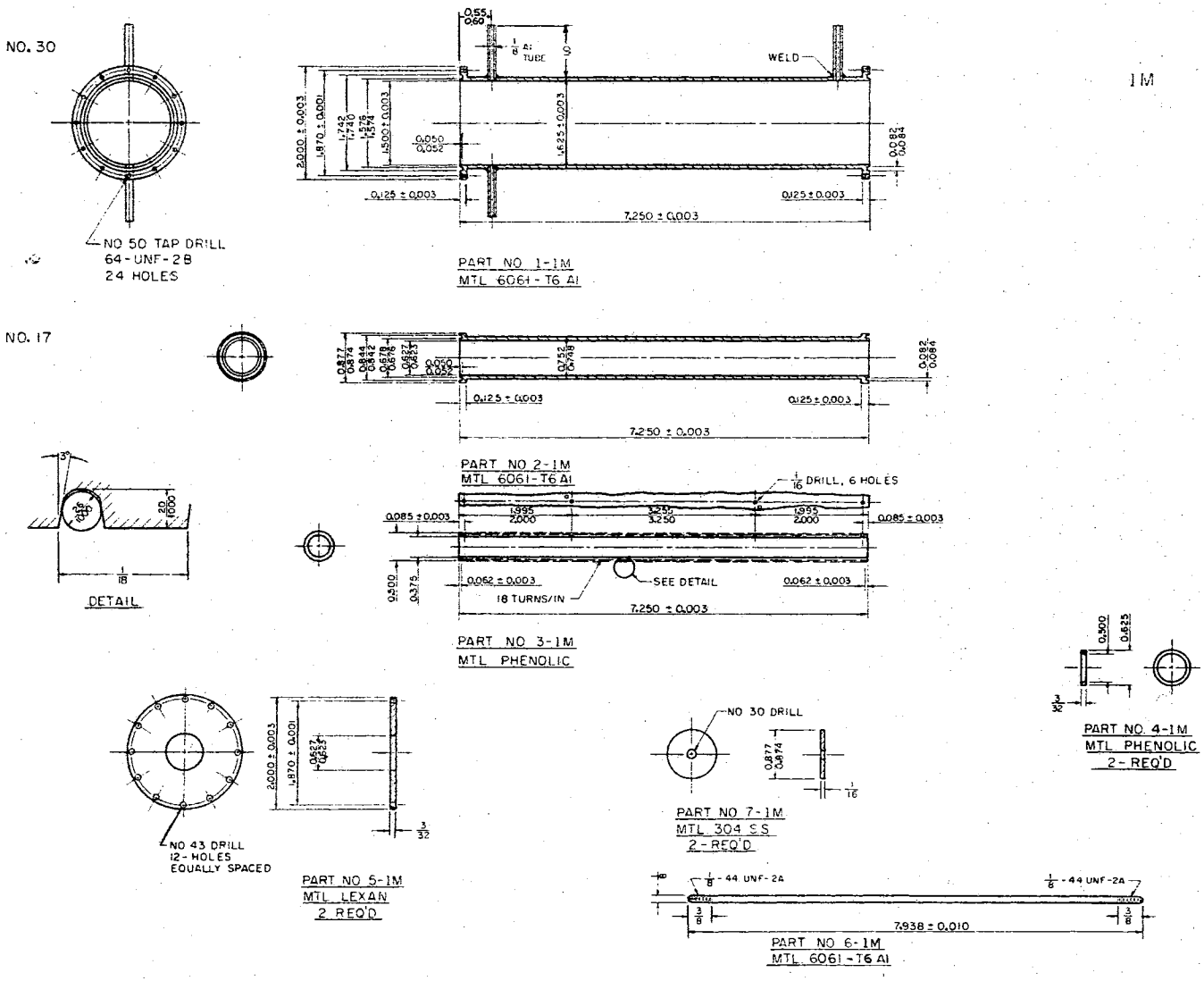

Figure 33. Test Section - 1M

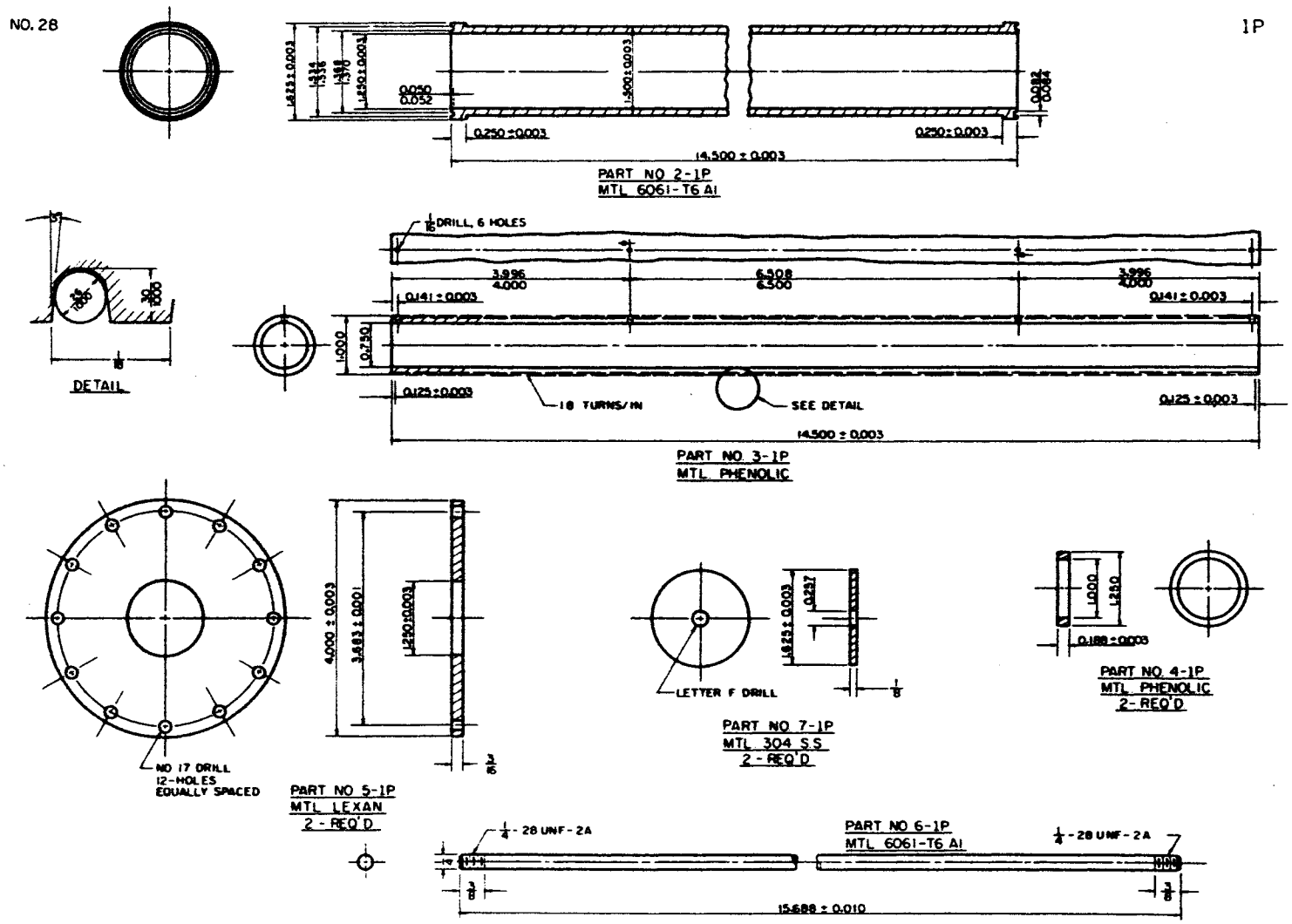

Figure 34. Test Section - 1P (Part One)

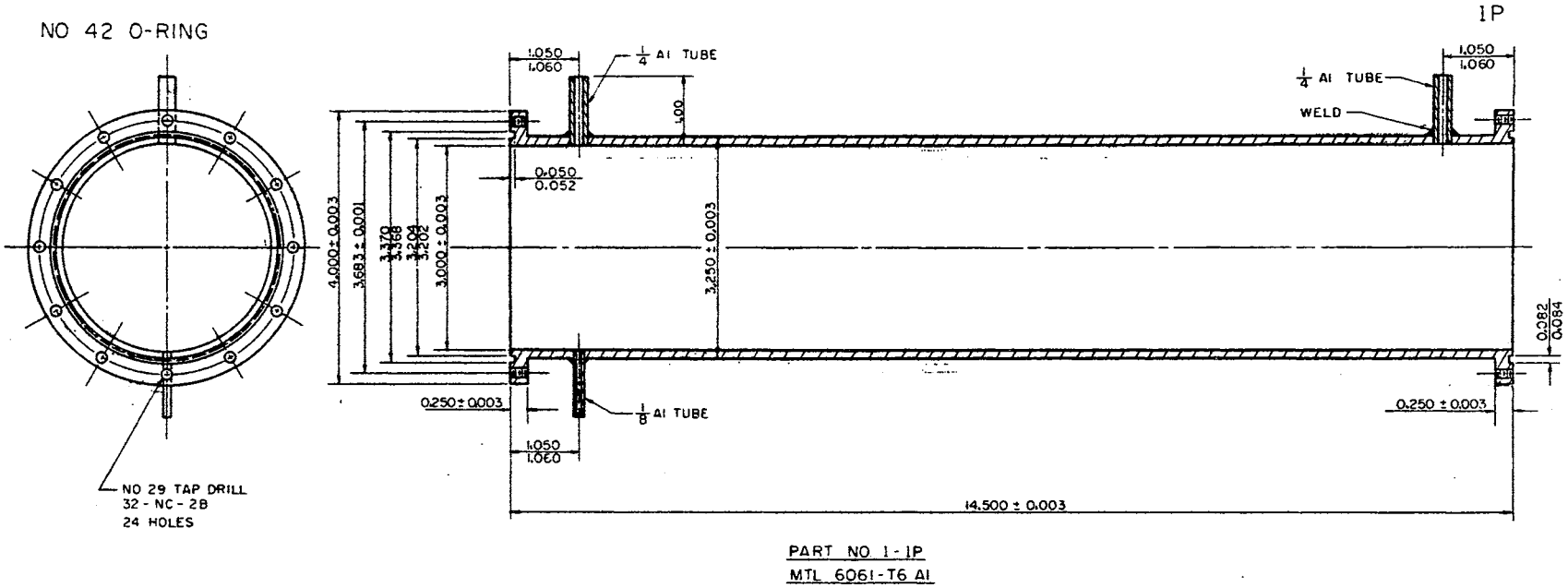

Figure 34. Test Section - 1P (Part Two)

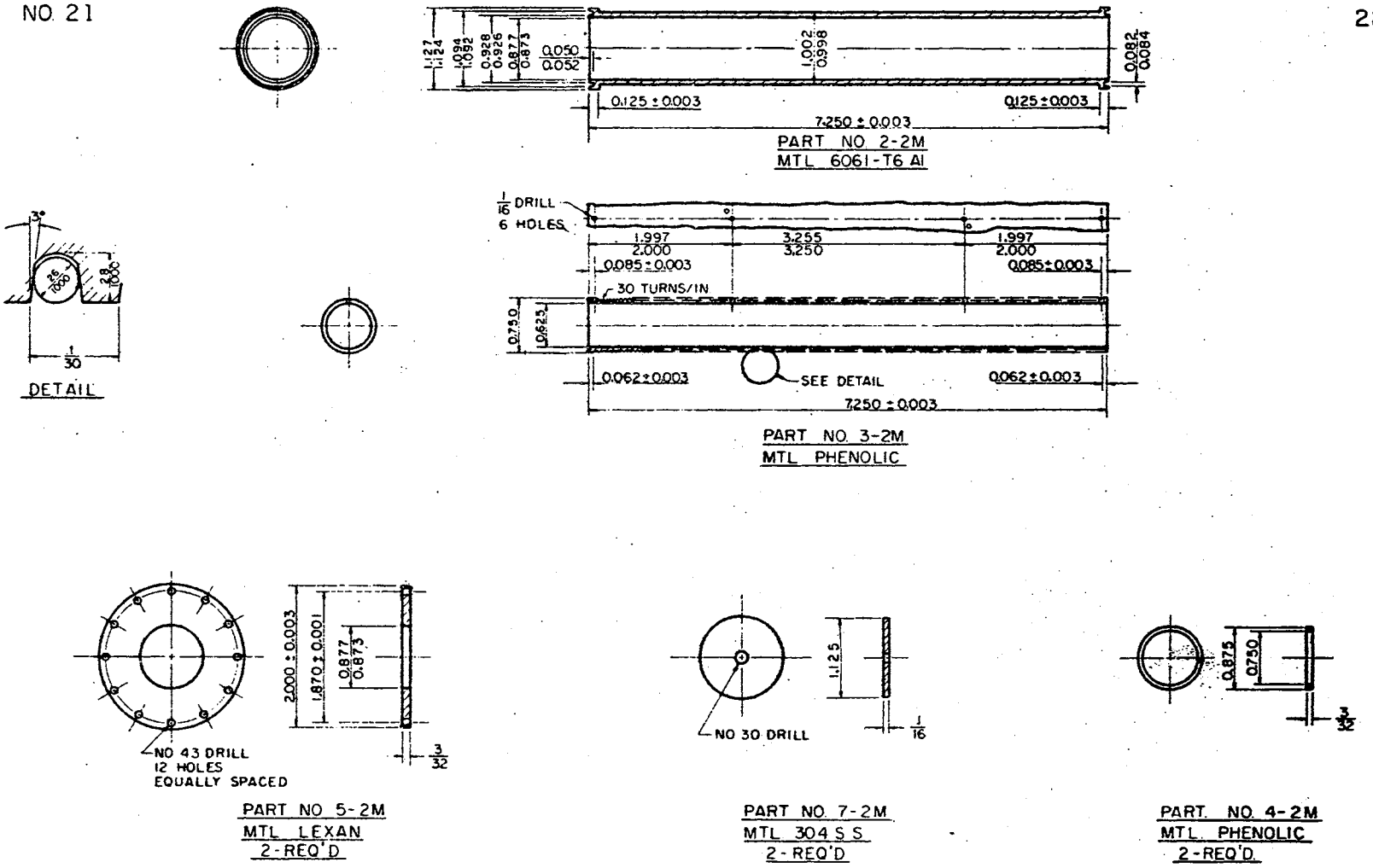

Figure 35. Test Section - 2M

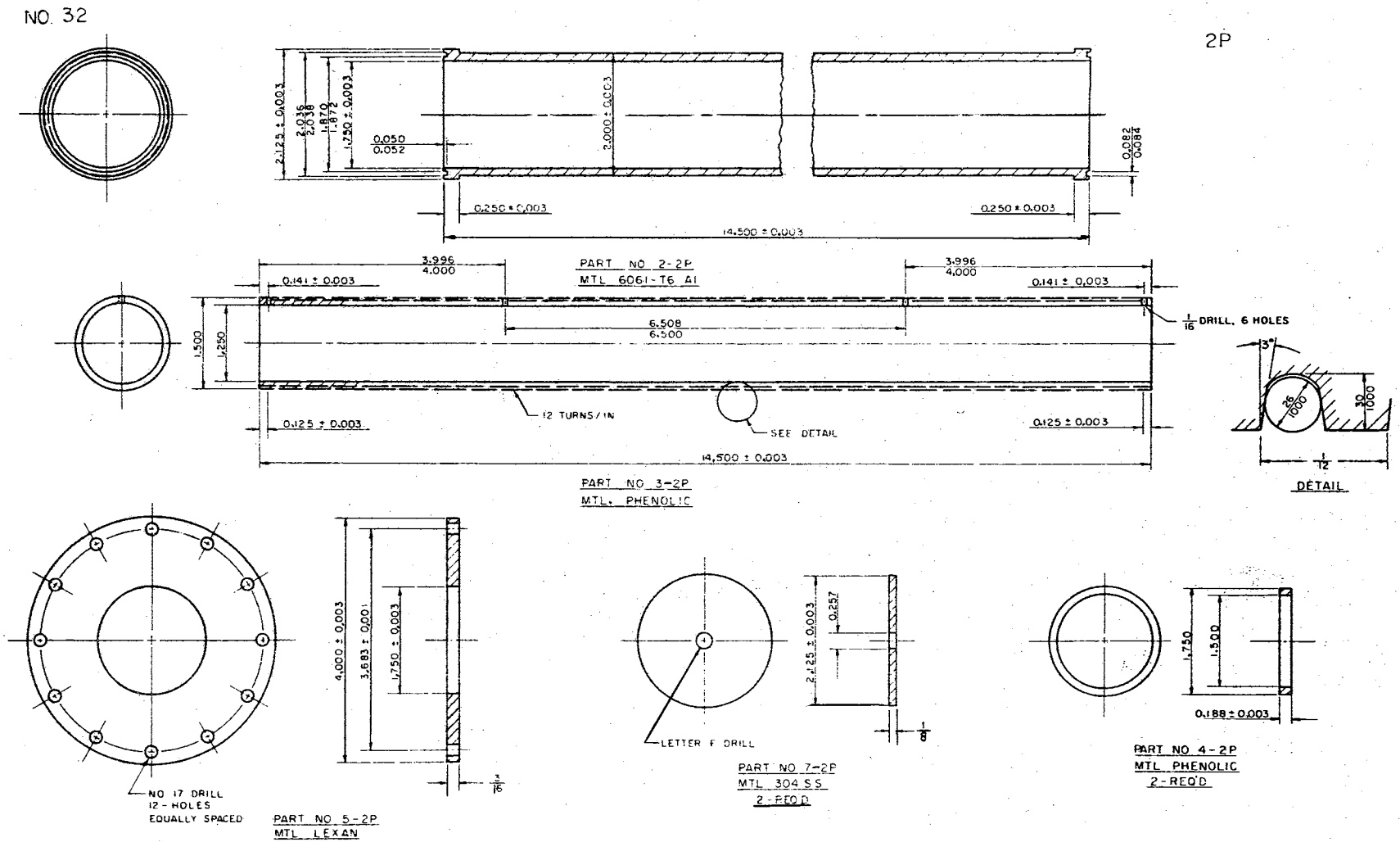

Figure 36. Test Section - 2P

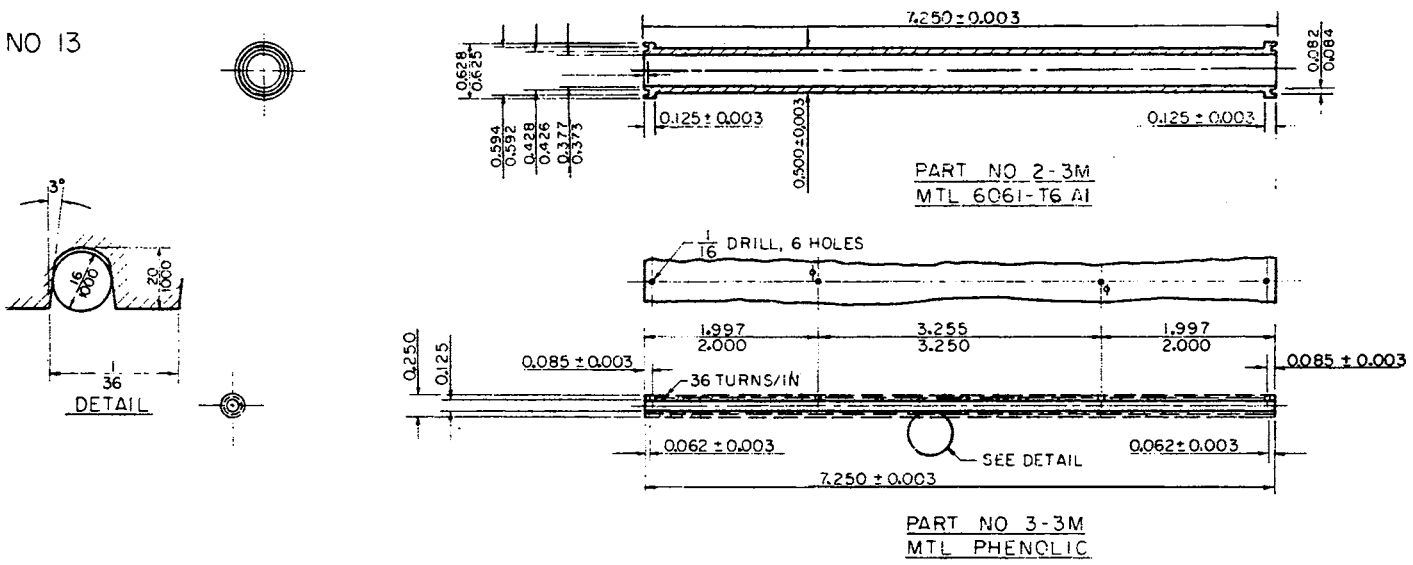

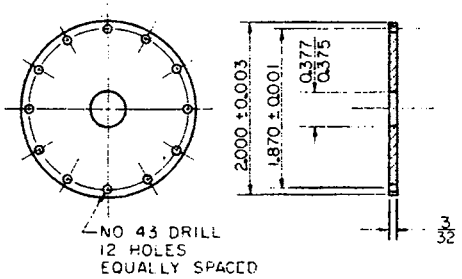

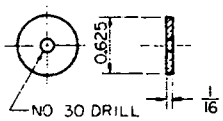

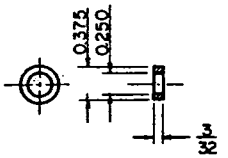

Figure 37. Test Section - 3M

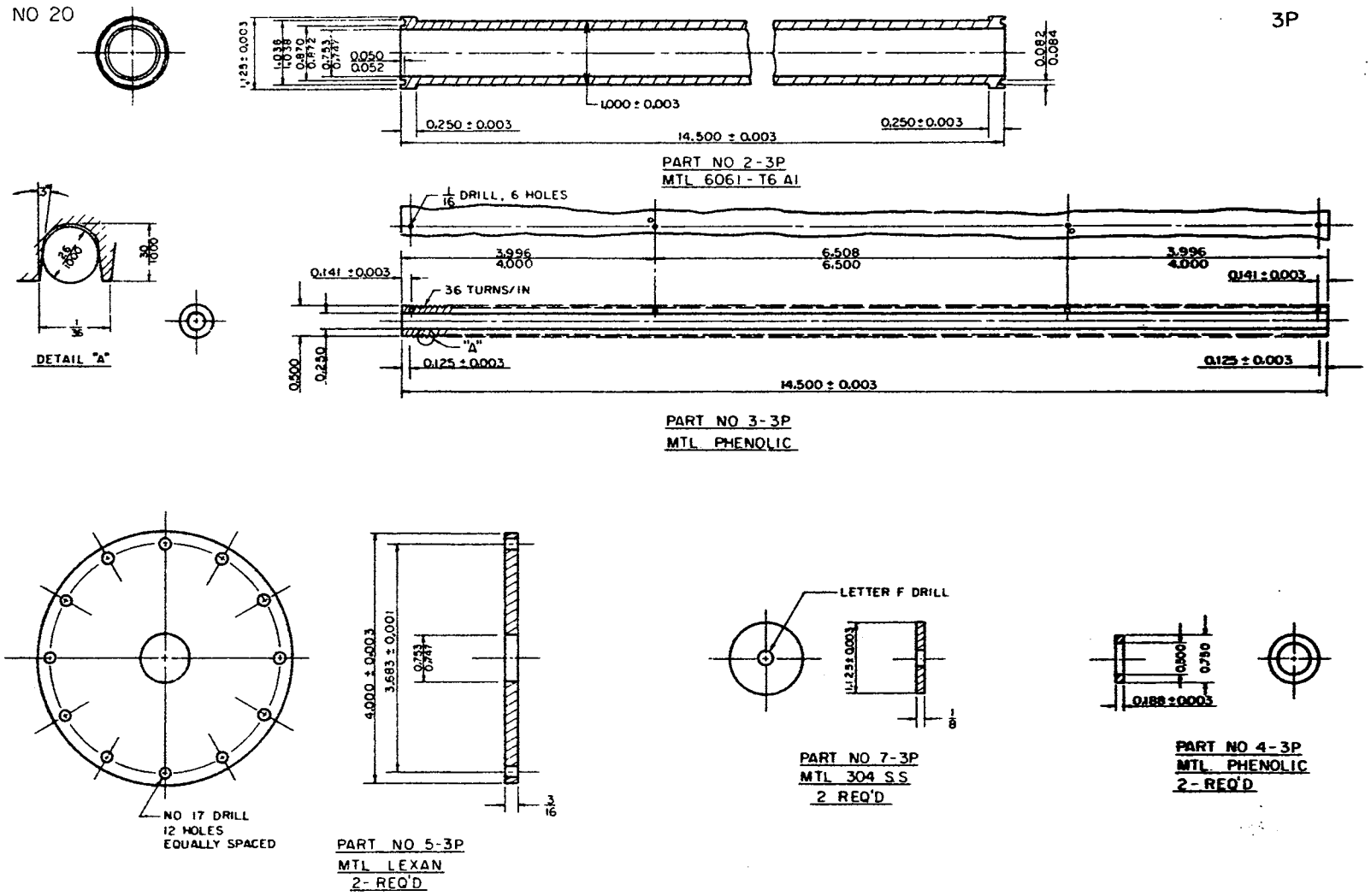

Figure 38. Test Section - 3P

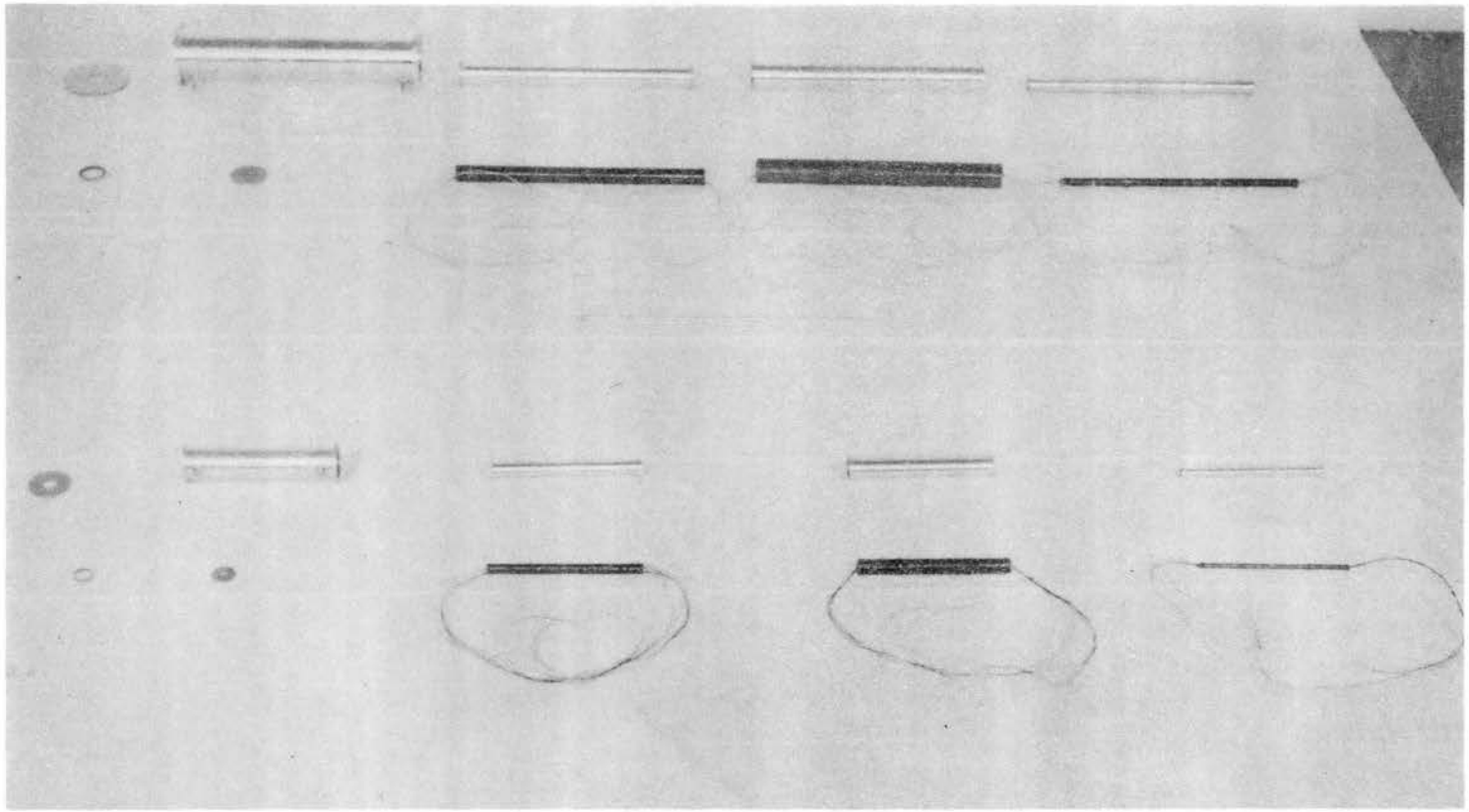

Figure 39. Photograph of Model and Prototype.

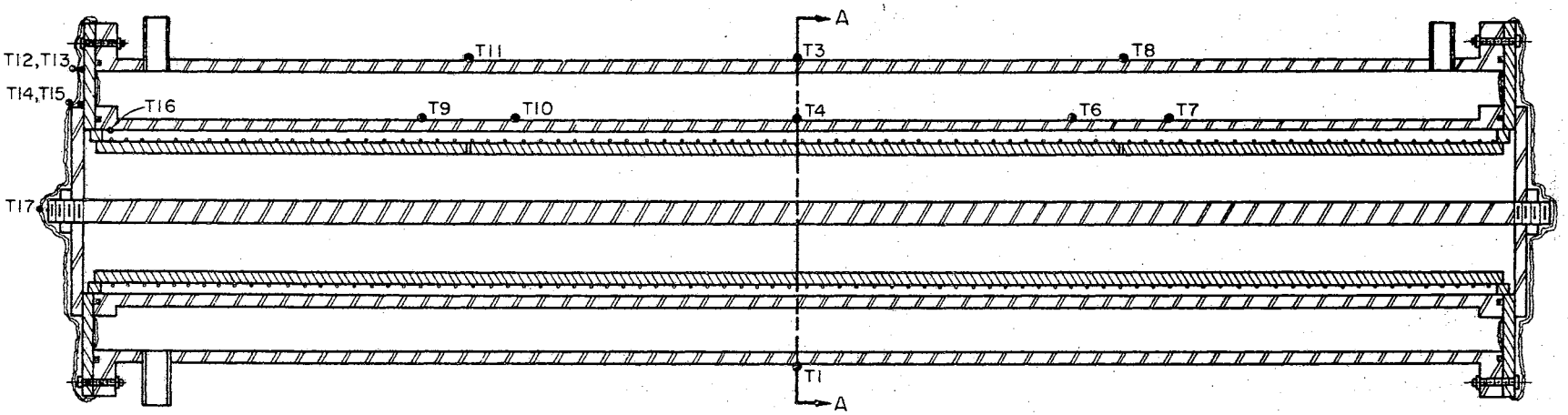

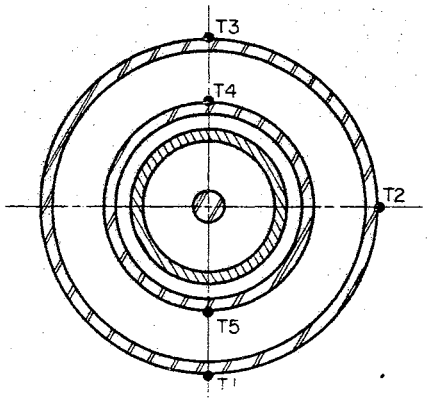

SECTION A-A

Figure 40. Location of Thermocouples on Test Section

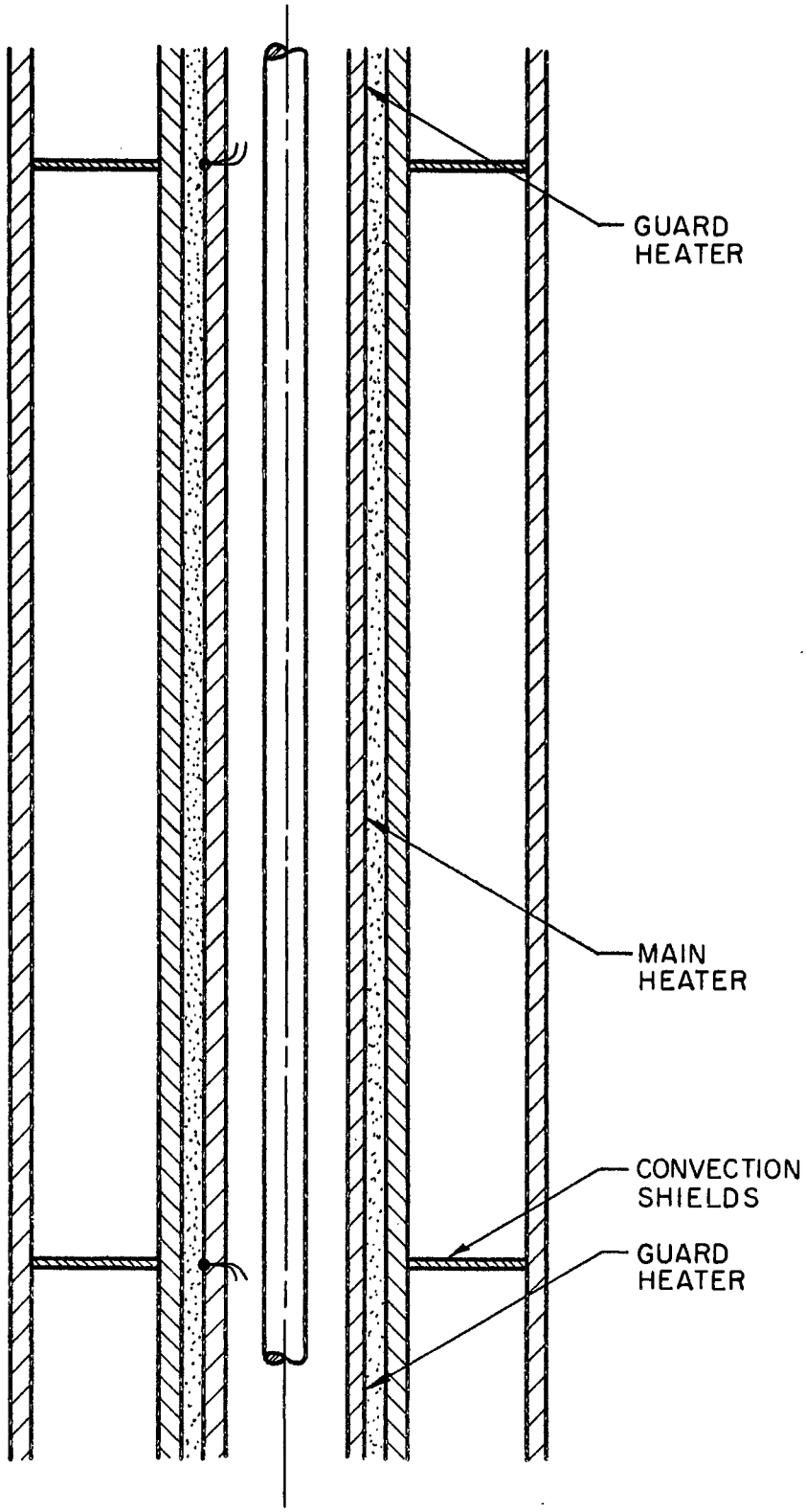

Figure 41. Schematic of Mid-Section for System IP Located Vertically

CHAPTER VI

EXPERIMENTAL PROGRAM

The thermal modeling criteria for a radiation-conduction-convection coupled heat transfer problem were developed in Chapter III. In order to verify this modeling criteria, the systems described in Chapter V were constructed and tested. The modeling criteria were used to predict the thermal behavior of a prototype from tests performed on a geometrically similar model. Tests were then performed on the prototype in order to verify the predicted results.

All test were conducted with each test section located inside a space simulation chamber. The chamber provided the necessary low temperature-low pressure environment so that an accurate prediction of the energy exchange between the system and the surroundings could be made. A description of the test facility and the experimental procedure is given in the following sections.

Description of Test Facility

The test facility consisted of a space simulation chamber, power supply equipment, data measuring equipment, and the concentric cylinder test sections. The test sections were described in Chapter V. A schematic of the test facility is shown in Figure 42 and photographs are shown in Figure 43.

Space Simulation Chamber

The space simulation chamber was a standard piece of test equipment in the heat transfer laboratory. The chamber consisted of a horizontal stainless steel cylinder, four feet long and two feet in diameter, and two removable stainless steel flanges. The chamber pressure was reduced to approximately 1×10^{-5} torr (mm of Hg) by a rotary mechanical pump in series with a six inch oil diffusion pump (See Figure 44) for pump-down characteristics. A freon cooled baffle was used to prevent diffusion pump oil from entering the simulation chamber. The baffle was the evaporator of a small freon refrigeration system. The chamber was equipped with feed-throughs for thermocouples, heater power, potential leads, liquid nitrogen, and gas to control the density between the concentric cylinders.

In order to obtain a low temperature environment, the main chamber was equipped with an inner chamber liner. The liner was constructed of copper and consisted of a twenty-six inch long, twenty inch diameter cylinder with an optically tight baffle on one end and a removable flange on the other end. A continuous piece of one quarter inch diameter copper tubing was attached to each part of the baffle and spiral wrapped around the cylinder. Liquid nitrogen was forced through the copper tubing and discharged to the atmosphere. A liquid level controller was used in conjunction with a solenoidally operated valve to control the flow of nitrogen and to ensure that liquid was in the tubing at all times during a test. The inner wall of the liner was coated with flat black paint (velvet coating 101-C10) in order to ensure surfaces with high and uniform values of emittance and absorptance [26]. Conduction from the outer chamber wall to the liner was

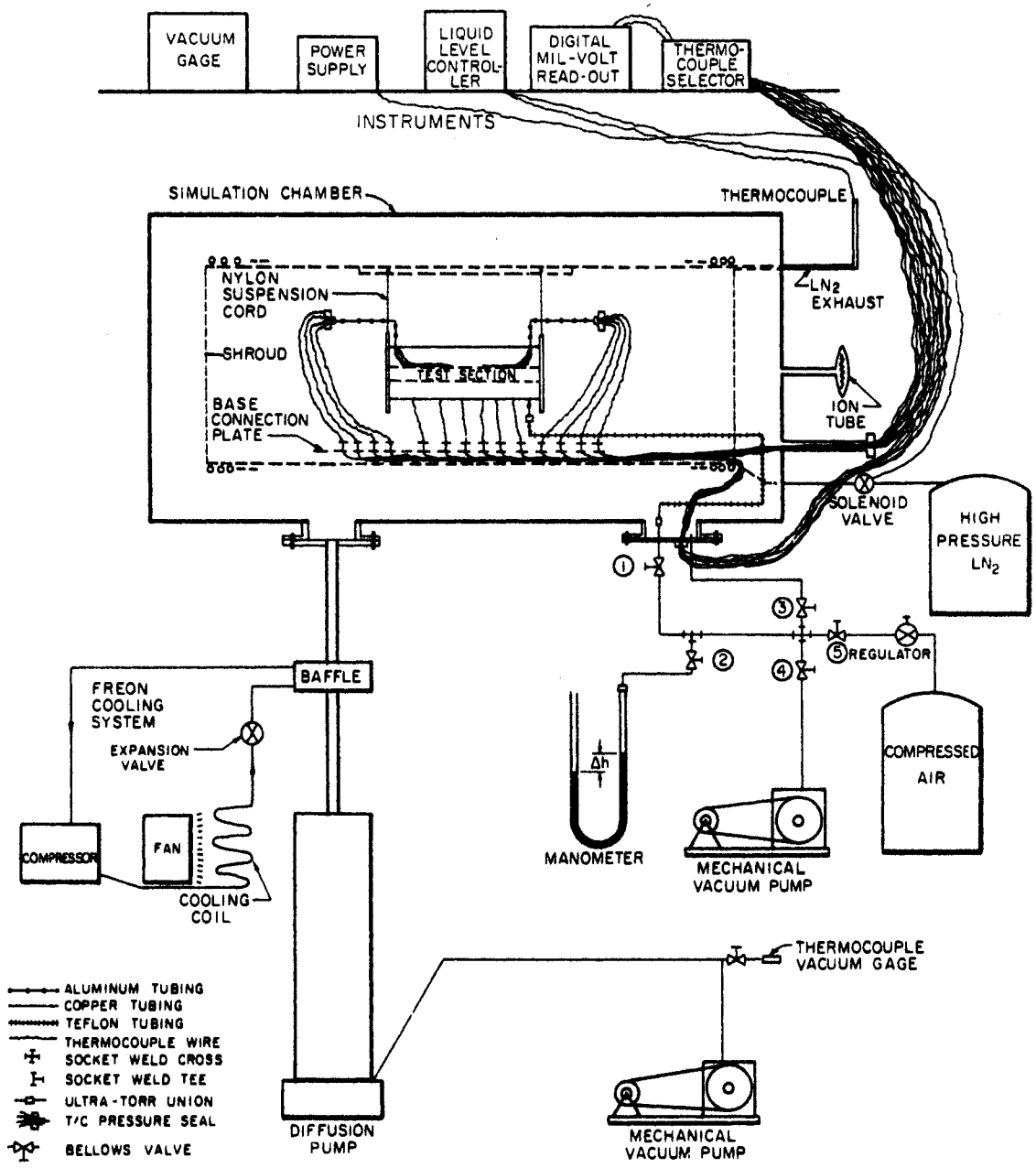

Figure 42. Schematic of Test Facility

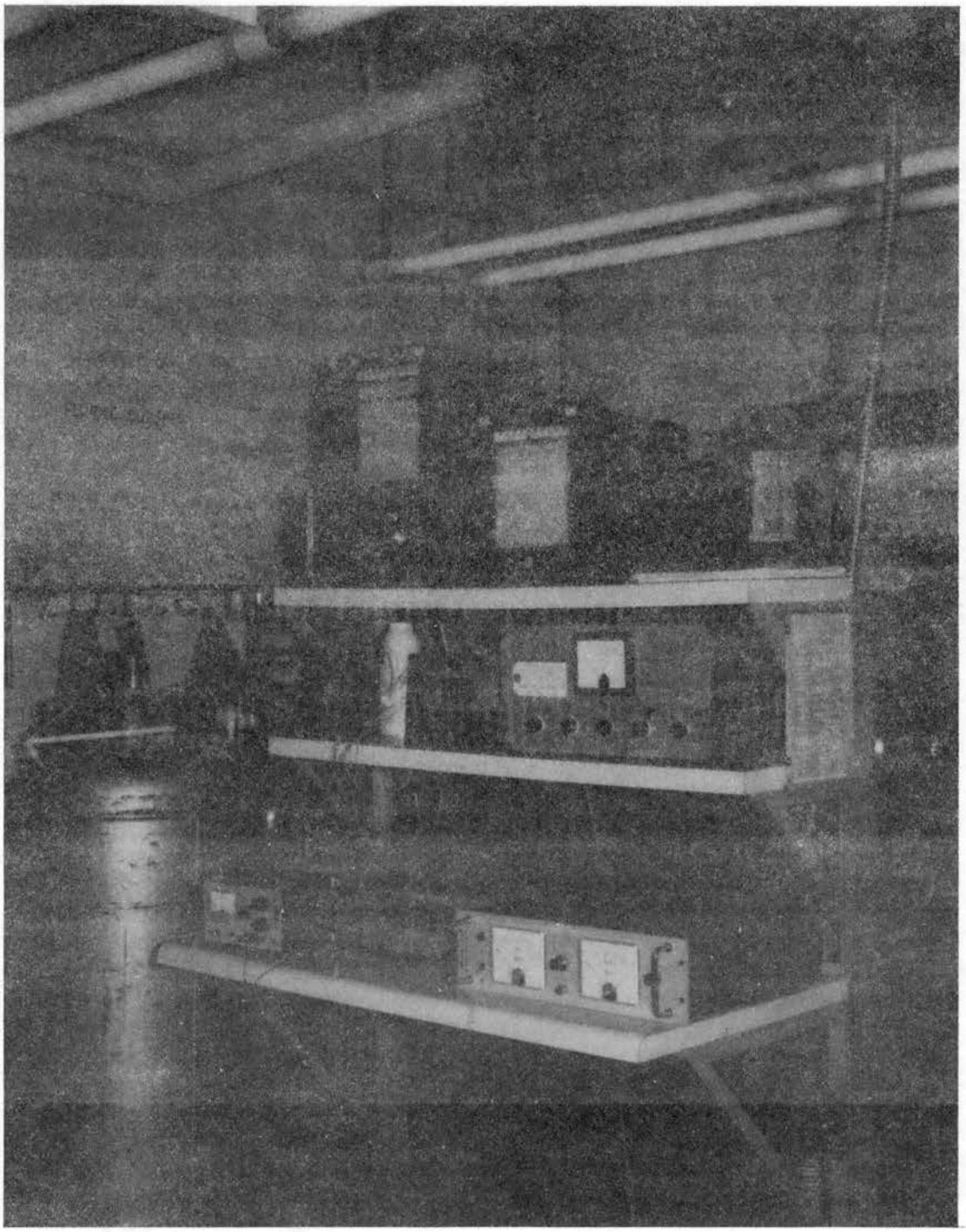

Figure 43. Photograph of Test Facility.

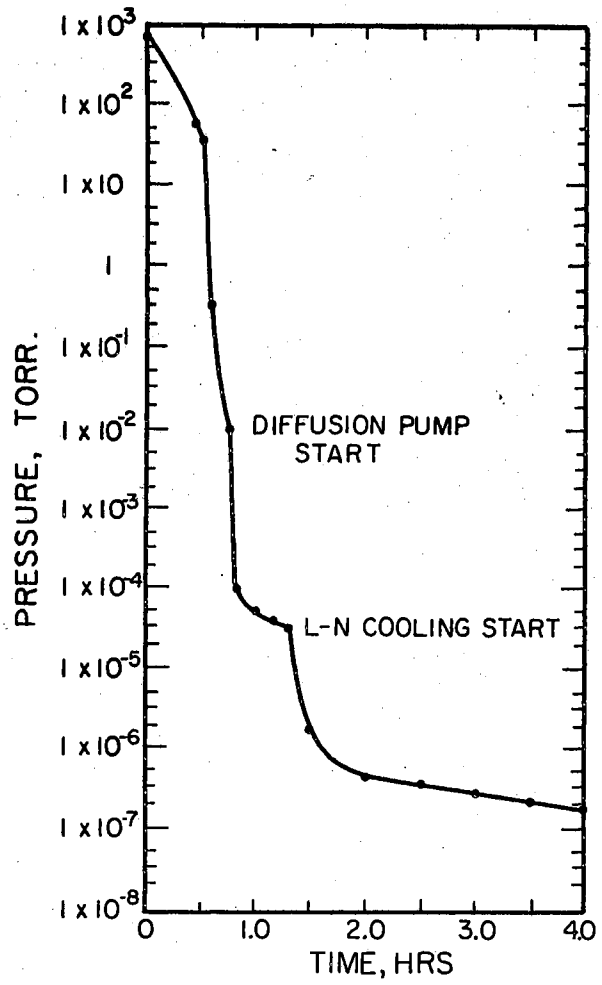

Figure 44. Pump-Down Characteristics of Chamber

minimized by supporting the liner on three legs. During testing, the chamber was maintained at a pressure below 1 x 10^{-6} torr. The cylinder and baffle end of the liner were maintained at a temperature of 160 degrees Rankine. Tests showed that the removable liner flange temperature was below 185 degrees Rankine.

Positions of Test Section

Various tests were performed with the test sections located in the horizontal and vertical positions. For these two positions, each test section was centrally located within the liner. The horizontal position was attained by extending nylon cords from a small rod passing through the liner to each end of a test section. The vertical position was attained by extending a single nylon cord from the rod to one end of the test section. The nylon cord was very long in comparison to the diameter in order to minimize conduction losses. Photographs of the two different positions of a test section are shown in Figure 45.

Temperature Measuring Equipment

The thermocouple output, for steady state conditions, was obtained from a digital voltmeter. This voltmeter had a reproducible accuracy of $\pm$ 0.005 millivolt or approximately $\pm$ 0.25 degree in the temperature range of the experimental work. The digital voltmeter was calibrated with a Leeds and Northrup Model 8686 portable potentiometer. During all tests, the thermocouple reference junction was maintained at $32^{o}F$ with an ice bath.

Before each test the test section was exposed to a vacuum environment at ambient temperature for several hours. At this equilibrium condition the output of all thermocouples on the test section and the liner were within $\pm$ 0.002 millivolt of each other. Therefore, it was reasonable to assume that temperatures were measured to an accuracy of at least + 0.75 degrees during steady state test.

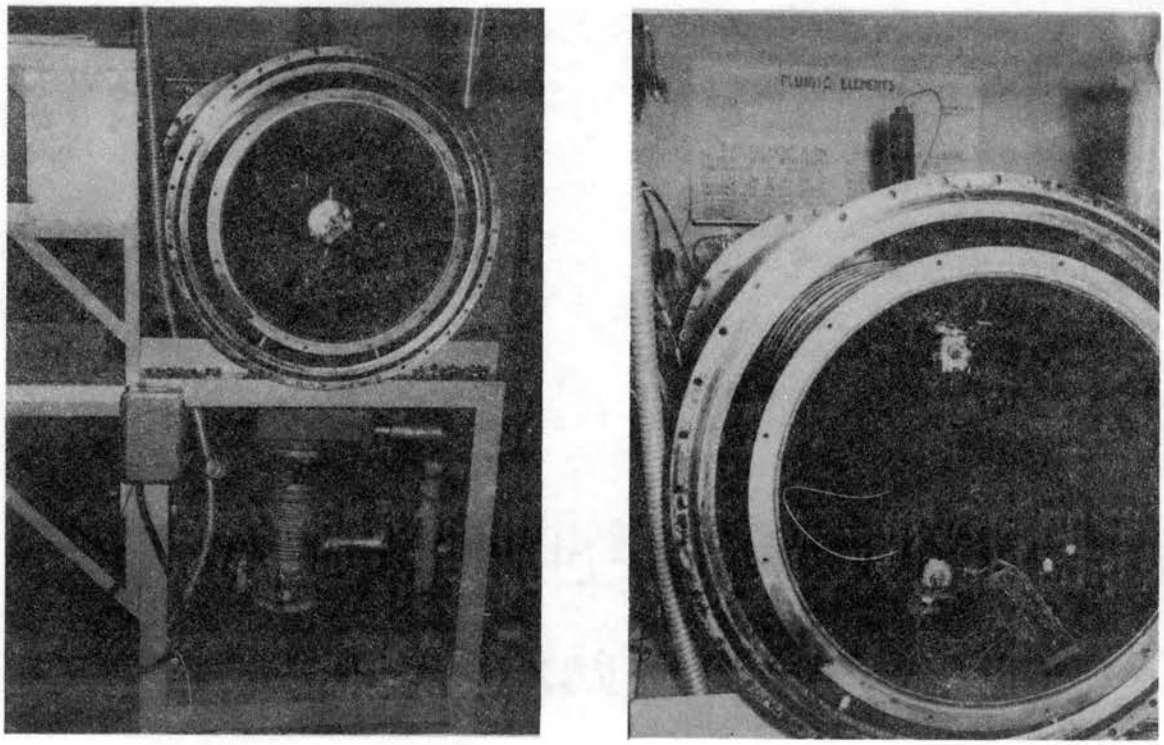

Figure 45. Photographs of Prototype Mounted Vertically and Horizontally in the Space Simulation Chamber.

Power Supply and Measuring Equipment

Steady state testing was performed on systems containing three heaters (two guard heaters and one main heater). For the steady state testing, separate D-C power supplies were used to provide power to each heater.

These power supplies were hand controlled to within ± 1 millivolt during test runs.

Current input to a heater was determined by measuring the voltage drop across a calibrated shunt in series with the heater. The voltage drop across the shunt was measured with the same self balancing potentiometer which was used to measure thermocouple output. The shunt resistance was measured to within ± 0.10 per cent with a Kelvin bridge. Separate leads were provided to each heater for potential measurement. The potential drop across each heater was measured with a digital voltmeter. This instrument had a four digital display and was calibrated to ± 0.01 volt accuracy. The input impedance of the digital voltmeter was greater than one megohm.

Pressure Measuring Equipment

The pressure of the gas between the concentric cylinders was measured with a mercury manometer connected in the gas supply heater as shown in Figure 42. This pressure was measured while the test section was at ambient temperature. The manometer was read to within about ± 0.025 inch. The space simulation chamber pressure was measured with an ion gage.

Experimental Procedure

A definite procedure was followed in installing and testing each test section. During testing, only one test section was located in the space simulation chamber.

Steady State Testing

The test section was installed within the liner, and the necessary feed-throughs were connected to the equipment located outside the chamber. After completing these connections the linear and chamber flanges were installed. Air was then supplied to the test section, through the gas fill line, until the desired density was obtained. The thermocouples were checked for equality of output and the pressure and temperature of the gas were recorded. All valves on the gas header were then closed and pump-down of the chamber was started.

After several hours of pumping, the chamber pressure reached an equilibrium state of approximately 1×10^{-5} torr. At this equilibrium state the pressure and temperature of the gas were checked to determine if any leaks had developed. If the density of the air within the test section was not affected by pump-down, then all valves on the gas header were closed and cool-down was started by allowing liquid nitrogen to flow through the copper tubing around the liner. The test section was protected from temperature extremes by adjusting the power input to the heater during the cool-down period. Cool-down time was approximately six hours. After cool-down the chamber pressure was approximately 1×10^{-6} torr.

After cool-down, the power input to the main heater was set to the desired value and the inputs to the guard heaters were adjusted until no temperature gradient existed in the axial direction. When thermal equilibrium existed all temperatures and power inputs were recorded. Thermal equilibrium was assumed to exist when the temperature charge at all thermocouples was less than one half degree per hour.

At this time, the power input to the main heater was changed to a high selected value and the inputs to the guard heaters were changed until no axial temperature gradient existed. Sufficient time was allowed for the test section to reach a new thermal equilibrium state. At this new thermal equilibrium state, all temperatures and power inputs were recorded. This process was continued until the selected range of power inputs to the main heater had been covered. After completing these tests, the flow of liquid nitrogen was stopped and sufficient time was allowed for the test section to return to ambient temperature. The test section was again protected from temperature extremes by controlling the power input to the heater. With the test section at ambient temperature, the gas pressure and temperature were checked to ensure that a constant density of gas was present during testing. The chamber pressure was approximately 1×10^{-5} torr.

At this point, the gas density was changed to a new selected value and the above procedure was repeated until the desired range of densities were covered. During one set of tests, the annulus between the concentric cylinders was exposed to chamber pressure. This was necessary in order to check the validity of the model used to predict the radiant exchange between the concentric cylinders.

Before performing tests on a geometrically similar model, the density of the air in the model had to be determined so that the convective heat transfer would be modeled. This was done by using the convective film coefficient correlation and the modeling criteria presented in Table V. The convective film coefficient correlation was determined from tests performed on the prototype (See Chapter VII). The resulting correlation is

$$Nu = (0.354 + 0.245\ \delta/di)(Gr)^{0.251}\, e^{-.015\delta/di} \qquad (6\text{-}1)$$

Equation (6-1) was applied to the model and the prototype and the following equation was obtained

$$\frac{\left(\frac{h\delta}{k}\right)_m}{\left(\frac{h\delta}{k}\right)_p} = \left[\frac{Gr_\delta}{Gr_\delta}\right]_p^{0.25}_m . \qquad (6\text{-}2)$$

For Technique I of the modeling criteria listed in Table V, Equation (6-2) reduces to

$$\frac{\rho_m}{\rho_p} = \frac{\mu^* \delta^{*\frac{1}{2}}}{\sqrt{\Delta T^* \beta^*}} \left(\frac{h^*}{k^*}\right)^2 = 0.707 , \qquad (6\text{-}3)$$

and for the Zero Surroundings Technique with constant thermal properties within the solid components, Equation (6-3) reduces to

$$\frac{\rho_m}{\rho_p} = 2.828 \mu^* / k^{*2} . \qquad (6\text{-}4)$$

In order to check the validity of Technique I of the modeling criteria, the density of the air in the model was scaled according to Equation (6-3). During testing of the model, the power input to the main heater was scaled according to

$$\frac{q_m}{q_p} = e^{*2} . \qquad (6\text{-}5)$$

The same procedure was followed in testing the model as was followed in testing the prototype.

Tests were also conducted on each model in order to verify the Zero Surroundings Technique. The density of the air in the model was scaled according to Equation (6-4) and the power input to the main heater was scaled according to

$$q^* = \left(e^*\right)^{\frac{2}{3}}. \tag{6-6}$$

Equations (6-5) and (6-6) were developed in Chapter III.

CHAPTER VII

RESULTS OF EXPERIMENTAL INVESTIGATION

The experimental investigation was conducted using the facility described in Chapter VI. This investigation included steady-state testing of the concentric cylinder test sections described in Chapter V. The steady-state investigation included testing of three prototypes and three one-half scale models located in the horizontal position and one prototype and one model located in the vertical position. Each test section was tested in accordance with the procedure described in Chapter VI.

The results of the tests performed without air in the annulus were used to check the validity of the thermal modeling criteria for a radiation-conduction coupled heat transfer problem. These results were also used to check the validity of the mathematical model used to predict the radiant exchange between the concentric cylinders. Tests were also performed with air in the annulus of each test section. These results were used to check the validity of the modeling criteria for a radiation-conduction-convection coupled heat transfer problem.

Tests were performed on the prototypes and models in accordance with the parameters listed in Table XII. The values of the parameters T^* and q^* were obtained from the modeling criteria listed in Table VI for a scaling factor of one-half. The density ratio, for a given test, was obtained from the modeling criteria and the free-convection

TABLE XII

CALCULATED VALUES OF SIMILARITY PARAMETERS

		TECHNIQUE I						ZERO SURROUNDINGS TECHNIQUE					
		Horizontal Annuli			Vertical Annuli			Horizontal Annuli			Vertical Annuli		
TEST SECTION	TEST NO.	q^*	T^*	ε^*	q^*	T^*	ε^*	q^*	T^*	ε^*	q^*	T^*	ε^*
1 M	1	0.25	1.0	0.707	0.25	1.0	0.707	0.63	1.26	0.098	0.63	1.26	0.098
1 M	2	0.25	1.0	0.707	0.25	1.0	0.707	0.63	1.26	0.25	0.63	1.26	0.26
1 M	3	0.25	1.0	(Vac.)	0.25	1.0	(Vac.)	0.63	1.26	(Vac.)	0.63	1.26	(Vac.)
2 M	1	0.25	1.0	0.707				0.63	1.26	0.098			
2 M	2	0.25	1.0	0.707				0.63	1.26	0.257			
2 M	3	0.25	1.0	(Vac.)				0.63	1.26	(Vac.)			
3 M	1	0.25	1.0	0.707				0.63	1.26	0.101			
3 M	2	0.25	1.0	0.707				0.63	1.26	0.254			
3 M	3	0.25	1.0	(Vac.)				0.63	1.26	(Vac.)			

heat-transfer coefficient.

Free-Convection Heat-Transfer Coefficients

During testing, the test sections were located in two different positions (horizontal and vertical). Therefore, two different free-convection heat-transfer coefficients were necessary in order to predict the amount of energy convected across the annulus. These coefficients were obtained from steady-state tests performed on the prototypes. The procedure used to obtain these coefficients is presented in the following sections. Only the power input to the main heater was used in obtaining these coefficients.

Correlation of Data for Free-Convection Heat-Transfer Between Horizontal Concentric Cylinders

During testing with air in the annulus, energy was transferred between the concentric cylinders by radiation and convection. The power input to the main heater was equal to the total energy transferred across the annulus over a known length of the cylinders. This input was related to the exchange between the cylinders by

$$q = q_c + q_r \tag{7-1}$$

where q_r and q_c are the heat transfers across the annulus by radiation and convection, respectively. These two modes of heat transfer had to be separated in order to obtain the desired convection correlation.

The net radiant exchange between the concentric cylinders was calculated by

$$q_{2 \rightleftarrows 5} = \frac{A_2 \sigma \quad (T_2^4 - T_5^4)}{(\frac{1}{\epsilon_2} - 1)\ (1 + \frac{A_2}{A_5}) + 1} \qquad (7\text{-}2)$$

Tests performed on the prototype, without air in the annulus, were used to check the validity of Equation (7-2). The input to the main heater and the corresponding value predicted by Equation (7-2), for several tests, are shown in Table XIII. The maximum difference between the predicted and measured radiant exchanges was less than 5.0 per cent.

TABLE XIII

MEASURED AND PREDICTED RADIANT EXCHANGE BETWEEN THE CONCENTRIC CYLINDERS OF EACH TEST SECTION

Test Section No.	Per Cent Error	Input to Main Heater	Calculated From Eq. (7-2)
	Horizontal Test Section		
1p	-3.94	48.78	50.70
1p	-4.68	23.36	24.45
2p	-4.93	48.50	50.89
2p	-3.23	23.52	24.28
3p	-1.395	48.75	49.43
3p	-1.362	23.45	23.77
	Vertical Test Section		
1p	-3.04	46.40	47.81
1p	-3.97	22.40	23.29

The energy transferred across the annulus by convection was obtained from Equation (7-1) and the film coefficient was obtained from

$$q_c = h A \Delta T. \tag{7-3}$$

The desired correlation was obtained by using the method of least squares to obtain the constants n, m, and c in the following equation:

$$Nu = c\,(Gr)^m\, e^{n\left(\frac{\delta}{d_i}\right)}. \tag{7-4}$$

Details of the curve fit are given in Appendix E and the resulting correlation for the test sections located in the horizontal position is

$$Nu = (0.354 + 0.245\delta/d_i)(Gr)^{0.251}\, e^{-.015\delta/d_i}. \tag{7-5}$$

Equation (7-5) is shown in Figure 46. As a matter of comparison, a correlation from the literature is shown in this figure.

Correlation of Data for Free-Convection Heat-Transfer between Vertical Concentric Cylinders

The energy convected across the annulus, as a result of input to the main heater, was necessary in order to obtain the desired convection heat-transfer correlation. This was obtained from

$$q = q_c + q_r + q_k, \tag{7-6}$$

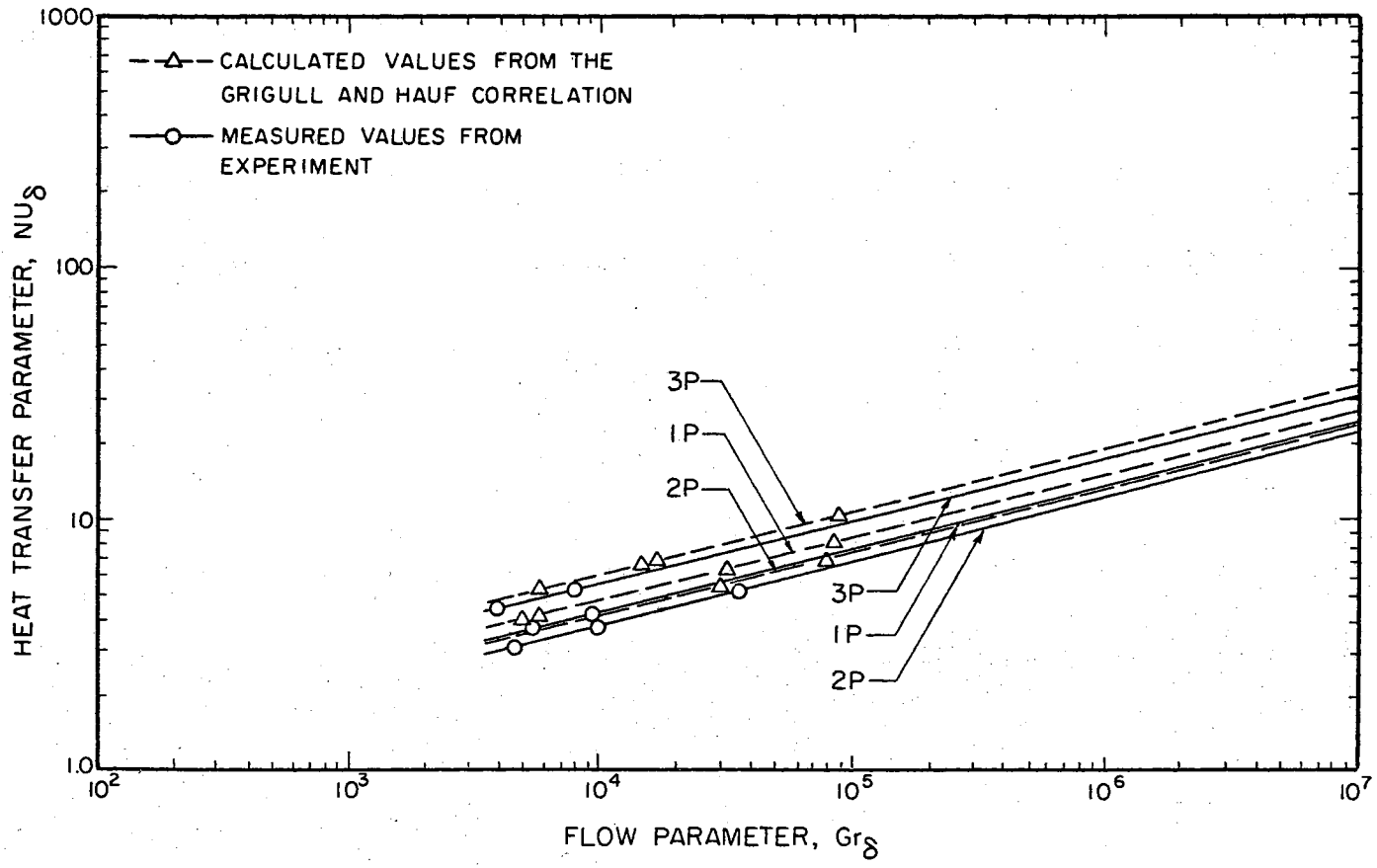

Figure 46. Comparison of Free-Convection Heat-Transfer Correlations for Horizontal Concentric Cylinders.

where q_k is the energy conducted across the annulus through the Lexan convection shields. The amount of energy transferred across the annulus through these shields was estimated by

$$q_k = 2\pi k L \frac{\Delta T}{\ln \frac{r_o}{r_i}} \tag{7-7}$$

The net radiant exchange was obtained from

$$q_r = \frac{A_2 \sigma \left(T_2^4 - T_5^4\right)}{\left(\frac{1}{\epsilon_2}\right) - \left(1 + \frac{A_2}{A_5}\right) + 1} . \tag{7-8}$$

Tests were performed on the prototype, without air in the annulus, in order to check the validity of Equation (7-8). The input to the main heater and the corresponding value predicted by Equation (7-8) are shown in Table XIII. The corrected input to the main heater was obtained by subtracting the amount of energy conducted across the annulus through the convective shields from the input to the main heater. The maximum difference between the predicted and measured radiant exchanges was less than 4.0 per cent.

The convection heat transfer correlation was obtained in a manner similar to that described in the preceding section. Details of establishing this correlation are given in Appendix F. The resulting correlation is

$$Nu = (.268)(Gr)^{0.2505} . \tag{7-9}$$

Results and Discussion

The results of the experimental investigation were presented in terms of the temperatures at corresponding points on the prototypes and one-half scale models for the steady-state studies.

Steady-State Investigation

The steady-state investigation was performed with the test sections located in two different positions (horizontal and vertical). Measurements of temperatures, power, and density were made in accordance with the procedure described in Chapter VI. The results of the investigation performed on the prototypes located in the horizontal position are shown in Tables XIV, XV, and XVI. Also shown in these tables are the temperatures predicted by the modeling criteria from tests performed on the models and the temperatures calculated by the analytical analysis (using the Grigull and Hauf [36] representation for the convection correlation) described in Chapter IV.

The temperatures predicted by Technique I and the Zero Surroundings Technique were in close agreement with those measured on the prototypes. The maximum difference was less than 3 degrees.

Some difference existed between the measured and computed temperatures. In the analytical analysis, the convection heat-transfer correlation was obtained from the literature [36]. When the correlation obtained in this investigation was used in the analytical analysis, the computed temperatures were in closer agreement with the measured temperatures. The maximum difference was less than 4 degrees for either of the above correlations.

TABLE XIV

STEADY-STATE TEMPERATURES OBTAINED FROM TEST SECTION 1P LOCATED HORIZONTALLY

THERMO-COUPLE NUMBER	TEST NO.	LOW ENERGY INPUT												HIGH ENERGY INPUT											
		POWER BTU/HR	DENSITY LB/FT^3	RAD HEAT TRANSFER BTU/HR	CONV HEAT TRANSFER BTU/HR	CONV FILM COEFF BTU/HR-FT2-°F	TEMPERATURE - °F MEASURED	PREDICTED TECH. I	PREDICTED ZERO TECH.	$(\Delta T)_1$	$(\frac{\Delta T}{T})_1$%	$(\Delta T)_2$	$(\frac{\Delta T}{T})_2$%	TEMPERATURE ANALYSIS °R	POWER BTU/HR	DENSITY LB/FT^3	RAD HEAT TRANSFER BTU/HR	CONV HEAT TRANSFER BTU/HR	CONV FILM COEFF BTU/HR-FT2-°F	TEMPERATURE - °F MEASURED	PREDICTED TECH. I	PREDICTED ZERO TECH	$(\Delta T)_1$	$(\frac{\Delta T}{T})_1$%	$(\Delta T)_2$	$(\frac{\Delta T}{T})_2$%	TEMPERATURE ANALYSIS °R
1							417.85	420.14	418.78	-2.19	-0.524	-0.83	-0.1985	420.14						500.80	503.67	502.86	-2.87	-0.573	-2.06	-0.4113	503.66
2							418.00	420.19	418.86	-2.19	-0.524	-0.86	-0.2057	420.14						501.49	503.72	502.93	-2.23	-0.444	-1.44	-0.2871	503.66
3							418.05	420.07	418.71	-2.02	-0.483	-0.66	-0.1578	420.14						500.69	503.63	502.79	-2.94	-0.587	-2.10	-0.419	503.66
4							563.37	560.15	560.0	3.22	0.571	3.37	0.598	560.15						675.75	672.67	672.72	3.08	0.4558	3.03	0.4484	672.67
5							563.00	560.21	560.10	2.79	0.4955	2.90	0.515	560.15						675.84	672.63	672.66	3.21	0.4749	3.18	0.4705	672.67
6	1	23.36	0.0000	23.36	0.0000	0.0000	563.74	560.49	560.16	3.25	0.576	2.58	0.457	560.15	48.78	0.0000	48.78	0.000	0.0000	676.10	672.91	672.78	3.19	0.4718	3.32	0.491	672.67
7							563.50	560.43	560.10	3.07	0.5448	3.40	0.6033	560.15						676.20	672.59	672.67	3.61	0.5338	3.53	0.522	672.67
8							417.78	420.31	418.87	-2.53	-0.6056	-1.09	-0.2609	420.14						499.49	503.87	502.97	-4.38	-0.8768	-3.48	-0.697	503.66
9							563.60	560.63	560.20	2.97	0.527	3.40	0.6032	560.15						676.20	672.81	672.77	3.39	0.502	3.43	0.5072	672.67
10							563.40	560.51	560.16	2.89	0.513	3.24	0.575	560.15						675.90	672.69	672.63	3.21	0.475	3.27	0.4839	672.67
11							417.96	420.29	418.77	-2.33	-0.5575	-0.81	-0.1937	420.14						501.01	503.81	502.94	-2.80	-0.5588	-1.93	-0.3852	503.66
LINER							160.19	160.07	160.11					160.00						160.20	160.11	159.96					160.00
1							418.85	420.50	419.14	-1.65	-0.3939	-0.29	-0.0692	420.49						502.02	503.85	503.05	-1.83	-0.3645	-1.03	-0.2051	503.85
2							418.73	420.53	419.06	-1.80	-0.4298	-0.33	-0.0788	420.49						501.84	503.82	503.10	-1.98	-0.394	-1.26	-0.251	503.85
3							418.92	420.58	419.21	-1.66	-0.3962	-0.29	-0.0692	420.49						502.50	503.89	502.99	-1.39	-0.277	-0.49	-0.0975	503.85
4							512.87	514.50	513.58	-1.63	-0.3178	-0.71	-0.1384	510.00						631.26	632.85	632.42	-1.59	-0.252	-1.16	-0.1837	628.36
5							512.03	514.53	513.55	-2.50	-0.4882	-1.52	-0.2968	510.00						630.00	632.87	632.31	-2.87	-0.455	-2.31	-0.3666	628.36
6	2	23.44	0.0281	13.37	10.07	0.50	511.93	514.59	513.66	-2.66	-0.5196	-1.73	-0.338	510.00	48.85	0.0283	33.18	15.67	0.57	631.52	632.59	632.50	-1.07	-0.169	-0.98	-0.1551	628.36
7							513.02	514.63	513.58	-1.61	-0.3138	-.56	-0.1091	510.00						632.00	632.71	632.38	-0.71	-0.1123	-0.38	-0.0601	628.36
8							418.34	420.72	419.25	-2.38	-0.5689	-0.91	-0.2175	420.49						502.31	504.10	503.17	-1.79	-0.356	-0.86	-0.1712	503.85
9							512.61	514.68	513.68	-2.07	-0.4038	-1.07	-0.2087	510.00						632.15	632.63	632.56	-0.53	-0.0838	-0.46	-0.0727	628.36
10							514.02	514.71	513.61	-0.69	-0.1342	-0.41	-0.0797	510.00						631.90	631.81	632.44	0.09	0.0142	-0.54	-0.085	628.36
11							418.39	420.63	419.17	-2.24	-0.5354	-0.78	-0.1864	420.49						502.20	503.99	503.14	-1.79	-0.356	-0.94	-0.1871	503.85
LINER							160.10	160.09	159.98					160.00						160.10	160.05	160.15					160.00
1							418.36	420.36	419.00	-2.00	-0.478	-0.64	-0.1529	420.36						501.74	503.74	502.94	-2.00	-0.3986	-1.20	-0.239	503.74
2							418.00	420.38	419.09	-2.38	-0.5694	-1.09	-0.2607	420.36						502.00	503.78	503.02	-1.78	-0.354	-1.02	-0.2032	503.74
3							417.82	420.37	418.97	-2.55	-0.610	-1.15	-0.2752	420.36						501.50	503.72	502.87	-2.22	-0.442	-1.37	-0.2732	503.74
4							476.87	479.37	477.75	-2.50	-0.524	-0.88	-0.1845	473.87						614.25	615.75	615.65	-1.50	-0.2442	-1.40	-0.2279	610.75
5							476.20	479.35	477.73	-3.15	-0.661	-1.53	-0.3213	473.87						614.03	615.78	615.62	-1.75	-0.285	-1.59	-0.2589	610.75
6	3	23.41	0.0735	10.56	12.85	0.77	476.38	479.52	477.86	-3.14	-0.659	-1.48	-0.3106	473.87	48.81	0.0740	27.50	21.31	0.89	613.95	615.81	615.76	-1.86	-0.303	-1.81	-0.2948	610.75
7							477.20	479.59	477.76	-2.39	-0.5008	-0.56	-0.1173	473.87						613.90	615.79	615.72	-1.89	-0.3078	-1.82	-0.2964	610.75
8							417.90	420.51	419.13	-2.61	-0.625	-1.23	-0.2943	420.36						501.06	503.86	503.03	-2.80	-0.5585	-1.97	-0.393	503.74
9							478.10	479.53	477.92	-1.43	-0.2991	0.18	0.0376	473.87						614.54	615.59	615.75	-1.05	-0.1708	-1.21	-0.197	610.75
10							476.92	479.42	477.86	-2.50	-0.5243	-0.94	-0.1970	473.87						614.75	615.63	615.63	-0.88	-0.1431	-0.88	-0.143	610.75
11							418.62	420.48	419.09	-1.86	-0.4443	-0.47	-0.1123	420.36						503.00	503.89	502.89	-0.89	-0.1769	0.11	0.0218	503.74
LINER							159.90	160.11	160.17					160.00						159.90	160.18	160.12					160.00

TABLE XV

STEADY-STATE TEMPERATURES OBTAINED FROM TEST SECTION 2P LOCATED HORIZONTALLY

THERMO-COUPLE NUMBER	TEST NO.	LOW ENERGY INPUT												HIGH ENERGY INPUT											
		POWER BTU/HR	DENSITY LB/FT^3	RAD HEAT TRANSFER BTU/HR	CONV HEAT TRANSFER BTU/HR	CONV FILM COEFF. BTU/HR-FT^2-°F	TEMPERATURE - °F			$(\Delta T)_I$	$\left(\frac{\Delta T}{T}\right)_I$%	$(\Delta T)_Z$	$\left(\frac{\Delta T}{T}\right)_Z$%	TEMPERATURE ANALYSIS °R	POWER BTU/HR	DENSITY LB/FT^3	RAD HEAT TRANSFER BTU/HR	CONV. HEAT TRANSFER BTU/HR	CONV. FILM COEFF. BTU/HR-FT^2-°F	TEMPERATURE - °F			$(\Delta T)_I$	$\left(\frac{\Delta T}{T}\right)_I$%	$(\Delta T)_Z$	$\left(\frac{\Delta T}{T}\right)_Z$%	TEMPERATURE ANALYSIS °R
							MEASURED	PREDICTED TECH. I	PREDICTED ZERO TECH.											MEASURED	PREDICTED TECH. I	PREDICTED ZERO TECH.					
1							419.02	420.84	419.49	-1.82	-0.4343	-0.47	-0.112	420.84						499.25	502.95	502.15	-3.70	-0.741	-2.90	-0.5808	502.95
2							418.61	420.90	419.52	-2.29	-0.547	-0.91	-0.2173	420.84						498.20	502.85	502.10	-4.65	-0.933	-3.90	-0.783	502.95
3							418.02	420.80	419.46	-2.78	-0.665	-1.44	-0.3444	420.84						497.84	503.05	502.20	-5.21	-1.046	-4.36	-0.8758	502.95
4							537.37	535.85	535.37	1.52	0.2828	2.00	+0.372	535.85						644.25	641.95	641.05	2.30	0.357	3.20	0.4967	641.46
5							537.46	535.79	535.35	1.67	0.3107	2.11	0.392	535.85						644.10	641.89	640.87	2.21	0.343	3.23	0.501	641.46
6	1	23.52	0.0000	23.52	0.000	0.000	538.02	535.98	535.42	2.04	0.3792	2.60	0.4832	535.85	48.50	0.0000	48.50	0.000	0.000	644.49	642.05	641.35	2.44	0.378	3.14	0.487	641.46
7							538.21	535.86	535.40	2.35	0.436	2.81	0.5221	535.85						644.38	641.91	641.32	2.47	0.383	3.06	0.4748	641.46
8							419.34	420.96	419.55	-1.62	-0.3863	-0.21	- .050	420.84						499.73	503.10	502.27	-3.37	-0.674	-2.54	-0.5083	502.95
9							538.09	535.99	535.47	2.10	0.39026	2.62	0.4869	535.85						644.51	642.99	641.22	1.52	0.2358	3.29	0.5105	641.46
10							538.41	536.02	535.43	2.39	0.44408	2.96	0.5534	535.85						644.60	642.84	641.19	1.76	0.27304	3.41	0.529	641.46
11							419.51	420.97	419.55	-1.46	-0.348	-0.04	-0.0095	420.84						500.03	503.06	502.15	-3.03	-0.6059	-2.12	-0.4239	502.95
LINER							159.80	160.11	160.01					160.00						160.23	160.19	160.10					160.00
1							418.10	420.32	418.96	-2.22	-0.5309	-0.86	-0.2056	420.32						501.00	503.64	502.84	-2.64	-0.5269	-1.84	-0.3672	503.64
2							417.69	420.40	418.93	-2.71	-0.6488	-1.24	-0.2968	420.32						500.93	503.60	502.78	-2.67	-0.533	-1.85	-0.3693	503.64
3							419.32	420.24	418.99	-0.92	-0.2194	0.33	+0.078	420.32						500.23	503.68	502.89	-3.45	-0.6897	-2.66	-0.5317	503.64
4							494.87	497.32	495.95	-2.45	-0.495	-1.08	-0.218	492.82						606.75	608.65	608.41	-1.90	-0.313	-1.66	-0.2735	604.65
5							494.83	497.29	495.90	-2.46	-0.4971	-1.07	-0.2162	492.82						606.00	608.61	608.33	-2.61	-0.4308	-2.33	-0.384	604.65
6	2	23.40	0.0281	13.59	9.81	0.450	495.10	497.35	496.05	-2.25	-0.4544	-0.95	0.1918	492.82	48.77	0.0279	33.51	15.26	0.510	606.82	608.71	608.47	-1.89	-0.3114	-1.65	-0.2719	604.65
7							494.50	497.21	496.04	-2.71	-0.548	1.54	0.3114	492.82						606.20	608.60	608.40	-2.40	-0.3959	-2.20	-0.3629	604.65
8							418.60	420.50	419.04	-1.90	-0.4539	-0.44	-0.1051	420.32						500.63	503.73	502.94	-3.10	-0.6192	-2.31	-0.4614	503.64
9							494.73	497.41	496.81	-2.68	-0.5417	-2.06	-0.4204	492.87						606.91	608.73	608.52	-1.82	-0.2998	-1.61	-0.2653	604.65
10							493.81	497.43	496.72	-3.62	-0.733	-2.91	-0.589	492.82						605.93	608.64	608.43	-2.71	-0.4472	-2.50	-0.4126	604.65
11							418.20	420.47	419.10	-2.27	-0.5428	-0.90	-0.2152	420.32						500.36	503.79	502.93	-3.43	-0.685	-2.57	-0.5136	503.64
LINER							161.05	160.07	160.08					160.00						159.34	160.02	159.96					160.00
1							417.90	419.88	418.52	-1.98	-0.4738	-0.62	-0.148	419.88						502.50	504.23	503.43	-1.73	-0.344	-0.93	-0.18507	504.23
2							417.60	419.80	418.46	-2.20	-0.5268	-0.86	-0.2059	419.88						502.10	504.30	503.36	-2.20	-0.438	-1.26	-0.2509	504.23
3							418.70	419.96	418.57	-1.26	-0.3009	-0.13	-0.031	419.88						501.96	504.16	503.49	-2.20	-0.438	-1.53	-0.3048	504.23
4							481.87	483.88	482.81	-2.01	-0.417	-0.94	-0.195	478.88						592.76	594.23	593.92	-1.47	-0.2479	-1.16	-0.1958	591.24
5							483.00	483.75	482.75	-0.75	-0.1553	-0.25	0.052	478.88						592.00	594.19	593.86	-2.19	-0.3699	-1.86	-0.314	591.24
6	3	23.30	0.0741	10.82	12.48	0.690	482.11	484.01	482.86	-1.90	-0.394	-0.75	-0.1555	478.88	49.00	0.0734	27.58	21.42	0.840	592.81	594.41	593.99	-1.60	-0.2699	-1.18	-0.199	591.24
7							482.36	484.05	482.82	-1.69	-0.3504	-0.46	-0.0953	478.88						592.01	594.39	593.93	-2.38	-0.402	-1.92	-0.324	591.24
8							417.32	420.03	418.63	-2.71	-0.649	-1.31	-0.3139	419.88						502.83	504.33	503.58	-1.50	-0.298	-0.75	-0.1491	504.23
9							482.01	484.10	482.93	-2.09	-0.4336	-0.92	-0.1909	478.88						593.04	594.46	594.07	-1.42	-0.2394	-1.03	-0.2089	591.24
10							482.09	483.99	482.96	-1.90	-0.394	-0.87	-0.1805	478.88						592.60	594.37	593.82	-1.77	-0.298	-1.22	-0.2058	591.24
11							417.92	419.78	418.67	-1.86	-0.445	-0.75	-0.17946	419.88						502.39	504.36	503.54	-1.97	-0.3921	-1.15	-0.2289	504.23
LINER							159.86	159.98	160.23					160.00						159.81	160.12	160.11					160.00

TABLE XVI

STEADY-STATE TEMPERATURES OBTAINED FROM TEST SECTION 3P LOCATED HORIZONTALLY

THERMO-COUPLE NUMBER	TEST NO	LOW ENERGY INPUT													HIGH ENERGY INPUT											
		POWER BTU/HR	DENSITY LB/FT^3	RAD HEAT TRANSFER BTU/HR	CONV HEAT TRANSFER BTU/HR	CONV FILM COEFF. BTU/HR-FT^2-°F	TEMPERATURE - °F MEASURED	PREDICTED TECH. I	PREDICTED ZERO TECH.	$(\Delta T)_1$	$\left(\frac{\Delta T}{T}\right)_1$%	$(\Delta T)_2$	$\left(\frac{\Delta T}{T}\right)_2$%	TEMPERATURE ANALYSIS °R	POWER BTU/HR	DENSITY LB/FT^3	RAD HEAT TRANSFER BTU/HR	CONV. HEAT TRANSFER BTU/HR	CONV FILM COEFF. BTU/HR-FT^2-°F	TEMPERATURE - °F MEASURED	PREDICTED TECH. I	PREDICTED ZERO TECH.	$(\Delta T)_1$	$\left(\frac{\Delta T}{T}\right)_1$%	$(\Delta T)_2$	$\left(\frac{\Delta T}{T}\right)_2$%	TEMPERATURE ANALYSIS °R
1							418.40	420.54	419.18	-2.14	-0.511	-0.78	-0.1864	420.54						501.50	503.59	502.79	-2.09	-0.4167	-1.29	-0.2572	503.59
2							418.20	420.60	419.14	-2.40	-0.574	-0.94	-0.2247	420.54						501.25	503.50	502.83	-2.25	-0.4488	-1.58	-0.3152	503.59
3							418.83	420.50	419.22	-1.67	-0.3987	-0.39	-0.09311	420.54						501.20	503.68	502.75	-2.48	-0.495	-1.55	-0.3093	503.59
4							603.37	602.54	602.52	0.83	0.1375	0.85	0.14087	602.55						724.25	723.60	723.44	0.65	0.0897	0.81	0.11186	723.10
5							603.48	602.60	602.47	0.88	0.1458	1.01	0.1674	602.55						724.21	723.49	723.46	0.72	0.0994	0.75	0.1036	723.10
6	1	23.45	0.0000	23.77	0.000	0.000	603.97	602.50	602.62	1.41	0.2335	1.29	0.2136	602.55	48.75	0.0000	49.43	0.000	0.000	724.61	723.80	723.56	0.81	0.11178	1.05	0.1449	723.10
7							604.10	602.65	602.55	1.45	0.240	1.55	0.2565	602.55						723.99	723.74	723.50	+0.25	0.0345	.25	0.0345	723.10
8							419.20	420.70	419.29	-1.50	-0.3578	-0.09	-0.0214	420.54						501.98	503.71	502.88	-1.73	-0.3446	-1.73	-0.3446	503.59
9							603.91	602.66	602.69	1.25	+0.207	1.22	0.202	602.55						725.03	723.74	723.63	1.29	0.1779	1.29	0.1779	723.10
10							603.51	602.71	602.60	0.80	+0.1326	0.91	0.1508	602.55						724.68	723.65	723.58	1.03	0.1421	1.03	0.1421	723.10
11							419.36	420.69	419.28	-1.33	-0.317	.08	0.019	420.55						502.06	503.63	502.92	-1.57	-0.3127	-1.57	-0.3127	503.59
LINER							159.8	160.08	160.11					160.00						159.7	160.16	160.01					160.00
1							417.95	420.05	418.70	-2.10	-0.5025	-0.75	-0.179	420.056						502.00	503.90	503.09	-1.90	-0.3785	-1.09	-0.2171	503.90
2							417.84	420.10	418.65	-2.26	-0.5409	-0.81	-0.193	420.06						501.93	503.93	503.05	-2.00	-0.3985	-1.12	-0.2231	503.90
3							417.73	419.99	418.75	-2.26	-0.541	-1.02	-0.244	420.06						501.83	503.87	503.14	-2.04	-0.406	-1.31	-0.26104	503.90
4							536.37	539.06	537.74	-2.69	-0.5015	-1.37	-0.2554	534.06						665.75	666.90	666.60	-1.15	-0.1727	-0.85	-0.12767	664.90
5							536.20	539.12	537.69	-2.92	-0.5445	-1.49	-0.278	534.06						665.75	666.80	666.49	-1.07	-0.1607	-0.76	-0.1141	664.90
6	2	23.34	0.0290	12.19	11.15	0.660	537.10	538.97	537.87	-1.87	-0.348	-0.77	-0.143	534.06	48.87	0.0284	31.01	17.86	0.77	665.94	666.82	666.595	-0.88	-0.1321	-0.66	-0.0991	664.90
7							536.90	539.22	537.82	-2.32	-0.432	-0.92	-0.1713	534.06						665.99	666.74	666.83	-0.75	-0.1126	-0.84	-0.12613	664.90
8							418.20	420.19	418.82	-1.99	-0.476	-0.62	-0.1482	420.06						502.06	504.01	503.26	-1.95	-0.3886	-1.20	-0.239	503.90
9							536.84	539.29	537.90	-2.45	-0.456	-1.06	-0.1975	534.06						666.09	666.84	666.75	-0.75	-0.1126	-0.66	-0.09908	664.90
10							535.98	539.31	537.86	-3.33	-0.621	-1.88	-0.3507	534.06						666.02	666.71	666.75	-0.69	+0.104	-0.73	-0.1096	664.90
11							418.10	420.20	418.85	-2.10	-0.502	-0.75	-0.1794	420.06						502.64	504.10	503.20	-1.66	-0.3304	-0.76	-0.1513	503.90
LINER							161.04	160.13	160.11					160.00						160.4	160.11	160.13					160.00
1							417.50	419.84	418.47	-2.34	-0.5605	-0.97	-0.2323	419.83						500.50	503.54	502.74	-3.04	-0.6073	-2.24	-0.4475	503.54
2							417.35	419.79	418.53	-2.44	-0.585	-1.18	-0.283	419.83						500.40	503.60	502.70	-3.20	-0.6395	-2.30	-0.4596	503.54
3							417.71	419.85	418.42	-2.14	-0.5123	-0.71	-0.1699	419.83						500.63	503.49	502.78	-2.86	-0.5713	-2.15	-0.429	503.54
4							514.87	516.84	516.09	-1.97	-0.3826	-1.22	-0.2369	512.84						642.76	645.55	644.82	-2.79	-0.434	-2.06	-0.3205	640.55
5							514.81	516.89	516.04	-2.08	-0.404	-1.23	-0.2389	512.84						642.83	645.61	644.76	-2.78	-0.4324	-1.93	-0.3002	640.55
6	3	23.29	0.0740	9.31	13.98	1.010	515.03	517.03	516.17	-2.00	-0.388	-1.14	-0.2213	512.84	48.73	0.0750	25.18	23.55	1.17	643.03	645.73	644.93	-2.70	-0.4198	-1.90	-0.2954	640.55
7							515.21	516.93	516.07	-1.72	-0.334	-0.86	-0.1669	512.84						642.91	645.69	644.87	-2.78	-0.432	-1.96	-0.3048	640.55
8							418.31	419.99	418.59	-1.68	-0.4016	-0.28	-0.0669	419.83						500.71	503.72	502.87	-3.01	-0.6011	-2.16	-0.4314	503.54
9							515.02	517.10	516.20	-2.08	-0.4038	-1.18	-0.229	512.84						642.51	645.80	644.86	-3.29	-0.512	-2.35	-0.3657	640.55
10							515.23	517.03	516.24	-1.80	-0.3493	-1.01	-0.19603	512.84						642.42	645.51	644.88	-3.09	-0.481	-2.46	-0.3829	640.55
11							418.26	420.03	418.58	-1.77	-0.4232	-0.32	-0.0765	419.83						500.43	503.69	502.88	-3.26	-0.6514	-2.45	-0.4895	503.54
LINER							160.50	159.86	160.11					160.00						160.5	160.18	160.08					160.00

The results of the tests performed on the three one-half scale models, located in the horizontal position, are shown in Tables XVII, XVIII, and XIX. Also shown in these tables are the temperatures computed from the theoretical analysis.

For the tests performed on the prototypes without air in the annulus, the measured, predicted, and calculated temperatures were in close agreement. The maximum difference was less than 3 degrees.

The results of the tests performed on the prototype located in the vertical position are shown in Table XX. Also shown in this table are the temperatures predicted by the modeling criteria from the tests performed on the model. As can be seen in this table, the predicted and measured temperatures were in close agreement. The maximum difference was less than 4 degrees. This difference was greater than the difference obtained with the test section located in the horizontal position. The results of the tests performed on the corresponding model are shown in Table XXI.

TABLE XVII

STEADY-STATE TEMPERATURES OBTAINED FROM TEST SECTION 1M LOCATED HORIZONTALLY.

THERMO-COUPLE NUMBER	TEST NO.	DATA USED TO PREDICT PROTOTYPE TEMPERATURE BY TECHNIQUE I — LOW ENERGY INPUT: POWER ACTUAL BTU/HR	POWER REQ. BTU/HR	DENSITY ACTUAL LB/FT³	DENSITY REQ. LB/FT³	RAD. HEAT TRANSFER BTU/HR	CONV. HEAT TRANSFER BTU/HR	CONV. COEFF. BTU/HR-FT²-°F	TEMP. °F	HIGH ENERGY INPUT: POWER ACTUAL BTU/HR	POWER REQ. BTU/HR	DENSITY ACTUAL LB/FT³	DENSITY REQ. LB/FT³	RAD. HEAT TRANSFER BTU/HR	CONV. HEAT TRANSFER BTU/HR	CONV. COEFF. BTU/HR-FT²-°F	TEMP. °F	DATA USED TO PREDICT PROTOTYPE TEMPERATURE BY ZERO SURROUNDINGS TECHNIQUE — LOW ENERGY INPUT: POWER ACTUAL BTU/HR	POWER REQ. BTU/HR	DENSITY ACTUAL LB/FT³	DENSITY REQ. LB/FT³	RAD. HEAT TRANSFER BTU/HR	CONV. HEAT TRANSFER BTU/HR	CONV. COEFF. BTU/HR-FT²-°F	TEMP. °F	HIGH ENERGY INPUT: POWER ACTUAL BTU/HR	POWER REQ. BTU/HR	DENSITY ACTUAL LB/FT³	DENSITY REQ. LB/FT³	RAD. HEAT TRANSFER BTU/HR	CONV. HEAT TRANSFER BTU/HR	CONV. COEFF. BTU/HR-FT²-°F	TEMP. °F
1									420.14								503.67								527.67								633.61
2									420.19								503.72								527.77								633.70
3									420.07								503.63								527.57								633.52
4									560.15								672.67								705.67								847.63
5									560.21								672.63								705.73								847.56
6	1	5.85	5.84	0.000	0.000	5.86	0.000	0.000	560.49	12.20	12.195	0.000	0.000	12.22	0.000	0.000	672.91	14.73	14.72	0.000	0.000	14.84	0.000	0.000	705.81	30.80	30.73	0.000	0.000	30.91	0.000	0.000	847.71
7									560.43								672.59								705.73								847.57
8									420.31								503.87								527.78								633.74
9									560.63								672.81								705.86								847.69
10									560.51								672.69								705.80								847.51
11									420.29								503.81								527.65								633.71
LINER									160.07								160.11								160.11								159.96
1									420.50								503.85								528.12								633.84
2									420.53								503.82								528.02								633.91
3									420.58								503.89								528.20								633.77
4									514.50								632.85								647.12								796.85
5									514.53								632.87								647.08								796.71
6	2	5.87	5.861	0.0199	0.0198	3.378	2.500	0.500	514.59	12.22	12.21	0.205	0.020	8.353	3.910	0.570	632.59	14.78	14.77	.098	.0974	8.50	6.33	1.000	647.21	30.80	30.77	.0970	.0979	21.05	9.88	1.14	796.95
7									514.63								632.71								647.11								796.80
8									420.72								504.10								528.26								634.00
9									514.68								632.63								647.24								797.03
10									514.71								637.81								647.16								796.87
11									420.62								503.99								528.16								633.96
LINER									160.09								160.05								159.98								160.15
1									420.36								503.74								527.95								633.71
2									420.38								503.78								528.05								633.80
3									420.37								503.72								527.90								633.62
4									479.37								615.75								601.96								775.72
5									479.35								615.78								601.94								775.69
6	3	5.86	5.85	0.0520	0.0516	1.88	4.078	1.30	479.52	12.21	12.20	0.0524	0.0523	6.91	5.30	0.890	615.81	14.77	14.75	0.250	0.254	4.67	10.23	2.60	602.11	30.76	30.75	.251	.2563	17.48	13.44	1.78	775.86
7									479.59								615.79								601.98								775.81
8									420.51								503.86								528.10								633.81
9									479.53								615.59								602.18								775.84
10									479.42								615.63								602.10								775.69
11									420.48								503.89								528.05								633.65
LINER									160.11								160.18								160.17								160.12

TABLE XVIII

STEADY-STATE TEMPERATURES OBTAINED FROM TEST SECTION 2M LOCATED HORIZONTALLY.

THERMO-COUPLE NUMBER	TEST NO	DATA USED TO PREDICT PROTOTYPE TEMPERATURE BY TECHNIQUE I — LOW ENERGY INPUT — POWER ACTUAL BTU/HR	POWER REQ. BTU/HR	DENSITY ACTUAL LB/FT^3	DENSITY REQ LB/FT^3	RAD. HEAT TRANSFER BTU/HR	CONV. HEAT TRANSFER BTU/HR	CONV. COEFF. BTU/HR-FT^2-°F	TEMP. °F	HIGH ENERGY INPUT — POWER ACTUAL BTU/HR	POWER REQ. BTU/HR	DENSITY ACTUAL LB/FT^3	DENSITY REQ. LB/FT^3	RAD. HEAT TRANSFER BTU/HR	CONV. HEAT TRANSFER BTU/HR	CONV. COEFF. BTU/HR-FT^2-°F	TEMP. °F	DATA USED TO PREDICT PROTOTYPE TEMPERATURE BY ZERO SURROUNDINGS TECHNIQUE — LOW ENERGY INPUT — POWER ACTUAL BTU/HR	POWER REQ. BTU/HR	DENSITY ACTUAL LB/FT^3	DENSITY REQ. LB/FT^3	RAD. HEAT TRANSFER BTU/HR	CONV. HEAT TRANSFER BTU/HR	CONV. COEFF. BTU/HR-FT^2-°F	TEMP. °F	HIGH ENERGY INPUT — POWER ACTUAL BTU/HR	POWER REQ. BTU/HR	DENSITY ACTUAL LB/FT^3	DENSITY REQ. LB/FT^3	RAD. HEAT TRANSFER BTU/HR	CONV. HEAT TRANSFER BTU/HR	CONV. COEFF. BTU/HR-FT^2-°F	TEMP. °F
1									420.84								502.95								528.56								632.71
2									420.90								502.85								528.60								632.65
3									420.80								503.05								528.52								632.77
4									535.85								641.95								674.57								807.72
5									535.79								641.89								674.54								807.49
6	1	5.89	5.88	0.00	0.00	5.90	0.000	0.000	535.98	12.13	12.125	0.00	0.00	12.225	0.000	0.000	642.05	14.83	14.82	0.000	0.000	14.90	0.000	0.000	674.63	30.56	30.55	0.000	0.000	30.65	0.000	0.000	808.10
7									535.86								641.91								674.60								808.06
8									420.96								503.10								528.63								632.86
9									535.99								642.99								674.69								807.94
10									536.02								642.84								674.64								807.90
11									420.97								503.06								528.64								632.71
LINER									160.11								160.19								160.01								160.10
1									420.32								503.64								527.89								633.58
2									420.40								503.60								527.85								633.51
3									420.24								503.68								527.93								633.65
4									497.32								608.65								624.90								766.60
5									497.29								608.61								624.84								766.50
6	2	5.86	5.85	0.019	0.0198	3.46	2.46	0.45	497.35								608.71	14.79	14.74	0.098	0.0974	8.64	6.19	0.90	625.03	30.74	30.72	0.097	0.0966	21.28	9.62	1.02	766.68
7									497.21	12.20	12.19	.019	.0197	8.42	3.80	0.51	608.60								625.01								766.59
8									420.50								503.73								528.00								633.70
9									497.41								608.73								625.98								766.73
10									497.43								608.64								625.87								766.62
11									420.47								503.79								528.06								633.69
LINER									160.07								160.02								160.08								159.96
1									419.88								504.23								527.33								634.32
2									419.80								504.30								527.26								634.24
3									419.96								504.16								527.40								634.40
4									483.88								594.23								608.34								748.34
5									483.75								594.19								608.26								748.26
6	3	5.83	5.825	0.052	.05239	2.742	3.131	0.69	484.01	12.26	12.25	.0518	.0519	6.935	5.36	0.84	594.41	14.71	14.67	0.257	0.2569	6.89	7.93	1.38	608.41	30.90	30.87	0.253	0.2542	17.52	13.58	1.68	748.43
7									484.05								594.39								608.35								748.35
8									420.03								504.33								527.48								634.51
9									484.10								594.46								608.49								748.53
10									483.99								594.37								608.53								748.22
11									419.78								504.36								527.53								634.46
LINER									159.98								160.12								160.23								160.11

TABLE XIX

STEADY-STATE TEMPERATURES OBTAINED FROM TEST SECTION 3M LOCATED HORIZONTALLY.

THERMO-COUPLE NUMBER	TEST NO.	DATA USED TO PREDICT PROTOTYPE TEMPERATURE BY TECHNIQUE I																DATA USED TO PREDICT PROTOTYPE TEMPERATURE BY ZERO SURROUNDINGS TECHNIQUE															
		LOW ENERGY INPUT								HIGH ENERGY INPUT								LOW ENERGY INPUT								HIGH ENERGY INPUT							
		POWER		DENSITY		RAD. HEAT TRANSFER	CONV. HEAT TRANSFER	CONV. COEFF.	TEMP.	POWER		DENSITY		RAD. HEAT TRANSFER	CONV. HEAT TRANSFER	CONV. COEFF.	TEMP.	POWER		DENSITY		RAD. HEAT TRANSFER	CONV. HEAT TRANSFER	CONV. COEFF.	TEMP	POWER		DENSITY		RAD. HEAT TRANSFER	CONV. HEAT TRANSFER	CONV. COEFF.	TEMP.
		ACTUAL BTU/HR	REQ'D. BTU/HR	ACTUAL LB/FT³	REQ'D. LB/FT³	BTU/HR	BTU/HR	BTU/HR-FT²-°F	°F	ACTUAL BTU/HR	REQ'D. BTU/HR	ACTUAL LB/FT³	REQ'D LB/FT³	BTU/HR	BTU/HR	BTU/HR-FT²-°F	°F	ACTUAL BTU/HR	REQ'D. BTU/HR	ACTUAL LB/FT³	REQ'D. LB/FT³	BTU/HR	BTU/HR	BTU/HR-FT²-°F	°F	ACTUAL BTU/HR	REQ'D. BTU/HR	ACTUAL LB/FT³	REQ'D. LB/FT³	BTU/HR	BTU/HR	BTU/HR-FT²-°F	°F
1									420.54								503.59								528.17								633.52
2									420.60								503.50								528.12								633.57
3									420.50								503.68								528.22								633.47
4									602.54								723.60								759.18								911.53
5									602.60								723.49								759.11								911.56
6	1	5.87	5.862	0.000	0.000	5.863	0.000	0.000	602.50	12.20	12.19	0.00	0.00	12.24	0.000	0.000	723.80	14.79	14.77	0.00	0.00	14.835	0.000	0.000	759.31	30.72	30.71	0.00	0.00	30.87	0.000	0.000	911.69
7									602.65								723.74								759.22								911.61
8									420.70								503.71								528.31								633.63
9									602.66								723.74								759.39								911.78
10									602.71								723.65								759.28								911.71
11									420.69								503.63								528.29								633.68
LINER									160.08								160.16								160.11								160.01
1									420.05								503.90								527.56								633.90
2									420.10								503.93								527.50								633.84
3									419.99								503.87								527.63								633.96
4									539.06								666.90								677.56								839.92
5									539.12								666.80								677.49								839.78
6	2	5.84	5.835	.0204	.0205	3.11	2.78	0.66	538.97	12.23	12.22	0.0200	0.02009	7.78	4.45	0.77	666.82	14.71	14.70	0.1010	0.1005	7.77	7.02	1.32	677.72	30.80	30.79	0.0980	0.0983	19.61	11.25	1.54	839.91
7									539.22								666.74								677.65								840.21
8									420.19								504.01								527.71								634.11
9									539.29								666.84								677.75								840.11
10									539.31								666.71								677.71								840.10
11									420.20								504.10								527.75								634.03
LINER									160.13								160.11								160.11								160.13
1									419.84								503.54								527.28								633.45
2									419.79								503.60								527.35								633.40
3									419.85								503.49								527.21								633.51
4									516.84								645.55								650.28								812.47
5									516.89								645.61								650.21								812.40
6	3	5.83	5.822	.052	.0523	2.35	3.47	1.01	517.03	12.19	12.18	0.0529	0.053	6.38	5.89	1.17	645.73	14.70	14.67	0.254	0.2561	5.92	8.81	2.02	650.38	30.71	30.70	0.2592	0.2597	16.02	14.85	2.34	812.61
7									516.93								645.69								650.25								812.54
8									419.99								503.72								527.42								633.62
9									517.10								645.80								650.41								812.53
10									517.03								645.51								650.46								812.55
11									420.03								503.69								527.41								633.63
LINER									159.86								160.18								160.11								160.08

TABLE XX

STEADY-STATE TEMPERATURES OBTAINED FROM TEST SECTION 1P LOCATED VERTICALLY

THERMO-COUPLE NUMBER	TEST NO	LOW ENERGY INPUT													HIGH ENERGY INPUT											
		POWER BTU/HR	DENSITY LB/FT^3	RAD HEAT TRANSFER BTU/HR	CONV. HEAT TRANSFER BTU/HR	CONV FILM COEFF. BTU/HR-FT2-°F	TEMPERATURE - °F MEASURED	PREDICTED TECH I	PREDICTED ZERO TECH	$(\Delta T)_1$	$(\frac{\Delta T}{T})_1$%	$(\Delta T)_2$	$(\frac{\Delta T}{T})_2$%	TEMPERATURE ANALYSIS °R	POWER BTU/HR	DENSITY LB/FT^3	RAD HEAT TRANSFER BTU/HR	CONV. HEAT TRANSFER BTU/HR	CONV FILM COEFF. BTU/HR-FT2-°F	TEMPERATURE - °F MEASURED	PREDICTED TECH I	PREDICTED ZERO TECH	$(\Delta T)_1$	$(\frac{\Delta T}{T})_1$%	$(\Delta T)_2$	$(\frac{\Delta T}{T})_2$%	TEMPERATURE ANALYSIS °R
1							414.0	415.85	414.45	-1.85	-0.4468	-0.45	-0.1087	415.85						495.00	497.47	496.64	-2.47	-0.4989	-1.64	-0.3313	497.47
2							413.90	415.81	414.69	-1.91	-0.4614	-0.59	-0.1425	415.85						496.83	497.36	496.69	-2.53	-0.5133	-1.86	-0.3758	497.47
3							413.78	415.89	414.61	-2.11	-0.5099	-0.63	-0.1522	415.85						494.71	497.52	496.60	-2.81	-0.568	-1.89	-0.382	497.47
4							556.99	554.86	554.16	2.13	0.382	2.85	0.5137	554.36						666.51	664.48	664.11	2.03	0.3045	2.40	0.360	664.48
5							556.83	554.83	554.21	2.00	0.359	2.62	0.4706	554.36						666.43	664.51	664.0	1.92	0.2881	2.43	0.3646	664.48
6	1	22.40	0.0000	22.40	0.000	0.000	556.41	555.00	554.31	1.41	0.2534	2.10	0.3774	554.36	46.40	0.0000	46.40	0.000	0.000	666.21	664.72	664.23	1.49	0.2236	1.98	0.2972	664.48
7							556.29	554.96	554.28	1.33	0.2388	2.01	0.3613	554.36						666.11	664.69	664.12	1.42	0.2131	1.99	0.2987	664.48
8							415.00	415.88	414.61	-0.88	-0.21205	0.39	0.0939	415.85						496.02	497.81	496.71	-1.79	-0.3608	- .69	-0.1391	497.47
9							557.03	554.92	554.37	-2.11	-0.3788	2.66	0.477	554.36						666.05	664.89	664.36	1.16	0.17416	1.69	0.2537	664.48
10							556.43	554.67	554.33	1.76	0.316	2.10	0.377	554.36						666.10	664.41	664.44	1.69	0.2537	1.66	0.2492	664.48
11							413.50	415.93	414.58	-2.43	-0.5876	1.08	0.2611	415.85						495.31	497.63	496.75	-2.32	-0.4684	-1.44	-0.2907	497.47
LINER							159.83	159.95	160.17					160.0						160.11	160.21	160.16					160.00
1							414.49	416.487	415.09	-1.997	-0.4818	-0.60	-0.1447	416.49						496.10	498.53	497.71	-2.43	-0.4898	-1.61	-0.3245	498.53
2							414.38	416.44	415.16	-2.06	-0.4971	-0.78	-0.1882	416.49						495.92	498.59	497.76	-2.67	-0.53839	-1.86	-0.371	498.53
3							414.60	416.52	415.0	-1.92	-0.463	-0.40	-0.0965	416.49						495.86	498.51	497.65	-2.65	-0.5346	-1.79	-0.361	498.53
4							506.5	508.489	507.158	-1.99	-0.3928	-0.66	-0.1303	505.51						621.50	623.535	623.12	-2.03	-0.3266	-1.62	-0.2606	623.04
5							506.28	508.471	507.22	-2.19	-0.4325	-0.94	-0.1856	505.51						621.41	623.56	623.08	-2.15	-0.3459	-1.67	-0.2687	623.04
6	2	22.54	0.0285	12.64	9.90	0.510	506.78	508.73	507.238	-1.95	-0.3845	-0.46	-0.0907	505.51	44.80	0.0281	30.86	15.94	0.600	621.23	623.69	623.18	-2.48	-0.3992	-1.97	-0.3171	623.04
7							506.99	508.51	507.12	-1.52	-0.2998	-0.13	-0.0256	505.51						620.71	623.71	623.10	-3.00	-0.4833	-2.39	-0.385	623.04
8							415.10	416.61	415.17	-1.51	-0.3637	-0.07	-0.0168	416.49						496.30	498.62	497.83	-2.32	-0.4674	-1.52	-0.3062	498.53
9							506.49	508.64	507.28	-2.15	-0.4265	-0.79	-0.1559	505.51						621.31	623.73	623.22	-2.42	-0.3894	-1.91	-0.3074	623.04
10							506.39	508.41	507.10	-2.04	-0.4028	-0.73	-0.1441	505.51						621.00	623.48	623.14	-2.48	-0.3993	-2.14	-0.3446	623.04
11							413.99	416.65	415.20	-2.66	-0.6425	-1.21	-0.292	416.49						496.32	498.67	497.85	-2.35	-0.4735	-1.53	-0.3082	498.04
LINER							159.87	160.08	160.21					160.0						160.08	160.11	160.08					160.00
1							413.85	415.98	413.99	-1.55	-0.3745	-0.14	-0.0338	415.40						495.50	497.737	496.91	-2.24	-0.452	-1.41	-0.284	497.74
2							413.75	415.31	413.89	-1.56	-0.3770	-0.14	-0.0338	415.40						495.30	497.79	496.98	-2.49	-0.5027	-1.68	-0.3392	497.74
3							414.20	415.48	414.09	-1.28	-0.309	0.11	0.2655	415.40						495.60	497.70	496.86	-2.10	-0.4237	-1.26	-0.254	497.74
4							490.50	492.40	490.98	-1.90	-0.3873	-0.48	-0.0978	488.21						604.00	605.74	604.85	-1.74	-0.288	-0.85	-0.1407	602.75
5							490.92	492.34	490.96	-1.42	-0.2892	-0.04	-0.0815	488.21						604.08	605.79	604.98	-1.71	-0.283	-0.90	-0.1489	602.75
6	3	22.30	0.0738	9.94	12.36	0.760	489.91	492.67	491.10	-2.76	-0.563	-1.19	-0.2429	488.21	46.50	0.0740	25.35	21.15	0.92	604.51	605.89	605.03	-1.38	-0.2283	-0.52	-0.086	602.75
7							489.99	492.61	490.98	-1.62	0.3306	-0.99	-0.202	488.21						604.31	605.73	604.97	-1.42	-0.2349	-0.66	-0.1092	602.75
8							415.21	415.64	414.11	-0.43	0.1035	1.10	0.224	415.40						495.03	497.86	497.06	-2.83	-0.571	-2.03	-0.410	497.74
9							491.00	492.53	491.13	-1.53	-0.3116	-0.13	-0.0265	488.21						604.21	605.91	606.94	-1.70	-0.2813	-0.73	-0.1208	602.75
10							491.05	492.54	490.95	-1.49	-0.3034	0.11	0.0223	488.21						603.94	605.76	604.83	-1.82	-0.3013	-0.89	-0.1473	602.75
11							413.10	415.53	414.05	-2.43	-0.5882	-0.95	-0.2299	415.40						495.08	497.89	496.81	-2.81	-0.5675	-1.73	-0.3494	497.74
LINER							159.99	160.17						160.0						160.12	160.31	160.12					160.00

TABLE XXI

STEADY-STATE TEMPERATURES OBTAINED FROM TEST SECTION 1M LOCATED VERTICALLY

DATA USED TO PREDICT PROTOTYPE TEMPERATURE BY TECHNIQUE 1

THERMO-COUPLE NUMBER	TEST NO.	LOW ENERGY INPUT: POWER ACTUAL BTU/HR	POWER REQ. BTU/HR	DENSITY ACTUAL LB/FT³	DENSITY REQ. LB/FT³	RAD. HEAT TRANSFER BTU/HR	CONV. HEAT TRANSFER BTU/HR	CONV. COEFF. BTU/HR-FT²-°F	TEMP. °F	HIGH ENERGY INPUT: POWER ACTUAL BTU/HR	POWER REQ. BTU/HR	DENSITY ACTUAL LB/FT³	DENSITY REQ. LB/FT³	RAD. HEAT TRANSFER BTU/HR	CONV. HEAT TRANSFER BTU/HR	CONV. COEFF. BTU/HR-FT²-°F	TEMP. °F
1									415.85								497.47
2									415.81								497.36
3									415.89								497.52
4									554.86								664.68
5									554.83								664.51
6	1	5.61	5.60	0.00	0.00	5.64	0.000	0.000	555.00	11.61	11.60	0.000	0.000	11.64	0.000	0.000	664.72
7									554.96								664.69
8									415.88								497.81
9									554.92								664.89
10									556.67								664.61
11									415.93								497.63
LINER									159.95								160.21
1									416.487								498.53
2									416.44								498.59
3									416.52								498.51
4									508.489								623.53
5									508.471								623.56
6	2	5.64	5.635	.0202	.02015	3.20	2.495	0.51	508.73	11.71	11.70	0.0199	0.0198	7.782	3.988	0.60	623.69
7									508.51								623.71
8									416.61								498.62
9									508.64								623.73
10									508.41								623.48
11									416.65								498.67
LINER									160.08								160.11
1									415.398								497.73
2									415.31								497.79
3									415.48								497.70
4									492.40								605.74
5									492.34								605.79
6	3	5.58	5.575	.0522	0.05217	2.525	3.112	0.76	492.67	11.63	11.625	0.0524	0.0523	6.377	5.2838	0.92	605.89
7									492.61								605.73
8									415.64								497.86
9									492.55								605.91
10									492.54								605.76
11									415.53								497.89
LINER									160.17								160.31

DATA USED TO PREDICT PROTOTYPE TEMPERATURE BY ZERO SURROUNDINGS TECHNIQUE

THERMO-COUPLE NUMBER	LOW ENERGY INPUT: POWER ACTUAL BTU/HR	POWER REQ. BTU/HR	DENSITY ACTUAL LB/FT³	DENSITY REQ. LB/FT³	RAD. HEAT TRANSFER BTU/HR	CONV. HEAT TRANSFER BTU/HR	CONV. COEFF. BTU/HR-FT²-°F	TEMP. °F	HIGH ENERGY INPUT: POWER ACTUAL BTU/HR	POWER REQ. BTU/HR	DENSITY ACTUAL LB/FT³	DENSITY REQ. LB/FT³	RAD. HEAT TRANSFER BTU/HR	CONV. HEAT TRANSFER BTU/HR	CONV. COEFF. BTU/HR-FT²-°F	TEMP. °F
1								522.21								625.77
2								522.26								625.83
3								522.16								625.72
4								698.22								836.78
5								698.30								836.64
6	14.13	14.112	0.000	0.000	14.21	0.000	0.000	698.43	29.25	29.23	0.000	0.000	29.33	0.000	0.000	836.93
7								698.39								836.79
8								522.41								625.86
9								698.51								837.10
10								698.46								837.20
11								522.38								625.91
LINER								160.17								160.16
1								523.02								627.11
2								523.10								627.18
3								522.90								627.05
4								639.02								785.13
5								639.10								785.08
6	14.21	14.20	.0981	.0988	8.00	6.292	1.020	639.12								785.21
7								638.97	29.69	29.68	.098	.0973	19.61	10.08	1.20	785.11
8								523.12								627.26
9								639.18								785.26
10								638.94								785.16
11								523.15								627.29
LINER								160.21								160.08
1								521.63								626.11
2								521.51								626.20
3								521.75								626.05
4								618.64								762.12
5								618.61								762.27
6	14.10	14.05	.260	.2558	6.31	7.84	1.52	618.79	29.31	29.30	.256	.2563	15.99	13.31	1.84	762.34
7								618.64								762.26
8								521.78								626.29
9								618.83								762.23
10								618.52								762.09
11								521.71								625.98
LINER								160.07								160.12

CHAPTER VIII

CONCLUSIONS AND RECOMMENDATIONS

The objective of this investigation was twofold. First, similarity parameters were developed to predict the thermal behavior of a prototype from observed model behavior for a radiation-conduction-convection coupled heat transfer problem. Second, an experimental investigation was performed in order to check the validity of the similarity parameters. This objective was accomplished.

The energy equation served as the starting point for the development of the similarity parameters. Two sets of similarity parameters were developed. The first set, Technique I, utilized scaling so that model and prototype temperatures were equal. The second set, Zero Surroundings Technique, required model temperatures higher than prototype temperatures by an amount related to the geometric scaling factor.

An analytical investigation was performed in order to facilitate the design of the test sections. This investigation pointed out the problems associated with separating the energy transferred by radiation from that transferred by convection. The analytical investigation also aided in the selection of a method to predict the radiant exchange.

The experimental investigation was conducted using concentric cylinder test sections located in a space simulation chamber.

Conclusions

The results of the investigation pointed out that it is possible to thermally model a radiation-conduction-convection coupled heat transfer problem. The success of modeling this type of problem lies in the empirical model used to predict the amount of energy transferred by convection. An accurate empirical model is necessary in order to determine the density of the fluid in the model.

The set of similarity parameters developed under the assumptions of Technique I were more accurate in predicting prototype temperatures than those developed under the assumptions of the Zero Surroundings Technique. This was as expected since the Zero Surroundings Technique places an additional constraint upon the thermal problem. This additional restraint was that of the surroundings being at a temperature of absolute zero. The two sets of similarity parameters were verified over a range of free convection from pseudo-conduction to fully developed laminar flow.

Both sets of similarity parameters were very accurate in predicting the steady-state temperatures on the horizontal prototypes. For the vertical test section, the accuracy of predicting the steady-state temperatures was less. This was due to inadequate models used to predict the energy transferred by convection. Nevertheless, the accuracy was close enough to validate the modeling criteria.

This investigation established the feasibility and accuracy of thermal modeling on simple geometries having complex thermal behavior. The models provided reliable forecasts of steady-state heat transfers for a scale ratio of one-half. The overall absolute temperature pre-

diction accuracy was approximately 3 per cent. The results provide substantial evidence that model studies can furnish reliable forecasts of full-scale thermal performance in the space environment.

The empirical correlation established in this investigation for the convective film coefficient in horizontal annuli was in close agreement with the correlation presented by Grigull and Hauf. This correlation deviated from other correlations reported in the literature. Due to the success obtained in modeling the convection heat transfer, it was concluded that the correlation reported by Grigull and Hauf was accurate over the convective regimes encountered in this investigation.

In searching the literature, no correlations of convective film coefficients in vertical annuli were found. Thus, no comparison can be made between existing correlations and the correlation obtained in this investigation.

Recommendations

Recommendations for future investigations in the area of thermal modeling include:

1. Testing the existing systems with various surface coatings.
2. Testing the existing systems in different environments.
3. Transient testing of existing systems.
4. Testing of one-quarter and one-eight scale models.
5. Testing different geometric shapes for a radiation-conduction-convection coupled heat transfer problem.
6. Developing and verifying similarity parameters for geometrically distorted systems containing the three modes of heat

transfer.

7. Investigating the feasibility of modeling systems containing a gas which participates in the radiant exchange.
8. Investigating modeling of a radiation-conduction-convection coupled heat transfer problem with nonuniform heat flux.

BIBLIOGRAPHY

1. Langhaar, H. L. Dimensional Analysis and Theory of Models. John Wiley and Sons, Inc., New York, 1951.

2. Kline, S. J. Similitude and Approximation Theory. McGraw Hill Book Company, Inc., New York, 1965.

3. Ipsen, D. C. Units, Dimensions, and Dimensionless Numbers. McGraw Hill Book Company, Inc., New York, 1960.

4. Wainwright, J. B., L. R. Kelly, and T. H. Keese. "Modeling Criteria and Testing Techniques for the Simulation of Space Environments." Fourth Annual Symposium on Space Environment Simulation, 1-14, May, 1963.

5. Hrycak, P. and B. A. Unger. "General Criteria for Solar Simulation and Model Testing." Proceedings 1964 Annual Technical Meeting of the Institute of Environment Sciences, 257-263, April 1964.

6. Jones, B. P. "Similitude Research in Space Vehicle Thermal Problems." Proceedings of Conference on Thermal Scale Modeling, NASA/OART, 17-35, February 1964.

7. Jones, B. P. "Thermal Similitude Studies." J. Spacecraft and Rockets, 1, Nr. 4, 364-369, July - August 1964.

8. Chao, B. T. and G. L. Weedkind. "Similiarity Criteria for Thermal Modeling of Spacecraft." Journal of Spacecraft and Rockets, 2, Nr. 2, 146-152, March - April 1965.

9. Rolling, R. E. "Results of Transient Thermal Modeling in a Simulated Space Environment." AIAA Thermophysics Specialist Conference, Monterey, California, Paper Nr. 65-659, September 1965.

10. Rolling, R. E. "Thermal Modeling of a Truncated Cone in a Simulated Space Environment." AIAA Space Simulation Conference, Houston, Texas, September 1966.

11. Adkins, D. L. "Thermal Modeling of Bodies with Transient Temperature Gradients." AIAA Thermophysics Specialist Conference, Monterey, California, Paper Nr. 65-660, September 1965.

12. Young, R. L. and Shanklin, R. V. "Thermal Similarity Study of a Typical Space Vehicle Element." Presented at the AIAA Aero-

space Sciences Meeting, New York, New York, January 1966.

13. Shih, C. "Thermal Similitude of Manned Spacecraft." Presented at The AIAA Aerospace Sciences Meeting, New York, New York, January 1966.

14. Miller, P. L. "Thermal Modeling in a Simulated Space Environment." Ph.D. Dissertation at Oklahoma State University, July 1966.

15. Matheny, J. D. "Thermal Design Studies." Final Report, Contract NAS8-5270, September 1965.

16. Kokorev, D. T. "Experimental Methods Applied to the Determination of Some Temperature Radiation Parameters." Int. J. Heat Mass Transfer, 1, 23-27, 1960.

17. Kokorev, D. T. "Method for Determining Size and Shape of Optically Black Emitting Systems." Int. J. Heat Mass Transfer, 5, 981-983, 1962.

18. Clark, L. G. and K. A. Laband. "Orbital Station Temperature Control." Astronautics, 40-43, September 1962.

19. Katz, A. J. "Thermal Testing." Space/Aeronautics (Aerospace Test Engineering - Part 2), 30-34, October 1962.

20. Vickers, J. M. F. "Thermal Scale Modeling: Basic Considerations." Jet Propulsion Laboratory Space Programs Summary IV, No. 37-18, 80-85, December 1962.

21. Katzoff, S. "Similitude in Thermal Models of Spacecraft." NASA TN-D-1631, April 1963.

22. Watkins, J. R. "Thermal Similitude Using Brand's Theorem." Proceedings of Conference on Thermal Scale Modeling, NASA/OART, 3-16, February 1964.

23. Vickers, J. M. F. "A Study of Thermal Modeling Techniques." Proceeding of Symposium on Aeroelastic and Dynamic Modeling Technology, USAF RTD-TOR-63-4197 (Part I), 97-126, March 1964.

24. Vickers, J. M. F. "Thermal Scale Modeling." Astronautics and Aeronautics, 34-39, May 1965.

25. Watkins, J. R. "Sets of Similarity Ratios for Thermal Modeling." NASA TND- (1966).

26. Fowle, A. A., F. Gabron, and Vickers, J. M. F. "Thermal Scale Modeling of Spacecraft: An Experimental Investigation." AIAA Space Simulation and Testing Conference, Pasadena, California, November 1964.

27. Gabron, F., R. W. Johnson, and J. M. F. Vickers. "Thermal Scale Modeling of a Modified Prototype of the Mariner Mars 64 Spacecraft." AIAA Second Annual Meeting, San Francisco, California, Paper Nr. 65-386, July 1965.

28. Gabron, F., R. W. Johnson, J. M. F. Vickers, and J. W. Lucas. "Thermal Scale Modeling of the Mariner IV Spacecraft." AIAA Third Aerospace Sciences Meeting, New York, New York, Paper Nr. 66-23, January 1966.

29. Rhodes, C. A., and J. W. Lucas. "Additional Tests on the Half-Scale Thermal Model of the Mariner IV Spacecraft." Presented at the AIAA Space Simulation Conference; Houston, Texas, September 1966.

30. Folkmann, N. R., F. L. Baldwin, and J. B. Wainwright. "Tests on a Thermally Scaled Model Station in a Simulated Solar Environment." AIAA Thermophysics Specialist Conference, Monterey, California, Paper Nr. 65-658, September 1965.

31. Jones, B. P. and J. K. Harrison. "A Set of Experiments of Thermal Similitude." NASA TMX-53346, October 1965.

32. Thompson, R. K., V. G. Klockzien, and G. E. Dufoe. "Analysis and Tests of Full-Size and Scaled Spacecraft Models in a Simulated Space Environment." Presented at the AIAA Space Simulation Conference, Houston, Texas, September 1966.

33. Lucks, G. F., and H. W. Deem. "Thermal Properties of Thirteen Metals." American Society for Testing Materials Special Tech. Publication 227, 1958.

34. Wiebelt, J. A. Engineering Radiation Heat Transfer. Holt, Rinehart and Winston, Inc., New York, 1966.

35. Leuenberger, H. and R. A. Person. "Compilation of Radiation Shape Factors for Cylindrical Assemblies." ASME Annual Meeting, New York, New York, Paper Nr. 56-A-144, November 1956.

36. Grigull, U. and W. Hauf. "Natural Convection in Horizontal Cylindrical Annuli." Proceedings of the Third International Heat Transfer Conference, Chicago, Illinois, Paper Nr. 41-80-Volume II, August 1966.

37. Lis, J. "Experimental Investigation of Natural Convection Heat Transfer in Simple and Obstructed Horizontal Annuli." Proceedings of the Third International Heat Transfer Conference, Chicago, Illinois, August 1966.

38. Beckmann, W. "Die Warmeubertragung in zylindrischen Gasschichten bei natwilicher Konvecktion." Forsch. a. d. Gebiete Ingenieurswesen, Bd. 2, Heft 5, 1931. pp. 165-178.

39. Kraussold, H. "Warmeabgable von zylindrischen Flussigkeitsschich-

ten bei naturlicher Konvecktion." Forsch. a. d. Gebiete Ingeniewiswesen, Bd. 5, Heft 4, 1934, pp. 186-188.

40. Liu, C. Y., W. K. Mueller, and F. Landis. "Natural Convection Heat Transfer in Long Horizontal Cylindrical Annuli." International Developments in Heat Transfer, Paper 117, ASME 1962, pp. 976-984.

41. Crawford, L. and R. Lemlich. "Natural Convection in Horizontal Concentric Cylindrical Annuli." I and E. C. Fundamentals, Vol. 1, No. 4, November 1962, pp. 260-264.

42. Reid, R. C. and J. K. Sherwood. Properties of Gases and Liquids. McGraw Hill Company, Inc., 1950.

43. Jackob, M. and Hawkins, G. A. Elements of Heat Transfer and Insulation. John Wiley and Sons, Inc., New York, 1950.

44. Light, W., and D. G. Stechert. J. Phys. Chem. 48:23, 1944.

45. Oshima, K. and F. Tamaki. "The Space/Solar Simulators of ISAS Univ. Tokyo." Presented at the AIAA Space Simulation Conference, Houston, Texas, September 1966.

46. Schlichting, H. Boundary Layer Theory, Fourth Edition. McGraw-Hill Co., Inc., 1960.

47. Bishop, E. H. and C. T. Carley. "Photographic Studies of Natural Convection Between Concentric Cylinders." Proceedings of the Heat Transfer and Fluid Mechanics Institute, June 1966.

48. Kreith, F. Principles of Heat Transfer. International Textbook Company, 1965.

APPENDIX A

DEVELOPMENT OF MODELING CRITERIA

DEVELOPMENT OF MODELING CRITERIA

Either of two principles, theory of similitude or dimensional analysis, may be used to develop the modeling criteria. The development of the criteria by dimensional analysis is accomplished by writing down all the pertinent variables and applying the principles of dimensionless analysis. One disadvantage in using the dimensional analysis approach is that it requires some insight into the problem and preferably the knowledge of at least one combination of dimensional groups used in the modeling criteria.

The similitude approach consists of writing the governing differential equation, which describes the thermal behavior of the model and prototype, in dimensionless form. Since the governing differential equation can be established, the similitude approach was selected for developing the modeling criteria.

The Governing Differential Equation

Before applying the theory of similitude, the governing differential equation must be obtained. The general differential equation, expressing the energy balance for the i th element of the test section, can be expressed as:

$$\rho_i V_i C_{p_i} \frac{\partial T_i}{\partial \theta} = q_i + \sum_{s=1}^{S} \sum_{j=1}^{J} \alpha_{sj} \phi_{js} A_s + \sum_{n=1}^{N} k_n A_n \frac{\partial T_{i-n}}{\partial L_{i-n}}$$

$$- \sum_{s=1}^{S} \epsilon_s \sigma A_s T_i^4 + \sum_{j=1}^{J} A_n C_s (T_i - T_j) + \sum_{j=1}^{J} h_s A_n (T_i - T_j). \qquad \text{(A-1)}$$

This element may or may not include an exposed surface. In Equation (A-1), $\rho_i V_i C_{p_i} \partial T_i/\partial\theta$ is the rate of change in internal energy of the element, $\varepsilon_s \sigma A_s T_i^4$ is the rate at which energy is emitted from surface s, q_i is the internal heat generation within the element, $A_n C_s(T_i-T_j)$ is the heat transfer by interfacial conductance between the i and j elements along the path n, $k_n A_n \frac{\partial T_{i-n}}{\partial L_{i-n}}$ is the heat transfer by solid conduction to or from element i along the path n, $h_s A_n(T_i-T_j)$ is the heat transfer by convection between the i and j element along the path n, and $\alpha_{sj} \phi_{js} A_s$ is the heat transfer from surface j which is absorbed at surface s of element i. Equation (A-1) has been widely used to predict the temperatures of regions of satellites and other space vehicles. This equation was used for establishing the modeling criteria.

Formulation of Modeling Criteria

If a geometrically similar, though different sized, model is constructed for the prototype, then it is possible to write the same relation for geometrically identical locations on the model and the prototype. Equation (A-1) written for the prototype and model is:

Prototype equation

$$\frac{\rho_p V_p C_{p_p} T_p}{\theta_p}\left\{\bar{\rho}_i \bar{V}_i \bar{C}_{p_i} \frac{\partial \bar{T}_i}{\partial \bar{\theta}}\right\}_p = q_p \left\{\bar{q}_i\right\}_p + \sum_{s=1}^{S}\sum_{j=1}^{J} (\alpha_{sj} \phi_{js} A_s)_p \cdot$$

$$\left\{\bar{\alpha}_{sj} \bar{\phi}_{js} \bar{A}_s\right\}_p + \sum_{n=1}^{N} \frac{k_{np} A_{np} C_{p_p} T_p}{L_p} \bar{k}_n \bar{A}_n \frac{\partial \bar{T}_{i-n}}{\partial \bar{L}_{i-n}} +$$

$$\sum_{j=1}^{J} A_{np}\, C_{sp}\, T_p \left\{ \overline{A}_n\, \overline{C}_s (\overline{T}_i - \overline{T}_j) \right\}_p + \sum_{j=1}^{J} h_{sp}\, A_{np}\, T_p \left\{ \overline{h}_s\, \overline{A}_n (\overline{T}_i - \overline{T}_j) \right\}_p -$$

$$- \sum_{s=1}^{S} \epsilon_{sp}\, \sigma\, A_{sp}\, T_p^4 \left\{ \overline{\epsilon}_s\, \sigma\, \overline{A}_s\, \overline{T}_i^4 \right\}_p , \qquad \text{(A-2)}$$

Model Equation

$$\left(\frac{\rho\, V\, C_p\, T}{\theta} \right)_m \left\{ \overline{\rho}_i\, \overline{V}_i\, \overline{C}_{p_i}\, \frac{\partial \overline{T}_i}{\partial \overline{\theta}} \right\}_m = q_m \left[\overline{q}_i \right]_m + \sum_{s=1}^{S} \sum_{j=1}^{J} (\alpha_{sj}\, \phi_{js}\, A_s)_m \cdot$$

$$\left[\overline{\alpha}_{sj}\, \overline{\phi}_{js}\, \overline{A}_s \right]_m + \sum_{n=1}^{N} \left(\frac{k_n\, A_n\, T}{L} \right)_m \left\{ \overline{k}_n\, \overline{A}_n\, \frac{\partial \overline{T}_{i-n}}{\partial \overline{L}_{i-n}} \right\}_m$$

$$+ \sum_{j=1}^{J} (A_n\, C_s\, T)_m \left[\overline{A}_n\, \overline{C}_s (\overline{T}_i - \overline{T}_j) \right]_m + \sum_{j=1}^{J} (h_s\, A_n\, T)_m \left[h_s\, A_n (T_i - T_j) \right]_m -$$

$$- \sum_{s=1}^{S} (\epsilon_s\, \sigma\, A_s\, T^4)_m \left[\overline{\epsilon}_s\, \sigma\, \overline{A}_s\, \overline{T}_i^4 \right] . \qquad \text{(A-3)}$$

The only differences between the model and prototype equations occur in the coefficients $\rho\, V\, C_p\, T/\theta$, q, $\alpha_{sj}\, \phi_{js}\, A_s$, etc. For point-to-point similarity to exist between the model and the prototype, the ratios of corresponding coefficients must be the same. Equating the ratios of correpsonding coefficients the following identities were obtained:

$$\frac{\rho^* V^* C_p^* T^*}{\theta^*} = q^* = \alpha_{sj}^* \phi_{js}^* A_s^* = \epsilon_s^* A_s^* T^{*4} =$$

$$\frac{k_n^* A_n^* T^*}{L^*} = A_n^* C_s^* T^* = A_n^* h_s^* T^* \; ;$$

$$j=1,2,3,\ldots,J$$

$$n=1,2,3,\ldots,N \; ,$$

$$s=1,2,3,\ldots,S \qquad \text{(A-4)}$$

where the ratios of properties at similar points on the model and the prototype is represented by a superscript starred quantity (T^*, V^*, etc.). Equations (A-4) are subject to the following restrictions:

1. Perfect geometric similarity between the model and the prototype.
2. The ratios of the properties (L^*, P^*, T^*, etc.) must be constants at all points in the model for all test conditions and thermal levels.

The length, area and volume ratios have been retained in the parametric equations. Thus, slight distortions in geometric scaling may be permitted when it can be shown that they have little or no effect on the temperature fields which exist in the system.

APPENDIX B

7040 COMPUTER PROGRAM FOR CONFIGURATION FACTOR EVALUATION

7040 COMPUTER PROGRAM FOR CONFIGURATION FACTOR EVALUATION

The term "shape factor," or its synonyms, "view factor," "configuration factor," "form factor," "F factor," as related to radiant energy transfer between two surfaces, is defined as the fraction of the total radiation leaving one surface in all directions which is intercepted by the other surface. The shape factor is a function of the shapes and relative position of the two surfaces under consideration. The above definition also covers the special case of the shape factor of a surface itself.

The configuration factors presented in Equations (4-18), (4-19), (4-20), and (4-21) were developed in Reference [35]. These equations were solved on the 7040 digital computer and the program which furnished the solution is listed in this appendix. In order to facilitate programming, the equations were written in the following form.

$$F21 = \frac{RI}{RO}\left\{1 - \frac{1}{\pi}\left\{\cos^{-1}\frac{EL^2-RO^2+RI^2}{EL^2+RO^2-RI^2} - \frac{1}{2RI(EL)}\left\{\sqrt{(EL^2+RO^2+RI^2)^2-(2RI\cdot RO)^2}\cdot \right.\right.\right.$$

$$\left.\left.\left.\cos^{-1}\frac{RI}{RO}\frac{EL^2-RO^2+RI^2}{EL^2+RO^2-RI^2} + (EL^2-RO^2+RI^2)\sin^{-1}\frac{RI}{RO} - \frac{\pi}{2}(EL^2+RO^2-RI^2)\right\}\right\}\right\}, \quad \text{(B-1)}$$

$$F22 = 1 - \frac{RI}{RO} + \frac{1}{\pi}\left\{\frac{2RI}{RO}\tan^{-1}\frac{2\sqrt{RO^2-RI^2}}{EL} - \frac{EL}{2RO}\left\{\frac{\sqrt{4RO^2+EL^2}}{EL}\cdot \right.\right.$$

$$\left.\left.\sin^{-1}\frac{4(RO^2-RI^2)+\frac{EL^2}{RO^2}(RO^2-2RI^2)}{EL^2+4(RO^2-RI^2)} - \sin\frac{RO^2-2RI^2}{RO^2} + \frac{\pi}{2}\left\{\frac{4RO^2+EL^2}{EL} - 1\right\}\right\}\right\}, \quad \text{(B-2)}$$

$$F34 = 1 - \left(\frac{EL}{RO^2-RI^2}\right)\left\{RI-RO(F22+2F21-1)\right\} , \qquad (B-3)$$

$$F23 = \frac{1}{2}\,(1-F21-F22) , \qquad (B-4)$$

where $F21 = F_{21}$,

$F22 = F_{22}$, $\qquad EL = L$,

$F34 = F_{34}$, $\qquad RI = R_i$,

$F23 = F_{23}$, $\qquad RO = R_o$.

```
      C     CONFIGURATION FACTORS FOR TWO EQUAL LENGTH-CONCENTRIC CYLINDERS
      C     D. MAPLES
      C     RI-RADIUS OF INNER CYLINDER
      C     RO-RADIUS OF OUTER CYLINDER
      C     EL-LENGTH OF CYLINDERS
1       500 FORMAT(F16.8,F16.8,F16.8)
2       100 FORMAT(F10.7,F10.7,F10.7,F10.7,F10.7,F10.7,F10.7)
3       200 FORMAT(3X,2HRI,8X,2HRO,9X,1HL,8X,3HF21,7X,3HF22,7X,3HF34,7X,3HF23)
4           WRITE(6,200)
5         3 READ(5,500) RI,RO,EL
      C     CALCULATIONS FOR CONFIGURATION FACTOR F21
6           D=RI/RO
7           E=(EL**2.0-RO**2.0+RI**2.0)/(EL**2.0+RO**2.0-RI**2.0)
10          P=ABS(E)
11          Q=D*P
12          X=(EL**2.0+RO**2.0+RI**2.0)**2.0-(2.0*RI*RO)**2.0
13          T=SQRT(1.0-P**2.0)/P
14          U=SQRT(1.0-Q**2.0)/Q
15          W=D/SQRT(1.0-D**2.0)
16          BAT=SQRT(X)*ATAN(U)+(EL**2.0-RO**2.0+RI**2.0)*ATAN(W)
17          CAT=(3.1415927/2.0)*(EL**2.0+RO**2.0-RI**2.0)
20          RAT=1.0/(2.0*RI*EL)
21          F21=D*(1.0-(1.0/3.1415927)*(ATAN(T)-(RAT)*(BAT-CAT)))
      C     CALCULATIONS FOR CONFIGURATION FACTOR F22
22          W1=SQRT(4.0*RO**2.0+EL**2.0)/EL
23          W2=(RO**2.0-2.0*RI**2.0)/RO**2.0
24          W3=4.0*(RO**2.0-RI**2.0)+(EL**2.0/RO**2.0)*(RO**2.0-2.0*RI**2.0)
25          W4=EL**2.0+4.0*(RO**2.0-RI**2.0)
26          W5=W3/W4
27          W6=(2.0/EL)*SQRT(RO**2.0-RI**2.0)
30          U1=W5/SQRT(1.0-W5**2.0)
31          U2=W2/SQRT(1.0-W2**2.0)
32          VT=W1*ATAN(U1)-ATAN(U2)+3.1415927/2.0*(W1-1.0)
33          F22=1.0-D+1.0/3.1415927*(2.0*D*ATAN(W6)-EL/(2.0*RO)*(VT))
      C     CALCULATION OF CONFIGURATION FACTOR F34
34          F34=1.0-(EL/(RO**2.0-RI**2.0))*(RI-RO*(F22+2.0*F21-1.0))
      C     CALCULATION OF CONFIGURATION FACTOR F23
35          F23=0.5*(1.0-F21-F22)
36          WRITE(6,100) RI,RO,EL,F21,F22,F34,F23
37          GO TO 3
40        5 STOP
41          END
```

APPENDIX C

7040 COMPUTER PROGRAM FOR RADIOSITY EVALUATION

7040 COMPUTER PROGRAM FOR RADIOSITY EVALUATION

For gray surfaces which follow Lambert's cosine law and reflect diffusely, the radiation from such surfaces can be treated conveniently in terms of the radiosity. The radiosity is defined as the rate at which radiation leaves a given surface per unit area. Therefore, the radiosity is the sum of the radiation emitted, reflected, and transmitted. The radiosities of the surfaces in the enclosure considered in performing the thermal analysis were generated from Equation (4-22). These radiosity relations were written in the following form to facilitate programming.

$$\begin{aligned}
&\partial_{11}\, x_1 + \partial_{12}\, x_2 + \cdots + \partial_{1n}\, x_1 = b_1 \,, \\
&\partial_{21}\, x_1 + \partial_{22}\, x_2 + \cdots + \partial_{2n}\, x_2 = b_2 \,, \\
&\quad\cdot \qquad\qquad\qquad\qquad\quad \cdot \,, \\
&\quad\cdot \qquad\qquad\qquad\qquad\quad \cdot \,, \\
&\quad\cdot \qquad\qquad\qquad\qquad\quad \cdot \,, \\
&\partial_{n1}\, x_1 + \partial_{n2}\, x_2 + \cdots + \partial_{nn}\, x_n = b_n \,.
\end{aligned} \tag{C-1}$$

where

$$\partial_{11} = -1.0 \qquad \partial_{21} = \frac{\bar{\bar{\rho}}_2\, F_{21}}{1-\bar{\bar{\rho}}_2 F_{22}} \qquad \cdots \qquad \partial_{n1} = \frac{\bar{\bar{\rho}}_n\, F_{n1}}{1-\bar{\bar{\rho}}_n F_{nn}}$$

$$\partial_{12} = \frac{\bar{\bar{\rho}}_1\, F_{12}}{1-\bar{\bar{\rho}}_1 F_{11}} \qquad \partial_{22} = -1.0 \qquad \cdots \qquad \partial_{n2} = \frac{\bar{\bar{\rho}}_n\, F_{n2}}{1-\bar{\bar{\rho}}_n F_{nn}}$$

$$\partial_{13} = \frac{\bar{\bar{\rho}}_1 F_{13}}{1-\bar{\bar{\rho}}_1 F_{11}} \qquad \partial_{23} = \frac{\bar{\bar{\rho}}_2 F_{23}}{1-\bar{\bar{\rho}}_2 F_{22}} \quad . \quad . \quad . \quad .$$

$$\partial_{1n} = \frac{\bar{\bar{\rho}}_1 F_{1n}}{1-\bar{\bar{\rho}}_1 F_{11}} \qquad \partial_{2n} = \frac{\bar{\bar{\rho}}_2 F_{2n}}{1-\bar{\bar{\rho}}_2 F_{22}} \quad . \quad . \quad . \quad \partial_{nn} = -1.0 \qquad \text{(C-2)}$$

$$b_1 = \frac{\epsilon_1 E_{b1}}{1-\bar{\bar{\rho}}_1 F_{11}}$$

$$b_2 = \frac{\epsilon_2 E_{b2}}{1-\bar{\bar{\rho}}_2 F_{22}}$$

$$b_n = \frac{\epsilon_n E_{bn}}{1-\bar{\bar{\rho}}_n F_{nn}} \quad . \qquad \text{(C-3)}$$

Equation (C-1) was solved by the method of determinants. The program for the solution is listed below.

```
      C     GAUSS-ELIMINATION WITH ALL COEFFICIENTS
1           DIMENSION A(10,10)
2           READ(5,51)N
3        55 FORMAT(29HINDEX TO UNKNOWNS    UNKNOWNS)
4        51 FORMAT(I3)
5        52 FORMAT(I3,14X,F16.8)
6       301 FORMAT(F16.8)
      C     I=INDEX CORRESPONDING TO THE UNKNOWN VARIABLE
      C     MATRIX COEFFICIENT FOR SOLUTION TO THE SET OF EQUATIONS  BELOW
7           A(1,1)=-1000.0
10          A(1,2)=0.0
11          A(1,3)=0.0
12          A(1,4)=24.969888
13          A(1,5)=2.500527
14          A(1,6)=0.001074
15          A(1,7)=2.515056
16          A(1,8)=0.004344
17          A(1,9)=-215344.656
20          A(2,1)=0.0
21          A(2,2)=-1000.0
22          A(2,3)=0.0
23          A(2,4)=1.538775
24          A(2,5)=26.858709
25          A(2,6)=1.538775
26          A(2,7)=0.031632
27          A(2,8)=0.031632
30          A(2,9)=-215344.656
31          A(3,1)=0.0
32          A(3,2)=0.0
33          A(3,3)=-1000.0
34          A(3,4)=0.001074
35          A(3,5)=2.500527
36          A(3,6)=24.969888
37          A(3,7)=0.004344
40          A(3,8)=2.515056
41          A(3,9)=-215344.656
42          A(4,1)=8.45963156
43          A(4,2)=0.84537246
44          A(4,3)=0.0003640906
45          A(4,4)=-1000.0
46          A(4,5)=2.9454832
47          A(4,6)=0.05416024
50          A(4,7)=3.873537
51          A(4,8)=0.0259938
52          A(4,9)=-105329.20
53          A(5,1)=0.521171205
54          A(5,2)=9.09955155
55          A(5,3)=0.521171205
56          A(5,4)=1.8164336
57          A(5,5)=-1000.0
60          A(5,6)=1.8164336
61          A(5,7)=0.16726972
62          A(5,8)=0.16726972
63          A(5,9)=-105551.80
64          A(6,1)=0.00036409067
65          A(6,2)=0.84537246
66          A(6,3)=8.459631588
```

```
      A(6,4)=0.054160238
      A(6,5)=2.9454832
      A(6,6)=-1000.0
      A(6,7)=0.0259938
      A(6,8)=3.873537
      A(6,9)=-105329.20
      A(7,1)=150.90336
      A(7,2)=3.1068
      A(7,3)=0.260388
      A(7,4)=687.4497
      A(7,5)=47.237733
      A(7,6)=4.60791
      A(7,7)=-1000.0
      A(7,8)=5.53284
      A(7,9)=-15675.02
      A(8,1)=0.260388
      A(8,2)=3.1068
      A(8,3)=150.90336
      A(8,4)=4.60791
      A(8,5)=47.237733
      A(8,6)=687.4497
      A(8,7)=5.53284
      A(8,8)=-1000.0
      A(8,9)=-15675.02
      A(9,1)=0.0
      A(9,2)=0.0
      A(9,3)=0.0
      A(9,4)=0.0
      A(9,5)=0.0
      A(9,6)=0.0
      A(9,7)=0.0
      A(9,8)=0.0
      A(9,9)=0.0
      DO 500 I=1,8
      DO 500 J=1,9
  500 WRITE(6,301)A(I,J)
      WRITE(6,55)
      M=N-1
      LM=M
      LP=M+1
    9 IF(A(1,1)) 13,14,13
   14 STOP
   13 DO 15 J=1,M
   15 A(LP,J)=A(1,J+1)/A(1,1)
      DO 16 I=2,M
      D=A(I,1)
      DO 16 J=1,M
      C=A(I,J+1)-D*A(LP,J)
   16 A(I-1,J)=C
      DO 17 J=1,M
   17 A(M,J)=A(LP,J)
      LM=LM-1
  113 IF(LM) 114,114,9
  114 DO 59 I=1,N
   59 WRITE(6,52)I,A(I,1)
   98 STOP
      END
$ENTRY
```

APPENDIX D

7040 COMPUTER PROGRAM FOR LEAST SQUARE CURVE FIT

7040 COMPUTER PROGRAM FOR LEAST SQUARE CURVE FIT

The purpose of the least square program was to determine the coefficients for Equation (5-38), Chapter IV. The program is a standard IBM share program and is presented below. All instructions necessary to operate the program are stated within the program.

```
      C     CURVE FIT.
1           DIMENSION A(3,3),B(3,1)
2           DIMENSION X(200),Y(200),Z(200),C(200,15)
3           READ(5,1) N,M
4         1 FORMAT(2I10)
5           DO 62 KIM=1,3
6           WRITE (6,100)
7       100 FORMAT(1H1,17HTHE COEFFICIENTS ,
           121HOE THE POLYNOMIAL IN ,20HINCREASING ORDER ARE)
10          READ(5,101)(X(I),Y(I),I=1,N)
11      101 FORMAT(2F10.0)
12          CALL LSQR (X,Y,N,A,B,M,1,C)
13          WRITE (6,102) (B(I,1),I=1,M)
14      102 FORMAT(1HO,E20.8)
15          DO 60 I=1,N
16          Z(I)=0.0
17          DO 60 L=1,M
20          R=X(I)**(L-1)*B(L,1)
21          Z(I)= Z(I) + R
22       60 CONTINUE
23          WRITE(6,103)
24      103 FORMAT(1HO)
25          WRITE(6,104)
26      104 FORMAT(1HO,5X,20HINDEPENDENT VARIABLE,
           16X,18HDEPENDENT VARIABLE,7X,19HCOMPUTED VALUE OF Y)
27          DO 61 J=1,N
30          WRITE (6,105) X(J),Y(J),Z(J)
31      105 FORMAT (1HO,3(5X,E20.8))
32       61 CONTINUE
33       62 CONTINUE
34          STOP
35          END
36          SUBROUTINE LSQR(X,Y,N,A,B,M,L,C)
      C     LEAST SQUARES CURVE FIT
      C    THE COEFFICIENTS OF THE POLUNOMIAL ARE STORED IN THE B(M,L) MATRIX.
      C    X IS THE ARRAY OF INDEPENDENT VARIABLE VALUES.
      C    Y IS THE ARRAY OF DEPENDENT VARIABLE VALUES.
      C    N IS THE NUMBER OF VALUES OF X.
      C    A IS THE ARRAY THAT IS GENERATED IN THE LEAST SQUARES COMPUTATION9
      C       A IS DIMENSIONED (M,M).
      C    B IS THE ARRAY THAT CONTAINS THE POLYNOMIAL DOEFFICIENTS IN ORDER OF
      C       DECREASING DEGREE9  B IS TWO DIMENSIONAL (M,L..
      C    M IS THE NUMBER OF COEFFICIENTS IN THE FITTED POLYNOMIAL9
      C    L IS THE NUMBER OF SETS OF Y DATA USUALLY L = 1)
37          DIMENSION A(M,M), B(M,L)
40          DIMENSION X(N),Y(N),C(200,10)
      C    GENERATE THE A AND B ARRAY.
41          1 DO 2 I= 1,N
42          2 C(I,1) = 1.
43            DO 3 J=2,M
44            DO 3 I=1,N
45          3 C(I,J) = C(I,J-1) * X(I)
46            DO 4 I= 1,M
47            DO 4 J= 1,M
50            A(I,J) = 0
51            DO 4 K= 1,N
52          4 A(I,J) =  A(I,J) + C(K,I) *C(K,J)
53            DO 5 I = 1,M
54            B(I,L) = 0
55            DO 5 K= 1,N
56          5 B(I,L) = B(I,L) + C(K,I) * Y(K)
      C    CALL AUBURN UNIV. MATRIX INVERSION SUBROUTINE.
57            CALL MATINV(A,M,B,L,DETERM)
      C    DIMENSIONS ARE A(M,M), B(M,L)
60            RETURN
61            END
```

APPENDIX E

7040 COMPUTER PROGRAM FOR THERMAL ANALYSIS OF HORIZONTAL CONCENTRIC CYLINDER SYSTEM

7040 COMPUTER PROGRAM FOR THERMAL ANALYSIS OF HORIZONTAL CONCENTRIC CYLINDER SYSTEM

Theoretical calculations of temperatures on models and prototypes for various energy inputs and convective film coefficient correlations were obtained on a digital computer. Prototype calculations were made for a range of power inputs to the main heater from 20 to 80 Btu/hr and two different convective film coefficient correlations. The input to the model was obtained by scaling the input to the prototype according to the similarity parameters developed in the Zero Surroundings Technique and Technique I. The correlations by Grigull and Hauf [36] and Liu, Mueller, and Landis [40] were used to represent the convective film coefficient correlations for the horizontal annuli.

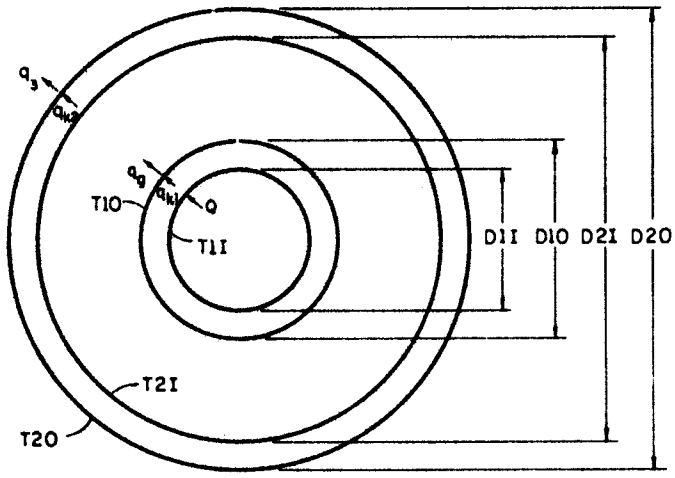

ASSUMPTIONS:

1. RADIAL CONDUCTION THROUGH CYLINDER WALL
2. RADIATION EXCHANGE BETWEEN INNER AND OUTER CYLINDER CAN BE EVALUATED BY INFINITE CYLINDER CALCULATION
3. THE CONVECTION FILM COEFFICIENT CAN BE REPRESENTED BY THE EMPIRICAL CORRELATIONS PRESENTED IN TABLE IX

Figure 47. Nomenclature Used in Computer Program

Computations were obtained by solving Equations (4-10), (4-11), (4-12), and (4-25). These equations were written in the following form to facilitate programming.

Heat transferred across the horizontal annuli:

$$q_g = \frac{\sigma \quad (A10)\left[(T10)^4 - (T2I)^4\right]}{(\frac{1}{\epsilon} - 1) + \frac{A10}{A2I}(\frac{1}{\epsilon} - 1) + 1} + h\,(A10)(T10-T2I), \qquad (E\text{-}1)$$

Heat transferred away from the outer cylinder:

$$q_3 = \sigma\,\epsilon\,(A20)\left\{(T20)^4 - (TW)^4\right\}, \qquad (E\text{-}2)$$

Heat conducted through the cylindrical walls:

$$q_{k1} = 2\pi\,k\,\ell\,\frac{(T10 - T1I)}{\ln\frac{r_{10}}{r_{1i}}}, \qquad (E\text{-}3)$$

and

$$q_{k2} = 2\pi\,k\,\ell\,\frac{(T20 - T2I)}{\ln\frac{r_{20}}{r_{2i}}}. \qquad (E\text{-}4)$$

For this one-dimensional problem, the following expression can be written:

$$Q = q_{k1} = q_{k2} = q_g = q_3 . \qquad (E\text{-}5)$$

Results obtained from the solution to these equations are presented in Table XXII.

```
C     THE FOLLOWING VARIABLES PRETAIN TO THE PROTOTYPE PROPERTIES.
C
C     PROTOTYPE NUMBER 1P.
C     T2O = OUTSIDE TEMPERATURE OF OUTER CYLINDER.
C     T2I = INSIDE TEMPERATURE OF OUTER CYLINDER.
C     T1O = OUTSIDE TEMPERATURE OF INNER CYLINDER.
C     T1I = INSIDE TEMPERATURE OF INNER CYLINDER.
C     D2O = OUTSIDE DIAMETER OF OUTER CYLINDER.
C     D2I = INSIDE DIAMETER OF OUTER CYLINDER.
C     D1O = OUTSIDE DIAMETER OF INNER CYLINDER.
C     D1I = INSIDE DIAMETER OF INNER CYLINDER.
C     Q = HEAT TRANSFER THRU CYLINDERS.
C     EL = LENGTH OF CYLINDER.
C     P = PRESSURE OF FLUID IN PSIF.
C     TG = THERMAL CONDUCTIVITY OF GAS.
C     H = CONVECTION COEFFICIENT.
C     GR = GRASHOF NUMBER.
C     THE FOLLOWING VARIABLES PRETAIN TO MODEL PROPERTIES.
C
C     T2OM = OUTSIDE TEMPERATURE OF OUTER CYCLINDER.
C     T2IM = INSIDE TEMPERATURE OF OUTER CYLINDER.
C     T1OM = OUTSIDE TEMPERATURE OF INNER CYLINDER.
C     T1IM = INSIDE TEMPERATURE OF INNER CYLINDER.
C     A2OM = OUTSIDE AREA OF OUTER CYLINDER.
C     A1OM = OUTSIDE AREA OF INNER CYLINDER.
C     A2IM = INSIDE AREA OF OUTER CYLINDER.
C     QM = HEAT TRANSFER THRU CYLINDER.
C     ELM = LENGTH OF CYLINDER.
C     PM = PRESSURE OF FLUID IN PSIF.
C     TGM = THERMAL CONDUCTIVITY OF GAS.
C     HM = CONVECTIVE COEFFICIENT.
C     GRM = GRASHOF NUMBER.
C     COMMON VARIABLES BETWEEN MODEL AND PROTOTYPE.
C
C     TW = CHAMBER WALL TEMPERATURE.
C     SIGMA = STEFAN - BOLTZMANN CONSTANT.
C     EPSON = EMISSIVITY.
C     R = GAS CONSTANT.
C     G = LOCAL ACCELERATION OF GRAVITY.
C     TS = THERMAL CONDUCTIVITY OF SOLID.
1       51 FORMAT(6F12.5)
2       52 FORMAT(E16.8)
3       53 FORMAT(F16.8)
4       54 FORMAT(4F12.5)
5       55 FORMAT(10F12.4)
6       70 FORMAT(1H1)
7          WRITE(6,70)
10      60 FORMAT(7X,3HT1I,9X,3HT1O,9X,3HT2I,9X,3HT2O,11X,1HQ,11X,1HP
          111X,1HH,10X,2HTM,10X,2HQR,10X,2HQC/)
11      62 FORMAT(52X,10HSYSTEM--1P/)
12      63 FORMAT(34X,60HCONVECTIVE COEFFICIENT CORRELATION--LIU, MUELLER, AN
          1D LANDIS/)
13         WRITE(6,62)
14         WRITE(6,63)
15         WRITE(6,60)
16         READ(5,51)TW,D2O,D2I,D1O,D1I,TS
17         READ(5,54)EPSON,EL,R,G
```

```
20          READ(5,52)SIGMA
21        5 READ(5,53)ROW
      C     PROTOTYPE  CALCULATIONS
22          TV=0.0
23        4 READ(5,53)Q
24          A2O=3.1415927*D2O*EL
25          A1O=3.1415927*D1O*EL
26          A2I=3.1415927*D2I*EL
27          TV=TV+1.0
30          T2O=(Q/(SIGMA*EPSON*A2O)+TW**4.0)**0.25
31          ZLOG=ALOG(D2O/D2I)
32          T2I=(Q/(2.0*3.1415927*TS*EL))*ZLOG+T2O
33          T1O=T2I+0.50
34        2 T1O=T1O+0.50
35          TM=(T1O+T2I)/2.0
36          A=0.35145532E-03
37          B=0.32041684E-04
40          C=-0.10027234E-07
41          D=0.22337353E-11
42          TG=A+B*TM+C*TM**2.0+D*TM**3.0
43          UM=TM**1.5/(375.0*TM+77700.0)
44          DELTA=(D2I-D1O)/2.0
45          DTM=T1O-T2I
46          GR=ROW**2.0/TM*DTM*DELTA**3.0/UM**2.0*G
47          P=ROW*R*TM
50          CON=0.20+0.145*(DELTA/D1O)
51          EP=-0.02*(DELTA/D1O)
52          CO=(2.72)**EP
53          A1=0.77661161
54          B1=-0.18508948E-03
55          C1=0.11816195E-06
56          ZL=ALOG(D2I/D1O)
57          PR=A1+B1*TM+C1*TM**2.0
60          TP=PR**2.0*GR/(1.36+PR)
61          S=ALOG(TP)
62          U=6.9077552
63          H=(2.0*TG/(D1O*ZL))*0.135*(TP)**0.278
64       16 CONTINUE
65          BT=(1.0/EPSON-1.0)*(1.0+A1O/A2I)+1.0
66          QC=H*A1O*(T1O-T2I)
67          QR=A1O*SIGMA*EPSON/BT*(T1O**4.0-T2I**4.0)
70          Z=-Q+QR+QC
71          IF(Z) 2,3,3
72        3 WLOG=ALOG(D1O/D1I)
73          T1I=Q/(2.0*3.1415927*TS*EL)*WLOG+T1O
      C     MODEL  CALCULATIONS
74          HM=2.0*H
75          QM=0.63*Q
76          A2OM=0.25*A2O
77          A1OM=0.25*A1O
100         A2IM=0.25*A2I
101         ELM=0.50*EL
102         T2OM=(QM/(SIGMA*EPSON*A2OM)+TW**4.0)**0.25
103         T2IM=(QM/(2.0*3.1415927*TS*ELM))*ZLOG+T2OM
104         T1OM=T2IM+1.0
105       6 T1OM=T1OM+1.0
106         TMM=(T1OM+T2IM)/2.0
107         DTMM=T1OM-T2IM

110         DELTAM=DELTA/2.0
111         TGM=A+B*TMM+C*TMM**2.0+D*TMM**3.0
112         UMM=TMM**1.5/(375.0*TMM+77700.0)
113         GRM=GR*(DELTAM*TG*HM/(DELTA*TGM*H))**4.0
114         BTM=(1.0/EPSON-1.0)*(1.0+A1OM/A2IM)+1.0
115         QCM=HM*A1OM*(T1OM-T2IM)
116         QRM=A1OM*SIGMA*EPSON/BTM*(T1OM**4.0-T2IM**4.0)
117         ZM=-QM+QRM+QCM
120         IF(ZM) 6,7,7
121       7 T1IM=QM/(2.0*3.1415927*TS*ELM)*WLOG+T1OM
122         ROWM=(GRM*UMM**2.0*TMM/(G*DTMM*DELTAM**3.0))**0.50
123         PM=ROWM*R*TMM
124         WRITE(6,55)T1I,T1O,T2I,T2O,Q,P,H,TM,QR,QC
125         IF(TV-4.0) 4,5,5
126      11 STOP
127         END
      $ENTRY
```

TABLE XXII

SYSTEM--1P

CONVECTIVE COEFFICIENT CORRELATION--LIU, MUELLER, AND LANDIS

T11	T10	T21	T20	Q	P	H	TM	QR	QC
747.9692	747.9264	569.4264	569.4076	80.0000	366.4875	0.2610	658.6764	70.1847	9.9115
693.2148	693.1826	530.1826	530.1685	60.0000	340.3402	0.2526	611.6826	51.2974	8.7575
622.0881	622.0667	479.5667	479.5573	40.0000	306.4744	0.2407	550.8167	32.7137	7.2975
515.5169	515.5062	404.5062	404.5015	20.0000	255.9474	0.2207	460.0062	14.8107	5.2110
738.4692	738.4264	569.4264	569.4076	80.0000	909.6116	0.4276	653.9264	64.9160	15.3714
682.7148	682.6826	530.1826	530.1685	60.0000	843.5478	0.4123	606.4326	46.6784	13.3750
611.0881	611.0667	479.5667	479.5573	40.0000	758.5355	0.3915	545.3167	29.2299	10.9498
503.0169	503.0062	404.5062	404.5015	20.0000	631.1748	0.3549	453.7562	12.5799	7.4355
733.4692	733.4264	569.4264	569.4076	80.0000	1272.0728	0.5119	651.4264	62.2235	17.8558
677.7148	677.6826	530.1826	530.1685	60.0000	1179.3294	0.4931	603.9326	44.5526	15.4710
605.5881	605.5667	479.5667	479.5573	40.0000	1059.4971	0.4669	542.5667	27.5571	12.5136
498.0169	498.0062	404.5062	404.5015	20.0000	881.1904	0.4222	451.2562	11.7329	8.3962
727.9692	727.9264	569.4264	569.4076	80.0000	1797.6768	0.6157	648.6764	59.3246	20.7580
672.2148	672.1826	530.1826	530.1685	60.0000	1666.0574	0.5925	601.1826	42.2678	17.8960
599.5881	599.5667	479.5667	479.5573	40.0000	1495.3012	0.5593	539.5667	25.7834	14.2757
492.0169	492.0062	404.5062	404.5015	20.0000	1242.2523	0.5032	448.2562	10.7496	9.3655
720.9692	720.9264	569.4264	569.4076	80.0000	2692.3210	0.7630	645.1764	55.7289	24.5871
664.7148	664.6826	530.1826	530.1685	60.0000	2493.0863	0.7323	597.4326	39.2414	20.9507
592.0881	592.0667	479.5667	479.5573	40.0000	2235.9630	0.6892	535.8167	23.6400	15.4935
484.5169	484.5062	404.5062	404.5015	20.0000	1854.9242	0.6158	444.5062	9.5700	10.4783

SYSTEM-- 1-P

CONVECTIVE COEFFICIENT CORRELATION--GRIGULL AND HAUF

T11	T10	T21	T20	Q	P	H	TM	QR	QC
737.9692	737.9264	569.4264	569.4076	80.0000	363.7055	0.4344	653.6764	64.6443	15.5683
682.7148	682.6826	530.1826	530.1685	60.0000	337.4191	0.4177	606.4326	46.6784	13.5499
610.5881	610.5667	479.5667	479.5573	40.0000	303.2751	0.3941	545.0667	29.0759	10.9807
503.0169	503.0062	404.5062	404.5015	20.0000	252.4699	0.3543	453.7562	12.5799	7.4242
725.4692	725.4264	569.4264	569.4076	80.0000	900.5701	0.6725	647.4264	58.0284	22.3143
669.2148	669.1826	530.1826	530.1685	60.0000	834.1585	0.6440	599.6826	41.0450	19.0400
597.0881	597.0667	479.5667	479.5573	40.0000	748.7985	0.6049	538.3167	25.0600	15.1191
489.5169	489.5062	404.5062	404.5015	20.0000	621.7856	0.5385	447.0062	10.3503	9.7356
719.4692	719.4264	569.4264	569.4076	80.0000	1258.4036	0.7883	644.4264	54.9719	25.1520
663.7148	663.6826	530.1826	530.1685	60.0000	1165.6602	0.7547	596.9326	38.8455	21.4305
591.0881	591.0667	479.5667	479.5573	40.0000	1045.3397	0.7066	535.3167	23.3603	16.7598
484.0169	484.0062	404.5062	404.5015	20.0000	867.5212	0.6267	444.2562	9.4933	10.5974
712.9692	712.9264	569.4264	569.4076	80.0000	1776.8921	0.9279	641.1764	51.7459	28.3223
657.2148	657.1826	530.1826	530.1685	60.0000	1645.2726	0.8870	593.6826	36.3156	23.9610
584.5881	584.5667	479.5667	479.5573	40.0000	1474.5164	0.8283	532.0667	21.5766	18.5001
478.0169	478.0062	404.5062	404.5015	20.0000	1222.8532	0.7311	441.2562	8.5911	11.4304
704.9692	704.9264	569.4264	569.4076	80.0000	2658.9370	1.1211	637.1764	47.8947	32.3116
648.7148	648.6826	530.1826	530.1685	60.0000	2459.7023	1.0683	589.4326	33.1187	26.9270
577.0881	577.0667	479.5667	479.5573	40.0000	2204.6656	0.9964	528.3167	19.5910	20.6652
471.5169	471.5062	404.5062	404.5015	20.0000	1827.7997	0.8754	438.0062	7.6513	12.4759

SYSTEM--2P

CONVECTIVE COEFFICIENT CORRELATION--LIU, MUELLER, AND LANDIS

T11	T10	T21	T20	Q	P	H	TM	QR	QC
716.4577	716.4263	569.4263	569.4075	80.0000	357.7242	0.2256	642.9263	70.9466	9.4035
664.2061	664.1826	530.1826	530.1685	60.0000	332.2724	0.2181	597.1826	51.8024	8.2907
597.0824	597.0667	479.5667	479.5573	40.0000	299.5194	0.2081	538.3167	33.2495	6.9363
496.0140	496.0062	404.5062	404.5015	20.0000	250.5225	0.1908	450.2562	15.1270	4.9526
708.4577	708.4263	569.4263	569.4075	80.0000	888.7465	0.3694	638.9263	65.7608	14.5614
655.7061	655.6826	530.1826	530.1685	60.0000	824.7692	0.3563	592.9326	47.4229	12.6811
587.5824	587.5667	479.5667	479.5573	40.0000	742.1913	0.3381	533.5667	29.7103	10.3563
486.0140	486.0062	404.5062	404.5015	20.0000	619.3513	0.3073	445.2562	13.0047	7.1024
704.4577	704.4263	569.4263	569.4075	80.0000	1243.7579	0.4423	636.9263	63.2329	16.9342
651.7061	651.6826	530.1826	530.1685	60.0000	1153.9436	0.4262	590.9326	45.4200	14.6872
583.5824	583.5667	479.5667	479.5573	40.0000	1038.0168	0.4039	531.5667	28.2705	11.9126
481.5140	481.5062	404.5062	404.5015	20.0000	865.0803	0.3651	443.0062	12.0915	7.9723
699.9577	699.9263	569.4263	569.4075	80.0000	1758.8785	0.5321	634.5763	60.4400	19.6934
647.2061	647.1826	530.1826	530.1685	60.0000	1631.4160	0.5122	588.6826	43.2104	15.9963
578.5824	578.5667	479.5667	479.5573	40.0000	1466.2025	0.4838	529.0667	26.5120	13.5829
477.0140	477.0062	404.5062	404.5015	20.0000	1221.4675	0.4359	440.7562	11.2035	8.9637
693.9577	693.9263	569.4263	569.4075	80.0000	2635.9853	0.6591	631.6763	56.7991	23.2713
641.2061	641.1826	530.1826	530.1685	60.0000	2444.0534	0.6334	585.6826	40.3351	19.9410
572.5824	572.5667	479.5667	479.5573	40.0000	2195.2763	0.5966	526.0667	24.4611	15.7357
471.0140	471.0062	404.5062	404.5015	20.0000	1826.7564	0.5340	437.7562	10.0579	10.0717

SYSTEM--2-P

CONVECTIVE COEFFICIENT CORRELATION--GRIGULL AND HAUF

T11	T10	T21	T20	Q	P	H	TM	QR	QC
706.9577	706.9263	569.4263	569.4075	80.0000	355.0813	0.3963	638.1763	64.8078	15.4543
654.2061	654.1826	530.1826	530.1685	60.0000	329.4904	0.3808	592.1826	46.6675	13.3909
586.0824	586.0667	479.5667	479.5573	40.0000	296.4592	0.3593	532.8167	29.1669	10.8513
484.5140	484.5062	404.5062	404.5015	20.0000	247.3232	0.3231	444.5062	12.6975	7.3309
696.4577	696.4263	569.4263	569.4075	80.0000	880.4005	0.6133	632.9263	58.3048	22.0913
643.2061	643.1826	530.1826	530.1685	60.0000	816.0755	0.5872	586.6826	41.2846	18.8183
575.0824	575.0667	479.5667	479.5573	40.0000	733.4975	0.5517	527.3167	25.3079	14.9421
473.5140	473.5062	404.5062	404.5015	20.0000	610.6576	0.4912	439.0062	10.5299	9.6118
691.4577	691.4263	569.4263	569.4075	80.0000	1231.0650	0.7189	630.4263	55.3097	24.8744
638.7061	638.6826	530.1826	530.1685	60.0000	1141.2507	0.6882	584.4326	39.1607	21.1769
570.0824	570.0667	479.5667	479.5573	40.0000	1024.8358	0.6443	524.8167	23.6254	16.5380
469.0140	469.0062	404.5062	404.5015	20.0000	852.8756	0.5717	436.7562	9.6857	10.4576
685.9577	685.9263	569.4263	569.4075	80.0000	1739.4794	0.8459	627.6763	52.0893	27.9493
633.2061	633.1826	530.1826	530.1685	60.0000	1612.0169	0.8085	581.6826	36.6250	23.6185
564.5824	564.5667	479.5667	479.5573	40.0000	1446.8034	0.7549	522.0667	21.8251	18.1982
464.0140	464.0062	404.5062	404.5015	20.0000	1203.4541	0.6667	434.2562	8.7757	11.2506
679.4577	679.4263	569.4263	569.4075	80.0000	2605.7311	1.0222	624.4263	48.3820	31.8905
626.2061	626.1826	530.1826	530.1685	60.0000	2412.7559	0.9737	578.1826	33.4920	26.5112
558.5824	558.5667	479.5667	479.5573	40.0000	2166.0653	0.9085	519.0667	19.9203	20.3560
458.5140	458.5062	404.5062	404.5015	20.0000	1800.6752	0.7975	431.5062	7.8081	12.2146

SYSTEM--3P

CONVECTIVE COEFFICIENT CORRELATION--LIU, MUELLER, AND LANDIS

T11	T10	T21	T20	Q	P	H	TM	QR	QC
800.4940	800.4263	569.4263	569.4075	80.0000	381.0930	0.3388	684.9263	69.0973	11.0975
740.7333	740.6826	530.1826	530.1685	60.0000	353.5547	0.3275	635.4326	50.2290	9.7772
663.6005	663.5667	479.5667	479.5573	40.0000	318.0197	0.3121	571.5667	31.9056	8.1437
547.5231	547.5062	404.5062	404.5015	20.0000	264.8498	0.2858	476.0062	14.2759	5.7957
786.9940	786.9263	569.4263	569.4075	80.0000	943.3433	0.5539	678.1763	62.9874	17.0843
726.7333	726.6826	530.1826	530.1685	60.0000	874.1497	0.5342	628.4326	45.2237	14.8857
648.1005	648.0667	479.5667	479.5573	40.0000	784.2690	0.5062	563.8167	27.9476	12.0963
530.5231	530.5062	404.5062	404.5015	20.0000	650.3011	0.4585	467.5062	11.8656	8.1917
780.9940	780.9263	569.4263	569.4075	80.0000	1318.4506	0.6634	675.1763	60.3709	19.8965
720.2333	720.1826	530.1826	530.1685	60.0000	1220.8253	0.6387	625.1826	42.9960	17.2098
641.1005	641.0667	479.5667	479.5573	40.0000	1094.1584	0.6037	560.3167	26.2507	13.8273
523.0231	523.0062	404.5062	404.5015	20.0000	905.5998	0.5438	463.7562	10.8732	9.1388
773.4940	773.4263	569.4263	569.4075	80.0000	1860.7238	0.7974	671.4263	57.1840	23.0682
712.2333	712.1826	530.1826	530.1685	60.0000	1721.4833	0.7663	621.1826	40.3358	19.7762
633.1005	633.0667	479.5667	479.5573	40.0000	1541.7204	0.7227	556.3167	24.3783	15.7308
515.0231	515.0062	404.5062	404.5015	20.0000	1274.1222	0.6475	459.7562	9.8608	10.1455
763.4940	763.4263	569.4263	569.4075	80.0000	2780.9971	0.9865	666.4263	53.0766	27.1403
702.2333	702.1826	530.1826	530.1685	60.0000	2571.3299	0.9463	616.1826	37.1343	23.0809
622.6005	622.5667	479.5667	479.5573	40.0000	2299.6013	0.8888	551.0667	22.0262	18.0239
505.5231	505.5062	404.5062	404.5015	20.0000	1898.7407	0.7921	455.0062	8.7183	11.3447

SYSTEM--3-P

CONVECTIVE COEFFICIENT CORRELATION--GRIGULL AND HAUF

T11	T10	T21	T20	Q	P	H	TM	QR	QC
787.4940	787.4263	569.4263	569.4075	80.0000	377.4764	0.5441	678.4263	63.2081	16.8213
727.2333	727.1826	530.1826	530.1685	60.0000	349.7990	0.5230	628.6826	45.3976	14.6107
649.1005	649.0667	479.5667	479.5573	40.0000	313.9858	0.4935	564.3167	28.1945	11.8620
532.0231	532.0062	404.5062	404.5015	20.0000	260.5377	0.4435	468.2562	12.0691	8.0190
770.9940	770.9263	569.4263	569.4075	80.0000	932.2153	0.8417	670.1763	56.1420	24.0498
709.7333	709.6826	530.1826	530.1685	60.0000	862.3262	0.8058	619.9326	39.5227	20.5111
631.1005	631.0667	479.5667	479.5573	40.0000	772.4455	0.7564	555.3167	23.9211	16.2499
513.5231	513.5062	404.5062	404.5015	20.0000	638.4776	0.6718	459.0062	9.6761	10.3834
763.4940	763.4263	569.4263	569.4075	80.0000	1301.3640	0.9868	666.4263	53.0766	27.1471
702.2333	702.1826	530.1826	530.1685	60.0000	1203.2505	0.9435	616.1826	37.1343	23.0134
623.1005	623.0667	479.5667	479.5573	40.0000	1076.5837	0.8829	551.3167	22.1355	17.9664
506.0231	506.0062	404.5062	404.5015	20.0000	889.0014	0.7806	455.2562	8.7768	11.2362
754.9940	754.9263	569.4263	569.4075	80.0000	1835.0893	1.1611	662.1763	49.7099	30.5422
693.7333	693.6826	530.1826	530.1685	60.0000	1695.8488	1.1084	611.9326	34.5184	25.6991
614.6005	614.5667	479.5667	479.5573	40.0000	1516.0859	1.0343	547.0667	20.3122	19.8011
498.5231	498.5062	404.5062	404.5015	20.0000	1251.2590	0.9109	451.5062	7.9166	12.1418
743.9940	743.9263	569.4263	569.4075	80.0000	2740.3103	1.4010	656.6763	45.5187	34.6672
682.7333	682.6826	530.1826	530.1685	60.0000	2530.6432	1.3344	606.4326	31.2730	28.8569
604.1005	604.0667	479.5667	479.5573	40.0000	2261.0010	1.2415	541.8167	18.1619	21.9189
489.5231	489.5062	404.5062	404.5015	20.0000	1865.3567	1.0879	447.0062	6.9344	13.1131

SYSTEM--1M

HM=2.0*H, QM=0.63*Q

CONVECTIVE COEFFICIENT CORRELATION--LIEL, MUELLER, AND LANDIS

T1IM	T1OM	T2IM	T2OM	QM	PM	HM	TMM	QRM	QCM
942.8221	942.7681	716.7681	716.7444	50.4000	1066.2033	0.5221	829.7681	44.4208	6.2745
873.2021	873.1616	667.1616	667.1438	37.8000	989.6053	0.5052	770.1616	32.3548	5.5339
784.1204	784.0935	603.0935	603.0816	25.2000	887.8362	0.4815	693.5935	20.7468	4.6345
648.7755	648.7620	507.7620	507.7561	12.6000	739.9720	0.4414	578.2620	9.3460	3.3097
929.8221	929.7681	716.7681	716.7444	50.4000	2650.9493	0.8552	823.2681	40.8167	9.6867
860.2021	860.1616	667.1616	667.1438	37.8000	2450.9965	0.8246	763.6616	29.4963	8.4636
769.1204	769.0935	603.0935	603.0816	25.2000	2202.8532	0.7829	686.0935	18.3736	6.9113
632.7755	632.7620	507.7620	507.7561	12.6000	1825.4076	0.7098	570.2620	7.9240	4.7180
923.8221	923.7681	716.7681	716.7444	50.4000	3704.7990	1.0237	820.2681	39.2035	11.2687
854.2021	854.1616	667.1616	667.1438	37.8000	3423.8638	0.9862	760.6616	28.2199	9.8070
762.1204	762.0935	603.0935	603.0816	25.2000	3077.1689	0.9338	682.5935	17.3126	7.8955
625.7755	625.7620	507.7620	507.7561	12.6000	2554.5473	0.8443	566.7620	7.3349	5.2981
916.8221	916.7681	716.7681	716.7444	50.4000	5235.8350	1.2314	816.7681	37.3607	13.0965
846.2021	846.1616	667.1616	667.1438	37.8000	4848.3257	1.1850	756.6616	26.5594	11.2795
755.1204	755.0935	603.0935	603.0816	25.2000	4335.6174	1.1185	679.0935	16.2804	9.0412
618.7755	618.7620	507.7620	507.7561	12.6000	3593.0508	1.0064	563.2620	6.7651	5.9404
907.8221	907.7681	716.7681	716.7444	50.4000	7843.7379	1.5259	812.2681	35.0526	15.4988
837.2021	837.1616	667.1616	667.1438	37.8000	7246.0739	1.4666	752.1616	24.7469	13.2402
745.1204	745.0935	603.0935	603.0816	25.2000	6492.4864	1.3785	674.0935	14.8548	10.4092
609.7755	609.7620	507.7620	507.7561	12.6000	5352.9153	1.2315	558.7620	6.0605	6.6799

SYSTEM--1M

HM=2.0*H, QM=0.63*Q

CONVECTIVE COEFFICIENT CORRELATION--GRIGULL AND HAUF

T1IM	T1OM	T2IM	T2OM	QM	PM	HM	TMM	QRM	QCM
929.8221	929.7681	716.7681	716.7444	50.4000	1058.6583	0.8687	823.2681	40.8167	9.8399
859.2021	859.1616	667.1616	667.1438	37.8000	982.5396	0.8354	763.1616	29.2817	8.5298
769.1204	769.0935	603.0935	603.0816	25.2000	879.3109	0.7881	686.0935	18.3736	6.9572
632.7755	632.7620	507.7620	507.7561	12.6000	730.1631	0.7087	570.2620	7.9240	4.7108
913.8221	913.7681	716.7681	716.7444	50.4000	2622.0054	1.3449	815.2681	36.5837	14.0895
843.2021	843.1616	667.1616	667.1438	37.8000	2422.7633	1.2879	755.1616	25.9488	12.0541
751.1204	751.0935	603.0935	603.0816	25.2000	2176.3375	1.2098	677.0935	15.7033	9.5218
615.7755	615.7620	507.7620	507.7561	12.6000	1797.1523	1.0769	561.7620	6.5268	6.1850
906.8221	906.7681	716.7681	716.7444	50.4000	3658.8080	1.5766	811.7681	34.8004	15.9296
835.2021	835.1616	667.1616	667.1438	37.8000	3394.2688	1.5093	751.1616	24.3519	13.4844
744.1204	744.0935	603.0935	603.0816	25.2000	3032.8322	1.4133	673.5935	14.7154	10.5970
608.7755	608.7620	507.7620	507.7561	12.6000	2507.4561	1.2533	558.2620	5.9841	6.7317
897.8221	897.7681	716.7681	716.7444	50.4000	5175.1780	1.8557	807.2681	32.5674	17.8618
827.2021	827.1616	667.1616	667.1438	37.8000	4788.1782	1.7739	747.1616	22.8003	15.0935
736.1204	736.0935	603.0935	603.0816	25.2000	4274.6067	1.6566	669.5935	13.6199	11.7168
600.7755	600.7620	507.7620	507.7561	12.6000	3540.8036	1.4622	554.2620	5.3864	7.2315
887.8221	887.7681	716.7681	716.7444	50.4000	7741.5606	2.2421	802.2681	30.1638	20.3885
817.2021	817.1616	667.1616	667.1438	37.8000	7142.9267	2.1365	742.1616	20.9231	17.0424
726.1204	726.0935	603.0935	603.0816	25.2000	6402.2275	1.9928	664.5935	12.2999	13.0350
592.7755	592.7620	507.7620	507.7561	12.6000	5286.0404	1.7508	550.2620	4.8121	7.9138

SYSTEM--1M

HM=1.0*H, QM=0.25*Q

CONVECTIVE COEFFICIENT CORRELATION--LIU, MUELLER, AND LANDIS

T1IM	T1OM	T2IM	T2OM	QM	PM	HM	TMM	QRM	QCM
748.4384	748.4170	569.4170	569.4076	20.0000	258.8427	0.2610	658.9170	17.6162	2.4848
693.1916	693.1756	530.1756	530.1685	15.0000	240.6551	0.2526	611.6756	12.8239	2.1894
622.5727	622.5620	479.5620	479.5573	10.0000	216.3985	0.2407	551.0620	8.2189	1.8308
515.5092	515.5038	404.5038	404.5015	5.0000	188.9816	0.2287	460.0038	3.7026	1.3329
738.4384	738.4170	569.4170	569.4076	20.0000	643.1866	0.4276	653.9170	16.2283	3.8428
683.1916	683.1756	530.1756	530.1685	15.0000	595.6510	0.4123	606.6756	11.7230	3.3547
611.5727	611.5620	479.5620	479.5573	10.0000	535.4977	0.3915	545.5620	7.3459	2.7478
503.5092	503.5038	404.5038	404.5015	5.0000	445.3302	0.3549	454.0038	3.1665	1.8683
733.4384	733.4170	569.4170	569.4076	20.0000	899.4831	0.5119	651.4170	15.5552	4.4637
678.1916	678.1756	530.1756	530.1685	15.0000	832.7181	0.4931	604.1756	11.1904	3.8809
605.5727	605.5620	479.5620	479.5573	10.0000	749.1736	0.4669	542.5620	6.8891	3.1284
497.5092	497.5038	404.5038	404.5015	5.0000	624.5516	0.4222	451.0038	2.9123	2.0878
728.4384	728.4170	569.4170	569.4076	20.0000	1269.4433	0.6157	648.9170	14.8957	5.2059
672.1916	672.1756	530.1756	530.1685	15.0000	1178.0718	0.5925	601.1756	10.5666	4.4743
599.5727	599.5620	479.5620	479.5573	10.0000	1057.3319	0.5593	539.5620	6.4457	3.5689
492.5092	492.5038	404.5038	404.5015	5.0000	876.2063	0.5032	448.5038	2.7075	2.3548
721.4384	721.4170	569.4170	569.4076	20.0000	1901.0670	0.7630	645.4170	13.9950	6.1671
665.1916	665.1756	530.1756	530.1685	15.0000	1760.0547	0.7323	597.6756	9.8596	5.2571
592.5727	592.5620	479.5620	479.5573	10.0000	1578.0092	0.6892	536.0620	5.9449	4.1417
484.5092	484.5038	404.5038	404.5015	5.0000	1311.6253	0.6158	444.5038	2.3925	2.6196

SYSTEM--1M

HM=1.0*H, QM=0.25*Q

CONVECTIVE COEFFICIENT CORRELATION--GRIGULL AND HAUF

T1IM	T1OM	T2IM	T2OM	QM	PM	HM	TMM	QRM	QCM
738.4384	738.4170	569.4170	569.4076	20.0000	256.8570	0.4344	653.9170	16.2283	3.9036
683.1916	683.1756	530.1756	530.1685	15.0000	238.2604	0.4177	606.6756	11.7230	3.3986
610.5727	610.5620	479.5620	479.5573	10.0000	214.4468	0.3941	545.0620	7.2688	2.7452
503.5092	503.5038	404.5038	404.5015	5.0000	178.1321	0.3543	454.0038	3.1665	1.8655
725.4384	725.4170	569.4170	569.4076	20.0000	636.7934	0.6725	647.4170	14.5065	5.5786
669.1916	669.1756	530.1756	530.1685	15.0000	589.8348	0.6440	599.6756	10.2609	4.7600
597.5727	597.5620	479.5620	479.5573	10.0000	528.5064	0.6049	538.5620	6.3008	3.7959
489.5092	489.5038	404.5038	404.5015	5.0000	439.6674	0.5385	447.0038	2.5875	2.4339
719.4384	719.4170	569.4170	569.4076	20.0000	889.8175	0.7883	644.4170	13.7424	6.2880
664.1916	664.1756	530.1756	530.1685	15.0000	822.9148	0.7547	597.1756	9.7605	5.3777
591.5727	591.5620	479.5620	479.5573	10.0000	737.7239	0.7066	535.5620	5.8748	4.2087
484.5092	484.5038	404.5038	404.5015	5.0000	611.7218	0.6267	444.5038	2.3925	2.6660
713.4384	713.4170	569.4170	569.4076	20.0000	1254.5628	0.9279	641.4170	12.9972	7.1052
657.1916	657.1756	530.1756	530.1685	15.0000	1163.3748	0.8870	593.6756	9.0786	5.9902
584.5727	584.5620	479.5620	479.5573	10.0000	1042.6347	0.8283	532.0620	5.3940	4.6250
478.5092	478.5038	404.5038	404.5015	5.0000	862.0620	0.7311	441.5038	2.1662	2.8770
705.4384	705.4170	569.4170	569.4076	20.0000	1877.1348	1.1211	637.4170	12.0324	8.1077
649.1916	649.1756	530.1756	530.1685	15.0000	1736.0581	1.0683	589.6756	8.3255	6.7602
576.5727	576.5620	479.5620	479.5573	10.0000	1562.4807	0.9964	528.0620	4.8652	5.1398
471.5092	471.5038	404.5038	404.5015	5.0000	1292.4451	0.8754	438.0038	1.9128	3.1190

SYSTEM--2M

HM=2.0*H, QM=0.63*Q

CONVECTIVE COEFFICIENT CORRELATION--LIU, MUELLER, AND LANDIS

T1IM	T1OM	T2IM	T2OM	QM	PM	HM	TMM	QRM	QCM
901.8076	901.7681	716.7681	716.7444	50.4000	1042.9105	0.4511	809.2681	44.5161	5.9172
837.1912	837.1616	667.1616	667.1438	37.8000	964.1927	0.4363	752.1616	32.8341	5.2590
751.1132	751.0935	603.0935	603.0816	25.2000	870.5351	0.4163	677.0935	20.8351	4.3684
623.7719	623.7620	507.7620	507.7561	12.6000	724.8206	0.3817	565.7620	9.5133	3.1394
891.8076	891.7681	716.7681	716.7444	50.4000	2590.3773	0.7387	804.2681	41.2840	9.1664
826.1912	826.1616	667.1616	667.1438	37.8000	2394.4344	0.7125	746.6616	29.9982	8.0330
740.1132	740.0935	603.0935	603.0816	25.2000	2150.3076	0.6762	671.5935	18.7917	6.5686
610.7719	610.7620	507.7620	507.7561	12.6000	1794.3305	0.6145	559.2620	8.1429	4.4880
887.8076	887.7681	716.7681	716.7444	50.4000	3615.4292	0.8846	802.2681	40.0212	10.7250
821.1912	821.1616	667.1616	667.1438	37.8000	3349.2507	0.8524	744.1616	28.7461	9.3079
734.1132	734.0935	603.0935	603.0816	25.2000	3016.5404	0.8077	668.5935	17.7148	7.5027
605.7719	605.7620	507.7620	507.7561	12.6000	2498.3648	0.7301	556.7620	7.6387	5.0733
881.8076	881.7681	716.7681	716.7444	50.4000	5116.5070	1.0642	799.2681	38.1588	12.4499
815.1912	815.1616	667.1616	667.1438	37.8000	4738.9202	1.0244	741.1616	27.2734	10.7498
728.1132	728.0935	603.0935	603.0816	25.2000	4256.2103	0.9675	665.5935	16.6641	8.5751
599.7719	599.7620	507.7620	507.7561	12.6000	3532.2032	0.8719	553.7620	7.0498	5.6873
873.8076	873.7681	716.7681	716.7444	50.4000	7676.1635	1.3181	795.2681	35.7341	14.6731
807.1912	807.1616	667.1616	667.1438	37.8000	7108.0413	1.2668	737.1616	25.3598	12.5754
720.1132	720.0935	603.0935	603.0816	25.2000	6382.5277	1.1932	661.5935	15.3029	9.8982
591.7719	591.7620	507.7620	507.7561	12.6000	5293.4118	1.0680	549.7620	6.2916	6.3611

SYSTEM--2M

HM=2.0*H, QM=0.63*Q

CONVECTIVE COEFFICIENT CORRELATION--GRIGULL AND HAUF

T1IM	T1OM	T2IM	T2OM	QM	PM	HM	TMM	QRM	QCM
890.8076	890.7681	716.7681	716.7444	50.4000	1032.6352	0.7926	803.7681	40.9667	9.7784
824.1912	824.1616	667.1616	667.1438	37.8000	956.8051	0.7615	745.6616	29.4946	8.4773
738.1132	738.0935	603.0935	603.0816	25.2000	859.1684	0.7185	670.5935	18.4298	6.8776
609.7719	609.7620	507.7620	507.7561	12.6000	713.7220	0.6462	558.7620	8.0411	4.6735
876.8076	876.7681	716.7681	716.7444	50.4000	2564.9308	1.2266	796.7681	36.6356	13.9158
810.1912	810.1616	667.1616	667.1438	37.8000	2369.9669	1.1744	738.6616	26.0708	11.9072
724.1132	724.0935	603.0935	603.0816	25.2000	2125.9139	1.1033	663.5935	15.9778	9.4659
594.7719	594.7620	507.7620	507.7561	12.6000	1770.9610	0.9823	551.2620	6.5723	6.0596
870.8076	870.7681	716.7681	716.7444	50.4000	3583.2722	1.4378	793.7681	34.8418	15.6994
804.1912	804.1616	667.1616	667.1438	37.8000	3317.3661	1.3764	735.6616	24.6567	13.3698
717.1132	717.0935	603.0935	603.0816	25.2000	2977.8522	1.2886	660.0935	14.8040	10.4162
589.7719	589.7620	507.7620	507.7561	12.6000	2464.1702	1.1433	548.7620	6.1068	6.6474
863.8076	863.7681	716.7681	716.7444	50.4000	5063.6277	1.6918	790.2681	32.7954	17.6332
797.1912	797.1616	667.1616	667.1438	37.8000	4686.3533	1.6170	732.1616	23.0465	14.9049
711.1132	711.0935	603.0935	603.0816	25.2000	4187.5236	1.5098	657.0935	13.8248	11.5612
583.7719	583.7620	507.7620	507.7561	12.6000	3469.5308	1.3334	545.7620	5.5636	7.1852
855.8076	855.7681	716.7681	716.7444	50.4000	7579.7708	2.0444	786.2681	30.5167	20.1490
789.1912	789.1616	667.1616	667.1438	37.8000	6992.1202	1.9474	728.1616	21.2575	16.8456
703.1132	703.0935	603.0935	603.0816	25.2000	6279.4951	1.8170	653.0935	12.5573	12.8836
576.7719	576.7620	507.7620	507.7561	12.6000	5190.2144	1.5951	542.2620	4.9506	7.8038

SYSTEM--2M

HM=1.0*H, QM=0.25*Q

CONVECTIVE COEFFICIENT CORRELATION--LITI, MUELLER, AND LANDIS

T11M	T10M	T21M	T20M	QM	PM	HM	TMM	QRM	QCM
716.4326	716.4169	569.4169	569.4075	20.0000	252.9469	0.2256	642.9169	17.7359	2.3509
664.1873	664.1755	530.1755	530.1685	15.0000	234.9503	0.2181	597.1755	12.9501	2.0727
597.5698	597.5620	479.5620	479.5573	10.0000	211.4026	0.2081	538.5620	8.3599	1.7414
496.5077	496.5038	404.5038	404.5015	5.0000	176.7244	0.1908	450.5038	3.8091	1.2449
708.4326	708.4169	569.4169	569.4075	20.0000	628.4329	0.3694	638.9169	16.4395	3.6404
656.1873	656.1755	530.1755	530.1685	15.0000	582.1896	0.3563	593.1755	11.9185	3.1829
587.5698	587.5620	479.5620	479.5573	10.0000	524.8056	0.3381	533.5620	7.4274	2.5891
486.5077	486.5038	404.5038	404.5015	5.0000	436.7610	0.3073	445.5038	3.2769	1.7865
704.4326	704.4169	569.4169	569.4075	20.0000	879.4615	0.4423	636.9169	15.8075	4.2335
652.1873	652.1755	530.1755	530.1685	15.0000	814.4953	0.4262	591.1755	11.4167	3.6869
583.5698	583.5620	479.5620	479.5573	10.0000	733.9848	0.4039	531.5620	7.0674	2.9782
481.5077	481.5038	404.5038	404.5015	5.0000	611.7021	0.3651	443.0038	3.0228	1.9931
700.4326	700.4169	569.4169	569.4075	20.0000	1241.6325	0.5321	634.9169	15.1863	4.9422
647.1873	647.1755	530.1755	530.1685	15.0000	1153.5768	0.5122	588.6755	10.8022	4.2491
578.5698	578.5620	479.5620	479.5573	10.0000	1036.7559	0.4838	529.0620	6.6278	3.3957
476.5077	476.5038	404.5038	404.5015	5.0000	866.3933	0.4359	440.5038	2.7765	2.2255
694.4326	694.4169	569.4169	569.4075	20.0000	1860.6329	0.6591	631.9169	14.2741	5.8412
641.1873	641.1755	530.1755	530.1685	15.0000	1728.1939	0.6334	585.6755	10.0834	4.9853
572.5698	572.5620	479.5620	479.5573	10.0000	1552.2860	0.5966	526.0620	6.1151	3.9339
471.5077	471.5038	404.5038	404.5015	5.0000	1287.3353	0.5340	438.0038	2.5379	2.5369

SYSTEM--2M

HM=1.0*H, QM=0.25*Q

CONVECTIVE COEFFICIENT CORRELATION--GRIGULL AND HAUF

T11M	T10M	T21M	T20M	QM	PM	HM	TMM	QRM	QCM
707.4326	707.4169	569.4169	569.4075	20.0000	250.6841	0.3963	638.4169	16.2805	3.8776
654.1873	654.1755	530.1755	530.1685	15.0000	232.9832	0.3808	592.1755	11.6665	3.3477
586.5698	586.5620	479.5620	479.5573	10.0000	209.1975	0.3593	533.0620	7.3367	2.7256
484.5077	484.5038	404.5038	404.5015	5.0000	174.8834	0.3231	444.5038	3.1743	1.8327
696.4326	696.4169	569.4169	569.4075	20.0000	622.5314	0.6133	632.9169	14.5755	5.5228
643.1873	643.1755	530.1755	530.1685	15.0000	577.0482	0.5872	586.6755	10.3208	4.7046
574.5698	574.5620	479.5620	479.5573	10.0000	519.8689	0.5517	527.0620	6.2842	3.7160
473.5077	473.5038	404.5038	404.5015	5.0000	431.7986	0.4912	439.0038	2.6324	2.4029
691.4326	691.4169	569.4169	569.4075	20.0000	870.4861	0.7189	630.4169	13.8268	6.2186
638.1873	638.1755	530.1755	530.1685	15.0000	808.6313	0.6882	584.1755	9.7315	5.2698
570.5698	570.5620	479.5620	479.5573	10.0000	722.8834	0.6443	525.0620	5.9478	4.1573
469.5077	469.5038	404.5038	404.5015	5.0000	600.9618	0.5717	437.0038	2.4445	2.6347
686.4326	686.4169	569.4169	569.4075	20.0000	1227.6597	0.8459	627.9169	13.0941	7.0173
633.1873	633.1755	530.1755	530.1685	15.0000	1139.6597	0.8085	581.6755	9.1559	5.9046
564.5698	564.5620	479.5620	479.5573	10.0000	1023.0388	0.7549	522.0620	5.4561	4.5495
464.5077	464.5038	404.5038	404.5015	5.0000	847.7179	0.6667	434.5038	2.2163	2.8363
679.4326	679.4169	569.4169	569.4075	20.0000	1842.5128	1.0222	624.4169	12.0950	7.9726
626.1873	626.1755	530.1755	530.1685	15.0000	1706.0631	0.9737	578.1755	8.3727	6.6278
558.5698	558.5620	479.5620	479.5573	10.0000	1531.6309	0.9085	519.0620	4.9799	5.0890
458.5077	458.5038	404.5038	404.5015	5.0000	1273.2652	0.7975	431.5038	1.9520	3.0537

SYSTEM--3M

HM=2.0*H, QM=0.63*Q

CONVECTIVE COEFFICIENT CORRELATION--LIN, MUELLER, AND LANDIS

T11M	T10M	T21M	T20M	QM	PM	HM	TMM	QRM	QCM
1007.8533	1007.7681	716.7681	716.7444	50.4000	1111.7215	0.6776	862.2681	43.4203	6.9900
933.2255	933.1616	667.1616	667.1438	37.8000	1028.7354	0.6551	800.1616	31.6906	6.1775
836.1360	836.0935	603.0935	603.0816	25.2000	922.9469	0.6242	719.5935	20.1620	5.1562
688.7833	688.7620	507.7620	507.7561	12.6000	767.0184	0.5716	598.2620	8.9714	3.6679
991.8533	991.7681	716.7681	716.7444	50.4000	2747.4598	1.1078	854.2681	39.8018	10.8004
915.2255	915.1616	667.1616	667.1438	37.8000	2544.2900	1.0684	791.1616	28.4752	9.3935
816.1360	816.0935	603.0935	603.0816	25.2000	2277.2331	1.0124	709.5935	17.6101	7.6452
667.7833	667.7620	507.7620	507.7561	12.6000	1880.5680	0.9169	587.7620	7.4882	5.2011
983.8533	983.7681	716.7681	716.7444	50.4000	3842.0048	1.3268	850.2681	38.0571	12.5588
907.2255	907.1616	667.1616	667.1438	37.8000	3551.8059	1.2775	787.1616	27.1057	10.8693
807.1360	807.0935	603.0935	603.0816	25.2000	3177.7373	1.2075	705.0935	16.5213	8.7328
657.7833	657.7620	507.7620	507.7561	12.6000	2622.1932	1.0877	582.7620	6.8293	5.7841
973.8533	973.7681	716.7681	716.7444	50.4000	5426.1802	1.5948	845.2681	35.9351	14.5307
897.2255	897.1616	667.1616	667.1438	37.8000	5006.9308	1.5325	782.1616	25.4440	12.4960
797.1360	797.0935	603.0935	603.0816	25.2000	4476.1699	1.4453	700.0935	15.3535	9.9406
647.7833	647.7620	507.7620	507.7561	12.6000	3687.6898	1.2949	577.7620	6.1999	6.4270
961.8533	961.7681	716.7681	716.7444	50.4000	8100.7989	1.9730	839.2681	33.4737	17.1374
884.2255	884.1616	667.1616	667.1438	37.8000	7482.8375	1.8926	775.6616	23.3653	14.5598
784.1360	784.0935	603.0935	603.0816	25.2000	6671.5980	1.7776	693.5935	13.8997	11.4068
635.7833	635.7620	507.7620	507.7561	12.6000	5494.5765	1.5842	571.7620	5.4821	7.1887

SYSTEM--3M

HM=2.0*H, QM=0.63*Q

CONVECTIVE COEFFICIENT CORRELATION--GRIGULL AND HAUF

T11M	T10M	T21M	T20M	QM	PM	HM	TMM	QRM	QCM
991.8533	991.7681	716.7681	716.7444	50.4000	1100.3976	1.0883	854.2681	39.8018	10.6098
916.2255	916.1616	667.1616	667.1438	37.8000	1017.5242	1.0460	791.6616	28.6489	9.2336
817.1360	817.0935	603.0935	603.0816	25.2000	912.1675	0.9870	710.0935	17.7334	7.4881
668.7833	668.7620	507.7620	507.7561	12.6000	755.1968	0.8870	588.2620	7.5557	5.0630
970.8533	970.7681	716.7681	716.7444	50.4000	2717.7650	1.6833	843.7681	35.3112	15.1579
894.2255	894.1616	667.1616	667.1438	37.8000	2507.2726	1.6116	780.6616	24.9562	12.9694
794.1360	794.0935	603.0935	603.0816	25.2000	2244.9296	1.5127	698.5935	15.0116	10.2433
645.7833	645.7620	507.7620	507.7561	12.6000	1848.4964	1.3435	576.7620	6.0774	6.5730
961.8533	961.7681	716.7681	716.7444	50.4000	3790.7586	1.9736	839.2681	33.4737	17.1419
884.2255	884.1616	667.1616	667.1438	37.8000	3501.5842	1.8870	775.6616	23.3653	14.5172
784.1360	784.0935	603.0935	603.0816	25.2000	3127.9596	1.7658	693.5935	13.8997	11.3307
636.7833	636.7620	507.7620	507.7561	12.6000	2569.4537	1.5613	572.2620	5.5403	7.1403
950.8533	950.7681	716.7681	716.7444	50.4000	5347.3309	2.3221	833.7681	31.2968	19.2638
873.2255	873.1616	667.1616	667.1438	37.8000	4937.3126	2.2168	770.1616	21.6766	16.1897
774.1360	774.0935	603.0935	603.0816	25.2000	4396.6777	2.0686	688.5935	12.8295	12.5407
626.7833	626.7620	507.7620	507.7561	12.6000	3622.4712	1.8217	567.2620	4.9697	7.6855
936.8533	936.7681	716.7681	716.7444	50.4000	7985.8193	2.8019	826.7681	28.6335	21.8533
860.2255	860.1616	667.1616	667.1438	37.8000	7352.9904	2.6688	763.6616	19.7615	18.2602
760.1360	760.0935	603.0935	603.0816	25.2000	6568.5948	2.4830	681.5935	11.3993	13.8203
615.7833	615.7620	507.7620	507.7561	12.6000	5391.4566	2.1758	561.7620	4.3728	8.3307

SYSTEM--3M

HM=1.0*H, QM=0.25*Q

CONVECTIVE COEFFICIENT CORRELATION--LIU, MUELLER, AND LANDIS

T11M	T10M	T21M	T20M	QM	PM	HM	TMM	QRM	QCM
800.4507	800.4169	569.4169	569.4075	20.0000	269.4712	0.3388	684.9169	17.2736	2.7744
741.2009	741.1755	530.1755	530.1685	15.0000	249.7641	0.3275	635.6755	12.6029	2.4501
663.5789	663.5620	479.5620	479.5573	10.0000	224.8728	0.3121	571.5620	7.9762	2.0359
547.5122	547.5038	404.5038	404.5015	5.0000	187.2765	0.2858	476.0038	3.5689	1.4489
787.4507	787.4169	569.4169	569.4075	20.0000	666.4273	0.5539	678.4169	15.8014	4.2809
727.2009	727.1755	530.1755	530.1685	15.0000	617.4809	0.5342	628.6755	11.3490	3.7309
648.5789	648.5620	479.5620	479.5573	10.0000	553.8901	0.5062	564.0620	7.0176	3.0330
530.5122	530.5038	404.5038	404.5015	5.0000	459.8308	0.4585	467.5038	2.9663	2.0479
780.4507	780.4169	569.4169	569.4075	20.0000	933.1644	0.6634	674.9169	15.0383	4.9624
720.2009	720.1755	530.1755	530.1685	15.0000	863.2476	0.6387	625.1755	10.7486	4.3024
641.5789	641.5620	479.5620	479.5573	10.0000	772.7012	0.6037	560.5620	6.5924	3.4675
523.5122	523.5038	404.5038	404.5015	5.0000	639.2204	0.5438	464.0038	2.7345	2.2943
773.4507	773.4169	569.4169	569.4075	20.0000	1315.7189	0.7974	671.4169	14.2954	5.7670
712.2009	712.1755	530.1755	530.1685	15.0000	1217.2638	0.7663	621.1755	10.0836	4.9441
633.5789	633.5620	479.5620	479.5573	10.0000	1088.6867	0.7227	556.5620	6.1232	3.9455
515.5122	515.5038	404.5038	404.5015	5.0000	899.2091	0.6475	460.0038	2.4806	2.5478
763.4507	763.4169	569.4169	569.4075	20.0000	1966.4444	0.9865	666.4169	13.2686	6.7850
702.2009	702.1755	530.1755	530.1685	15.0000	1818.1917	0.9463	616.1755	9.2833	5.7702
622.5789	622.5620	479.5620	479.5573	10.0000	1626.0551	0.8888	551.0620	5.5064	4.5060
505.5123	505.5038	404.5038	404.5015	5.0000	1342.6080	0.7921	455.0038	2.1795	2.8362

SYSTEM--3M

HM=1.0*H, QM=0.25*Q

CONVECTIVE COEFFICIENT CORRELATION--GRIGULL AND HAUF

T11M	T10M	T21M	T20M	QM	PM	HM	TMM	QRM	QCM
787.4507	787.4169	569.4169	569.4075	20.0000	266.9138	0.5441	678.4169	15.8014	4.2053
727.2009	727.1755	530.1755	530.1685	15.0000	247.3435	0.5230	628.6755	11.3490	3.6527
649.5789	649.5620	479.5620	479.5573	10.0000	221.7544	0.4935	564.5620	7.0794	2.9742
532.5122	532.5038	404.5038	404.5015	5.0000	183.9281	0.4435	468.5038	3.0343	2.0126
771.4507	771.4169	569.4169	569.4075	20.0000	658.5074	0.8417	670.4169	14.0868	6.0274
710.2009	710.1755	530.1755	530.1685	15.0000	609.0577	0.8058	620.1755	9.9208	5.1421
630.5789	630.5620	479.5620	479.5573	10.0000	546.9497	0.7564	555.0620	5.9517	4.0491
513.5122	513.5038	404.5038	404.5015	5.0000	451.4703	0.6718	459.0038	2.4190	2.5958
763.4507	763.4169	569.4169	569.4075	20.0000	920.1951	0.9868	666.4169	13.2686	6.7868
702.2009	702.1755	530.1755	530.1685	15.0000	850.8205	0.9435	616.1755	9.2833	5.7534
623.5789	623.5620	479.5620	479.5573	10.0000	760.1458	0.8829	551.5620	5.5611	4.5072
506.5123	506.5038	404.5038	404.5015	5.0000	627.2878	0.7806	455.5038	2.2089	2.8229
755.4507	755.4169	569.4169	569.4075	20.0000	1296.1533	1.1611	662.4169	12.4757	7.6561
694.2009	694.1755	530.1755	530.1685	15.0000	1197.6123	1.1084	612.1755	8.6671	6.4444
614.5789	614.5620	479.5620	479.5573	10.0000	1072.0289	1.0343	547.0620	5.0779	4.9503
498.5123	498.5038	404.5038	404.5015	5.0000	884.7708	0.9109	451.5038	1.9791	3.0355
744.4507	744.4169	569.4169	569.4075	20.0000	1935.3652	1.4010	656.9169	11.4258	8.6916
683.2009	683.1755	530.1755	530.1685	15.0000	1786.9534	1.3344	606.6755	7.8540	7.2379
604.5789	604.5620	479.5620	479.5573	10.0000	1596.0149	1.2415	542.0620	4.5653	5.5017
489.5123	489.5038	404.5038	404.5015	5.0000	1319.0020	1.0879	447.0038	1.7336	3.2783

APPENDIX F

7040 COMPUTER PROGRAM FOR EXPERIMENTAL DATA ANALYSIS

7040 COMPUTER PROGRAM FOR EXPERIMENTAL DATA ANALYSIS

This program was used in conjunction with the least square curve fit program to establish the empirical correlations for the convective film coefficients. A correlation of the form $Nu = A(Gr)^{x}e^{y}$ was established for horizontal cylindrical annuli and another of the form $Nu = B(Gr)^{z}$ was established for vertical cylindrical annuli. In establishing these correlations it was necessary to obtain the logarithm of the Nusselt and Grashof numbers. These values were obtained from the program listed below. After the logarithm values were obtained, a curve was fit to log Nu vs. log Gr through the use of the program listed in Appendix D. This permitted the evaluation of the constants in the correlations. All necessary instructions to use the Experimental Data Analysis Program are stated within the program.

```
C      ANALYSIS OF EXPERIMENTAL DATA FOR MODEL AND PROTOTYPE.
C      T2O = OUTSIDE TEMPERATURE OF OUTER CYLINDER.
C      T2I = INSIDE TEMPERATURE OF OUTER CYLINDER.
C      T1O = OUTSIDE TEMPERATURE OF INNER CYLINDER.
C      T1I = INSIDE TEMPERATURE OF INNER CYLINDER.
C      D2O = OUTSIDE DIAMETER OF OUTER CYLINDER.
C      D2I = INSIDE DIAMETER OF OUTER CYLINDER.
C      D1O = OUTSIDE DIAMETER OF INNER CYLINDER.
C      D1I = INSIDE DIAMETER OF INNER CYLINDER.
C      Q = HEAT TRANSFER THRU CYLINDERS.
C      EL = LENGTH OF CYLINDER.
C      P = PRESSURE OF FLUID IN PSIF.
C      TG = THERMAL CONDUCTIVITY OF GAS.
C      H = CONVECTION COEFFICIENT.
C      GR = GRASHOF NUMBER.
C      TW = CHAMBER WALL TEMPERATURE.
C      SIGMA = STEFAN - BOLTZMANN CONSTANT.
C      EPSON = EMISSIVITY.
C      R = GAS CONSTANT.
C      G = LOCAL ACCELERATION OF GRAVITY.
C      TS = THERMAL CONDUCTIVITY OF SOLID.
C      QR = RADIATION HEAT TRANSFER BETWEEN CYLINDERS.
C      QC = CONVECTION HEAT TRANSFER BETWEEN CYLINDERS.
C      NU = NUSSELT NUMBER.
C      ROW = DENSITY.
   51 FORMAT(6F12.5)
   52 FORMAT(E16.8)
   53 FORMAT(F16.8)
   54 FORMAT(4F12.5)
   55 FORMAT(3F14.5)
   58 FORMAT(9F12.5)
   60 FORMAT(6X,2HQR,10X,2HQC,10X,1HH,11X,2HNU,10X,2HGR,10X,3HROW,9X,
     1 1HX,11X,1HY,10X,2HTV)
   70 FORMAT(1H1)
      WRITE(6,70)
      READ(5,51)TW,D2O,D2I,D1O,D1I,TS
      READ(5,54)EPSON,EL,R,G
      READ(5,52)SIGMA
      REAL NU
      TV=0.0
    4 READ(5,54)Q,P,T1O,T2O
      A2O=3.1415927*D2O*EL
      A1O=3.1415927*D1O*EL
      A2I=3.1415927*D2I*EL
      TV=TV+1.0
      T2O=(Q/(SIGMA*EPSON*A2O)+TW**4.0)**0.25
      ZLOG=ALOG(D2O/D2I)
      T2I=(Q/(2.0*3.1415927*TS*EL))*ZLOG+T2O
      TM=(T1O+T2I)/2.0
      A=0.35145532E-03
      B=0.32041684E-04
      C=-0.10027234E-07
      D=0.22337353E-11
      TG=A+B*TM+C*TM**2.0+D*TM**3.0
      UM=TM**1.5/(375.0*TM+77700.0)
      DELTA=(D2I-D1O)/2.0
      BT=(1.0/EPSON-1.0)*(1.0+A1O/A2I)+1.0
      QR=A1O*SIGMA*EPSON/BT*(T1O**4.0-T2I**4.0)
      QC=Q-QR
      H=QC/(A1O*(T1O-T2I))
      NU=H*DELTA/TG
      DTM=T1O-T2I
      GR=P**2.0/((R**2.0)*TM**3.0)*G*DTM*DELTA**3.0/UM**2.0
      ROW=P/(R*TM)
      X=ALOG(NU)
      Y=ALOG(GR)
      WRITE(6,60)
      WRITE(6,58)QR,QC,H,NU,GR,ROW,X,Y,TV
      IF(TV-4.0) 4,11,11
   11 STOP
      END
$ENTRY
$IBSYS
```

APPENDIX G

SOURCES OF ERROR

SOURCES OF ERROR

The accuracy of predicting prototype temperatures from observed model temperatures was affected by uncertainties associated with two distinctly separate phases of this investigation. A portion of the overall error was introduced during design and construction of the test sections. Additional uncertainties were introduced during the experimental program and these were associated with random or systematic experimental errors. Since the overall accuracy was affected by these two independent sources they are treated separately in this appendix.

Design and Construction Errors

The design of the test sections used in this investigation was performed as much as possible in accordance with the modeling criteria. Thus, variations in thermal properties of materials, radiation properties of surfaces, dimensional tolerances, and thermal behavior of joints were controlled or eliminated during the design and construction phase of this investigation.

Slight geometric distortion was permitted on the ends of the inner cylinders and the gas fill line. These distortions were located within the guard heater sections. Thus, they had little effect upon the thermal behavior of the center portion of each test section during the steady-state investigation. Under transient conditions the error was more because of the energy stored in this extra mass of material. Nevertheless, this had little effect upon the thermal behavior of the center portion of each test section.

Errors Due to Thermal Variations in Properties

The variations in thermal properties of the solid components were considered in developing the similarity parameters for models and prototypes constructed of the same material. For Technique I, these variations presented no problem since the model and prototype were at the same temperature. Variations in thermal properties existed during tests performed to satisfy the Zero Surroundings Technique. These variations resulted from model temperatures being higher than prototype temperatures.

For the Zero Surroudings Technique, the effects of variations in thermal properties on the predicted thermal behavior of prototypes were estimated utilizing thermal property data reported by Lucks and Deem [33]. The variations in the thermal properties of 6061-T6 Aluminum are listed in Table XXIII. From the data listed in this table, the constants a, b, k_o, and C_{p_o} in the expressions were established. These constants are also listed in Table XXIII.

$$k = k_o T^a$$

$$c = c_{p_o} T^b$$

TABLE XXIII

COEFFICIENTS FOR THERMAL CONDUCTIVITY AND SPECIFIC HEAT

	k		C_p					
Material	273°K	360°K	273°K	360°K	a	b	k_o	C_{p_o}
6061 Al	0.41	0.42	0.230	0.237	0.07	0.11	0.025	0.075

An estimate of the error produced by assuming constant thermal properties was obtained by selecting a typical model temperature of 650°R and applying the Zero Surroundings Technique similarity parameters. For one-half scaling, the prototype temperature was 516°R for constant thermal properties and 513°R for variable properties. The time required for the prototype to reach a selected thermal level, for a model time of 50 minutes, was 200 minutes for constant thermal properties and 197.8 minutes for variable properties. A list of the controlling similarity parameters for constant and variable thermal properties is given in Table XXIV. The results of this analysis illustrate that variations in thermal properties had little effect during this investigation.

TABLE XXIV

SIMILARITY PARAMETER VARIATIONS WITH VARIATIONS IN THERMAL PROPERTIES

Parameter	Constant Thermal Properties	Variable Thermal Properties
T^*	1.26	1.267
θ	0.25	0.253
q^*	0.63	0.644

Since the percentage of alloying elements in a particular material is different for each batch from a particular manufacturer or for materials with the same alloy specifications from different manufacturers, there was a possibility that the model and prototype had slightly different thermal properties. Miller [14] pointed out that these variations could cause errors in predicting the prototype temperatures from observed model temperatures. These variations may be accounted for by measuring the thermal properties of the material. In this investigation these properties were not measured but the same material was purchased from the same manufacturer.

Experimental Error

The accuracy of the experimental measurements performed during model tests was governed by the same sources of error as the accuracy achieved during full-scale testing. For the tests conducted in this investigation the major sources of error were in temperature measurement, control of input to heaters, and pressure measurement. An estimate of the probable experimental error can be obtained by considering the accuracy of each of these independent contributing sources.

Temperature Measurement

The thermocouple output was measured with the following accuracy:

Steady-state readout accuracy	$\pm$ 0.25°R
Response uncertainty	$\pm$ 0.50°R
Thermocouple calibration	$\pm$ 0.50°R
Estimated maximum error for steady-state	$\pm$ 0.75°R

Power Input

The power input to the main heater was measured with the following accuracy:

Power readout accuracy	± 0.12 watt
Power variations due to voltage fluctuations	± 0.08 watt
Estimated maximum error	± 0.20 watt

Pressure Measurement

The gas pressure in the annulus was measured with the following accuracy:

Pressure readout accuracy	± 0.012 psi

Effect of Error in Power Input on Temperature

Errors in measurement on control of power input were directly related to errors in test section temperatures. Since the energy input to the test sections was in balance with that emitted to the surroundings (during steady-state), then variations in energy input were related to variations in overall model temperature through the 4th power of absolute temperature. For certain local regions in the test sections, this dependence does not apply since convection plays a strong part in distributing the energy to other regions. In these regions a change in energy rate causes a change in temperature with other than 4th power dependence. The exact dependence was not established in this investigation for these regions. Therefore, the 4th power dependence was used in obtaining an overall estimate of error. Thus, it was assumed that

$$k\ \Delta E = \Delta(T^4), \qquad (G\text{-}1)$$

where

ΔE = small variation in power input

k = constant

$\Delta(T^4)$ = small variation in 4th power of test section temperature.

The thermal error caused by power measurement or control can be expressed by

$$\frac{\Delta E}{4\ E} = \frac{\Delta T}{T} \qquad (G\text{-}2)$$

For E = 20 watts and the measurement errors estimated above, the result is

Estimated maximum error due to power measurement or control $\quad \frac{\Delta T}{T} = \pm 0.0025$

For a model inner cylinder temperature of $600^{\circ}R$, the following estimated overall maximum errors could have occurred:

Technique I

Estimated maximum error for steady-state $\quad \pm 2.25^{\circ}R$

Zero Surroundings Technique

Estimated maximum error for steady-state $\quad \pm 5.00^{\circ}R$

VITA

Dago Maples

Candidate for the Degree of

Doctor of Philosophy

Thesis: A STUDY OF SPACECRAFT TEMPERATURE PREDICTION BY THERMAL MODELING

Major Field: Mechanical Engineering

Biographical:

Personal Data: Born August 20, 1939, in Tiger Branch, Mississippi, the son of George and Betty Maples.

Education: Received the Bachelor of Science degree and Master of Science degree from Mississippi State University, with a major in Mechanical Engineering, in January, 1962 and August, 1963, respectively. Completed the requirements for the Doctor of Philosophy degree in May, 1969.

Professional Experience: Employed by Mississippi State University from September, 1962 to May, 1964 as Instructor of Mechanical Engineering. Employed by the School of Mechanical Engineering at Oklahoma State University, as a Teaching Assistant during 1964-65.